5. Meteorological Aspects

Storm surges occur because of meteorological problems associated with extratropical and tropical cyclones. This chapter will discuss the dynamics of extratropical cyclones and tropical cyclones and the meteorological problems associated with these cyclones in the Pacific, Atlantic, and Indian oceans, as well as in other smaller water bodies. The problems associated with obtaining wind stress data for synoptic scale and mesoscale weather systems will be examined in detail.

5.1 Extratropical Cyclones

5.1.1 Development Theory

The treatment in this section follows closely PETTERSSEN (1956) and WARNECKE (1997). FITZ-ROY (1863) appears to be among the first to propose a model of an extratropical cyclone as originating on the boundary between two different air masses (e.g. a warm and moist air mass originating in subtropical latitudes and a colder and drier air mass originating in the polar regions). Some later authors who recognized that discontinuities in temperature, moisture content, and speed of motion were essential for cyclone development were BLASIUS (1875), HELMHOLTZ (1888, 1889), MARGULES (1905) and SHAW (1921).

BJERKNES (1919) proposed the first dynamical model for cyclones and agreed with MARGULES (1905) that the kinetic energy of the cyclones comes from the potential energy due to the juxtaposition of warm and cold air masses and a decrease of the potential energy that follows the development of a cyclone. According to Bjerknes the cold air forms a wedge under the warm air, with a slope of separation of about 1 : 100, and the cyclonic disturbances travel along the frontal surface similar to waves traveling along a discontinuity.

The life cycle of a cyclone has several stages. In the initial stage, a small amplitude wave forms on a more or less straight quasi-stationary front. The currents on either side of the front could be in the same direction or in opposite directions. In the second stage, the warm air rises to higher levels over the warm front and the cold front wedges in under the warm air. In the third stage, the warm air sectors become progressively narrower and the cold front tends to overtake the warm front. At this stage the cyclone has reached the occlusion stage (Fig. 5.1).

It is customary to refer to cyclone families (Fig. 5.2), rather than individual cyclones (FITZ-ROY, 1863). Usually there would be two to four or five cyclones in a series, one following the other and all moving in a general southwest to northeast direction. BJERKNES and SOLBERG (1921, 1922) accounted for cyclone families as wave disturbances on the polar front. In a family of four cyclones, typically the first one would be old and occluded, the second would be somewhat younger, the third would be a young wave cyclone, and the fourth would be a nascent cyclone wave. On the average, a cyclone family takes 5–6 d to pass a given location. The occurrence of cyclone families is a regular phenomenon over the North Atlantic and Western Europe (because of regular major polar outbreaks from the Greenland-Labrador area) and not as regular over North America and Central Eurasia.

Usually, cyclone formation begins near sea level and develops to higher levels in the atmosphere as the occlusion develops. Once a complete occlusion occurs, generally a closed cyclonic circulation can be found in the middle and upper troposphere (located over the cold rear of the occluded sea level cyclone). Sometimes, the depression in the pressure field aloft

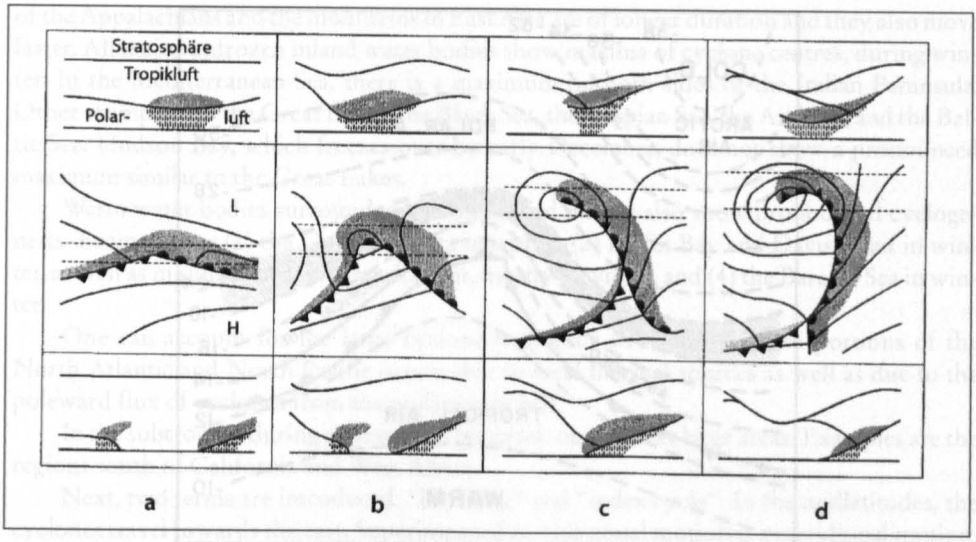

Fig. 5.1: Stages of cyclogenesis (WARNECKE, 1997)

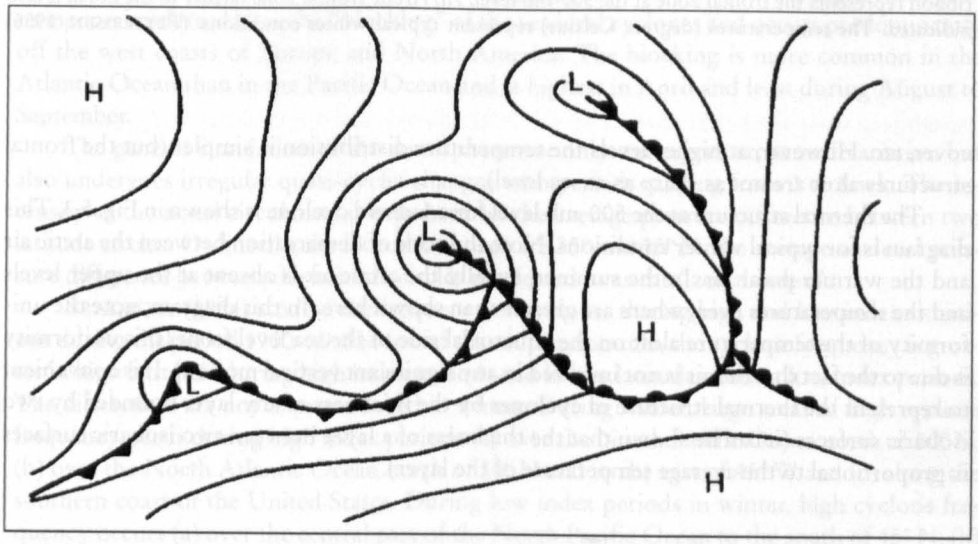

Fig. 5.2: Cyclone families (WARNECKE, 1997)

may merge with the semipermanent low over the polar region. When this happens, a high-level trough can be noticed in the rear of the occluded sea level cyclone. Thus, these upper level troughs represent the vertical extension of the cyclones. However, sometimes (particularly during winter), cyclone development may begin at the higher levels and at other times simultaneously with the lower level development. One refers to these more or less independent developments aloft (middle and upper troposphere) as "cutoff" cyclones.

Next, the thermal structure of cyclones will be briefly examined. At sea level there is no definite thermal pattern and irregularities occur because of the diurnal variations, cloud

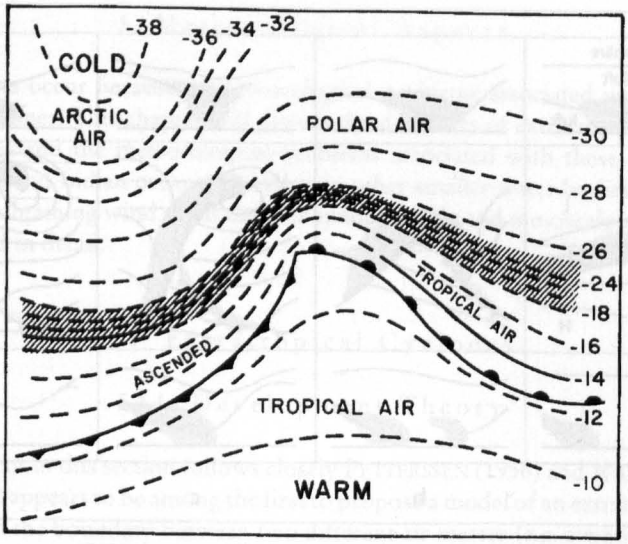

Fig. 5.3: Schematic representation of the isotherms at the 500-mb level associated with a wave cyclone. The front at sea level is represented by conventional symbols (warm front; cold front) and a hatched ribbon represents the frontal zone at the 500-mb level. An Arctic frontal zone farther to the north is also indicated. The temperatures (degrees Celsius) represent typical winter conditions. (PETTERSSEN, 1956)

cover, etc. However, at higher levels the temperature distribution is simpler (but the frontal structures aloft are not as sharp as at sea level).

The thermal structure at the 500-mb level for a 1-d-old cyclone is shown in Fig. 5.3. This diagram is for typical winter conditions. Note the zone of demarcation between the arctic air and the warmer polar air. In the summer, usually the arctic air is absent at the upper levels and the temperatures everywhere are greater than shown here. In this diagram, note the uniformity of the temperature aloft on the equatorial side of the sea level front (this uniformity is due to the fact that the air is not involved in any significant vertical motion). It is convenient to represent the thermal structure of cyclones by the thickness of any layer bounded by two isobaric surfaces (it can be shown that the thickness of a layer between two isobaric surfaces is proportional to the average temperature of the layer).

Cyclone Patterns

The patterns of cyclogenesis during winter will be examined first. In the North Pacific Ocean a zonal pattern exists around 30–35°N. Also, over the continents, large maxima of cyclogenesis occur in the lee of great mountain chains. These patterns are not sensitive to seasonal variations. Three pronounced maxima are associated with the Rockies: Sierra Nevada, Colorado, and Alberta regions. Similar maxima can be located to the east of the Appalachian mountains, the Scandinavian mountains, and also in East Asia.

If the frequency of cyclone centres is examined, the influence of mountain ranges can be seen even more. Examples are the leeward side of the Colorado and Alberta ranges. The cyclones that develop here are mostly of short duration, whereas those that develop in the lee

of the Appalachians and the mountains in East Asia are of longer duration and they also move faster. All major unfrozen inland water bodies show maxima of cyclone centres, during winter. In the Mediterranean Sea, there is a maximum on both sides of the Italian Peninsula. Other examples are the Great Lakes, the Black Sea, the Caspian Sea, the Aral Sea, and the Baltic Sea. Hudson Bay, which freezes over by early December, does not show a pronounced maximum similar to the Great Lakes.

Warm water bodies surrounded by colder land masses also show pronounced cyclogenesis. Examples are (1) the Gulf of Alaska in winter, (2) Baffin Bay and Davis Strait in winter, as well as in summer, (3) Denmark Strait, mostly in winter, and (4) the Barents Sea in winter.

One can account for the large cyclone frequency over the northern portions of the North Atlantic and North Pacific oceans due to local thermal sources as well as due to the poleward flux of cyclones from the midlatitude belt.

In the subtropics, during summer, cyclogenesis occurs over large areas. Examples are the regions south of California and West Africa.

Next, two terms are introduced: "blocking" and "index cycle". In the midlatitudes, the cyclones travel towards the east. Superimposed on this zonal motion is a meridional motion. The thermal wind in the middle troposphere to some extent guides the movement of the cyclones. Sometimes, when a warm cutoff high forms in the middle and upper troposphere, cyclones at sea level are steered either to the south or to the north of these highs. This phenomenon is referred to as the "blocking" of the sea level cyclones and occurs predominantly off the west coasts of Europe and North America. The blocking is more common in the Atlantic Ocean than in the Pacific Ocean and is highest in April and least during August to September.

The general circulation of the atmosphere not only undergoes an annual variation but also undergoes irregular quasi-cyclic changes with periods ranging from 3 to 8 wk. The intensity of the zonal circulation is expressed by the average pressure difference between two latitude circles. Ordinarily, the latitudes chosen are 35° and 55° N, the average sea level pressure difference between the latitude circles is referred to as the "zonal index".

BRADBURY (1954) studied the frequency of cyclones during high and low index situations during the period 1900–39. She found that during summer, the cyclone frequency is greater in high latitudes during high index periods and in low latitudes during low index periods. The differences are not as pronounced in winter. During winter, large areas of high cyclone frequency occur during high index periods (a) over the North Pacific Ocean north of 50° N, (b) over the North Atlantic Ocean north of 50° N and to the east of 45° W and (c) along the southern coast of the United States. During low index periods in winter, high cyclone frequency occurs (a) over the central part of the North Pacific Ocean to the south of 45° N, (b) over the western part of the North Atlantic Ocean and (c) over the Mediterranean Sea.

Instability Theories

MARGULES (1905) speculated that the potential energy associated with horizontal temperature gradients provides the kinetic energy of cyclones. SOLBERG (1936) showed that frontal cyclones would grow as a result of the inherent instability of the polar front (similar to the growth of a wave at a discontinuity). CHARNEY (1947), EADY (1949), BERSON (1949), and FJORTOFT (1950) have shown that the baroclinicity of the zonal current may lead to instability in which the kinetic energy of the growing perturbations is derived from the potential

and internal energies due to horizontal thermal gradients. KUO (1949) and FJORTOFT (1950) showed that certain categories of horizontal velocity patterns across a zonal current would lead to instability.

It has generally been observed that cyclones develop within a period of 1–3 d. In this short time scale, it is customary to assume that the motion is adiabatic and frictionless. Another assumption is that even during growth, the energy of an unstable zonal current is conserved. Let *K*, *P*, and *E* denote the kinetic, potential, and internal energies, respectively. Hence, according to the above assumptions:

$$K + P + E = \text{constant}$$

The kinetic energy per unit mass can be expressed as

$$\frac{1}{2}V^2 = \frac{1}{2}\overline{V}^2 + \overline{V}.V' + \frac{1}{2}V'^2 \tag{5.1}$$

where, V is the averaged velocity of the undisturbed current and V' is a deviation from this value. The kinetic energy K can be determined by integration over the total mass. During this integration, the second term on the right side of the above equation disappears. Hence

$$K = K_m + K_d \tag{5.2}$$

where, K_m and K_d are the integrated forms of the first and third terms, respectively, and these are referred to as the kinetic energy of the mean current and the kinetic energy of the perturbation. Equation (5.2) may be rewritten as

$$K_m + K_d + P + E = \text{constant} \tag{5.3}$$

Since K_d represents the average intensity of all the disturbances, for the growth of these, K_d must increase with time. This means that K_d can increase only at the expense of one of the three sources K_m, P, or E or from combinations of these.

Next, the potential energy of a column of air of unit cross-section is given by

$$P = \int_0^\infty gz\rho \, dz$$

Using the hydrostatic equation $dp = g\rho \, dz$ and integrating by parts:

$$p = \int_0^{\rho_0} z \, d\rho = [zp]_{p=p_0} - [zp]_{p=0} - \int_0^{\rho_0} p \frac{\partial z}{\partial p} dp$$

where, p_0 is the pressure at the bottom of the air column. In this equation, on the right side the first term becomes zero at $z = 0$ (bottom of the air column) and the second term vanishes because $pz \to 0$ as $p \to 0$. The third term becomes, after noting $\alpha = 1/\rho$ where αt is the specific volume.

The equation of state is

$$\alpha P = RT$$

Using this, the above equation becomes

$$P = R\int_0^\infty T\rho dz \tag{5.4}$$

The internal energy of the air column may be written as

$$E = C_v\int_0^\infty T\rho dz \tag{5.5}$$

where, C_v, is the specific heat of air at constant volume. Hence

$$\frac{P}{E} = \frac{R}{C_V} \sim 0.4 \tag{5.6}$$

Thus, it can be seen that the potential and internal energies of a column of air (from the sea level to the top of the atmosphere) will change proportionately to each other. For this reason, the potential and internal energies in eq. (5.3) should not be treated as two different energy sources; hence, only two energy sources exist for the perturbations to amplify: (1) the kinetic energy K_m of the mean motion and (2) the sum of the potential and internal energies P + E.

The perturbations of the basic zonal current may grow through three different types of instability. The first one is the so-called linear current instability. The energy for the perturbations is derived from the kinetic energy of the basic current. This instability mechanism is similar to the hydrodynamic instability of a linear flow of a homogeneous and incompressible fluid between two parallel walls. The second type of instability is referred to as baroclinic instability. In this case, the potential and internal energies of the basic baroclinic current supply the energy for the growth of the disturbances. The third type of instability is referred to as Solberg-Holland instability. SOLBERG (1936) considered a system that initially consists of two barotropic layers separated by a sloping frontal surface in the east-west direction. Both layers are assumed to move towards the east, with the warmer (southern) layer moving faster. He found that waves with lengths less than a few kilometres and also those with lengths between 1000 and 3000 km will amplify and waves with lengths in the remaining range will dissipate. The growth of the waves with lengths shorter than a few kilometers is similar to the classical Helmholtz instability problem, and these short waves are of no relevance to the cyclone problem. A sharp discontinuity is essential for their generation. The growth of waves with lengths of 1000–3000 km can account for the growth of cyclone disturbances.

It can be shown that each of these barotropic layers can give rise to stable wave motion. The wave motion in each layer can be tuned so that each can grow as a result of a resonance effect. In this type of instability the disturbances derive energy from the kinetic energy of the mean motion whereas the potential and internal energies are sink terms.

Some Examples of Cyclone Development

REITAN (1974) summarized the frequencies of cyclones and cyclogenesis for North America. DANARD and ELLENTON (1980) examined the physical influences on the cyclogenesis on the east coast of North America making use of an eight-level primitive equation model. This model includes sensible and latent heat from the ocean surface, parameterized convective and large-scale precipitation and release of latent heat, surface frictional drag and

orography. One of the important results of this study is that input of heat and water vapour from the ocean surface did not contribute significantly during the deepening of the low. However, these fluxes produced an initial vertical distribution of temperature and moisture that helped subsequent development.

BRAND and GUARD (1979) studied the evolution of extratropical storms from tropical cyclones. According to these authors, a tropical cyclone is identified as becoming extratropical when it loses its tropical nature (i.e. northward displacement from the tropics as well as the conversion of the cyclone's primary energy source from latent heat release to baroclinic processes). The movement of recurved tropical cyclones is difficult to predict. According to BURROUGHS and BRAND (1973), errors as high as 30 % could occur. Even when the recurved tropical cyclone becomes somewhat weaker, if it becomes an extratropical cyclone, it could

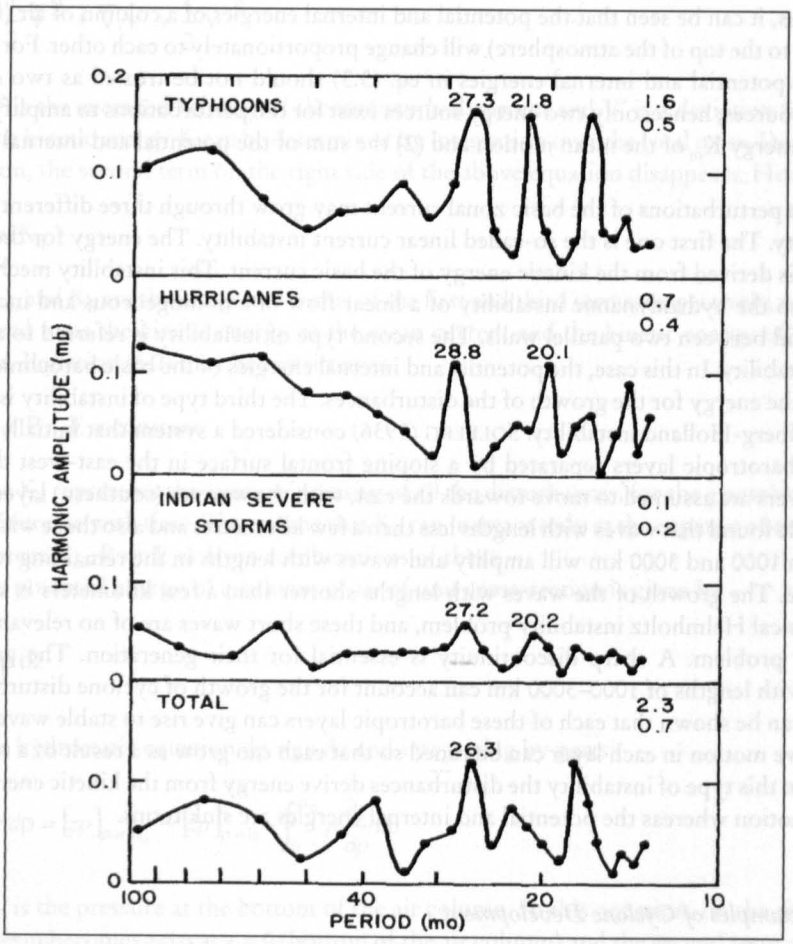

Fig. 5.4: Harmonic amplitude of the mean monthly frequency of North Pacific typhoons, North Atlantic hurricanes, severe storms (winds greater than 25 m s^{-1}) in the vicinity of India, and the total of all three. Numbers above the peaks indicate the dominant quasibiennial periods of oscillation (months). The two numbers in the upper right-hand corner represent the harmonic amplitudes of the annual (upper number) and semiannual (lower number) oscillations in surface pressure at the station. (ANGELL et al., 1969)

still be important. For typhoons to the east of China, during the period 1971–75, the average value of the maximum wind when the cyclones extratropical at 34° N and at that time the maximum wind speed was 51 m s^{-1}.

According to SEKIOKA (1970, 1972a, 1972b) and MATANO and SEKIOKA (1971a, 1971b), this transformation of tropical cyclones to extratropical cyclones can occur at least in two ways: (1) a tropical cyclone meets an already existing front causing a new extratropical cyclone to form and grow on the front and (2) a pre-existing extratropical cyclone merges with a tropical cyclone and usurps the tropical vortex.

ANGELL et al. (1969) detected a quasi-biennial (period of about 28 mo) variation in the centres of action such as the Icelandic and Aleutian low pressure centers. They related the frequency of hurricanes and typhoons to this quasi-biennial activity. Mean monthly surface pressures at stations with long data records were subjected to harmonic analysis. The following important results emerged.

Quasi-biennial variations in the surface pressure occur near the North Atlantic and North Pacific subtropical highs and subpolar lows, with amplitudes up to 0.4 mb. The quasi-biennial variations in latitude and longitude of the subtropical highs are about 1°.

The Atlantic high moves in a northwest-southeast direction. Hurricanes in the North Atlantic, typhoons in the North Pacific, and severe storms in the vicinity of India show a quasi-biennial variation in frequency (Fig. 5.4).

It is possible that the relatively large annual oscillation may contaminate the harmonic analysis for the quasi-biennial band. For this reason ANGELL et al. (1969) also performed an alternate analysis. In the so-called even-minus-odd-year difference method, the number of hurricanes or typhoons in the odd-numbered years is subtracted, year-by-year, from the number in the even-numbered years, and these first differences are smoothed through determination of a 3-yr running average. The results agree reasonably with observations.

It will not be discussed here in detail, but it must be considered that the work on reason and results of the existence of storm tracks continues. HOSKINS and VALDES (1990) investigate the question, why concentrated regions of eddy activity exist, i.e. storm tracks in the Northern Hemisphere. They have found that "the direct thermal effect of the eddies does indeed act against the storm tracks. Their vorticity fluxes lead to some reduction of this effect. It is argued that the mean diabatic heating in the storm track region is an indirect eddy effect." (HOSKINS and VALDES, 1990).

5.1.2 Regions of occurrence

Extratropical Storm Surges in Canada

Storm surges are generated in Canada by extratropical storms and occasionally by a hurricane that has transformed into an extratropical storm. In eastern Canada, storm surges occur in the Great Lakes, St. Lawrence Estuary, Gulf of St. Lawrence, Bay of Fundy and along the Atlantic coast. Storm surges also occur in Hudson Bay, James Bay, Lake Winnipeg, Beaufort Sea, Hecate Strait and Queen Charlotte Sound. The main storm surge season is autumn and early winter, and occasionally, storm surges could occur in summer and in late winter. Since all the surge-producing storms are extratropical in origin, the calculation of the meteorological forcing terms from the weather charts is straightforward (it does not necessarily mean the values are accurate). For convenience, Alaska will be discussed in this section along with western Canada. Similarly, the Great Lakes will be treated in this section. How-

ever, meteorological problems associated with mesoscale systems such as squall lines will be deferred to section 5.7.

Principal tracks of intense storms (based on the data for the period 1963–67) are shown in Fig. 5.5 (A) for January to March, in Fig. 5.5 (B) for July and August, and in Fig. 5.5 (C) for October to December. The tracks of storms of tropical origin are shown in Fig. 5.6, and the tracks of storms for the Hudson Bay region for different months are shown in Fig. 5.7A–5.7D. However, occasionally, rather irregular tracks can occur. In Fig. 5.8 are shown the tracks for four storms in 1969 over Hudson Bay. While the track for the November storm is not unusual, the tracks for the other three storms show forward – backward

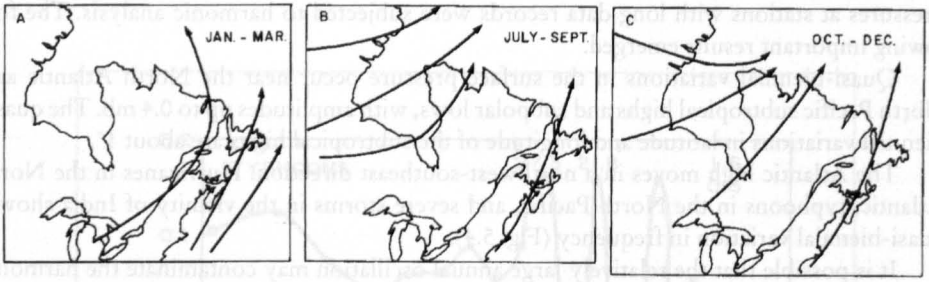

Fig. 5.5: Tracks of intense storms over eastern Canada (A) January–March, (B) July–September, and (C) October–December. (ARCHIBALD, 1945)

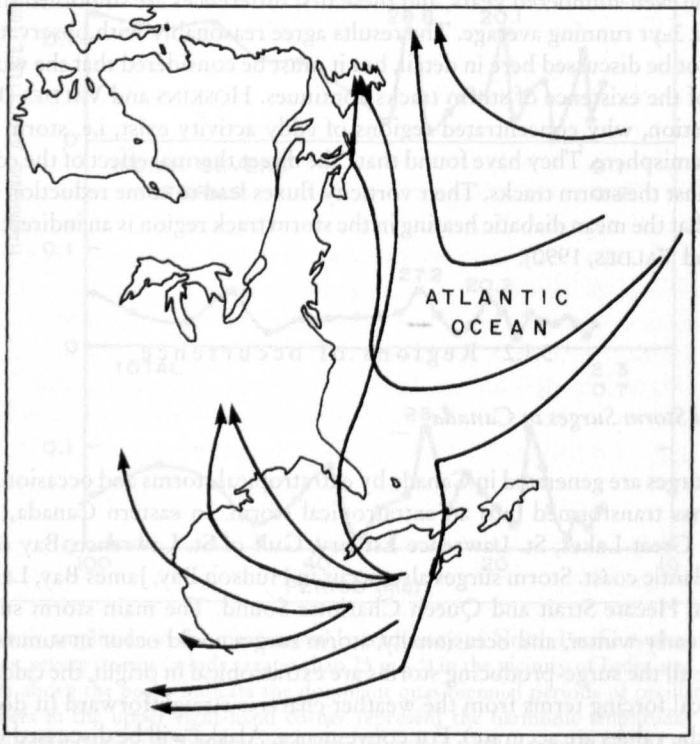

Fig. 5.6: Tracks of storms of tropical origin along the east coast of North America. (ARCHIBALD, 1945)

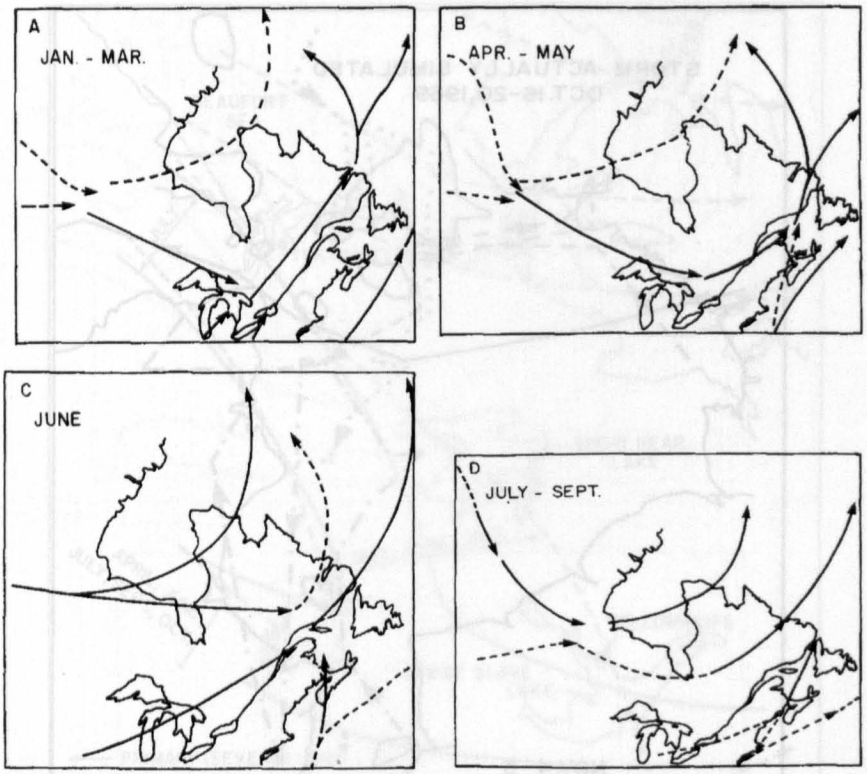

Fig. 5.7: Storm tracks over Hudson Bay and surroundings (A) January–March, (B) April and May, (C) June, and (D) July–September. (Archibald, 1945)

movements of the storm center, which could be the result of improper observations or could be real on certain occasions.

The corridors for the tracks of intense and ordinary storms in the northwestern part of Canada are shown in Fig. 5.9. The surface weather map for the Alaska area during a storm on October 3, 1963, is given in Fig. 5.10A. The distribution of the computed wind stress field is illustrated in Fig. 5.10B and the variation of the computed wind stress with time near Barrow, Alaska, is shown in Fig. 5.10C.

Great Lakes

BARRIENTOS (1970) discussed objective methods for predicting winds over Lakes Erie and Ontario. Making use of 1000-mb geostrophic wind and sea level pressure forecasts issued routinely for eight stations surrounding these lakes, as well as marine observations from anemometer-equipped vessels, two sets of regression equations were derived for predicting wind speed.

VENKATESH and DANARD (1976) used a one-level primitive equation model for computing the mesoscale influences of orography, friction, and heating on surface winds. They included the influence of atmospheric stability and land-water temperature contrast. ESTOQUE

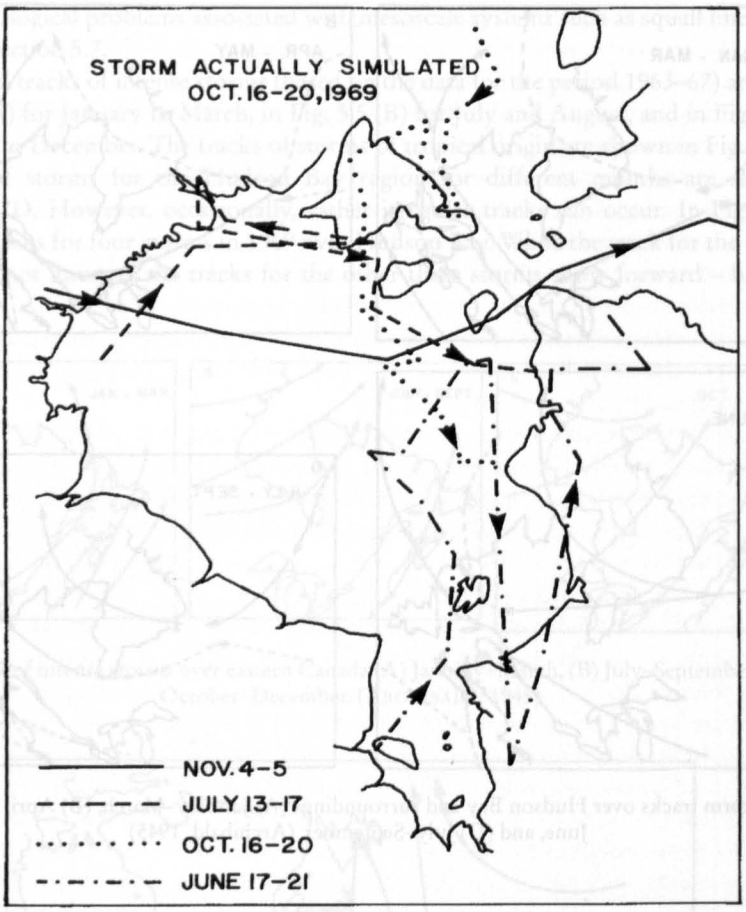

Fig. 5.8: Selected storm tracks over Hudson Bay for the year 1969

and GROSS (1979) discussed diurnal wind variations over Lake Ontario, as deduced from Rawinsonde data at six stations.

RESIO and VINCENT (1977) estimated winds over the Great Lakes knowing winds over adjacent land. FEIT and PORE (1978) discussed objective wind forecasting for all of the Great Lakes using a technique developed by FEIT and BARRIENTOS (1974). The predictors are the various forecast parameters computed by the National Meteorological Center's primitive equation (PE) model. The 12 locations at which wind forecasts are made at 6-h intervals, 36 h in advance, are shown in Fig. 5.11. Mean absolute error in wind speed is 5–8 knots (2.6–4.1 m. S^{-1}) and mean absolute error in wind direction is about 20° for short-term forecasts (6–12 h) and about 70° for long-term forecasts (30–36 h).

KEULEGAN (1953) took a somewhat different approach. He derived the wind stress and the roughness parameter for Lake Erie using water level data for a 50-yr period. In other words, he used the observed storm surge data to estimate the wind stress. He defined an effective lake wind velocity as the wind velocity that would be needed to produce the observed storm surge, assuming that the wind blows with this effective velocity along the lake axis. Recently, SCHWAB (1982) used a similar but more sophisticated inverse technique.

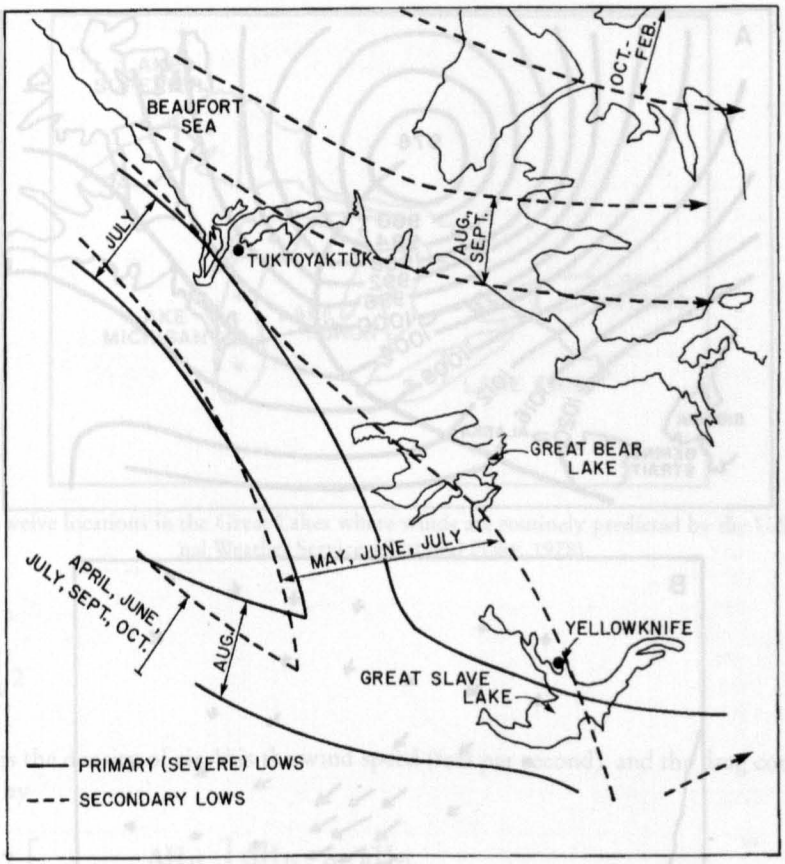

Fig. 5.9: Corridors of primary and secondary lows over the northwest part of Canada. (BURNS, 1973)

KEULEGAN (1953) used the following relationship to deduce the wind stress from the storm surge:

$$\frac{(\tau_S + \tau_0)}{\rho g H_0}\frac{L}{H_0} = 0.867\frac{\Delta H_0}{H_0} - 0.134\left(\frac{\Delta H_0}{H_0}\right)^2 \tag{5.7}$$

where, τ_S is the wind stress, τ_0 is the bottom stress, ρ is the density of water, g is gravity, H_0 is the average water depth, ΔH is the storm surge (feet), and L is the length of the lake (feet). The bottom stress τ_0 was related to the surface wind stress through

$$\tau_0 = n\tau_S \tag{5.8}$$

Then, eq. (5.7) becomes

$$\tau_S = \frac{1}{(1+n)}\left[0.867\frac{\Delta H_0}{H_0} - 0.134\left(\frac{\Delta H_0}{H_0}\right)^2\right]\frac{H_0}{L} \tag{5.9}$$

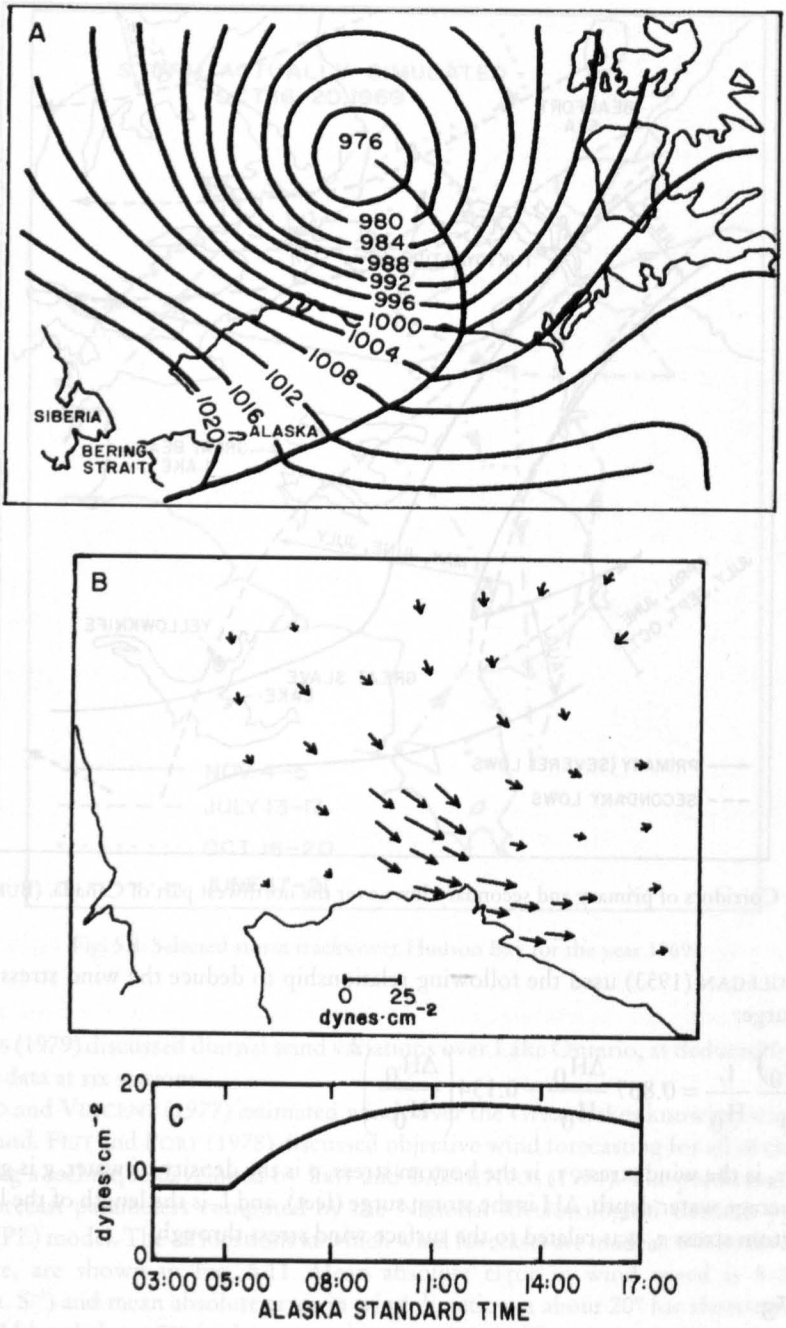

Fig. 5.10: (A) Simplified surface weather chart for October 3, 1963, at 11:00 (Alaska Standard Time); (B) computed wind stress field for 11:00–14:00; (C) variation of wind stress with time at Barrow, Alaska (1 dyne = 10 N). (SCHAFER, 1966)

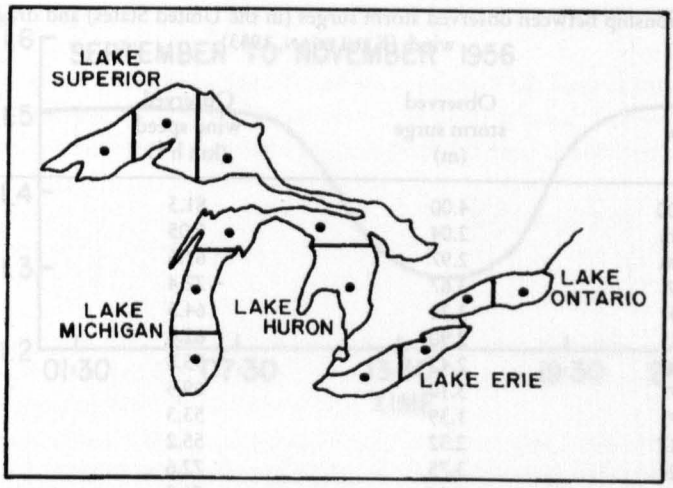

Fig. 5.11: Twelve locations in the Great Lakes where winds are routinely predicted by the U.S. National Weather Service. (FEIT and PORE, 1978)

Write

$$\tau_S = \gamma \rho_a V^2 \tag{5.10}$$

where, ρ_a is the density of air, V is the wind speed (feet per second), and the drag coefficient γ is given by

$$\gamma = \frac{0.867}{(1+n)}\left[1 - 0.16\,\frac{\Delta H_0}{H_0}\right]\frac{\Delta H_0}{H_0}\,\frac{\rho}{\rho_a}\,\frac{gH_0}{V^2} \tag{5.11}$$

The 22 storms during the period 1900–47 on Lake Erie, the observed wind speed, the observed storm surge (during westerly winds), and the calculated value of γ from eq. (5.11) are listed in Table 5.1.

HUNT (1959) discussed the relationship between the parameter α defined as

$$\alpha \equiv \frac{\tau_S + \tau_B}{\tau_S} \tag{5.12}$$

and D/K where D is the water depth, K is the bottom roughness coefficient, and τ_S and τ_B are the wind and bottom stresses. The relationship for Lake Erie is shown in Fig. 5.12. HUNT (1959) also gave diagrams showing the variation with time in fall and spring of the ratio U_W/U_L at Cleveland on Lake Erie (Fig. 5.13). Here, U_W and U_L are the overwater and overland wind speeds. The reason for examining this ratio is to account for atmospheric stability. The ratio U_W/U_L at four stations on Lake Erie for stable, adiabatic, and unstable atmospheric conditions is given in Table 5.2. The overwater wind speeds on Lake Erie at 21:00 on November 8, 1957, are shown in Fig. 5.14.

IRISH and PLATZMAN (1961) discussed the meteorological conditions associated with extreme storm surges on Lake Erie. The monthly frequency distributions of severe storms

Table 5.1: Relationship between observed storm surges (in the United States) and drag coefficients of wind. (KEULEGAN, 1953)

Date of storm surge	Observed storm surge (m)	Observed wind speed (km h^{-1})	Drag coefficient $\gamma \cdot 10^3$
Nov. 21, 1900	4.00	81.3	2.13
Oct. 20, 1905	2.04	5.05	2.87
Oct. 20, 1906	2.97	61.6	2.78
Jan. 20, 1907	3.67	77.4	2.17
Dec. 7, 1909	3.20	64.5	2.73
Dec. 31, 1911	2.90	62.6	2.63
Jan. 31, 1914	2.42	55.8	2.76
Dec. 9, 1917	3.10	69.5	2.23
Dec. 9, 1917	1.39	53.3	1.78
Dec. 10, 1917	2.32	55.2	2.71
Dec. 18, 1921	3.75	72.6	2.52
Dec. 8, 1927	4.04	76.3	2.44
Dec. 9, 1927	1.26	43.8	2.35
Dec. 9, 1927	1.05	42.0	2.15
Dec. 9, 1927	0.53	35.6	1.53
Apr. 1, 1929	4.06	82.6	2.88
Jan. 22, 1939	2.87	62.4	2.64
Sept. 25, 1941	2.76	57.5	2.96
Jan. 2, 1942	3.82	65.0	3.22
Jan. 3, 1942	0.73	31.4	2.68
Nov. 22, 1946	2.55	55.0	2.99
Mar. 25, 1947	2.54	57.5	2.77

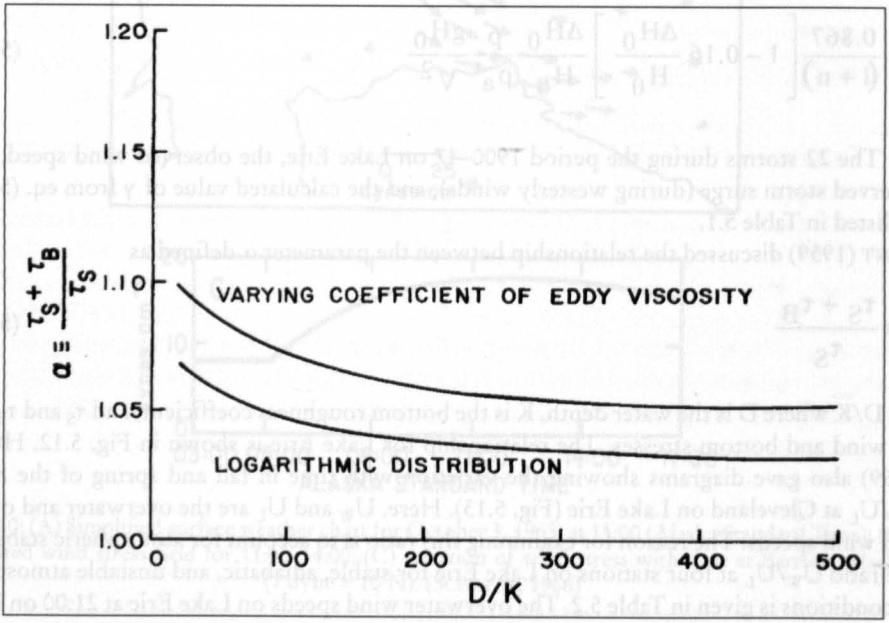

Fig. 5.12: Variation of a versus D/K (D = water depth, K = bottom roughness parameter, τ_S = wind stress, and τ_B = bottom stress). The relationship is shown for two different distributions of bottom stress. (HUNT, 1959)

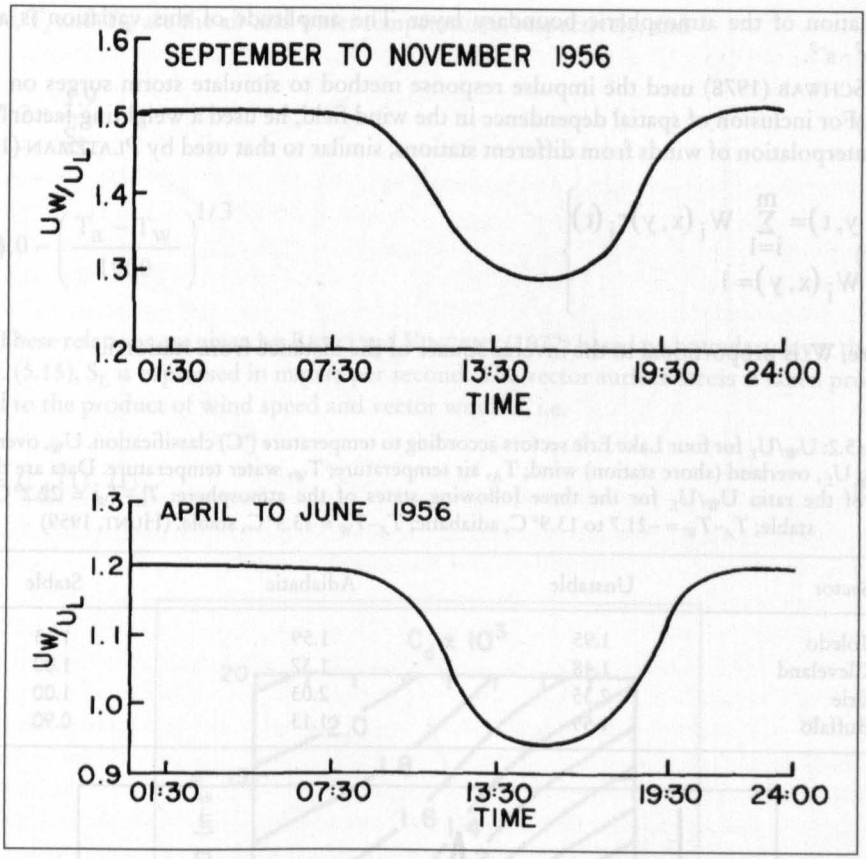

Fig. 5.13: Daily variation in U_W/U_L for southwesterly winds by season at Cleveland, Ohio, during 1956. (HUNT, 1959)

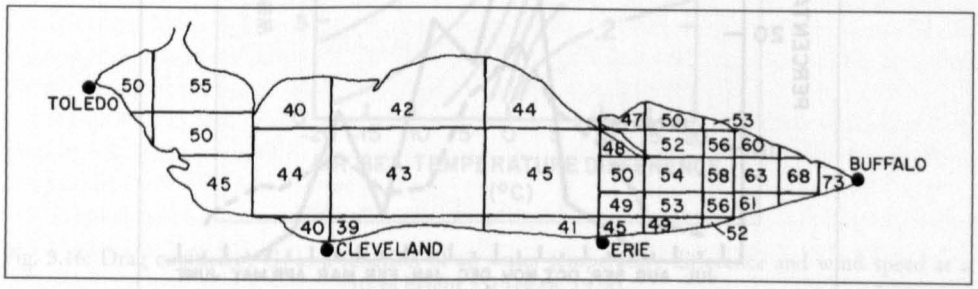

Fig. 5.14: Overwater wind speeds (feet per second) in Lake Erie (1 ft = 0.3048 m). (HUNT, 1959)

on the Great Lakes, as given by these authors for the period 1876–1900, are given in Fig. 5.15. It can be seen that maximum frequency occurs during October to December, November being the month of greatest frequency.

PLATZMAN (1965) showed that over Lake Erie, there is a distinct diurnal constituent of the longitudinal component of the wind square vector, with maximum in the direction Toledo to Buffalo shortly after noontime. This variation is due to the usual convective

oscillation of the atmospheric boundary layer. The amplitude of this variation is about 10 $m^2 \cdot s^{-2}$.

SCHWAB (1978) used the impulse response method to simulate storm surges on Lake Erie. For inclusion of spatial dependence in the wind field, he used a weighting factor W_i in the interpolation of winds from different stations, similar to that used by PLATZMAN (1963):

$$\left.\begin{aligned} \tau(x,y,t) &= \sum_{i=1}^{m} W_i(x,y)\tau_i(t) \\ \sum_{i=1} W_i(x,y) &= 1 \end{aligned}\right\} \qquad (5.13)$$

where, W_i is proportional to the inverse square of the distance from station i.

Table 5.2: U_W/U_L for four Lake Erie sectors according to temperature (°C) classification. U_W, overwater wind; U_L, overland (shore station) wind; T_A, air temperature; T_W, water temperature. Data are the values of the ratio U_W/U_L for the three following states of the atmosphere: $T_A - T_W$ = 22.2° C, unstable; $T_A - T_W$ = –21.7 to 13.9° C, adiabatic; $T_A - T_W$ = 13.3° C, stable. (HUNT, 1959)

Sector	Unstable	Adiabatic	Stable
Toledo	1.95	1.59	1.13
Cleveland	1.48	1.37	1.00
Erie	2.35	2.03	1.00
Buffalo	1.59	1.13	0.90

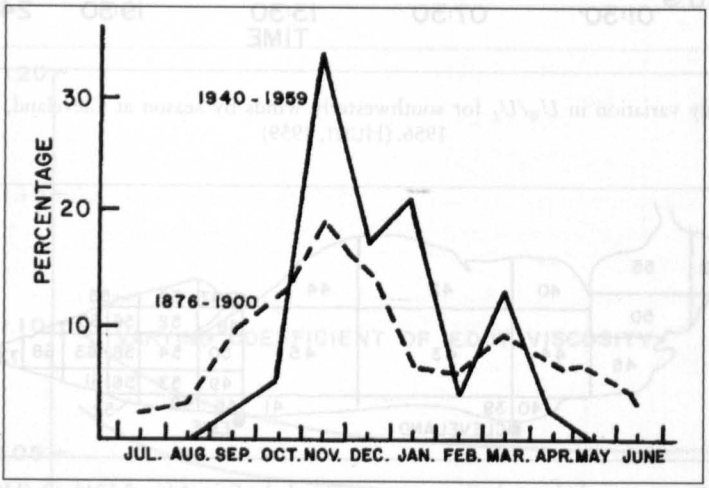

Fig. 5.15: Monthly frequency distribution of severe storms on the Great Lakes for the period 1940–59 (solid line) and for the period 1876–1900 (broken line). (IRISH and PLATZMAN, 1961)

SCHWAB (1978) converted the observed wind speeds S_L at the coastal stations into overlake wind speeds S_W through

$$\frac{S_W}{S_L} = \psi(S_L)\phi(T_a - T_W) \qquad (5.14)$$

where, T_a and T_W are the air and water temperatures, respectively, and

$$\psi = 1.2 + \frac{1.9}{S_L} \tag{5.15}$$

$$\phi = 1.0 - \left(\frac{T_a - T_W}{1900} \right)^{1/3} \tag{5.16}$$

These relations are given by RESIO and VINCENT (1977) based on boundary layer theory. In eq. (5.15), S_L is expressed in meters per second. The vector surface stress is taken proportional to the product of wind speed and vector wind U, i.e.

$$\frac{\tau_i}{\rho_a} = C_d \left| U_i \right| U_i \tag{5.17}$$

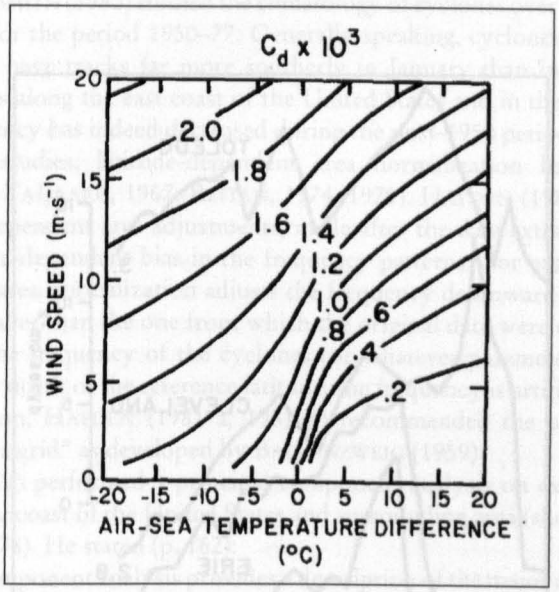

Fig. 5.16: Drag coefficient C_d as a function of air-water temperature difference and wind speed at a 10-m height. (SCHWAB, 1978)

The air density ρ_a is taken as $1.25 \times 10^{-3} g \cdot cm^{-3}$. The drag coefficient C_d as a function of $(T_a - T_W)$ and wind speed (at a 10-m height) is shown in Fig. 5.16.

HAMBLIN (1979) numerically simulated the storm surge of April 6, 1979, which produced a record set-up of 4.5 m on Lake Erie. The surface isobaric field for this storm is shown in Fig. 5.17 and the time variation of the wind stress at four stations is given in Fig. 5.18. HAMBLIN (1979) mentioned that the computed drag coefficients varied from 0.9×10^{-3} to 3.5×10^{-3} during the duration of the storm.

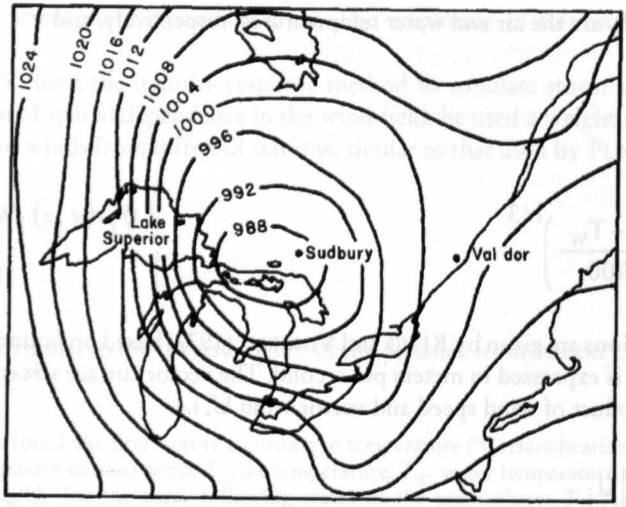

Fig. 5.17: Simplified surface weather chart at 01:00 (Eastern Standard Time) on April 6, 1979. The pressure field is in millibars. (HAMBLIN, 1979)

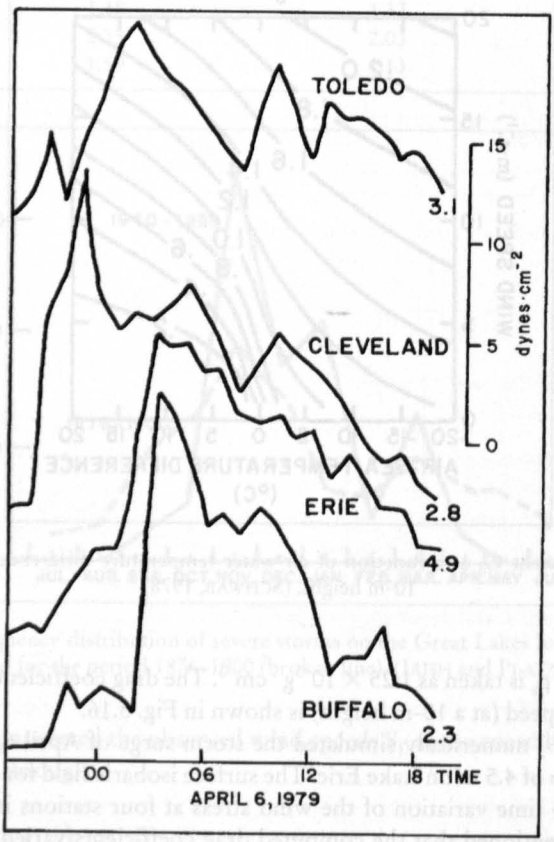

Fig. 5.18: Time history of wind stress at four locations on Lake Erie. (HAMBLIN, 1979)

SIMONS (1975) determined the effective wind stress over Lakes Erie and Ontario from long-term numerical water level simulations. He showed that the effective wind stress over water is greater than indicated by atmospheric boundary layer measurements over Lake Ontario; the theoretically derived drag coefficient appears to be about 1.85×10^{-3}. Over Lake Erie, the drag coefficient is about the same magnitude in spring and early summer, but increases to about 2.5×10^{-3} during the stormy autumn season. These results confirm DONELAN's (1975) study of the interaction between wind waves and the atmospheric boundary layer, whose primary result was that the drag coefficient increases significantly if the wave field is not completely adjusted to the wind field. Usually, boundary layer observations are made during steady winds (when no storms are present) and, hence, such measurements are not representative of drag coefficient during stormy periods.

Extratropical Storm Surges in the United States

REITAN (1979) extended his earlier study (REITAN, 1974) to cover the period 1949–76, which is characterized by gradually decreasing temperature in the Northern Hemisphere. This study showed a general trend for a decrease in the number of cyclonic events in recent years. ZISHKA and SMITH (1980) studied the climatology of cyclones over North America and surrounding area for the period 1950–77. Generally speaking, cyclones are more frequent, more intense, and have tracks far more southerly in January than in July. Predominant cyclogenesis occurs along the east coast of the United States and in the lee of the Rockies. The cyclone frequency has indeed decreased during the post-1950 period.

In a lot of studies, latitude-dependent area normalization has been used (e.g. O'CONNOR, 1964; TAIJAARD, 1967; REITAN, 1974, 1979). HAYDEN (1981a, 1981b) pointed out that latitude-dependent area adjustments, made after the data extraction is completed, introduce a latitude-dependent bias in the frequency patterns. For example, south of the reference latitude, area normalization adjusts the frequency downward and forces it to represent an area smaller than the one from which the original data were extracted. This artificially decreases the frequency of the cyclones (or whatever parameter being tabulated). On the other hand, north of the reference latitude, the frequency is artificially increased. To correct this situation, HAYDEN (1981 a, 1981 b) recommended the use of the so-called "practical equal area grid" as developed by BALLENZWEIG (1959).

HAYDEN (1981a) performed a principal component analysis on extratropical cyclone data for the Atlantic coast of the United States and surrounding area (shown in Fig. 5.19 for the period 1885–1978). He stated (p. 162):

... principal component analysis provides a description of the major modes of variability in the data set. Typically, each component is identified with some property of the data field. The analysis also provides an index, which measures the importance of each component within each year. Finally, the analysis provides an estimate of the total percent of variance in the data set, which can be explained on the basis of each component.

The objective of the analysis is to isolate characteristic, recurrent, and independent modes of covariance among variables into a new set of independent variables. Basically, the analysis transforms a set of intercorrelated variables into a new coordinate system in which the axes are linear combinations of the original variables and are mutually orthogonal. To prevent those grid cells with high mean cyclone frequencies (high latitudes) from dominating the total variance and consequently from dominating the eigenvector forms, the correlation matrix was used rather than the covariance matrix.

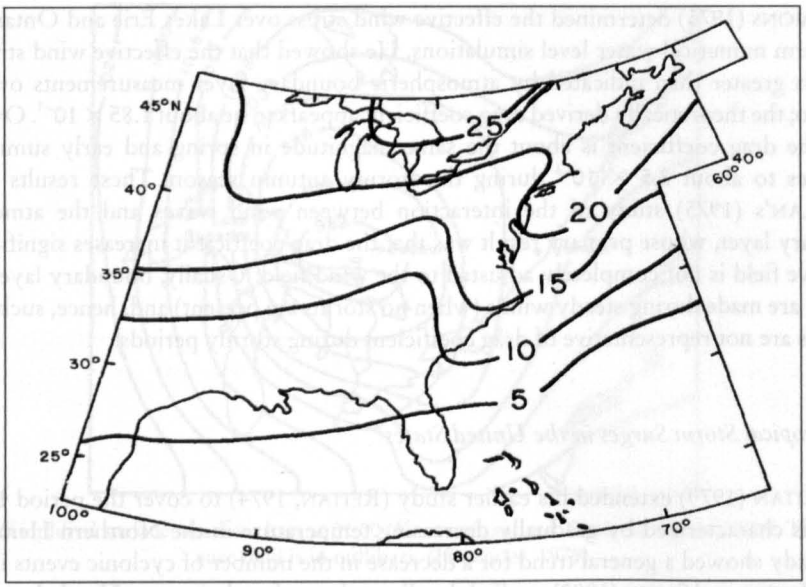

Fig. 5.19: Average annual frequency of extratropical cyclones over the eastern part of the United States. (HAYDEN, 1981a)

The area shown in Fig. 5.19 was divided into 74 rectangles (2.5° latitude by 5° longitude). The first principal component showed that, since the beginning of the twentieth century, the frequency of cyclones over the marine areas has increased whereas the frequency decreased over the continental areas. This trend peaked in the 1960s. The second principal component was identified as a cyclogenesis function for the east coast of the United States. This showed an increased cyclogenesis starting at the beginning of the twentieth century with a maximum in the 1950s. The third and fourth components explain the geographic variations in cyclogenesis in the Gulf coast and Great Lakes regions. The average cyclone frequencies over the eastern United States for the period 1885–1978 are also shown in Fig. 5.19.

Usually, one uses the Norwegian cyclone model to explain extratropical cyclogenesis. REED (1979) pointed out that it is not always necessary for the cyclone to originate as a wave perturbation on a polar front separating tropical and polar air masses. An alternate mechanism is the formation of cyclones in polar air streams behind or poleward of the polar front, as sometimes happens in winter over the oceans.

Cyclones that form in this manner are relatively small in size. One interesting feature is that, in their mature stage, these cyclones exhibit a comma-shaped pattern. A surface low pressure centre may not always be easily identifiable. When it exists, such a low pressure centre is situated beneath the head of the comma. Also, under the trailing edge of the comma tail, there is almost always a surface trough of low pressure. Thus, cyclones of this type somewhat resemble large frontal cyclones.

Wind Stress and pressure in extratropical cyclones over the United States

TANCRETO (1958) used the significant wave (wind waves) height as an indication of the intensity of the storm. An extratropical cyclone generated storm surge during March 1962

caused tremendous damage in Atlantic City (New Jersey). The surge was so severe it bisected a steel pier (PORE, 1964). Extratropical cyclone generated storm surges are not rare on this part of the east coast of the United States (e.g. February 1958).

MILLER (1957) showed that maximum surges at Norfolk are associated with east-northeast winds. There is a lag of 12 h between the wind and the surge. PORE (1964) studied 18 storm surges during the period 1956–61. For these 18 storms, there was a total of 1910 hourly observations available. Most of these storms passed over the southeastern United States and then moved offshore over the Atlantic Ocean. Maximum wind speeds varied from 22 to 50 knots (41–93 km h^{-1}). Three meteorological forcing terms were considered separately:

a) onshore component of the wind stress (which produces a set-up),
b) alongshore component of the wind stress (which generates alongshore currents, which then are deflected to the right by the Coriolis force, and this creates an upward slope of the water surface toward the right) and
c) atmospheric pressure (inverse barometer effect).

An interesting result of this study is that the storm surge at Atlantic City is strongly dependent on the alongshore component of the wind. There appears to be little difference between the results obtained using linear wind stress and quadratic wind stress.

WANG (1979) examined the response of the water level in Chesapeake Bay to the time scale of atmospheric forcing. For time scales longer than 7 d, the water levels in the bay were driven nonlocally by the coastal water levels. For periods between 4 and 7 d, the water level in the bay was driven both by the coastal sea level as well as the lateral component of the wind. For time scales of 1–3 d, the water level in the bay was driven by the longitudinal component of the wind.

SAUNDERS (1977) computed seasonal averages of wind stress over the eastern continental shelf of North America making use of about 1 million ship observations for the period 1941–72. He assumed a drag coefficient that increases with the wind speed from 1.0×10^{-3} at 5 m s^{-1} wind speed to 2.3×10^{-3} at 25 m s^{-1}. Atmospheric stratification was found to have little effect. The stress is strongest in winter (1–15 dynes cm^{-2}) and weakest in fall (0.25–0.5 dynes cm^{-2}). In summer the stress is directed towards the northeast whereas in the other three seasons it is directed south and east. The wind stress generally increases with increasing latitude, but local maxima are found over the Gulf of Maine and the Gulf of St. Lawrence. SAUNDERS (1977) attributed the local maxima and minima to cyclonic activity.

Storm Surges in Europe

Cyclones causing storm surges in the waters in and around Europe are mainly of the extratropical type, and the meteorological problems associated with these storms are somewhat simpler than those due to tropical cyclones. Most of the storm surges in Europe occur in the North Sea; other areas where surges occasionally occur are the Baltic Sea, the Irish Sea, Adriatic Sea, Ligurian Sea, the Atlantic coast of Portugal and the coasts of Norway and Sweden.

North Sea and Baltic Sea

A special meteorological situation must occur to induce storm surges in the North Sea. When a depression reaches the North Sea from west or northwest, an air stream develops.

The strength of an air stream depends on the pressure situation in the high, the location of the storm depression to the neighbouring high pressure area, the location of the fronts and speed and direction of the depression. For example, when the centre of the depression travels north of the Southern North Sea Coast wind there coming from west to northwest is generated and can lead to storm surges at this coast.

The depressions take different routes (Fig. 5.20). The meteorological situation leading to high or very high storm surges at the Southern North Sea Coast can be classified into three types (PETERSEN and ROHDE, 1991), here complemented by the fourth, called mixed type:

1. Jutland-Type
   It forms south of 60° N over Newfoundland and travels from west to east from England over the North Sea to Jutland and then either over the south of Sweden in easterly direction or turns off to northeast. These low pressure systems travel mostly very fast and cause strong storms for a short period. The winds change from southwest to northwest or north. As pointed out by GÖNNERT (1999), a fast increase of wind speed causes high storm surge peaks at the coast of the German Bight. Examples of the storm surge of February 23–24, 1967 and January 3, 1976 are shown in Fig. 5.21. The curve of the surge has mostly a steep slope. When high wind speed persists for more than 2–5 hours and water levels only drop slowly this type of cyclonic track can cause dangerous storm surges.
2. Scandinavia-Type:
   These depressions form over Greenland and Iceland and travel towards southeast. They cross Scandinavia between 60° N and 65° N. This type causes storms with long duration from northwest over the North Sea. Therefore more than one tidal peak (sometimes with 3–4 lower peaks following) is caused from this type of cyclone. The storm surge curve shows a slow ascent and a slow drop. Due to the long duration of this type of storm surge with its high water level dikes can become water-saturated, soggy and unstable.
   Examples for this type can be found on February 16–17, 1962 and January 20–22, 1976 (Fig. 5.22).
   Sometimes the tracks of the Jutland-Type and of the Scandinavia-Type are mixed. The Storm surge of November 22–23, 1981 started with a path of the Scandinavia-Type, but changed direction and travelled over Scandinavia to the southern Baltic Sea like the Jutland-Type.
3. Skagerrak-Type
   The tracks of these cyclones lie between both types described before. They cross the 8th degree of Longitude between 57° to 60° N. Mostly they travel from WNW to ESE, but sometimes they travel from W to E and NW to SE. The wind blows from WNW and NW towards the entire coast of the North Sea and causes storm surges. The storm surges of February 12, 1894, March 13, 1906, February 13 and 16, 1916, October 10, 1926, October 18 and 27, 1936 and November 16, 1973 were caused by this cyclonic type.
4. Mixed-Types
   Many surges are not caused by one type of meteorological situation only. The track of the depression is composed of different types. For example, the storm depression of February 1, 1953, which caused a very high storm surge at the coast of the Netherlands and at the east coast of the United Kingdom, took the direction of the Skagerrak-Type and then changed direction between Scotland and south of Norway to the south. Because of the change of direction at the German Coast only a small storm surge occurred. WEMELSFELDER (1954) mentioned that the meteorological conditions associated with the storm of February 1, 1953, were quite different from the traditional storm tracks that emerge over Scotland and disappear over Norway or Denmark. In this 1953 case, the storm track cros-

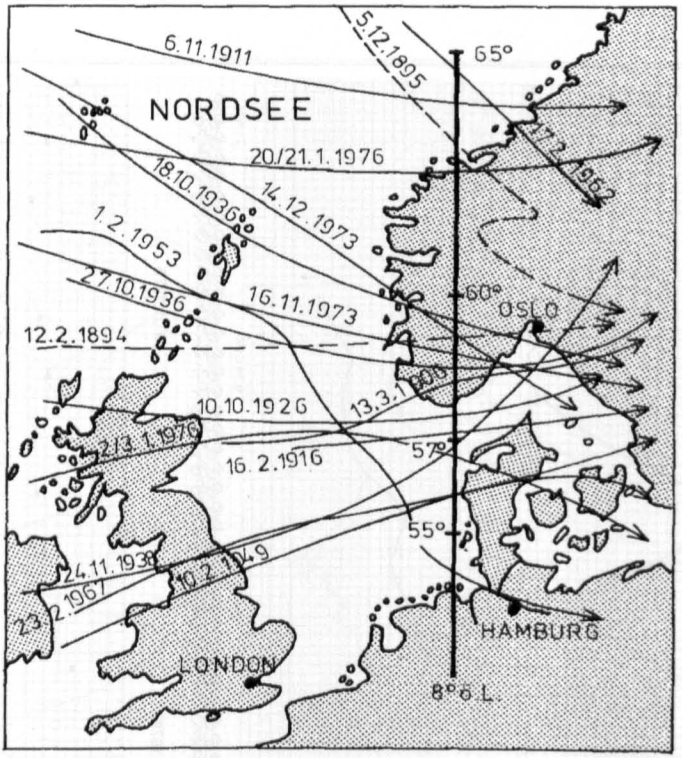

Fig. 5.20: Storm depression, which causes storm surge tracks at the North Sea Coast (PETERSEN and ROHDE, 1991)

sed the North Sea from Scotland to Hamburg. The Netherlands coast is very vulnerable to this type of track. Detailed meteorological data about this storm are presented by SNEYERS (1953).

DOODSON (1929) classified the meteorological situations for the Thames Estuary in the same way as presented here. Most of the major storm surges in the Thames Estuary are associated with type I meteorological situations. One example of type I is the storm of December 30–31, 1921, which reached a speed of 161 km/h (NNW) and caused a very high storm surge. The surface isobaric patterns at two different instants of time are shown in Fig. 5.23. DOODSON (1929) and DINES (1929) listed the storm surges in the Thames Estuary during the period 1912–28 (MURTY, 1984).

The Baltic Sea can be described as a relatively closed basin because the connection between North Sea and Baltic Sea is very small in relation to the surface of the bordering sea. Strong wind from southwest causes storm surges in the North and low water levels in the South. A change of wind direction to NNE causes high water levels in the southern part of the Baltic Sea. At the north-eastern as well as at the south-western part of the longitudinal axis of the Baltic Sea high water levels of more than 3 m over mean water level can be observed.

The special meteorological situation in Europe causes stormy weather and, with this, storm surges only during the period from September to April. The highest frequency occurs in the period from October to February, the highest level was reached in the same period. Fig. 5.24 shows the average annual distribution of storm surges at Cuxhaven for the period

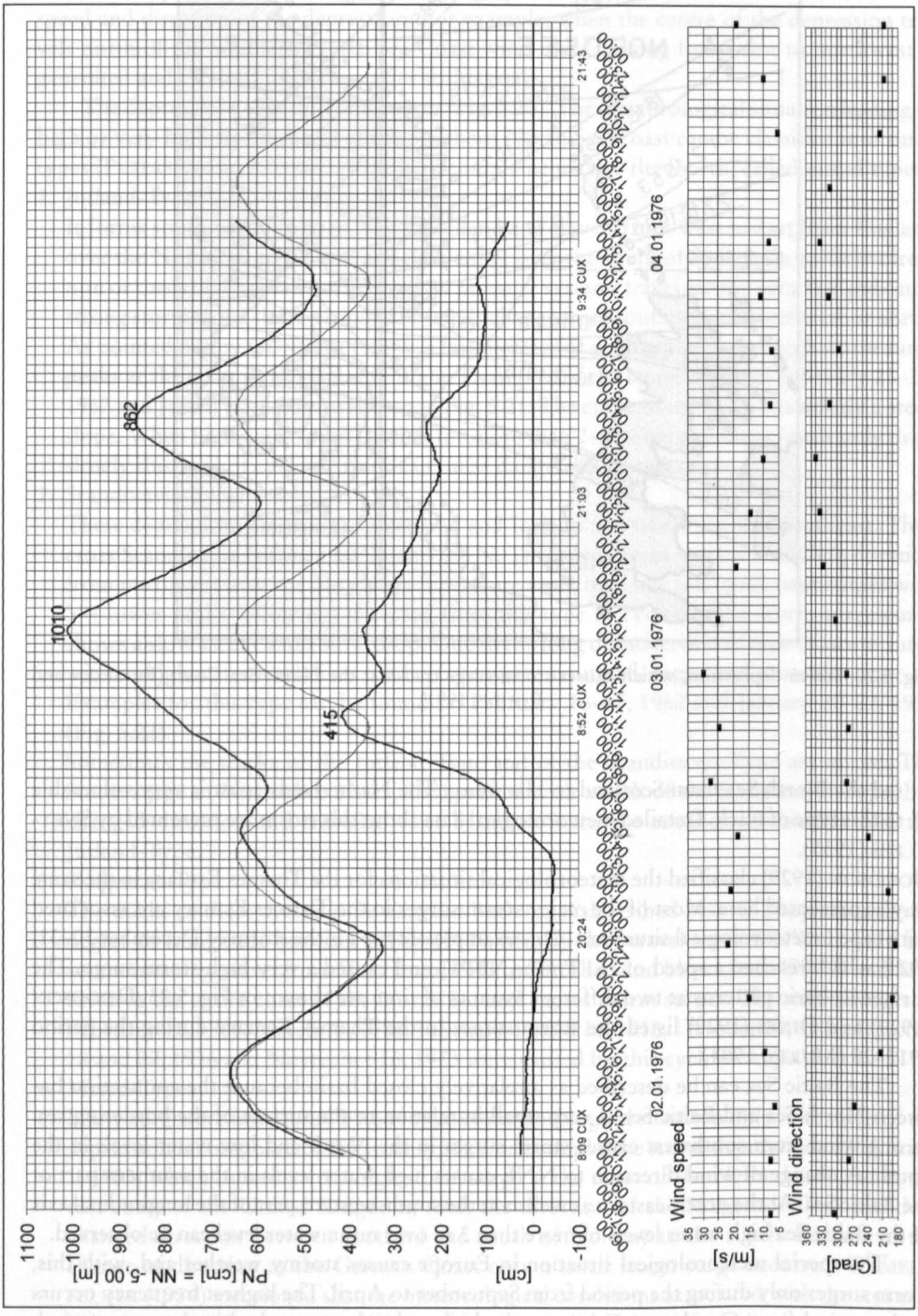

Fig. 5.21: Storm surge at Cuxhaven from January 3, 1976 (GÖNNERT and SIEFERT, 1998)

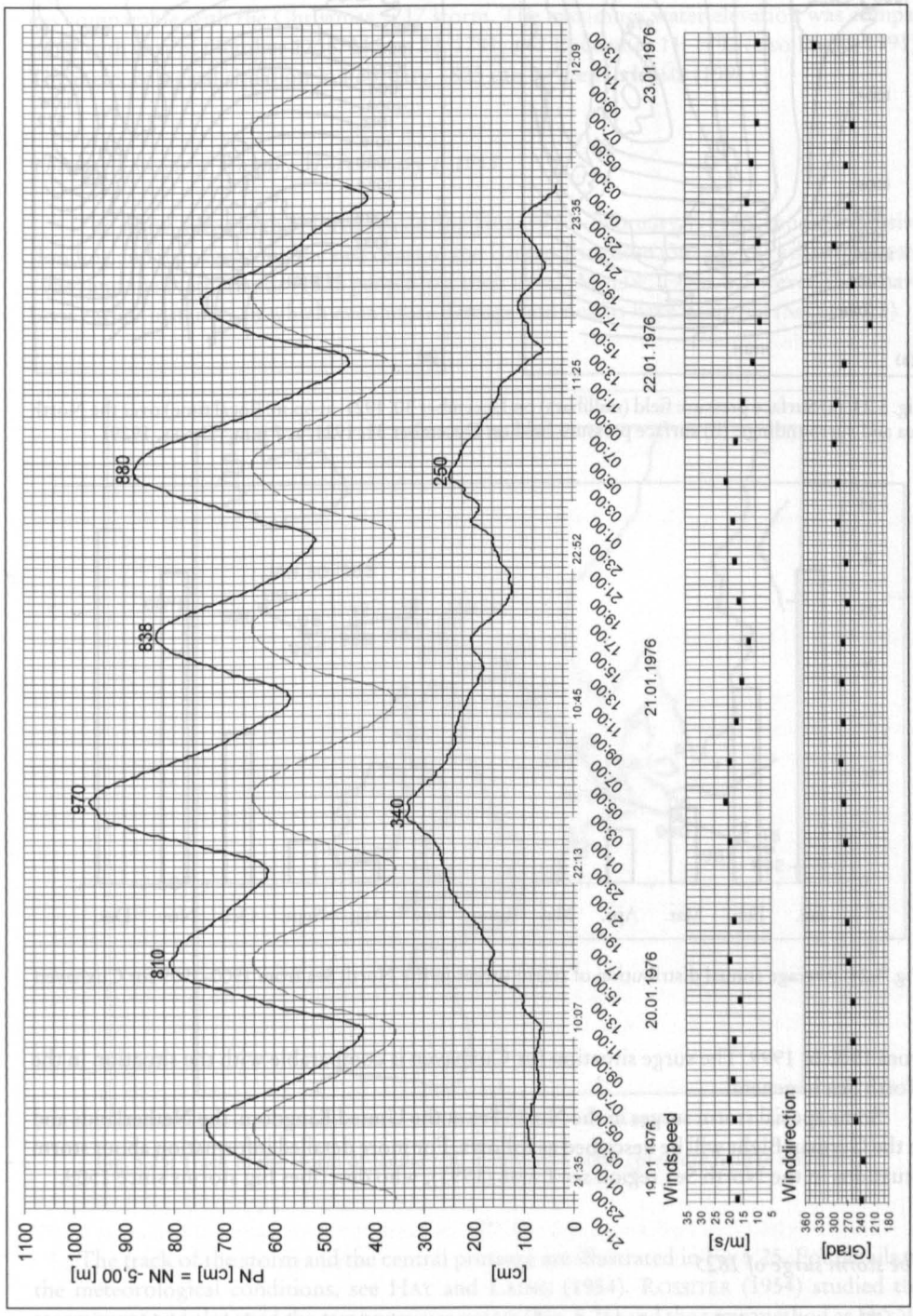

Fig. 5.22: Storm surge at Cuxhaven from January 20–22, 1976 (GÖNNERT and SIEFERT, 1998)

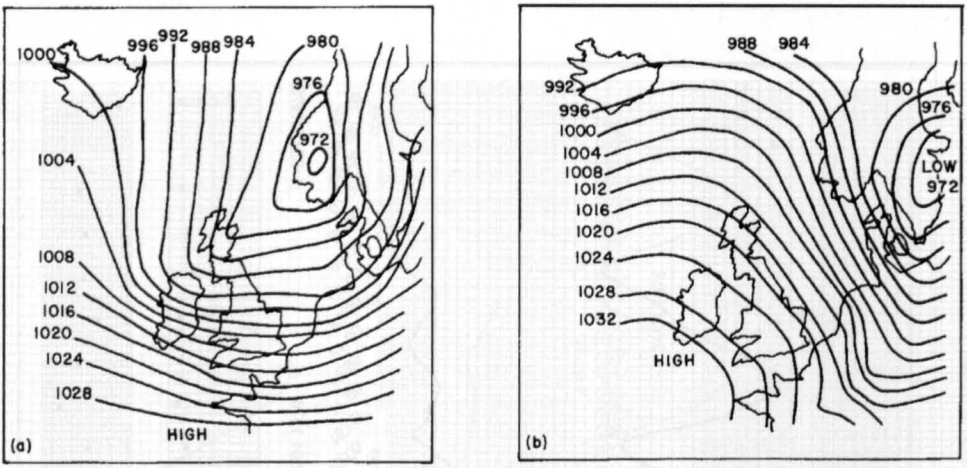

Fig. 5.23: (a) Surface pressure field (millibars) on December 30, 1921, at 6p.m. (local time) over the North Sea and surroundings; (b) surface pressure field on December 31, 1921, at 7 p.m. (DINES, 1929)

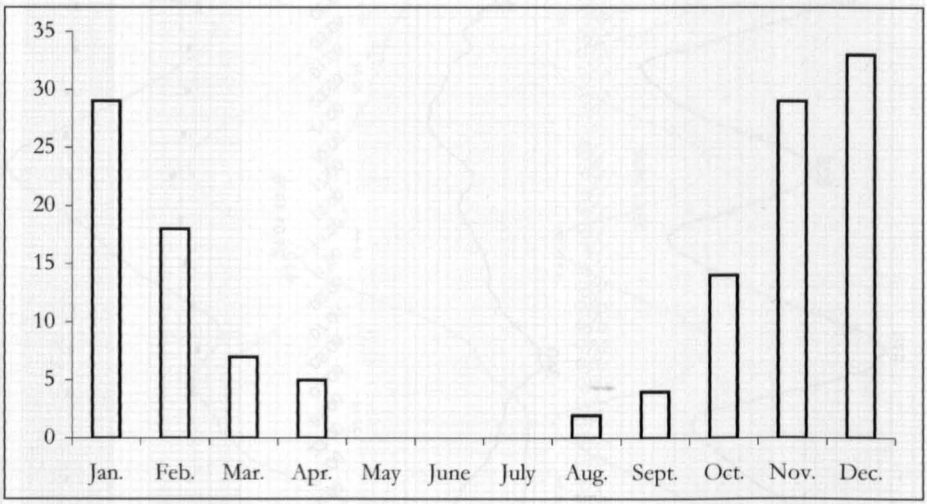

Fig. 5.24: Average annual distribution of storm surges in the North Sea from 1900–1999 for Cuxhaven

from 1900 to 1999. The surge situation for Cuxhaven is comparable with the situation in the North Sea in general.

Some special storm surges in the North Sea at the United Kingdom, the Netherlands and in the German Bight will be described as follows. For more detailed information about storm situations in the North Sea region see LAMB (1991), who describes big storms since 1509.

The storm surge of 1825

The storm of February 1–2, caused storm surges in Scotland and the neighbouring sea areas to north and east. The storm of February 2–5 caused a disastrous storm surge from

Holland to Denmark. The storm tide crest reached a level of more than 350 cm over mean high tide level at Cuxhaven (German Bight) and was therefore one of the highest storm surges comparable with the Christmas 1717 storm. The maximum water elevation was comparable with that of October 1756, March 22, 1791, and December 11, 1792 (also LAMB, 1991). The meteorological situation in February 1825 can be seen in LAMB (1991).

The storm surge of January 31–February 1, 1953

The storm surge in the North Sea during January 31–February 1, 1953, caused extensive flooding and damage along the east coast of the United Kingdom (307 people killed) (STEERS, 1954) and the Netherlands (1835 people lost their lives) (MALDE, 1996). However, there have been earlier instances in which even more damage and deaths have occurred (Section 7.3).

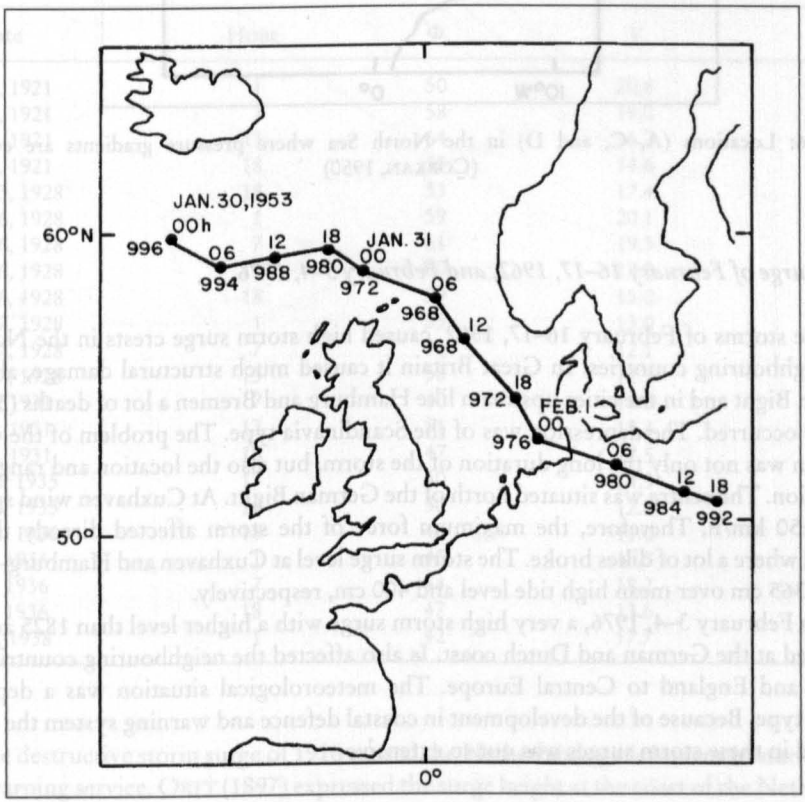

Fig. 5.25: Track of the storm of January 30–February 1, 1953 (pressure field in millibars).

The track of the storm and the central pressure are illustrated in Fig 5.25. For details on the meteorological conditions, see HAY and LAING (1954). ROSSITER (1954) studied this storm surge and also used the same pressure points (Fig. 5.26) and the same method as DOODSON (1924, 1929) and CORKAN (1948, 1950).

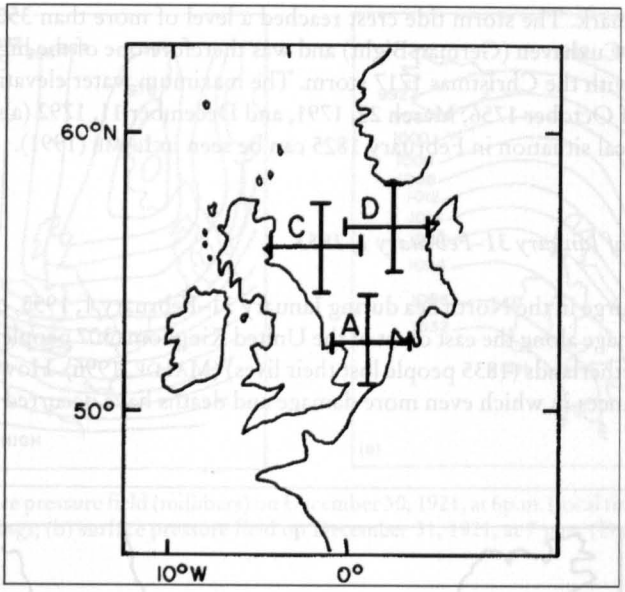

Fig. 5.26: Locations (A, C, and D) in the North Sea where pressure gradients are evaluated. (CORKAN, 1950)

Storm surge of February 16–17, 1962, and February 3–4, 1976

The storms of February 16–17, 1962, caused high storm surge crests in the North Sea and neighbouring countries. In Great Britain it caused much structural damage, along the German Bight and in the cities upstream like Hamburg and Bremen a lot of deaths (340) and damage occurred. The depression was of the Scandinavia type. The problem of the weather situation was not only the long duration of the storm, but also the location and range of the depression. The centre was situated north of the German Bight. At Cuxhaven wind speed reached 150 km/h. Therefore, the maximum force of the storm affected directly the Elbe estuary, where a lot of dikes broke. The storm surge level at Cuxhaven and Hamburg-St Pauli rose to 365 cm over mean high tide level and 400 cm, respectively.

On February 3–4, 1976, a very high storm surge with a higher level than 1825 and 1962 happened at the German and Dutch coast. Is also affected the neighbouring countries from Ireland and England to Central Europe. The meteorological situation was a depression Jutland type. Because of the development in coastal defence and warning system the damage incurred in these storm surges was not so extensive.

Surges in the German Bight and at the coast of the Netherlands

SCHALKWIJK (1947) gave a comprehensive analysis of storm surges at the coast of the Netherlands until 1940, and the following discussion is based on his paper.

Table 5.3: International and Bleck equivalents of the Beaufort Scale. (SCHALKWIJK, 1947)

Degrees Beaufort	International equivalent of wind speed ($m \cdot s^{-1}$)	Bleck equivalent of wind speed ($m \cdot s^{-1}$)	Degrees Beaufort	International equivalent of wind speed ($m \cdot s^{-1}$)	Bleck equivalent of wind speed ($m \cdot s^{-1}$)
1	1.1	1.8	7	13.8	17.4
2	2.5	4.4	8	16.7	20.0
3	4.3	7.0	9	19.9	22.6
4	6.3	9.6	10	23.3	25.2
5	8.6	12.2	11	27.1	27.8
6	11.1	14.8	12	>29.0	>29.0

Table 5.4: Values of deviation angle Ψ (degrees), wind speed V ($m \cdot s^{-1}$), and surge η (cm) for the storm surges at the Netherlands coast. (SCHALWIJK, 1947)

Date	Hour	Φ	V	η
Jan. 19, 1921	1	50	20.8	155
Jan. 19, 1921	7	58	19.0	134
Jan. 19, 1921	13	64	16.7	99
Jan. 19, 1921	18	55	14.6	70
Nov. 25, 1928	18	53	17.4	115
Nov. 26, 1928	1	59	20.1	172
Nov. 26, 1928	7	61	19.3	142
Nov. 26, 1928	13	60	17.0	105
Nov. 26, 1928	18	59	15.0	86
Nov. 27, 1928	1	55	13.0	74
Nov. 27, 1928	7	54	12.1	71
Nov. 27, 1928	13	58	12.3	71
Jan. 17, 1931	7	40	18.9	133
Jan. 17, 1931	13	51	18.4	139
Jan. 18, 1931	18	47	12.5	45
Oct. 30, 1935	13	50	14.3	71
Oct. 20, 1935	18	50	12.4	44
Oct. 20, 1936	18	46	11.0	54
Dec. 1, 1936	1	43	18.3	141
Dec. 1, 1936	7	44	18.2	176
Dec. 2, 1936	18	47	13.6	71
Jan. 30, 1938	1	42	17.7	119

The destructive storm surge of 1916 caused the Netherlands government to start a storm surge warning service. ORTT (1897) expressed the surge height at the coast of the Netherlands through

$$\eta = KR + R_b(76 - p) \tag{5.18}$$

where η is the storm surge (centimetres), K is a factor representing the influence of the strength of the wind, R is a factor representing the wind direction, R_b is a factor representing the effect of atmospheric pressure, and p is the atmospheric pressure (centimetres of mercury).

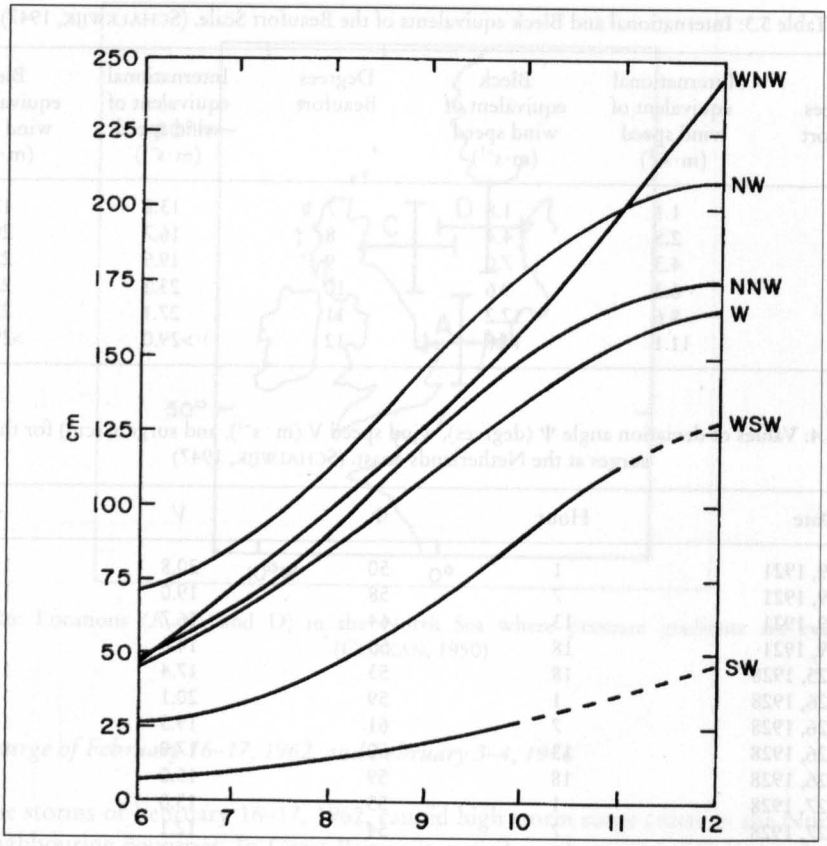

Fig. 5.27: Storm surge versus wind speed at Hook of Holland. Schalkwijk, based on earlier studies by a Netherlands Government committee, summarized these results. (SCHALKWIJK, 1947)

For the Netherlands coast

$$K = 0.14V^2 \tag{5.19}$$

where, V is the wind velocity. SCHALKWIJK (1947) gave tables of R and R_b for various wind directions. ORTT (1897) showed that large surges are produced by W to WNW winds and the smallest surges are produced by E to ESE winds and, in general, there is a lag of about 6 h between the wind and the surge.

The committee (Rotterdamsche Waterweg) established by the Netherlands government in 1920 studied 19 storm surges for the period 1887–1917. They related the surges to the wind but ignored time lag and atmospheric pressure gradients. The results of this study are shown in Fig. 5.27 (the Beaufort Scale is explained in Table 5.3). One interesting result is that the winds over the southern part of the North Sea are more relevant than the local winds in generating these surges.

$$\eta = \frac{aV^2 L \cos\psi}{H} \tag{5.20}$$

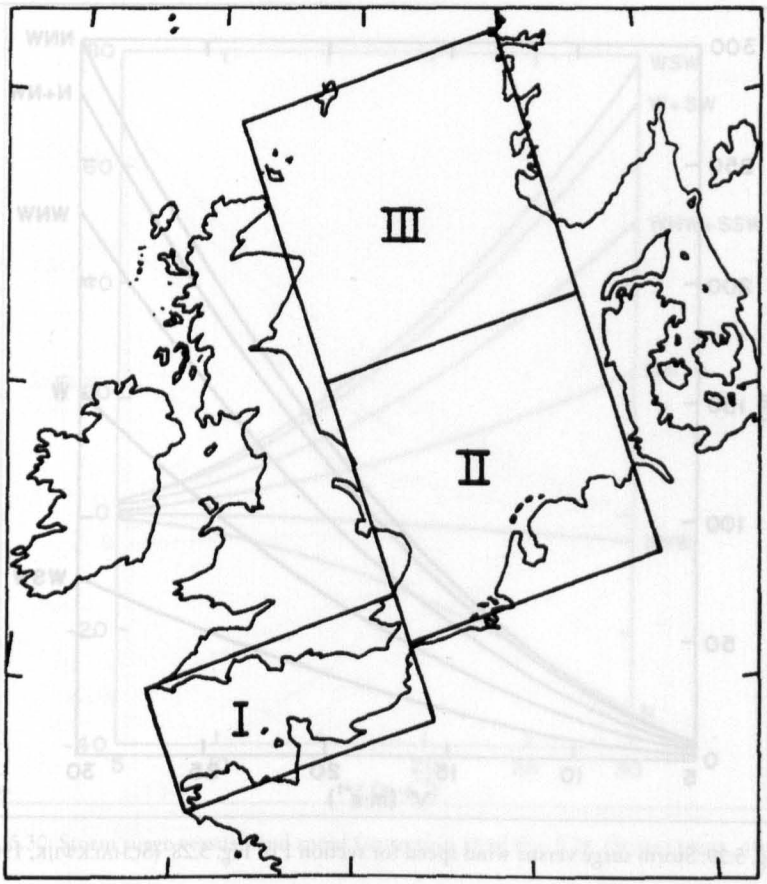

Fig. 5.28: Three sections of the North Sea for which the storm surge study was made. (SCHALKWIJK, 1947)

where, a = 0.0036, V is the wind velocity (metres per second), η is the surge (centimetres), H is the water depth (metres), L is the channel length (kilometres), and Ψ is the angle between the wind direction and the channel axis. COLDING (1880, 1881) used a slightly different formula:

$$\eta = \frac{0.048 L V^2 \cos^2 \psi}{H} \tag{5.21}$$

This formula was successfully used to hindcast the storm surges of November 12–14, 1872, on the Danish coast and in the Baltic Sea.

Based on several studies (MAZURE, 1937; PALMEN, 1932) and verified by more recent research (GÖNNERT, 1999), the following results can be deduced for the Southern North Sea coast. The time lag between the wind and surge is 3–6 h. The most effective wind direction in generating surges is NW. The relationship between the surge and atmospheric pressure gradient is related to the structure and movement of the pressure field. The surge in the southern part of the North Sea is closely related to the average wind over the whole North

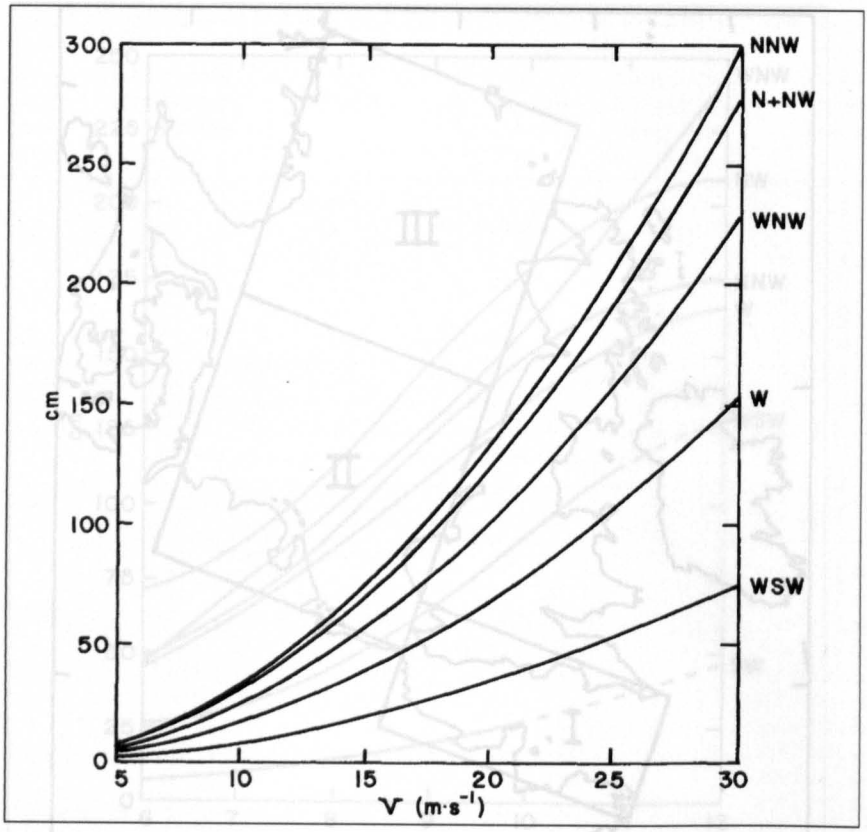

Fig. 5.29: Storm surge versus wind speed for section 1 of Fig. 5.28. (SCHALKWIJK, 1947)

Sea. Along the coast of the Netherlands, the variations in the surge south of Helder are not significant.

SCHALKWIJK (1947) developed an analytical theory applicable to an enclosed sea, a partly open sea, a bay of uniform depth, and a bay of variable depth. He included the influence of the Dover Strait and inhomogenities and time variations in the wind field. He selected 14 surges for the period 1920–40. These cases with factors Ψ, V, and η (from eq. 5.20) are listed in Table 5.4 (in this table, 22 cases appear because some cases are broken down into separate events).

Schalkwijk's 1947 study showed that the average deviation of the wind from the isobars is 8°, which is somewhat smaller than the values given by other authors, which ranged from 13 to 20°. He also found that on the rising part of the curve the time lag between wind and surge is 2.2 h whereas on the falling part of the curve the lag is 2.8 h.

The three separate regions of the North Sea for which this study is made are shown in Fig. 5.28. The results for sections 1, 11, and 111 are summarized in Fig. 5.29, 5.30, and 5.31, respectively. The results for the whole North Sea are shown in Fig. 5.32. Comparison of Fig. 5.27 and 5.32 shows that differences exist between the results of SCHALKWIJK'S (1947) study and the Netherlands government committee's earlier study.

Schalkwijk also examined the surges in the East Scheldt Estuary. The results for this case are summarized in Fig. 5.33.

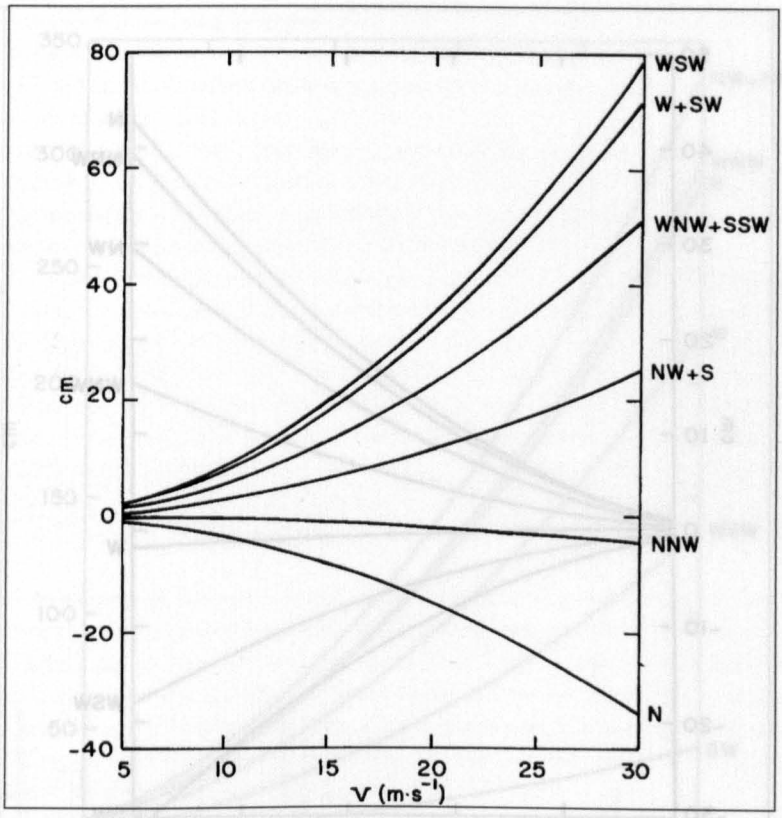

Fig. 5.30: Storm surge versus wind speed for section 11 of Fig. 5.28. (SCHALKWIJK, 1947)

Special Meteorological Influence on Storm Surges in the North Sea (Atmospheric Pressure Gradient / External Surges)

TIMMERMAN (1975) showed that storm surges can be generated in the North Sea not only by westerly winds over the continental shelf but also by atmospheric pressure gradients near the area of transition from deep to shallow water. He mentioned that this effect is usually disregarded in storm surge calculations. For the storm surge of February 16, 1962, the atmospheric pressure gradient effect was very significant. KOOPMAN (1963) studied the surge of October 16–17, 1963. In this case, atmospheric pressure gradients were also a significant factor. Other important storm surge dates are December 11–15, 1972, and January 29, 1974, where atmospheric pressure gradients were important (TIMMERMAN, 1975).

Until now the issue of externally generated surges in the German Bight has not been adequately addressed. External surges originated in deep water in the open sea (SCHMITZ 1965). Their genesis in the North Sea depends upon the speed of movement and the pressure deficit of the extratropical cyclone travelling over the Atlantic Ocean. Note that the amplitude of this external surge is completely independent of the local meteorological conditions over the German Bight. These external surges travel from Aberdeen to Immingham, then through the Straits of Dover to arrive at the Dutch and German coasts.

KOOPMANN (1962) investigated external surges for the period of 1956–1960; SCHMITZ et

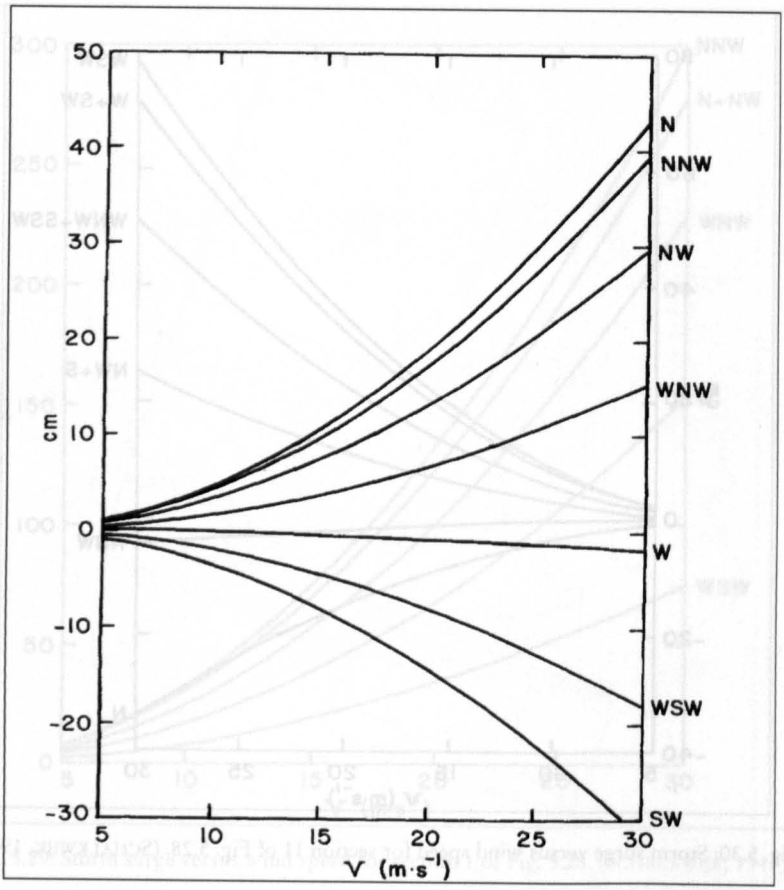

Fig. 5.31: Storm surge versus wind speed for section III of Fig. 5.28. (SCHALKWIJK, 1947)

al. (1988) specified the meteorological situation. GÖNNERT (1999) investigated this phenomenon in the North Sea and its influence on the normal tide level and storm surge level for the period of 1971–1995. The research showed that at Cuxhaven a peak level of 10 cm to 108 cm (Fig. 5.35) can occur. The peak external surge needs not coincide with the high tide at the coast. Normally it is disturbed over the entire tide, mostly 3 h before high tide and 3 h after high tide. External surges occur from October to March, sometimes also in August, September and April (Fig. 5.34). This is the same period as the storm surge period in the German Bight. Furthermore, for every 4th to 5th storm surge case an external surge influences the water level, till now mostly before and after the high water level. Because of the fact that external surges at Cuxhaven have a long duration they influence the storm surge. Till now, the peak external surge never coincided with the local surge peak.

Storm surges in the Irish Sea

Storm surge studies for the Irish Sea are fewer than those for the North Sea, although large surges occur in the Irish Sea. Surges in the Irish Sea originate in the Atlantic (AMIN, 1985). LENNON (1963) examined the meteorological situations associated with large surges

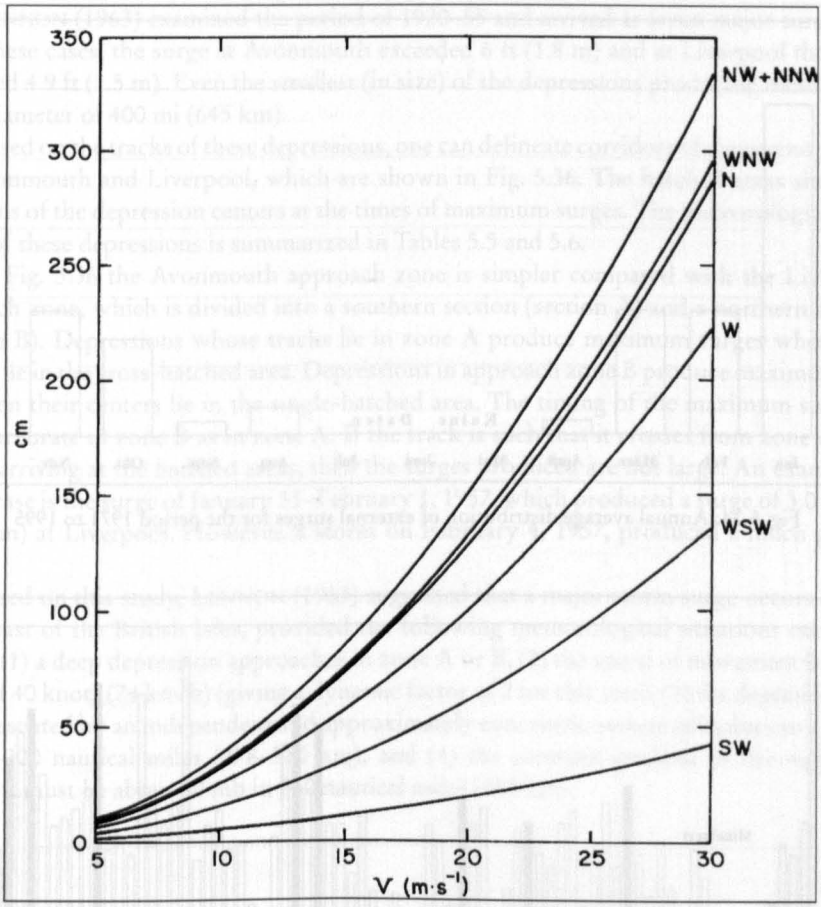

Fig. 5.32: Storm surge versus wind speed for the entire North Sea based on Schalkwijk's results (SCHALKWIJK, 1947)

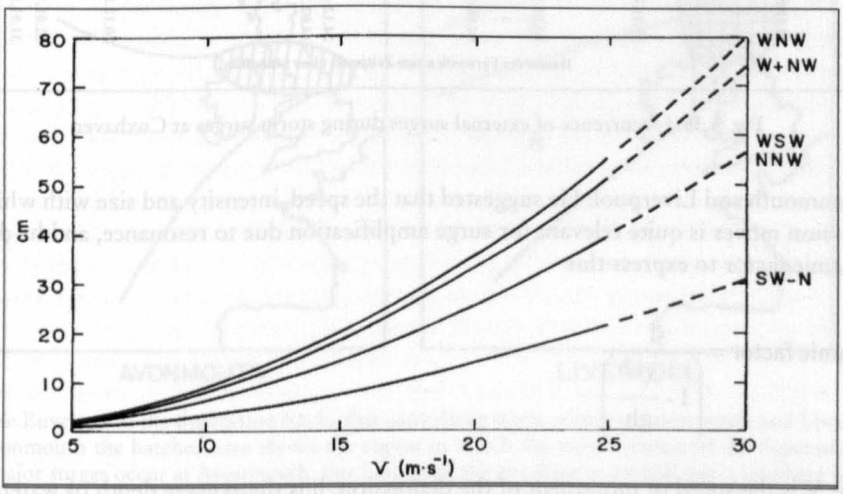

Fig. 5.33: Storm surge versus wind speed for the East Scheldt Estuary. (SCHALKWIJK, 1947)

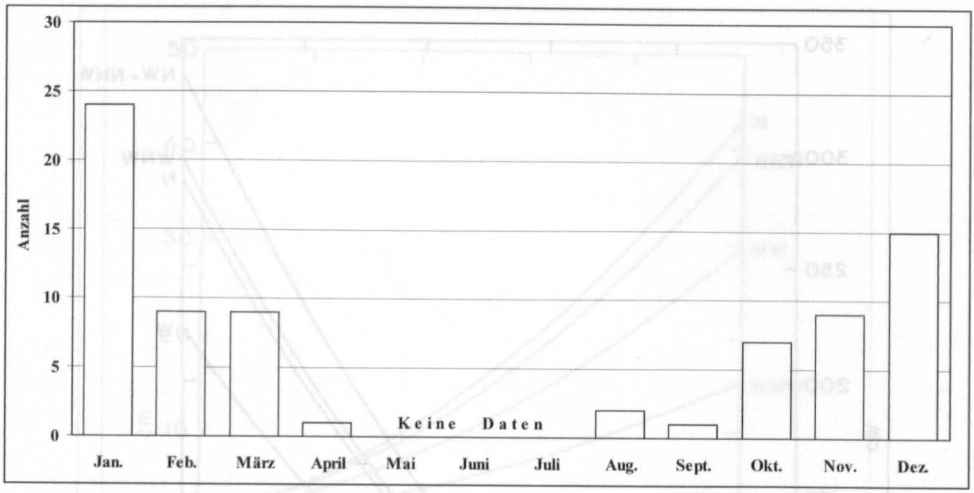

Fig. 5.34: Annual average distribution of external surges for the period 1971 to 1995

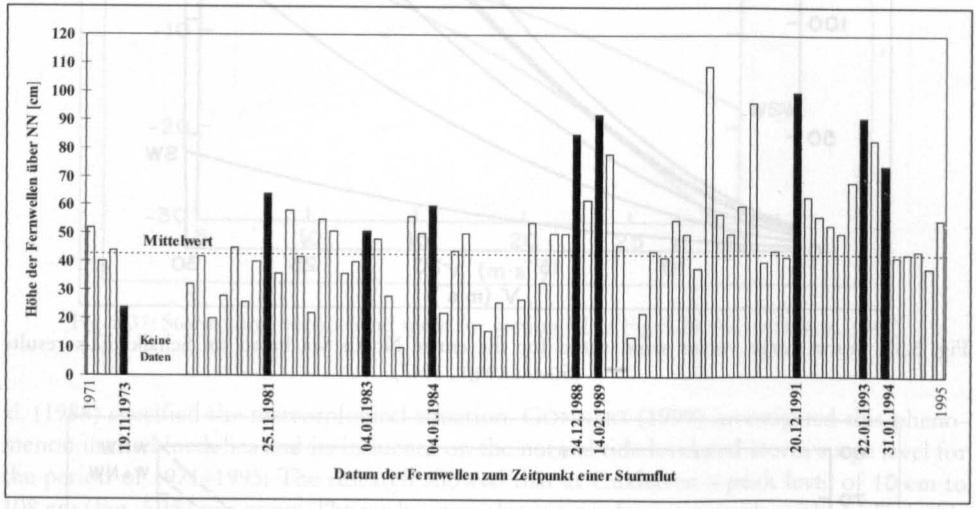

Fig. 5.35: Occurrence of external surges during storm surges at Cuxhaven

at Avonmouth and Liverpool. He suggested that the speed, intensity and size with which the depression moves is quite relevant for surge amplification due to resonance, and he defined a dynamic factor to express this:

$$\text{Dynamic factor} = \frac{1}{\left(1 - \frac{V^2}{gh}\right)} \qquad (5.22)$$

where, V is the speed of movement of the depression, h is the average depth of water, and g is the acceleration of gravity.

LENNON (1963) examined the period of 1920–55 and arrived at seven major surges; i.e. in all these cases, the surge at Avonmouth exceeded 6 ft (1.8 m) and at Liverpool the surge exceeded 4.9 ft (1.5 m). Even the smallest (in size) of the depressions producing these surges has a diameter of 400 mi (645 km).

Based on the tracks of these depressions, one can delineate corridors of dangerous zones for Avonmouth and Liverpool, which are shown in Fig. 5.36. The hatched areas show the positions of the depression centers at the times of maximum surges. The meteorological character of these depressions is summarized in Tables 5.5 and 5.6.

In Fig. 5.36 the Avonmouth approach zone is simpler compared with the Liverpool approach zone, which is divided into a southern section (section A) and a northern section (section B). Depressions whose tracks lie in zone A produce maximum surges when their centers lie in the cross-hatched area. Depressions in approach zone B produce maximum surges when their centers lie in the single-hatched area. The timing of the maximum surges is not as accurate in zone B as in zone A. If the track is such that it crosses from zone A to B before arriving at the hatched areas, then the surges produced are not large. An example of such a case is the surge of January 31–February 1, 1957, which produced a surge of 3.0 ft (less than 1 m) at Liverpool. However, a storm on February 4, 1957, produced a much greater surge.

Based on this study, LENNON (1963) suggested that a major storm surge occurs on the west coast of the British Isles, provided the following meteorological situations occur together: (1) a deep depression approaches in zone A or B, (2) the speed of movement is of the order of 40 knots (74 km/h) (giving a dynamic factor of 2 for this area), (3) the depression can be represented by an independent and approximately concentric system of isobars to a radius of 150–200 nautical miles (278–370 km), and (4) the pressure gradient in the right rear quadrant must be about 30 mb in 250 nautical miles (463 km).

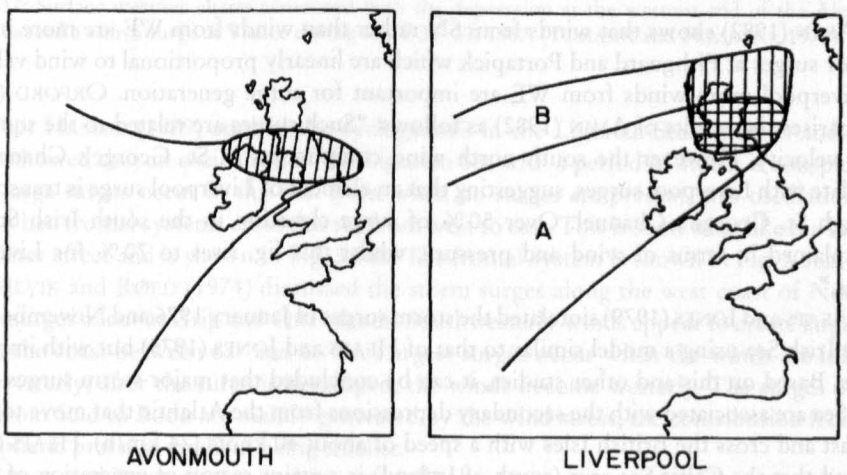

Fig. 5.36: Envelope of the depression tracks that cause large storm surges at Avonmouth and Liverpool. For Avonmouth the hatched area shows the region in which the storm centers of the depressions lie when major surges occur at Avonmouth. For Liverpool the envelope is divided into a southern section (A) and a northern section (B). The cross-hatched and single-hatched areas are, respectively, associated with zones A and B. (LENNON, 1963)

Table 5.5: Some details of the depressions that caused large storm surges at Avonmouth. (LENNON, 1963)

Date	Speed of movement (km/h)	Location of depression center at time of maximum surge	Radius of depression (km)	Pressure gradient (mb) over 463 km
Jan. 12, 1930	87	Irish Sea	241	24
Sept. 17, 1935	74	Irish Sea	333	32
Jan. 9, 1936	78	Ireland	296	34
Nov. 23, 1938	65	South Scotland	389	26
Mar. 16, 1947	72	North England	333	26
Apr. 23, 1947	74	North Ireland	370	28
Nov. 30, 1954	59	East England	333	38

Table 5.6: Some details of the depressions that caused large storm surges at Liverpool, U.K. (LENNON, 1963)

Date	Speed of movement (km/h)	Location of depression center at time of maximum surge	Radius of depression (km)	Pressure gradient (mb) over 463 km
Jan. 9, 1936	78	Ireland	296	34
Oct. 27, 1936	69	North of Scotland	278	32
Nov. 23, 1938	65	North England	389	26
Jan. 25, 1944	65	West Scotland	482	23
Dec. 2, 1946	70	Off West Scotland	333	23
Apr. 23, 1947	74	North Ireland	370	28
Nov. 30, 1954	59	East Ireland	296	34

AMIN (1982) shows that winds from SN rather than winds from WE are more important for surges at Fishguard and Portapick which are linearly proportional to wind velocity. At Liverpool more winds from WE are important for surge generation. ORFORD (1989) summarises the results of AMIN (1982) as follows: "Such surges are related to the square of wind velocity. However the south north wind components in St. George's Channel do correlate with Liverpool surges, suggesting that an element of Liverpool surge is transported through St. George's Channel. Over 50 % of surge elevation in the south Irish Sea can be explained in terms of wind and pressure, whilst this fig. rises to 70 % for Liverpool surges."

HEAPS and JONES (1979) simulated the storm surges of January 1976 and November 1977 in the Irish Sea using a model similar to that of HEAPS and JONES (1975) but with improvements. Based on this and other studies, it can be concluded that major storm surges in the Irish Sea are associated with the secondary depressions from the Atlantic that move towards the east and cross the British Isles with a speed of about 40 knots (74 km/h). HEAPS (1965) showed that the Celtic Sea area (south of Ireland) is a major region of generation of storm surges.

Meteorological conditions associated with storm surges in other parts of Europe

Storm surges occur on the northern part of the Atlantic coast of Portugal. MORAIS and ABECASIS (1975) discussed the storm surge that occurred on Leixoes during January 16–17, 1973.

In the city of Venice at the Adriatic Sea and the Ligurian Sea storm surges occur. The Ligurian Sea is a region of cyclogenesis. Depressions from the Atlantic reaching this sea are intensified here and then travel eastwards. Southeast winds appear to generate the greatest surges in the Venice area. The surface weather charts for two time slots during the surge of April 21–22, 1967, are shown in Fig. 5.37. Note the depression at the western end of the Alps.

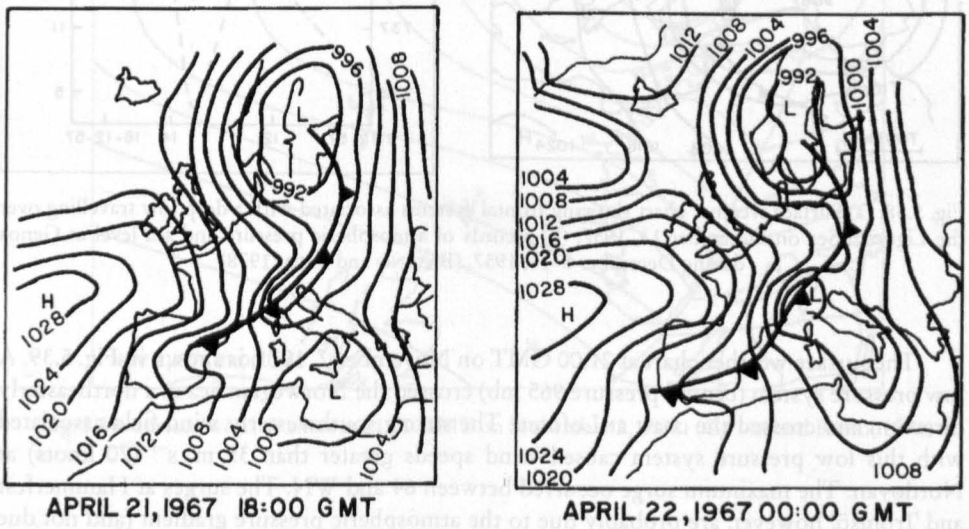

Fig. 5.37: Surface weather charts associated with the depression at the western end of the Alps that caused a storm surge at Venice during April 21–22, 1967. (TOMASIN and FRASETTO, 1979)

VAN HAMME (1979) studied the cyclogenesis in the Ligurian Sea. BASANO and PAPA (1978) showed that an oscillation of the Ligurian Sea with a period of 3.66 h is conspicuous when large surges occur in this sea. Even when no surges are present, this oscillation can occur when frontal systems cross this sea from west to east. This is somewhat like the inverse barometer effect and is shown in Fig. 5.38b. The frontal system is shown in Fig. 5.38a.

GJEVIK and RØED (1974) discussed the storm surges along the west coast of Norway. Severe surges occur at Grip and Ona islands. Southwesterly winds appear to create large surges on the coast between 62° and 66° N. Largest surges occur when the winds are initially southwesterly; after the surge is developed, the winds become westerly. The surges on the coast from Stad to Bodø are mainly generated by the wind stress, the contribution from the atmospheric pressure gradient being smaller.

GJEVIK and RØED (1974) studied especially three storm surges: (1) November 2, 1971, (2) December 30, 1972, and (3) December 31, 1972. The second and third are typical surges that frequently occur along the coast between 62 and 68° N. The first one is exceptional because the peak surge coincided with the peak tide along the coast between Sula and Sandnessjøen.

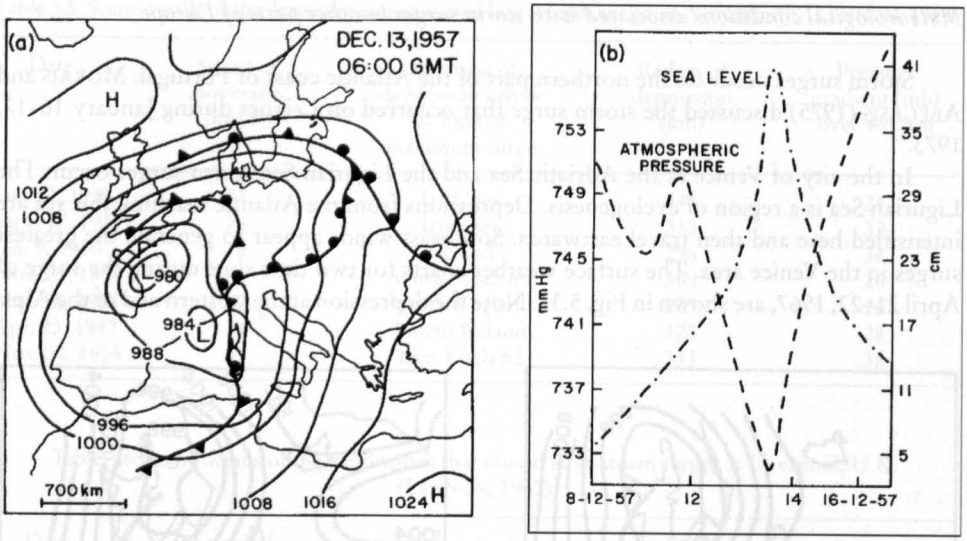

Fig. 5.38: (a) Surface weather chart showing frontal systems associated with a deep low travelling over the Ligurian Sea on December 13, 1957; (b) records of atmospheric pressure and sea level at Genoa during December 8–16, 1957. (BASANO and PAPA, 1978)

The surface weather chart at 21:00 GMT on November 2, 1971, is shown in Fig. 5.39. A low pressure system (central pressure 965 mb) crossed the Norwegian Sea in a northeasterly direction and crossed the coast at Lofoten. The strong southwesterly wind field associated with this low pressure system caused wind speeds greater than 35 m. s^{-1} (70 knots) at Nordøyan. The maximum surge occurred between 64 and WN. The surges at Hammerfest and Tromsö, however, are probably due to the atmospheric pressure gradient (and not due to wind stress) because these two stations are located to the north of the wind field associated with this system.

GJEVIK and RØED (1974) presented detailed surface weather charts for the three surge cases considered here. They showed that the meteorological situation was somewhat similar for cases 1 and 3. The peak of the wind field moved with an average speed of about 25 m s^{-1}. These authors used the following values of drag coefficients for different wind speeds:

$$C_D = \begin{cases} 2.5 \times 10^{-3} & \text{for } 25 \text{ m s}^{-1} \\ 3.0 \times 10^{-3} & \text{for } 30 \text{ m s}^{-1} \\ 3.5 \times 10^{-3} & \text{for } 35 \text{ m s}^{-1} \end{cases}$$

In the analytical model for the surges on the Norwegian coast, these authors considered surge development due to a wind field moving along the coast. The following forms are assumed for the wind stress components and the pressure field:

$$\tau_{S_x} = \rho T_{0x} F(x,t) e^{-\alpha y}$$

$$\tau_{S_y} = \rho T_{0y} G(x,t) e^{-\beta y} \qquad (5.23)$$

$$P_0 = \text{cons tan t}$$

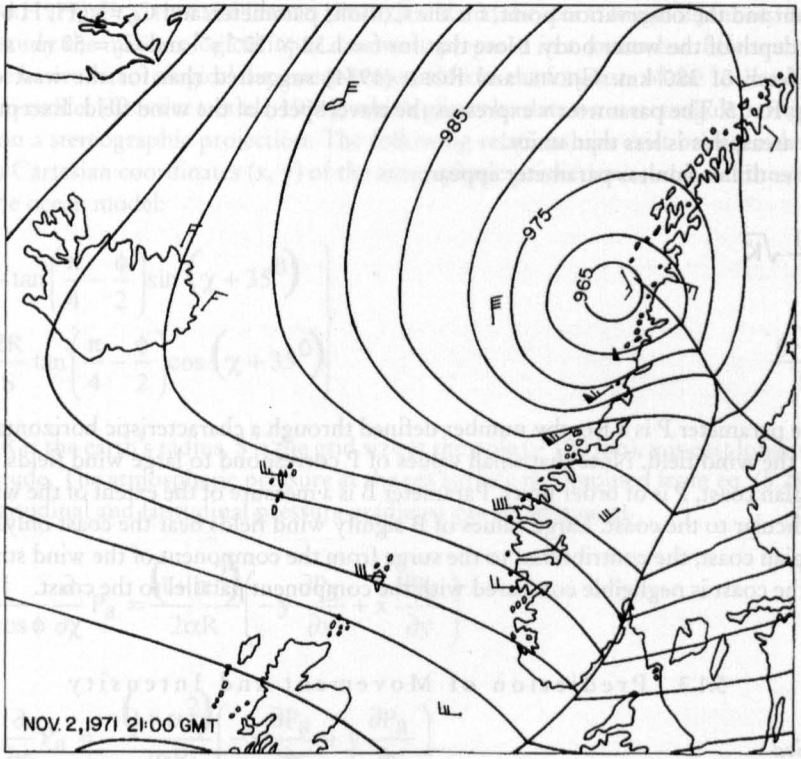

Fig. 5.39: Surface weather chart at 21:00 GMT on November 2, 1971. (GJEVIK and RØED, 1974)

for $t \geq 0$, where T_{0x}, T_{0y}, á, and â are constants and F and G are functions of x and t only. Here, ñ is the water density and the horizontal coordinate y is directed perpendicular to the coast. The following forms are prescribed for F and G:

$$\left.\begin{aligned} F &= e^{-K\left(x-u_0 t\right)^2} \\ G &= e^{-Kx^2} h(t) \end{aligned}\right\} \tag{5.24}$$

where, h (t) is a function of time and $0 \leq h(t) \leq 1$.

In the non-dimensionalisation of the equations of motion and continuity, the following two parameters appear:

$$R \equiv \frac{f}{C_0} x \tag{5.25}$$

where, R is a dimensionless wind fetch (i.e. distance between the initial position of the wind

$$v \equiv \frac{u_0}{C_0} \tag{5.26}$$

maximum and the observation point, f is the Coriolis parameter, and $C_0 = vgH$, H being the average depth of the water body. Note that for $f = 1.32 \times 10^{-4}\ s^{-1}$ and $C_0 = 50\ m \cdot s^{-1}$, R = 1 gives a fetch of 380 km. GJEVIK and RØED (1974) suggested that for the west coast of Norway, R < 5. The parameter v expresses the travel speed of the wind field. Except in very shallow areas, this is less than unity.
Two other dimensionless parameter appear:

$$P \equiv \frac{C_0}{f}\sqrt{K} \tag{5.27}$$

$$B \equiv \frac{\alpha C_0}{f} \tag{5.28}$$

The parameter P is a Rossby number defined through a characteristic horizontal length scale of the wind field. Note that small values of P correspond to large wind fields. For the Norwegian coast, P is of order unity. Parameter B is a measure of the extent of the wind field perpendicular to the coast. Large values of B signify wind fields near the coast only. For the Norwegian coast, the contribution to the surge from the component of the wind stress normal to the coast is negligible compared with the component parallel to the coast.

5.1.3 Prediction of Movement and Intensity

North Sea

DAVIES and FLATHER (1977) developed numerical models to study the storm surge of April 1–6, 1973. A coarse grid covered the whole northwestern European continental shelf and a fine grid covered only the North Sea. They determined the wind field from the geopotential height field extracted from 12-h weather charts for a period of 36 h. From the forecast data at 7 and 19 h, the geopotential height H of the 1000-mb level was used. The sea surface pressure p is calculated from

$$p = 1000 + \rho_a g H \tag{5.29}$$

where ρ_a. is the air density and g is gravity. From the pressure gradients the geostrophic wind was determined. The surface wind w is determined from the geostrophic wind w using the empirical relationship of HASSE and WAGNER (1971):

$$w = Aw + B \tag{5.30}$$

where, A = 0.56 and B has a range of values depending on atmospheric stability. The above formula is valid when w and w are in meters per second. FLATHER and DAVIES (1975, 1976) used the above formula with $B = 2.4\ m \cdot s^{-1}$. This gave reasonable results for the storm surge of March 26–30, 1972, but gave unsatisfactory results for the surge of April 1–6, 1973.

There was a series of storm surges in the North Sea during the period November 4–December 18, 1973. DAVIES and FLATHER (1978) simulated these numerically, again using a coarse model for the whole shelf and a fine model for the North Sea alone. The meteorological input data were obtained in a manner similar to their earlier study (DAVIES and

FLATHER, 1977). FLATHER and DAVIES (1978) simulated the storm surge of January 2–4, 1976. In this study the meteorological input data were prepared in a somewhat different manner.

The basic meteorological data were extracted from the forecasts of the 10-level Bushby-Timpson model (BENWELL et al., 1971), which gives the data on a rectangular array of grid points on a stereographic projection. The following relationships exist between the dimensionless Cartesian coordinates (x, y) of the atmospheric prediction model and the coordinates of the ocean model:

$$\left.\begin{aligned} x &= \frac{2R}{S}\tan\left(\frac{\pi}{4}-\frac{\phi}{2}\right)\sin\left(\chi+35^0\right) \\ y &= -\frac{2R}{S}\tan\left(\frac{\pi}{4}-\frac{\phi}{2}\right)\cos\left(\chi+35^0\right) \end{aligned}\right\} \tag{5.31}$$

where, R is the earth's radius, S is the grid size at the pole (~ 100 km), χ is east longitude, and ϕ is latitude. The atmospheric pressure at the sea surface is computed from eq. (5.29). Then, the longitudinal and latitudinal pressure gradients can be written as

$$P = \frac{1}{R\cos\phi}\frac{\partial}{\partial\chi}P_a = \frac{\left(1+\alpha^2\right)}{2\alpha R}\left(-y\frac{\partial P_a}{\partial x}+x\frac{\partial P_a}{\partial y}\right) \tag{5.32}$$

$$Q = \frac{1}{R}\frac{\partial}{\partial\phi}P_a = -\frac{\left(1+\alpha^2\right)}{2\alpha R}\left(-x\frac{\partial P_a}{\partial x}+y\frac{\partial P_a}{\partial y}\right)$$

where,

$$\alpha^2 \equiv \frac{S^2\left(x^2+y^2\right)}{4R^2} \tag{5.33}$$

The eastward and northward components of the geostrophic wind are

$$\hat{w}_x = -\left[\frac{\left(1+\alpha^2\right)}{\left(1-\alpha^2\right)}\right]\frac{Q}{2\omega\rho_a} \tag{5.34}$$

$$\hat{w}_\phi = -\left[\frac{\left(1+\alpha^2\right)}{\left(1-\alpha^2\right)}\right]\frac{P}{2\omega\rho_a}$$

where, ω is the angular velocity of the earth's rotation. A linear relationship was assumed between the geostrophic wind ^wand the surface wind w:

$$\left.\begin{aligned} w_\chi &= \left(\hat{w}_\chi\cos\delta-\hat{w}_\phi\sin\delta\right)\left(A\hat{w}+B\right)/\hat{w} \\ w_\phi &= \left(\hat{w}_\chi\sin\delta-\hat{w}_\phi\cos\delta\right)\left(A\hat{w}+B\right)\hat{w} \end{aligned}\right\} \tag{5.35}$$

where, δ is the angular deviation between the geostrophic and surface winds and a and b are empirical constants, as in the earlier model of DAVIES and FLATHER (1977).

FISCHER (1979) developed a combined atmosphere-ocean model to simulate the storm surge of January 3, 1976, in the North Sea. The atmospheric model has a grid size of 1.4° latitude and 2.8° longitude and has eight levels in the vertical. The ocean model has a 22-km grid. The surface wind calculated from the atmospheric model was used to determine the wind stress τ_0 in the following manner:

$$|\tau_0| = \rho_a C_D \gamma^2 |v_0| v_0 \tag{5.36}$$

where, v_0 is the wind at the anemometer level, C_D is the drag coefficient, $\gamma = 1$ (when observed winds were used) and $\gamma = 1.55$ (when predicted winds were used), and ρ_a is the density of air. Wind at the anemometer level is

$$|v_0| = 0.54 - 0.012\Delta\theta |v_{g0}| + 1.68 - 0.015\Delta\theta \tag{5.37}$$

where, the cross-isobar angle is 8° for an unstable atmosphere and 213° for the very stable case and è is the potential temperature. The drag coefficient is

$$C_D = \left(1.18 + 0.016|v_{g0}|\right) \times 10^{-3} \tag{5.38}$$

where, v_{g0} is in meters per second. Here, subscript 0 denotes the water surface.

The storm surge of January 11–12, 1978 (TOWNSEND, 1979), was the worst on record after the January 1953 surge in the North Sea. This surge was simulated successfully by using empirical methods (TOWNSEND 1979).

Storm surges in the Irish Sea

The next passage follows closely ORFORD (1989). HEAPS and JONES (1979, 1981) and FLATHER (1981) use running numerical models of Irish Sea conditions in which the dynamics of flow and velocity were addressed using first principle hydrodynamic equations to predict surge elevations. FLATHER (1987) give an example of this type of approach in which observed surge were modelled and predictive results indicate close approximation to observed data.

"He used a numerical model based on non-linear, depth-averaged hydrodynamical equations (FLATHER and PROCTER, 1983) to determine surface elevation, plus north and east components of current velocity, and predicted the water elevation due to combined tide and surge for a number of known parameterized storms over NW Europe (53 days of storm activity). Sea level elevation was obtained for grid points of size 0.5° lat.; 0.33° long. at hourly intervals through the storms. A re-run of the model without meteorological forcing allowed the prediction of tidal elevation per se. The differences between the two runs indicate the surge component. Surge values were calibrated against coastal data from PUGH and VASSIE (1979) for 50 year surge elevation status. The grided data was then interpolated using the nearest reference coastal sites that Pugh and Vassie cite. The resulting prediction of 50 year surge elevation was contoured as increments to the maximum tidal elevation in order to indicate the extreme 50 year height of water level above O.D.

Surge heights are 1–2 m on the west U.K. coast and 1.0–1.5 m on the Irish coast. Highest surge are predicted around the northeast margins of the basin. The joint probability of high

spring and 50 year surge achieves a sea-level elevation commensurate with the 100 year maximum seal-level elevation."

HEAPS and JONES (1975) used a two-and-a-half-dimensional model (they called it a three-dimensional model) of the Irish Sea to simulate storm surges for the period January 10–18, 1965. The first storm surge of this period was associated with a storm of January 13–14. A deep depression moved from the Atlantic with a speed of about 35 knots (65 km. h') on a track (towards the east) lying to the north of Ireland. Fronts from this depression swept across the Irish Sea and winds veered from south to west. The second storm (January 16–18) was associated with a large slow-moving depression to the north of Scotland.

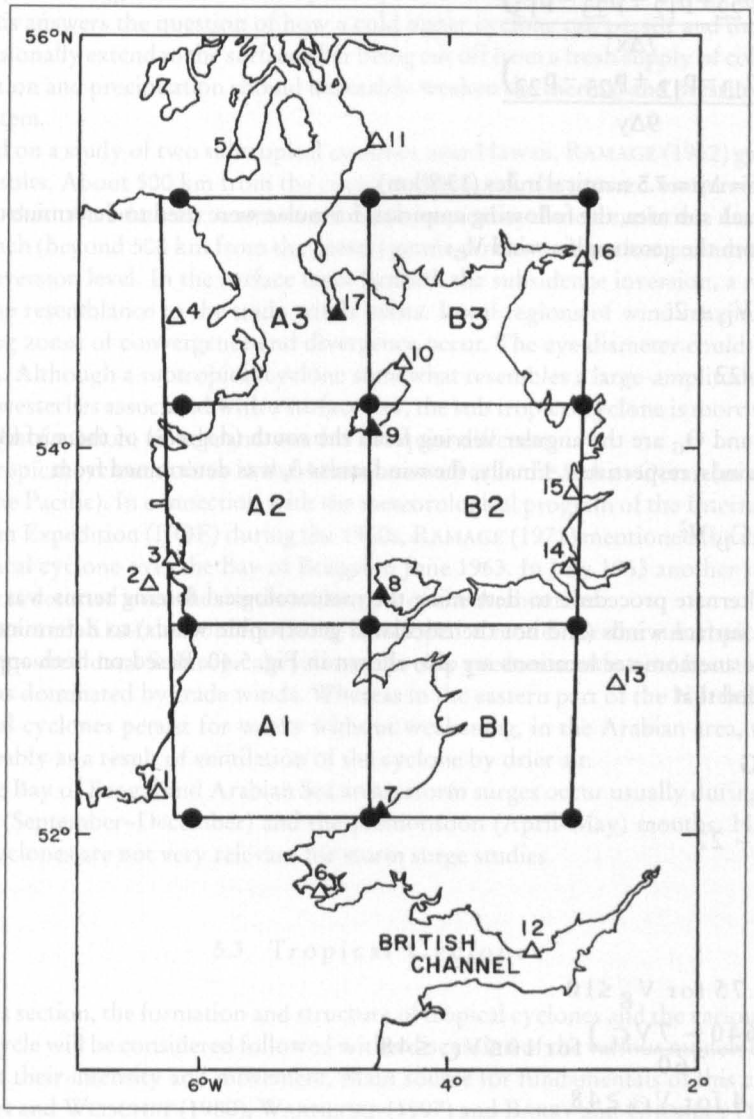

Fig. 5.40: Irish Sea model with six sub areas for determining atmospheric pressure gradients and wind stress. (HEAPS and JONES, 1975)

The following meteorological forcing terms were included in the numerical model: atmospheric pressure gradients over the water surface determined at 3-h intervals from pressure records and wind stress determined at 3-h intervals from geostrophic winds, or alternatively, at 6-h intervals from measured surface winds.

The six rectangular sub areas of the Irish Sea and surroundings (regions AI, A2, A3, B 1, B2, and B3) are shown in Fig. 5.40. From observations of atmospheric pressure, pi,j values were extrapolated for each grid point at each time step. The 16 meteorological stations whose pressure data are used are also shown. Heaps and Jones (1975) wrote the following for sub area A2

$$\frac{\partial p}{\partial x} = \frac{1}{2}\frac{(p_{22} - p_{12} + p_{23} - p_{13})}{7\Delta x} \tag{5.39}$$

$$\frac{\partial p}{\partial y} = \frac{1}{2}\frac{(p_{13} - p_{12} + p_{23} - p_{22})}{9\Delta y} \tag{5.40}$$

where, $\Delta x = \Delta y = 7.5$ nautical miles (13.8 km).

For each sub area, the following empirical formulae were used to determine the surface wind V from the geostrophic wind V_G:

$$V = 0.56\, V_G + 2. \tag{5.41}$$

$$\Theta = \Theta_G - 22 \tag{5.42}$$

where, Θ and Θ_G are the angular veering from the south (degrees) of the surface and geostrophic winds, respectively. Finally, the wind stress $\hat{o}_s$ was determined from

$$\tau_s = 12.5\, C_D\, V^2 \tag{5.43}$$

An alternate procedure to determine the meteorological forcing terms was to use the measured surface winds (and not the calculated geostrophic winds) to determine the wind stress. The anemometer locations are also shown in Fig. 5.40. Based on both approaches it was deduced that

$$V = \beta V_G$$

$$\theta = \theta_G - 22 \tag{5.44}$$

with

$$\beta = \begin{cases} 0.75 \text{ for } V_g \leq 10 \\ \dfrac{(640 - 7V_G)}{760} \text{ for } 10 \leq V_G \leq 48 \\ 0.4 \text{ for } V_G \geq 48 \end{cases} \tag{5.45}$$

where, V_G is in meters per second.

Die Küste, 63 Global Storm Surges (2001), 1-623

5.2 Subtropical Cyclones

SIMPSON (1952) referred to the upper level cutoff lows, which frequently develop over the eastern part of the North Pacific Ocean during winter, north of Hawaii (locally referred to as Kona storms and which occasionally cause heavy flooding in Hawaii), as subtropical cyclones. BARRY and CHORLEY (1992) use the same definition for this phenomenon, which is usually relatively weak near the surface, but well developed in the middle troposphere. These appear to be preceded by the injection of cold air aloft through the mechanism of large-amplitude troughs in the polar westerlies (PALMEN, 1949). The eye diameter could be of some 150 km with little cloud and precepatiomn about 300 km wide (BARRY and CHORLEY, 1992). RAMAGE (1962) suggested that subtropical cyclones indeed are direct energy-creating systems. This answers the question of how a cold upper cyclone can persist and intensify and even occasionally extend to the surface after being cut off from a fresh supply of cold air when condensation and precipitation should inevitably weaken the thermal and pressure gradients of the system.

Based on a study of two subtropical cyclones near Hawaii, RAMAGE (1962) gave the following results. About 500 km from the center and beyond, the upward motion is weak and resembles that of a relatively warm-cored weak tropical cyclone circulation. In the downward branch (beyond 500 km from the center) gentle downward motion extends to the subsidence inversion level. In the surface layer beneath the subsidence inversion, a regime that bears some resemblance to the trade winds exists. Local regions of wind maxima and corresponding zones of convergence and divergence occur. The eye diameter could be as large as 200 km. Although a subtropical cyclone somewhat resembles a large-amplitude trough in the polar westerlies associated with a surface low, the sub tropical cyclone is more symmetric and its field of motion, clouds, and weather are quite different.

Subtropical cyclones occur in the Atlantic as well as in the Indian Ocean (in addition to those in the Pacific). In connection with the meteorological program of the International Indian Ocean Expedition (IIOE) during the 1960s, RAMAGE (1971) mentioned the existence of a subtropical cyclone over the Bay of Bengal in June 1963. In July 1963 another subtropical cyclone was detected over the northeastern part of the Arabian Sea.

MILLER and KESHAVAMURTHY (1968) developed a model for the subtropical cyclone using composited data. Subtropical cyclones develop predominantly near heat troughs and in the areas dominated by trade winds. Whereas in the eastern part of the North Pacific, the subtropical cyclones persist for weeks without weakening, in the Arabian area, they dissipate, probably as a result of ventilation of the cyclone by drier air.

In the Bay of Bengal and Arabian Sea areas, storm surges occur usually during the post-monsoon (September–December) and the premonsoon (April–May) months. Hence, subtropical cyclones are not very relevant for storm surge studies.

5.3 Tropical Cyclones

In this section, the formation and structure of tropical cyclones and the various stages in their life cycle will be considered followed with a discussion of the various models being used to forecast their intensity and movement. Main source for fundamentals of this chapter are BLÜTHGEN and WEISCHET (1980), WARNECKE (1997) and BARRY and CHORLEY (1992).

5.3.1 Development Theory

The main source of material for this subsection is GRAY (1978a, 1978b, 1978c, 1978d, 1989) and BARRY and CHORLEY (1992).

Annually over the globe there are about 80 tropical cyclones with maximum sustained wind speeds of 20–25 $m \cdot s^{-1}$. About one half to two thirds of these cyclones reach hurricane strength (i.e. maximum sustained wind speeds greater than 33 $m \cdot s^{-1}$).

At first the necessary conditions for the development of tropical storms and hurricanes be described with six climatological genesis parameters:

(1) low level relative vorticity, ζ_r
(2) Coriolis parameter, f
(3) the inverse of the vertical shear S_z of the horizontal wind between the lower and upper troposphere, $1/S_z$
(4) ocean thermal energy, sea temperature excess above 26° C to a depth of 60 m, E
(5) vertical gradient of Θ_e, between the surface and 500 mb, $\partial\Theta_e/\partial p$, where Θ_e is the equivalent potential temperature of air and
(6) midtroposphere relative humidity, RH.

The rationale for selecting these parameters is the following. The first parameter is selected because, all things being equal, seasonal cyclone frequency should be related to the magnitude of the seasonal lower tropospheric relative vorticity. The Coriolis parameter is relevant because cyclones do not appear to form within 4–5° of the equator. Cyclogenesis does not occur near the equator because wind accelerations are small due to weak pressure gradients whereas frictional dissipation is as large as at any other latitude. The third parameter is relevant because tropical cyclones form when there is minimum vertical shear of the horizontal wind between the lower and upper troposphere.

The fourth parameter becomes relevant when recognizing that tropical cyclones can have considerable influence on the temperature of the water body over which they travel. The feedback effect of the altered ocean temperature influences the cyclone. It appears that the inner region of the average-sized hurricane (0–240 km) can consume up to 4000 $cal \cdot cm^{-2} \cdot d^{-1}$ from the ocean's sensible and latent heat energy (for details see LEIPPER and JENSEN, 1971; LEIPPER and VOLGENAU, 1972; HEFFERMAN, 1972; PERLROTH, 1967, 1969). On the other hand, MALKUS and RIEHL (1960) put this value at 3100 $cal \cdot cm^{-2} \cdot d^{-1}$. According to FRANK (1977) for Pacific typhoons for the inner 80 km, the consumption rate is around 1470 $cal \cdot cm^{-2} \cdot d^{-1}$. If a typhoon crosses the track of another typhoon, the second one may weaken sometimes because of the lowered sea surface temperature due to the upwelling caused by the first typhoon (BRAND, 1971).

The hurricane or typhoon can influence the ocean temperatures down to a depth of 60 m. LEIPPER and JENSEN (1971) and LEIPPER and VOLGENAU (1972) defined an ocean thermal energy potential (for cyclogenesis) E (calories per square centimeter) as the ocean thermal energy above 26T down to a depth of 60 m, i.e.

$$E = \int \rho_W C_W (T - 26) dz \tag{5.46}$$

where, the integral is from the surface down to a depth of 60 m (or to where T = 26° C). Here, ρ_w is the density of seawater, T is the ocean temperature (degrees Celsius) and C_w is the specific heat of water.

The importance of the fifth parameter is obvious when it is considered that cyclones do not form unless the lower and upper tropospheric flow patterns are well coupled. The pri-

mary mechanism for this coupling is the cumulonimbus convection. Hence, cyclogenesis should depend on the seasonally averaged moist buoyancy potential (i.e. the seasonal magnitude of the difference in the equivalent potential temperature Θ_e between the boundary layer and the middle troposphere). The importance of the sixth parameter can be seen from the observations that tropical cyclones form in areas where seasonal middle level humidity values are high. In other words, when the humidity is high, deep cumulus convection occurs leading to better coupling in the vertical.

Based on these considerations, GRAY (1978a, 1978b, 1978c, 1978d) defined a "seasonal genesis parameter" (SGP) as follows:

SGP = vorticity parameter × Coriolis parameter × vertical shear parameter × ocean energy parameter × moist stability parameter × humidity parameter (5.47)

Here, vorticity parameter = $\zeta_r + 5$ where ζ_r is in units of $10^{-6} \cdot s^{-1}$, Coriolis parameter = f, vertical shear parameter = $1/(S_z + 3)$ where $S_z = |\partial V/\partial p|$ is in units of meters per second per 750 mb and V is the wind vector, ocean energy parameter = E is defined by eq. 6.33 and is in units of 10^{-5} cal $\cdot$ cm^{-2}, moist stability parameter = $\partial\Theta_e/\partial p \pm 5$ where $\partial\Theta_e/\partial p$ is in K $\cdot$ 500 mb^{-1}, and humidity parameter = (RH –40)/30 where RH is the mean relative humidity between 500 and 700 mb but is zero for $RH \leq 40$ and for $RH \geq 70$. Note that in the above expressions, arbitrary units are added to enable daily values to be used instead of seasonal values.
Another interpretation of SGP is as follows:

SGP = dynamic potential × thermal potential (5.48)

where, dynamic potential = $f(\zeta r + 5)\,[1/(S_z + 3)]$ and thermal potential = $E(\partial\Theta_e/\partial p + 5)(RH)$. The thermal potential might be thought of as potential for cumulonimbus convection. The dynamic potential is in units of 10^{-11} s^{-2} (m $\cdot$ s^{-1})/750 mb and the thermal potential is in units of 10^{-5} cal $\cdot$ cm^{-2} $\cdot$ K $\cdot$ 500 mb^{-1}. The SGP is in units of 1.5×10^{-8} cal $\cdot$ K $\cdot$ s^{-1} $\cdot$ cm^{-3}. GRAY (1978a, 1978b, 1978c, 1978d) reported that there is very close agreement between the predicted (from SGP) and the observed cyclogenesis frequencies.

Life Cycle of a Tropical Cyclone

RIEHL (1979) summarized the life cycle of tropical cyclones. For storms with the strength of hurricanes, the duration from their birth to the time of landfall or recurvature into middle latitudes is usually about 6 d. The life cycle of a tropical cyclone may be considered to be made up of the following four stages: formative stage, immature stage, mature stage and terminal stage.

Tropical cyclones form in the vicinity of pre-existing weather systems. The deepening can occupy several days or may occur explosively in as short a time as 12 h. In the formative stage, winds are usually less than hurricane force (i.e. 1-min sustained winds are less than 74 mi $\cdot$ h^{-1} [119 km $\cdot$ h^{-1}]). Strongest winds occur in the quadrant that is to the east of the center and poleward. Surface pressure usually drops to 1000 mb.

Several of these incipient cyclones never deepen enough to become hurricanes. In those cases that do deepen, the lowest pressure rapidly decreases to less than 1000 mb. Winds with speeds of up to 74 mi $\cdot$ h^{-1} occur in a tight band around the centre (and not just in one quadrant). The disorganized squalls of the formative stage change into narrow and organized

bands of clouds spiralling inward. In this immature stage only a small area is involved in the intense inner core (30- to 50-km radius) although there may be a large outer core.

In the mature stage, the surface pressure at the center stops decreasing and the maximum wind speeds do not increase further. However, the area of intense circulation expands (up to 300-km radius in certain cases). The symmetry of the immature stage is destroyed and strong winds and bad weather preferentially occur to the right of the center looking downstream in the direction of movement of the cyclone. Some storms with a central low pressure as low as 950 mb could still be only 100–200 km in radius. RIEHL (1979) estimated that for a storm with an average surface pressure of 1000 mb, the total weight of air and water involved in the circulation is about 3×10^{11} to 1×10^{12} t (3.05×10^{14} to 1.016×10^{15} kg). However, another storm with a radius of 1000 km but with the same average surface pressure of 1000 mb will have a weight of about 5×10^{12} to 3×10^{13} t (5.8×10^{15} to 3.05×10^{16} kg). By comparison, in an ordinary midlatitude cyclone, the weight involved is about 5×10^{12} to 1×10^{13} t (5.8×10^{16} kg).

When the tropical cyclone hits land, usually its core size decreases and sometimes the storm dissipates within 1–2 d. Storms can dissipate even over the ocean if they travel over cold ocean currents (e.g. Northeast Pacific Ocean). Many cyclones recurve (both over land and ocean) into the westerlies and travel towards northeast or east (in the Northern Hemisphere).

Some Characteristics of Tropical Cyclones

RIEHL (1979) offered the following classification of tropical cyclones.

(A) Tropical depression: at most, winds barely acquire gale force in one quadrant.
(B) Tropical storm: winds acquire gale force but less than hurricane force of 64 knots (119 km · h^{-1} or 74 mi · h^{-1}).
(C) Minimal hurricane: winds above 64 knots only in one quadrant.
(D) Moderate hurricane: winds of 80–90 knots (148–167 km · h^{-1}) around the center, with the maximum wind being around 100 knots (185 km · h^{-1}) or more.
(E) Severe hurricane: maximum winds up to 200 knots (370 km · h^{-1}).

Tropical cyclone intensity classification is not uniformly used in the various meteorological services for the various regions of the globe. For example, in the western part of the Pacific Ocean, unless the maximum winds are about 150 knots (278 km · h^{-1}), a typhoon will not be considered severe.

RIEHL (1979) mentioned that the word "hurricane" means "big wind" in the Taino.

Next, some characteristics of tropical cyclones will be briefly examined with respect to their surface pressure, winds, and thermal structure. Since ordinarily, surface pressure varies only by about 3 mb (0.3 %) in the tropics whereas pressure varies 5–10 % below average sea level pressure during tropical cyclones, a useful tool for analysis is the sea level isobar field. Gradients of 0.5–2 mb km^{-1} can occur.

When the tropical cyclone is over an ocean, the increase of wind with height usually occurs in the first 100 m. Above that it increases slowly to about the 300-m level where the winds probably attain maximum values. For Hurricane Eloise of 1977 the wind speed at the 100-m level was 20 m · s^{-1}; from 200 to 500 m it was 22 m · s^{-1}. Then it decreased to 14 m · s^{-1} at 1200 m. Usually, the wind at 50 m is about three quarters the geostropic wind speed (RIEHL, 1979).

In hurricanes, in the inner 80-km core, winds up to 45 m · s^{-1} can occur. Winds are grea-

ter on the right side because here the carrying current and the circulation are in the same direction whereas to the left they oppose each other. One of the safest ways to identify tropical cyclones is to look for this asymmetry in the surface wind field. For convenience, one may think of the following four quadrants around the center: right front, right rear, left front, and left rear. Inward spiralling of streamlines is pronounced in the rear quadrants. Here, the radial component of the motion is strongest.

RIEHL (1979) gave the following relationship between pressure and wind fields in a tropical cyclone (this was derived empirically based on 28 yr of Pacific typhoon data):

$$V_m = 3.35(1010 - p_c)^{0.644} \tag{5.49}$$

where, V_m is the maximum wind (metres per second) and p_c is the central pressure (millibars).

The theory of vortex flows shows that in the center of every revolving vortex, there is a singular point. In a tropical cyclone this center is referred to as the eye, near which the circulation is weak. At the edge of the eye, strong precipitation abruptly stops and the sky may clear at least partly. The diameter of the eye in a mature hurricane ranges from 30 to 50 km and probably twice this value in a severe typhoon. The eye need not be circular and sometimes it is diffuse and has a double structure.

RIEHL (1979) mentioned that one of the earliest controversies about tropical cyclones concerned their vertical extent. Estimates varied from 3 to 10 km or greater. According to HAURWITZ (1935) the tropical cyclone extends through the troposphere, and high level observations substantiated this idea. However, a surprising result revealed from Rawinsonde data was that the circulation at higher levels is opposite to that at lower levels. This changeover level is at about 300 mb.

As expected, the air inside a tropical cyclone is less dense than its surroundings. For Hurricane Daisy of 1958 near Florida, in the mature stage, the surface pressure in the eye was 950 mb and the maximum wind was 50 m s^{-1}. Hurricane Daisy is considered to be a hurricane of moderate intensity, and even in this case more than half the temperature gradient needed for its existence was internally generated. RIEHL (1979), WARNECKE (1997) maintained that this is the main reason why intense hurricanes occur rarely. In contrast, in extratropical cyclones, the cyclone grows at the expense of the potential energy in a pre-existing temperature field, which becomes pronounced. On the other hand, in a tropical cyclone, the cyclone itself must generate most of the required temperature gradient.

RIEHL (1979) suggested that a hurricane may be regarded as a rankine vortex with a velocity profile defined by v_θ/r = constant in the inner core of maximum winds and $v_\theta r = constant$ in the outer core. Here, r is the radial coordinate and vo is the azimuthal velocity. The outer core can be defined as

$$v \cdot r^x = \text{constant}, \; 0.4 \cdot x \cdot 0.6 \tag{5.50}$$

In the outer core, with increasing distance from the center, v_θ tends to zero.

Momentum And Energy Budgets For Tropical Cyclones

Following RIEHL (1979), the energy and momentum budgets for hurricanes will be considered. In polar coordinates the equations of horizontal motion with the neglect of lateral friction are

$$\frac{dv_\theta}{dt} + \frac{v_\theta v_r}{r} + fv_r = -\frac{1}{\rho}\frac{\partial p}{r\partial\theta} + \frac{1}{\rho}\frac{\partial \tau_{\theta z}}{\partial z}$$

$$\frac{dv_r}{dt} - \frac{v_\theta^2}{r} - fv_\theta = -\frac{1}{\rho}\frac{\partial p}{r\partial r} + \frac{1}{\rho}\frac{\partial \tau_{rz}}{\partial z} \tag{5.51}$$

Here, v_r and v_θ are the radial and azimuthal velocities respectively. After certain algebra involving these two equations, it can be shown that

$$\frac{d}{dt}\left(v_\theta r + \frac{fr^2}{2}\right) - \frac{r^2}{2}\frac{df}{dt} = -\frac{1}{\rho}\frac{\partial p}{\partial\theta} + \frac{r}{\rho}\frac{\partial \tau_{\theta z}}{\partial z} \tag{5.52}$$

The component of the earth's angular momentum (per unit mass) about the vertical axis of the tropical cyclone is

$$\Omega = v_\theta r + \frac{fr^2}{2} = \text{cons tan t} \tag{5.53}$$

For symmetrical storms, eq. (5.53) is a good representation in the upper troposphere. If eq. (5.52) is integrated over the entire volume in the storm, by definition the pressure term will disappear, but the frictional term will not because of transfer of momentum from the atmosphere to the ocean. To compute the momentum budget, integrate eq. (5.67) over the volume of the storm to obtain expressions for the transport F_Ω (radial) at any radius and F_Ω (vertical) between two radii. These are

$$F_\Omega(\text{radial}) = -\frac{2\pi r^2}{g}\left[\int_{p2}^{p1} \bar{v}_\theta \bar{v}_r dp + \int_{p2}^{p1} \overline{v'_\theta v'_r} dp + \frac{fr}{2}\int_{p2}^{p1} \bar{v}_r dp\right] \tag{5.54}$$

$$F_\Omega(\text{vertical}) = -\frac{2\pi}{g}\left[\int_{r1}^{r2} \tilde{v}_\theta \tilde{\omega} r^2 dr + \int_{r1}^{r2} \tilde{v}^*_\theta \omega^* r^2 dr + \frac{f}{2}\int_{r1}^{r2} \tilde{\omega} r^3 dr\right] \tag{5.55}$$

where, $\omega = dp/dt$.

The surface transport to the ocean is given by

$$E_\Omega(\text{surface}) = 2\pi \int_{r_1}^{r} \tau_{\theta,0} r^2 dr \tag{5.56}$$

where $t_{\theta,0}$ is the stress at the ship's deck level (or anemometer level).

In eq. (5.54) the first term represents the transport by the mean ageostrophic circulation v_r, the second term denotes the deviation from symmetry when one goes round the perimeter and the third term is the influence due to the earth's rotation, assuming the Coriolis parameter to be constant.

Table 5.7: Transports through 1° radius (1012 kJ · s^{-1}) showing the radial energy balance in two different hurricanes (RIEHL, 1979)

Parameter	Hurricane Daisy (1960)	Hurricane Helene (1951)
Net latent heat inflow	+34.1	+31.9
Flux of latent and sensible heat from the sea	+3.4	+6.2
Import of kinetic energy	+0.4	+0.2
Total energy source	37.9	38.3
Less net export of (CpT + gz)	− 36.9	−37.4
Balance for radiation cooling	1.0	0.9

One can regard the atmosphere, and particularly a tropical cyclone, in the present situation as a thermal engine for which the efficiency (of converting heat to mechanical energy) is defined as the ratio of the mechanical energy produced to the heat released. For an average hurricane, the kinetic energy produced was estimated by RIEHL (1979) as 15×10^{18} ergs s^{-1} or 0.36×10^{12} kWh^{-1} (1 erg = 0.1 μJ, 1 kWh = 3.6 MJ). The latent heat released was 13.3×10^{12} kWh · d^{-1}. Thus, the efficiency E is 3 %. This is very low but is somewhat higher than for extratropical cyclones and the general circulation of the atmosphere. Hence, weather systems and the atmosphere are very inefficient heat engines. This low value of efficiency for the tropical cyclones indicates that the mechanism for energy release is in the central area with local oceanic heat source and not in the advection of large masses of water vapour into the system from outside.

The balance of radial energy for Hurricanes Helen of 1951 and Daisy of 1960 is shown in Table 5.7. Concerning oceanic input of energy, GRAY (1978a) provided the following analysis. In the tropical cyclone, moist static energy *h* can increase or decrease through latent and sensible heat exchange with the ocean *Es* through radiation *R* and through horizontal transport through the boundaries ∇. Vh. One can write for this energy balance

$$\frac{\partial h}{\partial t} = E_S + R - \nabla.Vh \tag{5.57}$$

where,

$$h = gz + C_pT + Lq \tag{5.58}$$

Note that all these terms have been integrated through the thickness of the troposphere.

For the inner 4° radius of tropical storms, E_S + R is slightly positive for weak disturbances, but for hurricanes it is highly positive because strong input of energy takes place from the ocean. The vertical circulations in a tropical cyclone will act as an energy sink dissipating the system and the main energy source is the ocean. For this reason, many tropical systems weaken or dissipate once they are not traveling over the ocean.

Frequency and region of occurrence

The conditions for development of tropical storms form the boundary of areas and period of generation of tropical cyclones. Fig. 5.41 shows over a 20-yr period these areas. Over the globe, the percentage change in the number of tropical cyclones over a recent 20-yr period (1958–77) varied from + 23 to – 13, with an average of 8 (Table 5.8). The ratio of the number of tropical cyclones in the Northern Hemisphere to those in the Southern Hemisphere varied from 1.5 to 4.0.

Month by month occurrences of tropical cyclones for the same 20-yr period for the Northern and Southern Hemispheres are shown separately in Table 5.9 and Table 5.10, respectively. The data for the various ocean basins, which are identified in Fig. 5.41, are shown in Table 5.11.

About 80 % of the tropical cyclones occur in the belt between 20° N and 20° S. The rest occurs poleward of 20° latitude, but mainly in the Northern Hemisphere. Annually, about two thirds of all tropical cyclones occur in the Northern Hemisphere; similarly, about two thirds occur in the Eastern Hemisphere (as opposed to the Western Hemisphere). Most of the tropical cyclones form in the latitudinal belt 5–15°, and rarely do they form within 4–5° from the equator. In the Southern Hemisphere, tropical cyclones do not form poleward of 22°, whereas in the Northern Hemisphere they form at latitudes up to 36°.

Considering longitude, there are three favoured locations for the formation of tropical cyclones: 90° E, 140° E, and 105° W. The western part of the North Pacific Ocean accounts for about one third of all tropical cyclones. Generally, summer is the favoured season for tropical cyclone formation, but they do occur in other seasons, especially in the western part of the North Pacific Ocean.

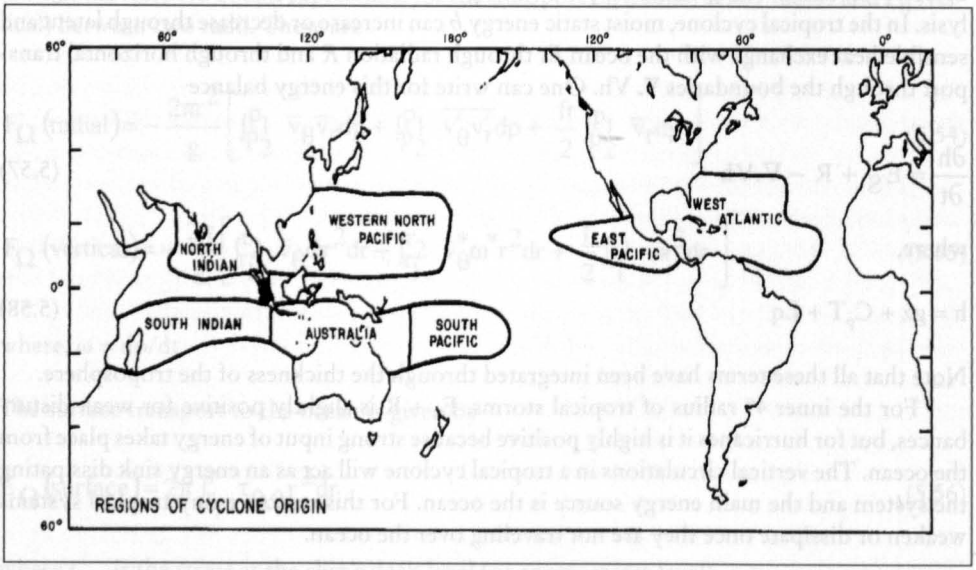

Fig. 5.41: Ocean basins for which tropical cyclone frequency is given in Table 5.10 (GRAY, 1978a)

Table 5.8: Tropical cyclone statistics for the period 1958–77. NH, Northern Hemisphere; SH, Southern Hemisphere (GRAY, 1978a)

Year		No. of cyclones			% deviation from 20-yr average	Ratio (NH:SH)
NH	SH	NH	SH	Total		
1958	1958–59	52	25	77	−3	2.1
1959	1959–60	48	21	69	−13	2.3
1960	1960–61	48	22	70	−12	2.2
1961	1961–62	58	23	81	+2	2.5
1962	1962–63	50	30	80	+1	1.7
1963	1963–64	49	23	72	−9	2.1
1964	1964–65	65	19	84	+6	3.4
1965	1965–66	56	22	78	−1	2.5
1966	1966–67	64	16	78	−1	4.0
1967	1967–68	63	28	91	+15	2.2
1968	1968–69	61	23	84	+6	2.6
1969	1969–70	49	23	72	−9	2.1
1970	1970–71	56	26	82	+4	2.1
1971	1971–72	70	27	97	+23	2.6
1972	1972–73	54	35	91	+15	1.5
1973	1973–74	46	28	74	−6	1.6
1974	1974–75	55	19	75	−5	2.9
1975	1975–76	47	29	76	−4	1.6
1976	1976–77	55	30	85	+7	1.8
1977	1977–78	47	20	67	−15	2.3
Total		1093	489	1583		
Average		54.6	24.5	79.1	±8	2.3

Table 5.9: Frequency of Northern Hemisphere tropical cyclone genesis by year and month (GRAY, 1978a)

Year	Jan.	Feb.	Mar.	Apr.	May	June	July	Aug.	Sept.	Oct.	Nov.	Dec.	Total
1958	1	0	0	0	2	5	10	9	11	9	4	1	52
1959	0	0	0	1	2	6	7	11	9	8	2	2	48
1960	0	0	0	1	3	7	6	14	6	8	2	1	48
1961	1	1	1	1	4	5	10	5	14	9	6	1	58
1962	0	1	0	1	3	2	7	11	11	7	4	3	50
1963	0	0	0	1	3	5	6	5	14	11	0	4	49
1964	0	0	0	0	3	4	11	15	12	8	10	2	65
1965	2	2	1	1	4	8	8	8	12	3	4	3	56
1966	0	0	0	2	2	3	9	13	20	5	7	3	64
1967	2	1	1	1	2	4	10	12	12	13	3	2	63
1968	0	0	0	1	2	5	7	17	11	11	6	1	61
1969	1	0	1	1	1	0	7	13	10	9	4	2	49
1970	0	1	0	0	4	6	11	10	9	8	7	0	56
1971	1	0	1	3	7	3	15	11	15	9	4	1	70
1972	1	0	0	1	4	2	9	12	12	6	4	3	54
1973	0	0	0	0	0	5	12	8	8	7	5	1	46
1974	1	0	0	2	4	6	5	14	13	6	4	0	55
1975	2	0	0	0	2	3	6	11	9	8	6	0	47
1976	1	1	0	3	2	7	9	15	10	4	0	3	55
1977	0	0	1	0	3	4	8	4	13	9	4	1	47
Total	13	7	6	20	57	90	173	218	231	158	86	34	1093
Average	0.7	0.3	0.3	1.0	2.9	4.5	8.6	10.9	11.5	7.9	4.3	1.7	54.6

Table 5.10: Frequency of Southern Hemisphere tropical cyclone genesis by year and month (GRAY, 1978a)

Year	Oct.	Nov.	Dec.	Jan.	Feb.	Mar.	Apr.	May	Total
1958–59	1	1	3	5	7	6	2	0	25
1959–60	0	1	4	3	2	7	4	0	21
1960–61	0	1	1	9	7	4	0	0	22
1961–62	0	1	4	6	8	2	2	0	23
1962–63	1	0	4	6	9	5	2	3	30
1963–64	0	1	3	7	3	7	1	1	23
1964–65	0	2	5	4	5	3	0	0	19
1965–66	0	0	3	7	6	6	0	0	22
1966–67	0	1	3	5	1	3	2	1	16
1967–68	0	2	4	8	7	3	4	0	28
1968–69	1	1	3	7	8	2	1	0	23
1969–70	0	1	0	5	6	7	3	1	23
1970–71	1	3	6	4	7	4	1	0	26
1971–72	0	1	6	3	10	3	2	2	27
1972–73	1	3	4	10	6	7	3	1	35
1973–74	1	3	5	7	4	6	2	0	28
1974–75	0	0	2	6	2	5	4	0	19
1975–76	0	4	4	8	5	4	3	1	29
1976–77	1	0	4	8	9	5	3	0	30
1977–78	0	3	4	3	4	4	2	0	20
Total	7	29	72	121	117	93	41	10	489
Average	0.4	1.5	3.6	6.1	5.9	4.7	2.1	0.5	24.5

Table 5.11: Yearly variation of tropical cyclones by ocean basins. SH, Southern Hemisphere; NW Atl., Northwest Atlantic Ocean; NE Pac., Northeast Pacific Ocean; NW Pac., Northwest Pacific Ocean; S. Pac., South Pacific Ocean; Aust., Australia; N. Ind., North Indian Ocean; S. Ind., South Indian Ocean (GRAY, 1978a)

Year	SH	NW Atl.	NE Pac.	NW Pac.	N. Ind.	S. Ind.	Aust.	S. Pac.	Total
1958	1958–59	12	13	22	5	11	11	7	81
1959	1959–60	11	13	18	6	6	13	2	69
1960	1960–61	6	10	28	4	6	8	8	70
1961	1961–62	11	12	29	6	12	7	4	81
1962	1962–63	6	9	30	5	8	17	3	78
1963	1963–64	9	9	25	6	9	7	7	72
1964	1964–65	13	6	39	7	6	9	4	84
1965	1965–66	5	11	34	6	12	7	4	79
1966	1966–67	11	13	31	9	5	5	6	80
1967	1967–68	8	14	35	6	11	9	8	91
1968	1968–69	7	20	27	7	8	7	8	84
1969	1969–70	14	10	19	6	10	7	6	72
1970	1970–71	8	18	23	7	11	12	3	82
1971	1971–72	14	16	34	6	7	14	6	97
1972	1972–73	4	14	28	6	13	12	10	88
1973	1973–74	7	12	21	6	4	16	8	74
1974	1974–75	8	17	23	7	6	10	3	74
1975	1975–76	8	16	17	6	8	16	5	76
1976	1976–77	8	18	24	5	9	12	9	85
1977	1977–78	6	17	19	5	6	7	7	67
Total		176	268	526	121	168	206	118	1583
Average		8.8	13.4	26.3	6.4	8.4	10.3	5.9	79.1

Die Küste, 63 Global Storm Surges (2001), 1-623

In the North Indian Ocean, there are two seasons of cyclone formation in the 5–15° latitude belt: a major period in the autumn associated with the retreat of the southwest monsoon and a minor period in the spring associated with the onset of the monsoon. Note that the Southeast Pacific Ocean and the South Atlantic Ocean are not regions of tropical cyclones. The seasonal location of the intertropical convergence zone (ITCZ) is a favoured region for tropical cyclogenesis.

According to GRAY (1978a, 1978b, 1978c, 1978d), tropical cyclones tend to cluster in time as well as in space. Within a period of 1–2 wk there may be as many as 5–15 tropical cyclones over the globe and then a lull for several weeks. During such active periods there may be as many as two to six times as many cyclones than in the less active periods. GRAY (1978a, 1978b, 1978c, 1978d) attributed this to the influence of the larger scale general circulation of the tropical atmosphere with time scales of 10–20 d.

About 80–85 % of the tropical cyclones originate in or near the poleward side of the ITCZ or the doldrums trough. The remainder occur in the trade winds at some distance from the ITCZ but usually in conjunction with an upper tropospheric trough to their northwest.

There are some anomalous warm core systems belonging to the class of subtropical or semitropical cyclones accounting for about 3–5 % of the tropical cyclones. These originate in the subtropics inside baroclinic regions where stagnant frontal zones exist to the cast of the westerly troughs aloft (e.g. Northwest Atlantic and Northwest Pacific oceans). These mixed type of tropical midlatitude cyclones usually do not generate intense cyclones.

Since tropical cyclones spend most of their lifespan over the warm waters of the tropical oceans, traditional data sources are not dense enough. Aircraft data have contributed significantly. However, for an accurate vertical structure determination, Rawinsonde data are the most pertinent. Since enough synoptic Rawinsonde data are not available, it is necessary to combine the data of different periods for similar weather systems.

Hurricane Movement Over Ocean and Land

Earlier, it was seen that hurricanes are born primarily over oceanic areas and they weaken when they travel over the continents. A numerical model simulation by CHANG and MADALA (1980) showed that hurricanes appear to move into areas of higher sea surface temperature (SST) if the SST gradient is perpendicular to the mean ambient flow vector (MAFV). An area of warmer SST located to the right of MAFV is more favorable for hurricane intensification than an area situated to the left.

SCHWERDT (1978) studied the reduction of the wind field when a hurricane moves from the ocean to over land. Once a hurricane crosses the coast from the ocean to the land its central pressure starts increasing and the wind fields start decreasing, and this so-called filling process is most pronounced in the inner portion of the hurricane.

According to PALMÉN and NEWTON (1969), filling occurs because the heat flux from the land is negligible, which causes a reduction of the excess temperature of the hurricane core. Consequently, the kinetic energy decreases. BERGERON (1954) showed that a reduction in the equivalent potential temperature of the ascending air in the core leads to the filling process. MILLER (1963) showed that surface friction plays a minor role in the filling process.

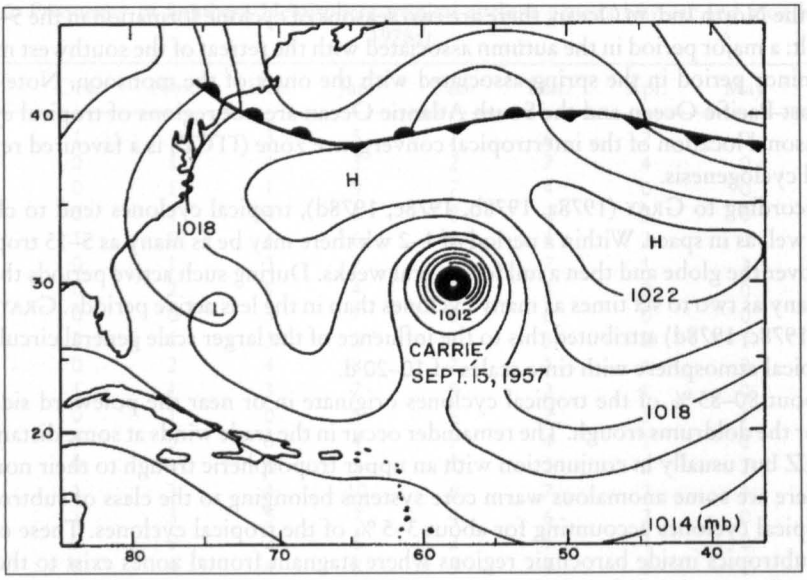

Fig. 5.42: Surface weather chart on September 15, 1957, showing Hurricane Carrie (SIMPSON and RIEHL, 1981)

SIMPSON and RIEHL (1981) defined the habitation layer as the lowest 500 m of the atmosphere. They considered the balance of forces in this layer at a coastal station as a hurricane approaches the station. The centrifugal force C_e and the Coriolis force C_0 are directed outwards, whereas the pressure gradient force Pg and the frictional force F_s are directed inward (perpendicular to the streamline). This leads to an acceleration of the tangential wind component as the air spirals inward. (Figs. 5.42, 5.43, 5.44, 5.45, 5.46, 5.67).

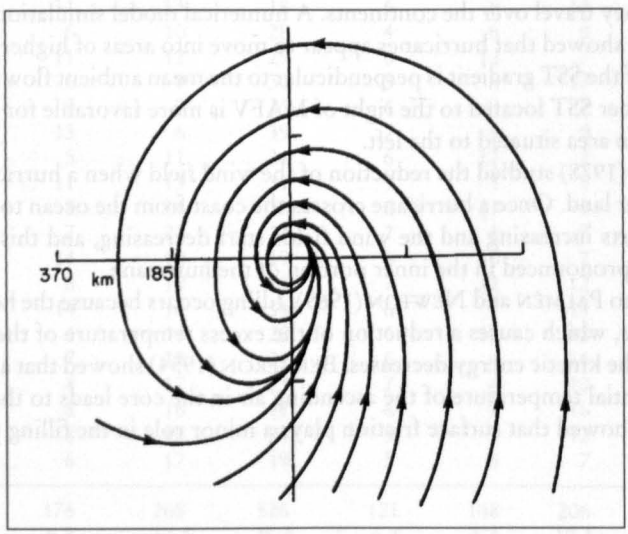

Fig. 5.43: Streamlines showing the circulation in a hurricane (SIMPSON and RIEHL, 1981)

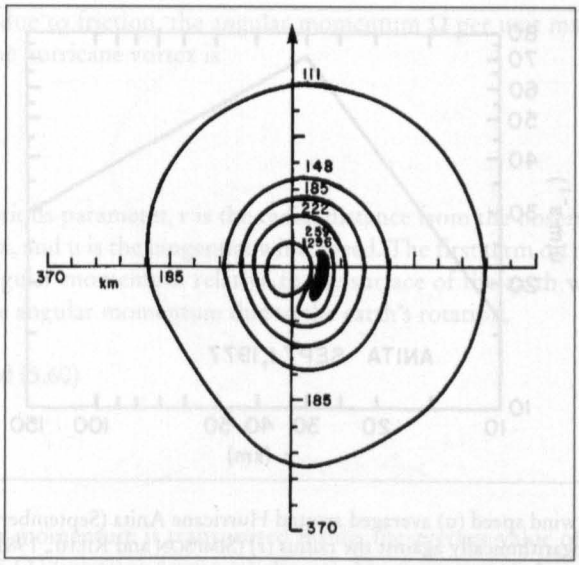

Fig. 5.44: Isotachs of surface wind speed (knots) in an intense hurricane. Black area shows the region of strongest winds (to the right of the eye) (1 knot = 1.852 km · h^{-1}) (SIMPSON and RIEHL, 1981)

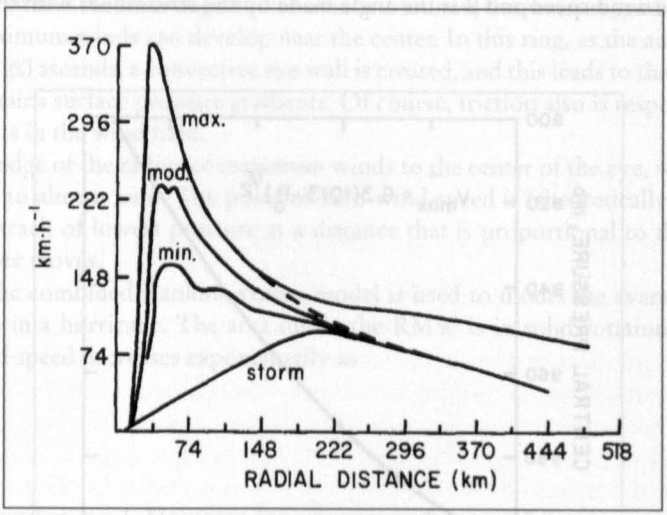

Fig. 5.45: Model of radial profiles of wind speed for three hurricane intensities and for a tropical storm (SIMPSON and RIEHL, 1981)

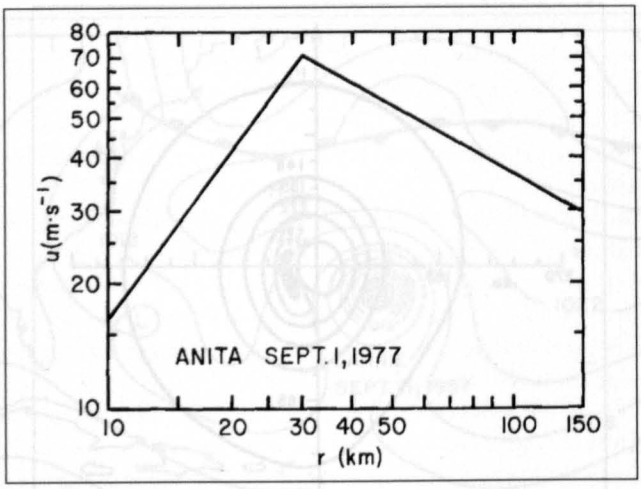

Fig. 5.46: Tangential wind speed (u) averaged around Hurricane Anita (September 1, 1977) and plotted logarithmically against the radius (r) (SIMPSON and RIEHL, 1981)

In a hurricane, mainly the tangential (rotational) component of the wind increases from the periphery of the vortex to the ring of maximum winds (RMW). According to SIMPSON and RIEHL (1981) this ring has a radius of less than 35 km:

$$u = V \cos \beta \tag{5.59}$$

where, V is the wind speed and β is the angle made by the streamlines with the isobars.

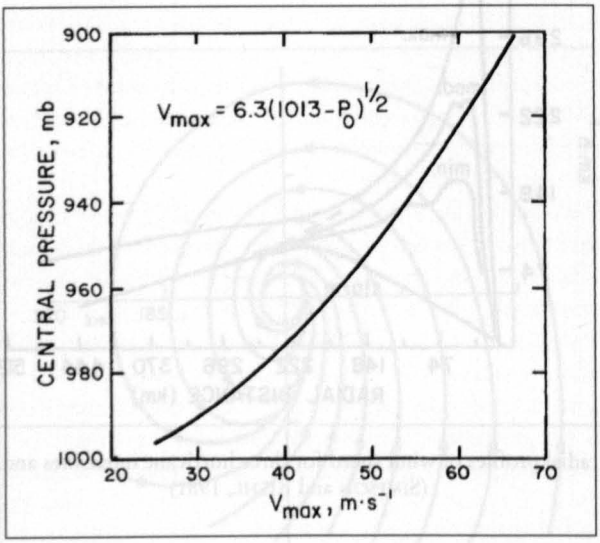

Fig. 5.47: Maximum sustained wind speed versus central pressure for Atlantic hurricanes (SIMPSON and RIEHL, 1981)

Neglecting losses due to friction, the angular momentum Ω per unit mass supplied by the surroundings to the hurricane vortex is

$$\Omega = ur + \frac{fr^2}{2} \tag{5.60}$$

where, f is the Coriolis parameter, r is the radial distance from the observation point to the centre of the vortex, and u is the tangential wind speed. The first term on the right side of eq. (5.60) gives the angular momentum relative to the surface of the earth whereas the second term represents the angular momentum due to the earth's rotation.

From eq. (5.59) and (5.60)

$$u = \frac{\Omega}{r} - \frac{fr}{2} \tag{5.61}$$

As the angular momentum is transported inside, the average value of u increases as can be seen from eq. (5.61) (ignoring frictional effects). The maximum value of u occurs for cyclostrophic balance (i.e. when the pressure gradient force balances the centrifugal plus Coriolis forces) and when β of eq. (5.59) tends to zero.

In principle, the increase of u with decreasing r would create centrifugal forces that would far exceed the pressure gradient forces, and the air should spiral outward towards higher pressure. However, surface friction reduces the value of Ω steadily and this outward spiralling tendency is offset. Hence, surface friction plays a dual role. First of all, it permits a crossing angle between the streamlines and isobars so that air from the surroundings is drawn towards the vortex center by pressure gradient forces. Second, it reduces the imported angular momentum so that the centrifugal forces cannot dominate the pressure gradient forces and a radius of maximum winds can develop near the center. In this ring, as the air (drawn from the surroundings) ascends, a convective eye wall is created, and this leads to the central warm core that maintains surface pressure gradients. Of course, friction also is responsible for the creation of gusts in the wind field.

From the edge of the radius of maximum winds to the center of the eye, wind decreases monotonically to almost zero. The point of zero wind speed is (theoretically) displaced to the left of the track of lowest pressure at a distance that is proportional to the speed with which the vortex moves.

Usually, the combined Rankine vortex model is used to model the average horizontal wind structure in a hurricane. The area inside the RMW is in solid rotation. Outside the RMW the wind speed decreases exponentially as

$$u = \frac{\text{cons tan t}}{r^x} \tag{5.62}$$

For a Rankine vortex, x = 1. However, for a hurricane, $0.4 < x < 0.8$.

Above the first few hundred meters, the strongest winds of a hurricane do not vary much up to 4–5 km of height. The wind speed variation with height in tropical cyclones is shown in Fig. 5.48.

The international standard for sustained winds is the average speed for a 10-min period. In the United States the sustained wind is a 1-min average. For extreme winds in the United

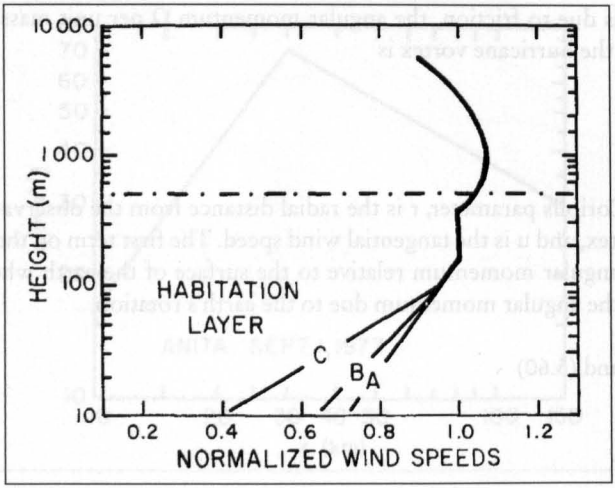

Fig. 5.48: Model of wind speed variation with height in tropical cyclones. Speeds are normalized with reference to wind speeds measured by aircraft in the 150- to 300-m layer. A, over water; B, over land; C, profile for 1/7-power law (BATES, 1977)

States the unit of measurement is the fastest mile (the highest speed at which 1 mi of wind passes the anemometer).

In the U. S. National Weather Service and in the U. S. Army Corps of Engineers, the ideas about Probable Maximum Hurricane (PMH) and Standard Project Hurricane (SPH) originated in the 1950s (e.g. GRAHAM and NUNN, 1959). The PMH is defined as a hypothetical hurricane having that combination of values of meteorological parameters that will make it the most severe that can probably occur at a particular coastal location. The SPH is defined as a hypothetical hurricane with the most severe combination of values of hurricane parameters reasonably characteristic of a specified geographic location, thus excluding extremely rare combinations (SCHWERDT, 1976; MOGOLESKO, 1976).

5.3.2 Prediction of Movement and Intensity

Modelling Of Hurricane Formation and Intensification

According to GRAY (1978a, 1978b) little effort has gone into numerically modelling tropical cyclogenesis. OOYAMA (1964), CHARNEY and ELIASSEN (1964), OGURA (1964), KUO (1965) and several later authors modelled the intensification of hurricanes. The low level winds for different classes of tropical disturbances were deduced from Rawinsonde composite studies. These winds are much smaller than the initial cyclone strength assumed by numerical modellers, as summarized in Table 5.13. According to GRAY (1978a, 1978b, 1978c, 1978d) the transformation of a disturbance to a cyclone has yet to be realistically modelled.

GRAY (1978a, 1978b, 1978c, 1978d) classified the disturbance stages and gave estimates of central pressure and maximum sustained surface winds. These are shown in Table 5.13. Even in a stage 6 cyclone (i.e. typhoon) approximately 50 % of the mass inflow at 4° radius takes place above the 900-mb layer. Hence, there is significantly more mass inflow than can be accounted for by boundary layer processes. In fact, mass convergence could occur in a layer as high as 400 mb.

Table 5.12: Some numerical modeling papers on tropical cyclone intensification and their assumed initial lower tropospheric cyclone strength (GRAY, 1978a)

Modellers	Assumed initial maximum wind velocity ($m\ s^{-1}$) and radius (km) of maximum wind		Vortex vorticity inside the radius of maximum winds ($10^{-6} \cdot s^{-1}$)	Type of vortex
KUO (1965)	10	141	142	Symmetrical
YAMASAKI (1968)	4.7	100	94	Symmetrical
OOYAMA (1969)	10	50	400	Symmetrical
MILLER (1969)	10	200	100	Real vortex
ROSENTHAL (1970)	7	250	56	Symmetrical
SUNDQVIST (1970a, 1970b)	15	200	150	Symmetrical
CARRIER (1971)	21	50	840	Symmetrical
ANTHES et al. (1971a, 1971b)	18	240	150	Asymmetrical
ANTHES (1972)	18	240	150	Asymmetrical
MATHUR (1972)	15	200	150	Asymmetrical
HARRISON (1973)	~10	~120[a]	~170	Asymmetrical
KURIHARA and TULEYA (1974)	12	200	120	Symmetrical
CESELSKI (1974)	17	~100–150	~200	Real vortex
KURIHARA and TULEYA (1974)	12	200	120	Symmetrical
ANTHES (1977)	18	240	150	Symmetrical
ROSENTHAL (1978)	7.2	220	65	Symmetrical

NOTE: Typical precyclone cloud cluster vorticity is 10×10^{-6} to $15 \times 10^{-6} \cdot s^{-1}$.
[a] Estimated from initial height field.

Table 5.13: Tropical disturbance classification stages and surface pressure and wind estimates at these various stages; two classes of nonintensifying disturbance and six stages of disturbance-to-cyclone intensification are shown. (GRAY, 1978a)

Disturbance classification	Stage	Estimated minimum sea level pressure (mb)	Estimate of maximum sustained surface winds ($m \cdot s^{-1}$)
General class of nondeveloping disturbances	0	1008	8
Nondeveloping disturbances of summer in cyclone genesis region	00	1008	8
Initial cluster	1	1007	8
Pre-typhoon cluster	2	1005	10
Genesis	3	1003	12
Intensifying	4	1000	18
Tropical storm (980–1000 mb)	5	990	25
Typhoon (950–980 mb)	6	965	40

Movement of Tropical Cyclones: Prediction and Modelling

Several different techniques are being used for predicting the tracks of tropical cyclones: empirical, statistical, and dynamical. Empirical techniques will be considered first. According to HEBERT (1979), these may be further classified into three categories:

(a) persistence and climatology,
(b) synoptic and
(c) satellite.

These techniques can be used for prediction of the hurricane track for 12–24 h in advance. Any extrapolation beyond 24 h will result in large errors, except possibly in the deep easterlies of the tropics.

In the persistence technique, one simply extrapolates linearly the last track, assuming uniform speed and no change of direction. One can use a higher order persistence forecast by allowing for variation of speed of movement and direction of the hurricane in the past 12–24 h. The simplicity of this technique is its chief advantage. It is obvious that errors could occur if the persistence assumption does not hold.

In a climatological forecast one makes use of the knowledge of the temporal and spatial frequency of past hurricanes in given grid areas (e.g. 2.5° latitude-longitude squares and time scales up to 5 d). This method works well when the frequency of occurrence is great. It fails with increasing latitude (due to recurvature) as well as for untypical situations. Other time it fails is when a bimodal structure is present.

In the persistence plus climatology forecasts (BELL, 1962; AOKI, 1979) one uses the formula np + mC where p and C represent the persistence and climatology, respectively, and n and m are weighting factors. Usually, n = m = 0.5 is used. AMADORE (1972) gave different weightings to get latitude and longitude components separately for the tropical cyclones east of the Philippines. However, according to HEBERT (1979), similar attempts for the South China Sea region did not significantly improve the results.

In the synoptic technique, the main assumption is that the air mass in which the tropical cyclone is embedded is homogeneous. In the surface geostrophic steering method, the zonal (east-west) and the meridional (north-south) components of the hurricane movement are determined by estimating (from the synoptic charts) the pressure gradient (millibars per degree of latitude) across the storm. Since the surrounding air mass is not uniform, one must apply a correction to the pressure gradient to account for the nonhomogeneity. The main advantage of this technique lies in the fact that almost all forecast centres have surface pressure analysis charts.

In the control point method (CHIN, 1970), which has been in use for several years at the Hong Kong Observatory, one makes use of the observed high correlation between the wind direction at certain locations in the midtroposphere and the direction of movement of the tropical cyclone. The disadvantage is that in areas of sparse data, midtropospheric analyses might be difficult to make.

In predicting the movement of cyclones, one should also consider the so-called Fujiwhara effect (FUJIWHARA, 1921) in which two vortices close to each other will rotate about a common point located on the line joining their centres.

Next, satellite techniques, which are playing an ever-increasing role in the prediction of the tracks of cyclones, will be considered. The basic principle is to relate past changes in cloud features to future changes in the direction of motion.

FETT and BRAND (1975) used six identifiable cloud patterns and extrapolated the rotation of one or more of these patterns during the previous 24 h to calculate the change in the motion direction for the next 24 h. In making this extrapolation, an analogy of the relationship of the turning of a tropical cyclone to its hyperbolic point was used.

The method that is occasionally used in the Australian Bureau of Meteorology was developed by LAJOIE and NICHOLLS (1974). From available satellite pictures, they identify certain cloud features and based on these, extrapolation is made for the next 12 h regarding

the change of direction of motion of the cyclone. The two main principles involved are as follows: tropical cyclones frequently move in the direction of the line connecting their centers to the most developed cumulonimbus cluster at or near the downstream end (i.e. in a cyclonic direction of the inflow current) of the outer cloud band and tropical cyclones usually do not move towards a cumulonimbus-free sector.

The advantage of the satellite techniques is that they can be used in regions where conventional data are sparse. The disadvantages are difficulty in obtaining good satellite pictures and the subjectivity involved in interpreting them. Nevertheless, certain simple concepts are useful in the prediction of the tracks. For example, RAMAGE (1973) noted the extent of cloudiness along the track of a tropical cyclone. In Japan, substantial observations exist to show that the successive positions of the spiral cloud band correlate well with the movement of recurving typhoons.

Cyclones moving towards the west sometimes recurve towards northeast after interaction with upper air troughs in the westerlies. CHAN (1978), based on a study of recurring typhoons in the western part of the North Pacific Ocean, suggested that the following two parameters, which can be determined from satellite imagery, can be used to estimate the recurvature: D/d, where D is the diameter of the central dense overcast of the tropical cyclone and d is the average width of the cloud band associated with the interacting trough, and Θ, which is the angle between the axis of the cloud band and the latitude of the tropical cyclone center. If $30° \leq \Theta \leq 40°$ and $D/d < 1.5$, then it is highly probable that a tropical cyclone will recurve.

Statistical Techniques of Track Prediction

Following NEUMANN (1979), statistical models will be discussed. These are broadly divided into two categories: models based on analogs and models based on regression equations. Regression equation models can be further classified into (i) models using predictors based on climatology and persistence, (ii) models that include, but are not limited to, predictors derived from observed synoptic data, and (iii) models that include, but are not limited to, predictors derived from numerically forecasted data. Models of type (i) are referred to as simulated analog, models of type (ii) are referred to as classical models (or statistico-synoptic), and models of type (iii) are called statistical-dynamical models.

The basic principle involved in these models is the recognition of the fact that temporal and spatial analyses of tracks reveal repetitiveness and close association with identifiable synoptic patterns.

The advantage of the analog method is that it is usually the first available forecast for the tracks. Its disadvantage is that it works well only for typical situations. Next, the regression methods will be considered. RIEHL (1956) gave the first objective technique for predicting the movement of tropical cyclones. In this method, known as the Riehl-Haggard technique, one makes use of the steering principle, namely that the tropical cyclone's movement speed is proportional to the speed of the vertically integrated flow surrounding the vortex. The 500-mb level was used for approximating this flow. This technique was originally used for the Atlantic hurricanes.

Dynamical Methods for Predicting Hurricane Movement

Following PELISSIER (1979), the numerical models that were developed for predicting hurricane motion will be considered. The numerical modelling effort has been slow until the 1970s principally because tropical storms mainly occur over the data-sparse areas of the tropical oceans, and it is difficult to provide the initial state of the atmosphere. From a grid resolution point, the scale of the intense part of the tropical cyclone is small compared with the synoptic weather disturbances. Generally, prediction of the tracks of tropical cyclones is more successful than prediction of the intensification because the movement of the storm is mainly related to the steering current in which the storm is embedded.

SANDERS and BURPEE (1968) originally developed a barotropic model, referred to as SANBAR, which was modified by PIKE (1972). In this model the tropical cyclone track is predicted based on the track of minimum stream function and maximum vorticity centers. On a Mercator projection using a grid size of 1.5° and extending from the equator to 55° N and from 36.5° W to 123.5° W and using a time step of 30 min, forecasts are made up to 72 h in advance. The initial observations are averaged over the 1000- to 100-mb layer.

After specifying the initial winds, the nondivergent part of the wind field is calculated through a relaxation of the stream function ψ in the interior of the grid using the relation

$$\nabla^2\psi = \frac{\partial v}{\partial x} - \frac{\partial u}{\partial y} + \frac{u \tan(\text{latitude})}{R_E} \tag{5.63}$$

where, u and v are the eastward and northward components, respectively, of the hurricane motion and R_E is the radius of the earth. One must specify the component of the wind parallel to the boundaries. Then, using the barotropic vorticity equation

$$\left(\nabla^2 - M\right)\frac{\partial\psi}{\partial t} = J\left(f + \nabla^2\psi, \psi\right) \tag{5.64}$$

one can determine ψ where J is the Jacobian, ∇^2 is the horizontal Laplacian, and M is the Helmholtz coefficient.

One can identify the storm center with a local minimum in x~ or a maximum in (or as an average between these two positions). Usually, the storm is replaced by an idealized circularly symmetric vortex defined by

$$v_\theta = 0.72 v_{max}\left\{\sin\left[\pi\left(\frac{r}{r_m}\right)\right]\right\}^{\left(\frac{\ln 0.5}{\ln r_c / r_m}\right)}{}^{1.5} \tag{5.65}$$

where, v_θ is the symmetric tangential wind field.

The Japan Meteorological Agency developed a balanced barotropic model for typhoon track prediction northward of 20 % using a 51 x 15 grid with a mesh length of 381 km at 60° N. At least three types of systematic errors appear: forecast positions for low latitude storms are occasionally poor due to a westward bias in the predicted tracks, the predicted speed of movement is usually smaller than observed values, and the predicted recurvature is usually less than the observed recurvature.

Table 5.14: Frequency distribution of direction using the balanced barotropic model. The angular intervals listed are the ranges of absolute differences between predicted and observed directions of displacement. Data listed under 24 and 48-h forecast periods are the number of typhoons that exhibited these directional deviations (PELISSIER, 1979)

Angular interval (degrees)	24-h forecast period	48-h forecast period
0–5	10	8
6–10	12	7
11–20	13	9
21–30	5	10
31–45	7	3
45	7	7

Table 5.15: Same as Table 5.14, except this is for eastward moving typhoons (PELISSIER, 1979)

Angular interval (degrees)	24-h forecast period	48-h forecast period
0–5	11	15
6–10	14	8
11–20	16	10
21–30	10	14
31–45	5	8
45	3	5

Table 5.16: Errors in predicted speed of movement relative to recurvature point. Overrun No. indicates number of typhoons that moved slower than the forecast. *R*, actual typhoon displacement; *F*, prediction by the balanced barotropic model (PELISSIER, 1979)

Typhoon position	24-h forecast period			48-h forecast period		
	Total No.	Overrun No.	$\frac{\lvert R-F\rvert}{R}$	Total No.	Overrun No.	$\frac{\lvert R-F\rvert}{R}$
Before recurvature	42	16	0.406	38	14	0.341
Near recurvature	45	13	0.334	34	12	0.498
After recurvature	20	0	0.340	9	0	0.379
Total (mean)	107	29	(0.381)	81	26	(0.401)

In this model the initial stream function ψ is determined from the geopotential by solving the balance equation

$$\nabla\cdot(f\nabla\psi)+2\left(\frac{\partial^2\psi}{\partial x^2}\frac{\partial^2\psi}{\partial y^2}-\frac{\partial^2\psi}{\partial x\partial y}\right)=\nabla^2\psi \qquad (5.66)$$

where, (Φ is the geopotential and f is the Coriolis parameter. Using ARAKAWA's (1966) finite-difference schemes, the equation is integrated in time. Based on the data at 00:00 and 12:00 GMT, forecasts are issued for 48 h in advance, twice daily.

The frequency distribution of direction errors for westward moving typhoons is shown in Table 5.14. In this table, the first row contains the ranges of absolute differences between observed and predicted directions of displacements. One can see that there is no directional bias in the forecast. The frequency distribution of the direction errors for eastward moving typhoons is shown in Table 5.15. The errors in the forecast speed of the hurricane are classified in Table 5.16 according to the location relative to the point of recurvature. The term "overrun" means the number of typhoons that moved slower than predicted. Usually, this happens before recurvature but never afterwards.

A primitive equation model is considered next. The Fleet Numerical Weather Center (FNWC) at Monterey, C-A, and the Joint Typhoon Warning Center (JTWC) at Guam use a primitive equation model referred to as the coarse mesh grid model (CMG), which is a simplified version of a more elaborate triple-nested grid model (HINSMAN, 1977). The primitive equations are expressed in the pressure coordinates as follows:

$$\frac{\partial u}{\partial t} = -L(u) + fv - M\frac{\partial \phi}{\partial x} + \frac{\partial \tau_{xx}}{\partial x} + \frac{\partial \tau_{yx}}{\partial y} \tag{5.67}$$

$$\frac{\partial v}{\partial t} = -L(v) - fu - M\frac{\partial \phi}{\partial y} + \frac{\partial \tau_{xy}}{\partial x} + \frac{\partial \tau_{yy}}{\partial y} \tag{5.68}$$

$$\frac{\partial \theta}{\partial t} = -L(\theta) \tag{5.69}$$

$$\frac{\partial \phi_{1000}}{\partial t} = -L(\phi_{1000}) \tag{5.70}$$

$$\frac{\partial w}{\partial p} = -M^2\left[\frac{\partial}{\partial x}\left(\frac{u}{M}\right) + \frac{\partial}{\partial y}\left(\frac{v}{M}\right)\right] \tag{5.71}$$

$$\frac{\partial \phi}{\partial p} = \phi C_p \frac{\partial}{\partial p}\left(\frac{p}{1000}\right)^{R/C_p} \tag{5.72}$$

where,

$$L(S) = M^2\left[\frac{\partial}{\partial x}\left(\frac{u_S}{M}\right) + \frac{\partial}{\partial y}\left(\frac{v_S}{M}\right)\right] + \frac{\partial}{\partial p}(w_S) \tag{5.73}$$

The region of computation is like a channel with cyclic boundary conditions in the east and west and free-slip conditions on the north and south walls. In the vertical there are three layers. A movable grid is placed over the tropical cyclone so that initially the storm is in the lower central portion of the grid, which covers a span of 56° of longitude and 48° of latitude, with a mesh interval of 2°. An objective analysis of the flow fields at the 850-, 700-, and 200-mb levels, as well as the temperature at the 850-mb level, serve as input. Using a time step of 10 min, the model is integrated in time. The errors in the predicted track for the western and eastern Pacific are shown separately and together in Table 5.17. The errors are in kilometres and the numbers in parentheses are the cases studied.

At the National Meteorological Center, a multilevel nested grid model was developed (HOVERMALE and LIVEZEY, 1978). This is referred to as the moving fine mesh (MFM) model.

This model appears to be unique in the sense that a nested high-resolution grid cantered over the tropical cyclone moves during the numerical integration through a coarse outer grid. The error analysis for the forecasts based on this model is given in Table 5.18 and comparison is made with the errors from other models. For a review of the forecast errors using barotropic models (SANDERS et al., 1978). HOPE and NEUMANN (1978) provided a survey of tropical cyclone models available worldwide. ELSBERRY (1979) summarized the three-dimensional models that are available for hurricane track prediction. In his survey he omitted the barotropic models. Since it is almost certain that all future forecasts will be made with baroclinic models, these three-dimensional models will be briefly reviewed. The features of some of the baroclinic models presently available are listed in Table 5.19. These models (except the FNWC-TCM) are capable of resolving the inner structure of the tropical cyclone. Although a 60-km grid such as that used by the NMC and NRL-NEPRF models can resolve the primary interaction between the vortex and the steering current, to predict intensification the inner core of the typhoon must be resolved. Since it is impractical to cover the whole region of the typhoon with a fine grid, one can use a nested grid, the fine grid having a resolution of 10 km. Also, this inner grid must be moved with the storm. At present, the JMA model has these capabilities, although the inner grid size is 36 km.

Table 5.17: Average forecast errors (km) for 1976 for the U. S. Navy primitive equation tropical cyclone prediction model (CMG). Number of cases in parentheses (PELISSIER, 1979)

Area	24-h forecast period	48-h forecast period	72-h forecast period
Western Pacific	287 (65)	480 (57)	693 (43)
Eastern Pacific	263 (18)	387 (15)	724 (15)
Both together	283 (81)	461 (72)	702 (58)

Table 5.18: Mean vector errors (km) of the MFM, official forecasts, and other operational objective techniques based on statistical, climatological, and persistence methods (homogeneous sample) for Hurricane Belle of August 7–8, 1976. MFM, movable fine mesh; NHC, National Hurricane Center; NHC-67, National Hurricane Center's 1967 model. For a description of SANBAR and CLIPER, see text (HOVERMALE and LIVEZEY, 1978)

Forecast period (h)	MFM	Official	NHC-67	NHC-72	NHC-73	SANBAR	CLIPER
12	124	87	67	72	67	86	76
24	213	185	200	226	152	228	204
36	215	–	241	365	270	426	454
48	280	404	311	507	369	644	748

Two types of boundary conditions are presently used in these models. In the one-way (OW) type, no feedback is allowed from the tropical cyclone to the hemispherical model. Note that the JMA nested grid model has a two-way (TW) interaction boundary condition for the inner grids. The statistics at 24 and 48 h for selected 1977 typhoons for official (JTWC), NMC-MFM, and FNWC-TCM models are shown in Table 5.20.

Table 5.19: Characteristics of several baroclinic models being applied for prediction of tropical cyclone motion based on operational data. NMC, National Meteorological Center (U.S.A.); MFM, movable fine mesh; FNWC, Fleet Numerical Weather Center (Monterey, CA); TCM, tropical cyclone model; NRL, Naval Research Laboratory; NEPRF, Naval Environmental Prediction Research Facility; PSU, Pennsylvania State University; NPS, Naval Post Graduate School (Monterey, CA); JMA, Japan Meteorological Agency; MNG, multiple-nested grid (ELSBERRY, 1979)

Agency-model	Vertical coordinate	No.of layers	Grid size (km)	No. of points	Relocatable grid	Lateral boundary conditions[a]
NMC-MFM	σ	10	60	50 x 50	Yes	OW
FNWC-TCM	ρ	3	205	32 x 24	No	OW
NRL-NEPRF	σ	5	60	51 x 51	No	OW
PSU-NPS	σ	5	120	40 x 40	No	OW
JMA-MNG	σ	3	291	31 x 31	No	OW
			145	31 x 31	Yes	TW
			73	31 x 31	Yes	TW
			36	31 x 31	Yes	TW

[a] OW, one-way interaction; TW, two-way interaction

Table 5.20: Track error (km) statistics at 24 and 48 h for selected 1977 typhoons for official (JTWC), NMC-MFM, and FNWC-TCM. JTWC, Joint Typhoon Warning Center, Guam (ELSBERRY, 1979)

Typhoon	Official		NW-MFM		FNWC-TCM	
	24 h	48 h	24 h	48 h	24 h	48 h
Vera-1	178	107	294	289	106	111
Ivy	226	472	109	248	–	–
Dinah-1	181	778	356	559	152	285
Thelma	159	707	96	148	146	574
Jean	126	578	339	441	–	–
Dinah-2	206	437	56	385	250	270
Babe	583	–	282	885	437	–
Dinah-3	204	693	115	324	52	350
Vera-2	300	444	254	181	143	52
Gilda	243	407	183	580	100	376
Babe	191	782	217	198	196	726
Homogeneous	250	544	206	333	176	343
Sample (N)		9	8			

One important data source should be mentioned. The National Climatic Center's (Asheville, NC) magnetic tape deck 993 contains 12-h tropical storm movements for all ocean basins (CRUTCHER et al., 1978) for the period 1886–1975, and this file is continually being updated. CRUTCHER (1971a, 1971b) and CRUTCHER and QUINLAN (1971) used the bivariate normal elliptical distribution as a model for the statistics of the distributions of hurricane movements. CRUTCHER et al. (1978) deduced tropical storm accelerations based on the data contained in this vast file.

Forcasting Tropical Cyclone Recurvature

Most of the forecast errors associated with storm track prediction occur when the cyclones turn (or recurve). CHAN et al. (1980) studied tropical cyclones in the West Indies area for the period 1961–77 using compositing. These studies indicated that through an observation of certain parameters around a tropical cyclone (e.g. wind rotation, vertical wind shear between 200 and 900 mb, or a gradient of tropospheric mean temperature), better forecasts for 24–36 h ahead could be made. The basis for this statement is the fact that significant differences exist in the large-scale wind fields at 200-, 500-, and 900-mb levels for left-turning, straight-moving, and right-turning cyclones.

This study was limited to those cyclones west of 55° W and with maximum sustained winds of at least 18 m · s^{-1}. Three categories are defined as follows (Fig. 5.49):

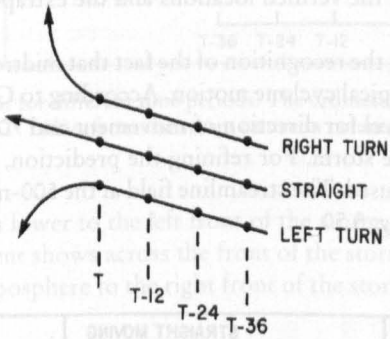

Fig. 5.49: Idealized picture of the three turn classes of tropical cyclones and of the time periods (hours) prior to the turn (CHAN et al., 1980)

Table 5.21: Average 24-h official tropical cyclone track forecast errors (km) issued by the National Hurricane Center, Miami. T, time when the storm begins to turn (CHAN et al., 1980)

Turn classification	T – 24	T	T + 24
Left turn (10 cases)	235	289	206
Straight (23 cases)	148	169	196
Right turn (22 cases)	178	324	239
Special right turn (16 cases)	148	417	245

Table 5.22: Directional deviation (degrees) of the mean 24-h forecast position made at turn time from the mean verifying position and the mean extrapolated track. A positive number means the forecast position is to the right of the verifying position of the extrapolated track (CHAN ET AL., 1980)

Turn classification	From mean extrapolated track	From mean verifying position
Left turn	21	50
Straight	9	11
Right turn	2	–38

$$\begin{aligned} &\text{Left-turning:} && D(T+12) - D(T) < -20 \\ &\text{Straight-moving:} && -10° < D(T+12) - D(T-12) \\ &\text{Right-turning:} && D(T+12) - D(T) > 20° \end{aligned} \qquad (5.74)$$

where, D is the direction of movement of the storm at a standard time T (00:00 or 12:00 GMT). A total of 16 left-turning, 33 straight-moving, and 28 right-turning storms were selected for this study.

The 24-h forecasts given by the National Hurricane Center were analysed for each case at three time periods: (a) 24 h before turn time, i.e. T – 24, (b) at turn time T, and (c) 24 h after turn time, i.e. T + 24. The forecast errors are listed in Tab 5.21. The special right-turn class is for those cases with an error greater than 350 km. The average directional deviation of the forecast locations from the verified locations and the extrapolated tracks are given in Table 5.22.

The basis for this study is the recognition of the fact that midtropospheric wind patterns have a strong influence on tropical cyclone motion. According to GEORGE and GRAY (1977), 500 mb is the best steering level for direction of movement and 700 mb is the best level for the speed of movement of the storm. For refining the prediction, flow fields at 900-, 700-, 500-, and 200-mb levels were used. The streamline field at the 500-mb level for the three classes of cyclones is shown in Fig. 5.50.

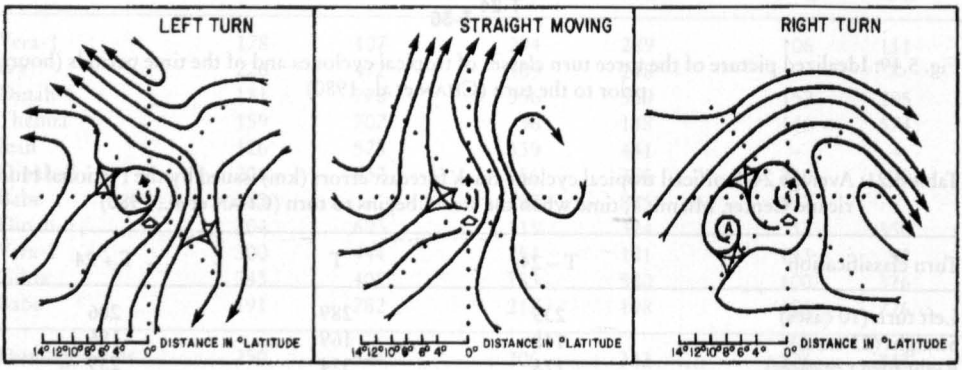

Fig. 5.50: Streamlines (500 mb) for the three turn cases shown in Fig. 5.49, at turn time. Open arrows indicate the instantaneous direction of storm motion. Solid arrows indicate the movement of the storm during the next 12 h (CHAN et al., 1980)

The vertical wind shear for these three classes is shown in Fig. 5.51. Here, V_P represents the wind component parallel to the track and V_N is the wind component perpendicular to the track. It can be seen from this diagram that usually the shear (i.e. V_P at 200 mb minus V_P at 900 mb) is greater than 5 m · s^{-1} for left-turning tropical cyclones, is in the range of – 5 to 5 m · s^{-1} for straight-moving storms, and is less than - 5 m · s^{-1} for right-turning cyclones.

Sometimes it may not be possible to derive satellite winds at the 900- and 200-mb levels because of extensive cloud cover. In these situations, the satellite sounder (which can measure tropospheric difference) could be used. Generally, for left-turning storms the mean tro-

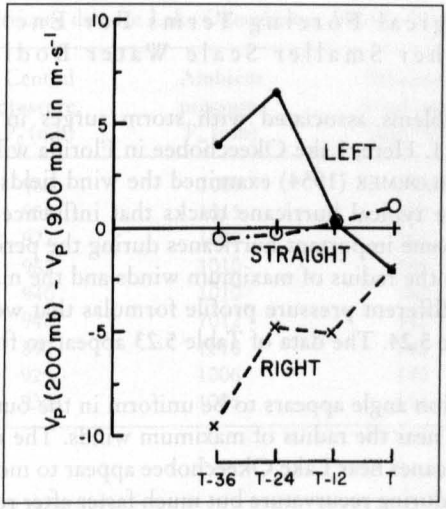

Fig. 5.51: Vertical wind shear for different time periods. The ordinate is the value of the average vertical wind shear within 7–11° radius from the storm centre in octants 1 and 5 (CHAN et al., 1980)

pospheric temperature is lower to the left front of the storm. For straight-moving storms a weak temperature gradient shows across the front of the storm. Right-moving storms indicate a relatively cold troposphere to the right front of the storm.

Project Stormfury

Project Storm fury is a scientific program aimed at studying the structure and dynamics of tropical cyclones and the possibility of modifying them, e.g. through cloud-seeding experiments (SHEETS and LASEUR, 1978). The project formally began in 1962, although some initial seeding experiments were done in 1961. These experiments are designed to effect a reduction in the maximum wind speeds in cyclones through changing the location of the energy released near the cyclone's centre. It is well known that the source of energy for a tropical cyclone is the latent heat released during convective overturning of the atmosphere. The active convective area in which updrafts of 10–20 m · s^{-1} occur is less than 1 % of the area of the hurricane. Hence, one must modify only a small area of the hurricane to change its characteristics. The dynamics of the modification through seeding is explained by SHEETS and LASEUR (1978, p. 281) as follows:

Injection of silver iodide particles into the upper portion of these clouds causes the droplets to freeze, releasing the latent heat of fusion. This additional heat causes that portion of the cloud to be warmer and thereafter lighter than the surrounding air and thus triggers an increase in the ascending flow. As the air rises, it expands and cools, and water vapour condenses or sublimates, releasing considerably more latent heat. The result is that the seeded cloud grows to the outflow level, providing a new convective conduit that intercepts the inflowing low level air. The result is that a new eye wall is formed at a greater distance from the storm centre than the initial eye wall.

The tests on Hurricane Debbie of 1969 showed that winds could be reduced by 15–30 %. For experiments on typhoon modification, see World Meteorological Organization (1975) report No. 408.

5.3.3 Meteorological Forcing Terms For Enclosed Lakes and other Smaller Scale Water Bodies

Meteorological problems associated with storm surges in the Great Lakes were considered in section 7. 1. Here, Lake Okeechobee in Florida will be used as an example of an enclosed lake. SCHLOEMER (1954) examined the wind fields over Lake Okeechobee due to hurricanes. Some typical hurricane tracks that influence this lake are shown in Fig. 5.52. The dates of some important hurricanes during the period 1925–50 are listed in Table 5.23 together with the radius of maximum winds and the maximum wind speed and the pressure field. Ten different pressure profile formulas that were used by SCHLOEMER (1954) are listed in Table 5.24. The data of Table 5.23 appear to fit the second equation of Table 5.24.

The average deflection angle appears to be uniform in the outer portion of the storm, and it decreased rapidly near the radius of maximum winds. The most common deflection angle was 35°. The hurricanes near Lake Okeechobee appear to move with a speed of about 16 km · h^{-1} prior to and during recurvature but much faster after recurvature. However, the maximum winds appear to occur before recurvature. Hurricane winds over lake Okeechobee for a synthesized storm at 0, 1 and 2 h are shown in Fig. 5.53. Notice the changes in pattern that could occur even in a 1-h time interval.

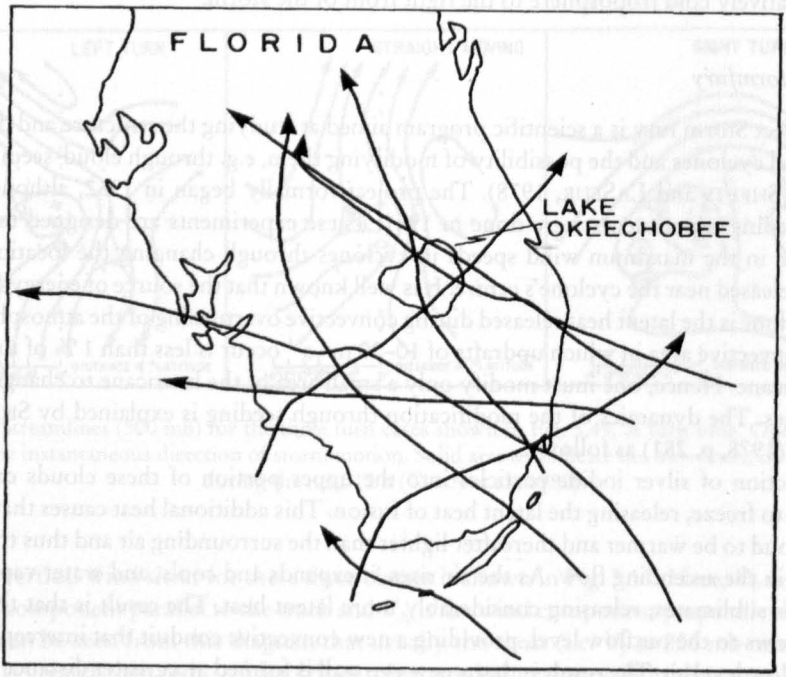

Fig. 5.52: Typical hurricane tracks over and near Lake Okeechobee, Florida (SCHLOEMER, 1954)

Table 5.23: Hurricane data for Lake Okeechobee, Florida (SCHLOEMER, 1954)

Date of hurricane	Central pressure, P_0 (mb)	Ambient pressure, P_∞ (mb)	Maximum wind speed ($km \cdot h^{-1}$)	Radius of maximum winds (km)
Sept. 18, 1926	960	1009	199	28
Sept. 16–17, 1928	955	1015	185	43
Sept. 2–3, 1935	977	1008	163	27
Sept. 15–16, 1945	962	1010	185	24
Sept. 17, 1947	940	1010	180	37
Sept. 21–22, 1948	946	1012	140	30
Oct. 5, 1948	892	1010	142	51
Aug. 26–27, 1949	929	1006	140	37
Oct. 17–18, 1950	935	1005	117	21

Table 5.24: Ten different forms used to approximate $(P - P_0)/(P_\infty - P_0)$ in a hurricane. Here, P is the pressure at a distance r from the centre, P_0 is the central pressure, and P_∞ is the ambient pressure. Parameters n, i, and j must be determined empirically (SCHLOEMER, 1954)

(1)	$1 - e^{-nri}$	(6)	$\frac{2}{\pi} \arctan \frac{1}{nr^i}$
(2)	$e^{-n/ri}$	(7)	$\frac{2}{\pi} \operatorname{arc\,cot} \frac{1}{nr^i}$
(3)	$\frac{1}{1 + 1/nr^i}$	(8)	$\frac{2}{\pi} \operatorname{arc\,sec} (1 + nr')$
(4)	$\frac{1}{(1 + 1\,nr)^j}$	(9)	$\frac{2}{\pi} \operatorname{arc\,cosec} (1 + 1/nr')$
(5)	$\frac{1}{(1 + 1\,nr^i)^j}$	(10)	$\tanh nr$ '

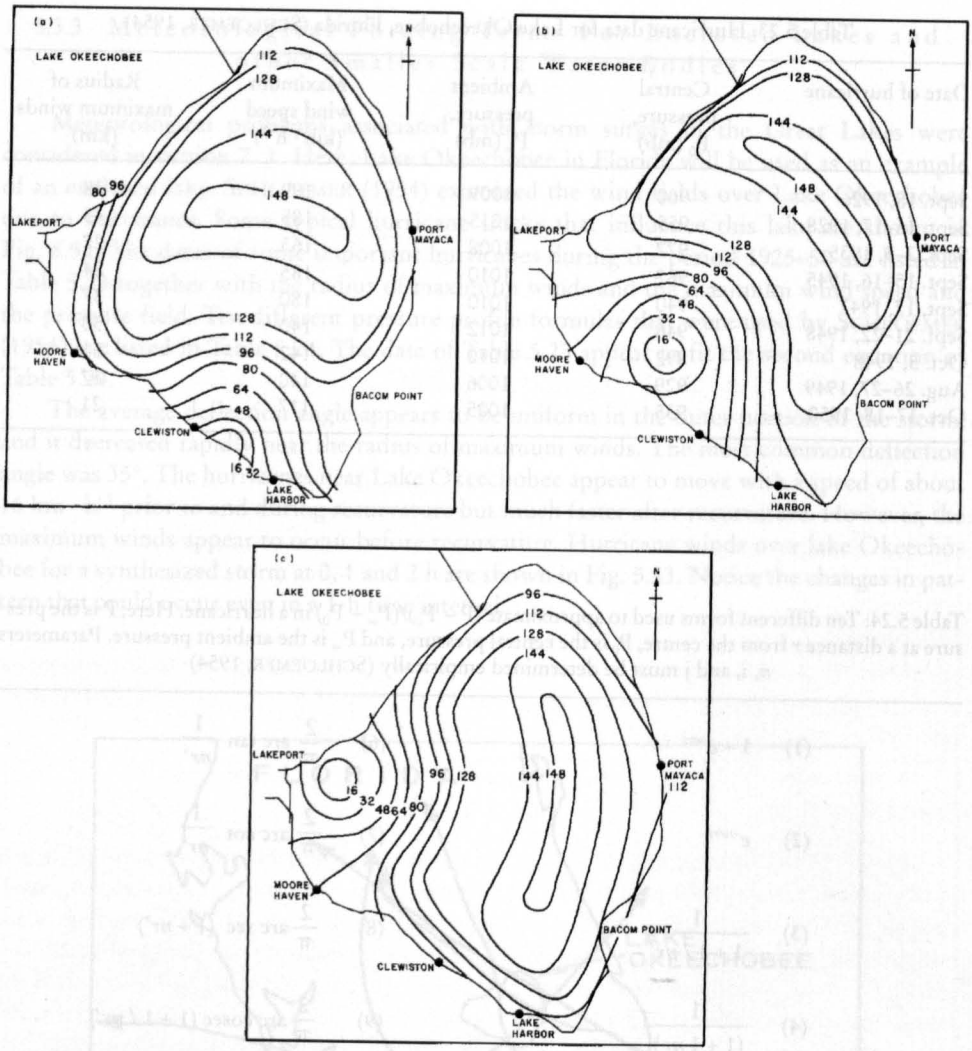

Fig. 5.53: Wind field (kilometers per hour) for a synthesized hurricane over Lake Okeechobee at (a) 0 h, (b) 1 h, and (c) 2 h after a specified zero time (SCHLOEMER, 1954)

Die Küste, 63 Global Storm Surges (2001), 1-623

5.4 Cyclones of the Pacific Ocean

Most of the damage from storm surges on the coast of the Pacific Ocean results from tropical storms. Hence, these will be emphasized in this section. Note that a storm surge is a rare event on the Pacific coasts of Canada and the United States (with the exception of Alaska); along these coasts, wind waves and swell are of primary importance.

Table 5.25: Record number of storms by basin based on data from 1968–1989 (1968/69 to 1989/90) for the Southern Hemisphere (NEUMANN, 1993)

	Tropical Strom or stronger (greater than 17 m/s sustained winds)			Hurricane / Typhoon / Severe Tropical Cyclone (greater than 33 m/s sustained winds)		
Basin	Most	Least	Average	Most	Least	Average
Atlantik *	18	4	9.7	12	2	5.4
NE Pacific	23	8	16.5	14	4	8.9
NW Pacific	35	19	25.7	24	11	16.0
N Indian	10	1	5.4	6	0	2.5
SW Indian	15	6	10.4	10	0	4.4
Aus SE Indian	11	1	6.9	7	0	3.4
Aus SW Pacific	16	2	9.0	11	2	4.3
Globally	103	7.5	83.7	65	34	44.9

* Note that the data include subtropical storms in the Atlantic basin numbers.

Table 5.26: Monthly average number of storms per year for each major ocean basin. T, tropical storms only; H, hurricanes only. For the North Indian Ocean, replace the term hurricane with cyclone (winds >– 89 kin -h-'). –, zero (CRUTCHER and QUAYLE, 1974)

	North Atlantic		Eastern North Pacific		Western North Pacific		Southwest Pacific and Australian area		Southwest Indian Ocean		North Indian Ocean	
Month	T	H	T	H	T	H	T	H	T	H	T	H
Jan.	–	–	–	0.2	0.3	2.7	0.7	2.0	1.3	0.1	–	
Feb.	–	–	–	0.3	0.2	2.8	1.1	2.2	1.1	–	–	
Mar.	–	–	–	0.3	0.2	2.4	1.3	1.7	0.8	–	–	
Apr.	–	–	–	0.2	0.7	1.3	0.3	0.6	0.4	0.1	0.1	
May	0.1	–	0.3	0.4	0.9	0.3	–	0.2	–	0.3	0.5	
June	0.4	0.3	1.5	0.6	0.5	1.2	0.2	–	–	–	0.5	0.2
July	0.3	0.4	2.8	0.9	1.2	2.7	–	0.1	–	–	0.5	0.1
Aug.	1.0	1.5	2.3	2.0	1.8	4.0	–	0.1	–	–	0.4	–
Sept.	1.5	2.7	2.3	1.8	1.5	4.1	–	–	–	–	0.4	0.1
Oct.	1.2	1.3	1.2	1.0	1.0	3.3	0.1	–	0.3	–	0.6	0.4
Nov.	0.4	0.3	0.3	–	0.8	2.1	0.4	0.3	0.3	–	0.5	0.6
Dec.	–	–	–	0.6	0.7	1.5	0.5	0.8	0.5	0.3	0.2	

Earlier it was mentioned that tropical cyclones form over all the tropical oceans except in the South Atlantic and in the South Pacific east of 140° W. The highest frequency of tropical cyclones occurs in the western Pacific, although maximum damage has occurred on the coasts surrounding the Bay of Bengal. Indeed one may say that tropical cyclones and their

associated storm surges together are probably the most devastating natural phenomena, even more so than earthquakes.

The number of tropical storms and hurricanes is listed by most, least and average for the period 1969–1989 and by month for various ocean basins in Table 5.25 and Table 5.26. It can be seen that the maximum frequency of tropical storms and Hurricans occurs in the western part of the North Pacific Ocean during the months of August and September. The preferred tropical cyclone tracks over the globe are shown in Fig. 5.54. Again, it can be seen that the tracks in the Pacific Ocean and Indian Ocean have more fine structure than those in the Atlantic Ocean. Contours of the speed of movement of tropical storms for various ocean basins are shown in Fig. 5.55. Maximum values of 35 knots (65 km · h^{-1}) occur in the western North Pacific, with maximum values of 30 knots (56 km · h^{-1}) in the Atlantic, and with maximum values of 27.5 (51 km · h^{-1}) in the eastern edge of the South Indian Ocean. In the following subsections, certain characteristics of tropical cyclones in the eastern North Pacific, central North Pacific, and western North Pacific will be detailed. There are shown for every region special examples and not the whole research.

5.4.1 Characteristics of Tropical Cyclones in the Eastern North Pacific

This discussion will be based on the tropical cyclone seasons of 1976, 1977 and 1978 (GUNTHER, 1977, 1978, 1979). For the 1976 season, tropical cyclone activity began on June 1 and ended on October 29. The season was average in the sense that there were eight hurricanes, six tropical storms, and four tropical depressions. The 1977 season began on May 25 and ended on October 23. Thus, the length of the 1977 season was 152 d whereas in 1976 it was 150 d. The total number of tropical storms in 1977 was 17 compared with 18 in 1976. However, in 1977 only 47 % of the storms reached hurricane intensity. Note that the number of tropical cyclones reaching storm or hurricane intensity in 1977 was 47 % less than the average for the period 1966–76. For the 1976 season, the highest sustained wind speed was 125 knots (231 km · h^{-1}) whereas for the 1977 season it was 90 knots (167 km · h^{-1}).

1978, the season began on May 30 and ended on October 20, with duration of 144 d. Although the 1978 season was 8 d shorter than the 1977 season, there was an increase of 24 % in cyclone activity. The number of cyclones reaching storm or hurricane intensity was 86 % in 1978 compared with 47 % in 1977. The highest sustained wind speed in the 1978 season was 120 knots (222 km · h^{-1}).

The first tropical cyclone to hit southern California since 1939 was Hurricane Kathleen in 1976. In the 1977 season, Hurricane Doreen struck again and in the 1978 season Hurricane Norman reached the coast. Though none of these three hurricanes caused any storm surge activity on the California coast, the heavy rains associated with these caused extensive damage.

During the hurricane season bulletins are issued four times per day from the Eastern Pacific Hurricane Center in San Francisco. The number of eastern North Pacific tropical storms reaching hurricane intensity is given in Table 5.27. The tracks of Hurricanes Kathleen of September 1976 and Doreen of August 1977 are shown in Fig. 5.56. All the tropical cyclones during 1977 did not reach land, as they were dissipated over the ocean. Hence, the damage in the 1977 season was less than in the 1976 season (during this season, several hurricanes moved onshore). In the 1978 season, only three cyclones moved onshore. Hurricane statistics prior to 1966 were not used in this study because satellite coverage was not adequate prior to 1966 and some hurricanes might have been missed.

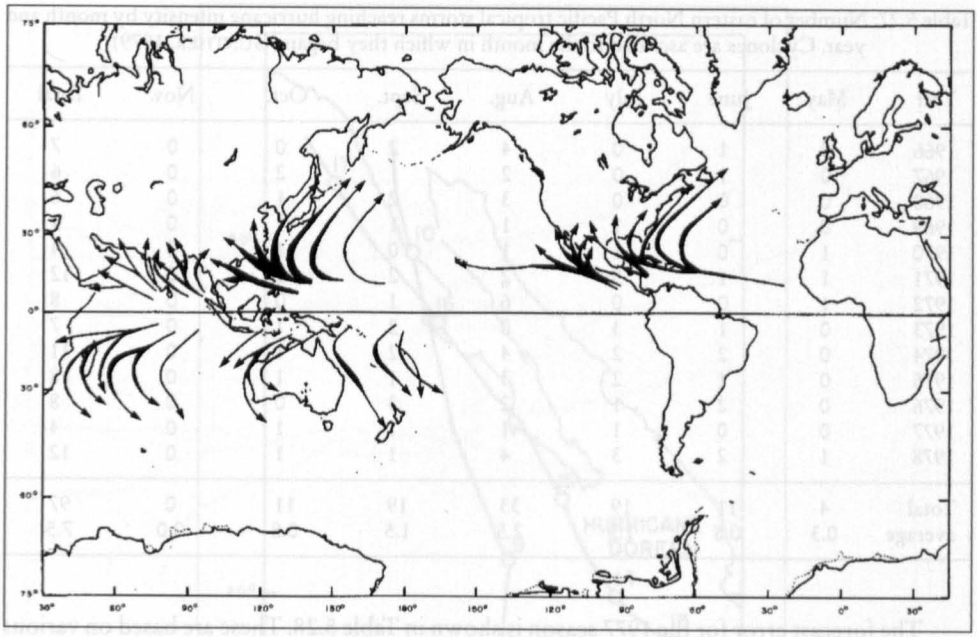

Fig. 5.54: Preferred annual tropical cyclone paths. Arrow widths are proportional to storm frequencies along indicated paths (CRUTCHER and QUAYLE, 1974)

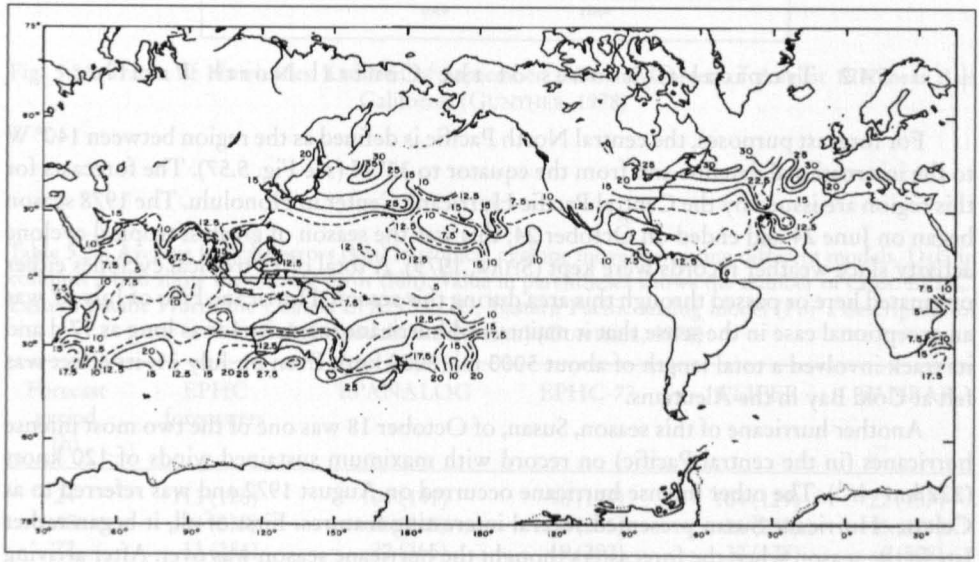

Fig. 5.55: Average (for annual data) speeds (knots) of storm movement (1 knot = 1852 km · h^{-1}) (CRUTCHER and QUAYLE, 1974)

Table 5.27: Number of eastern North Pacific tropical storms reaching hurricane intensity by month and year. Cyclones are ascribed to the month in which they began (GUNTHER, 1979)

Year	May	June	July	Aug.	Sept.	Oct.	Nov.	Total
1966	0	1	0	4	2	0	0	7
1967	0	1	0	2	1	2	0	6
1968	0	0	0	3	2	1	0	6
1969	0	0	1	1	1	1	0	4
1970	1	0	1	1	0	1	0	4
1971	1	1	5	2	2	1	0	12
1972	1	0	0	6	1	0	0	8
1973	0	1	3	0	2	1	0	7
1974	0	2	2	4	2	1	0	11
1975	0	1	2	3	1	1	0	8
1976	0	2	1	2	3	0	0	8
1977	0	0	1	1	1	1	0	4
1978	1	2	3	4	1	1	0	12
Total	4	11	19	33	19	11	0	97
average	0.3	0.8	1.5	2.5	1.5	0.8	0.0	7.5

The forecast error for the 1977 season is shown in Table 5.28. These are based on various computer models available at the National Hurricane Center in Miami. In this table, EPI-IC stands for the Eastern Pacific Hurricane Center, CLIPER is a simulated analog model, EPHC77 is a statistical synoptic model, EPRANALOG is an analog model, and SANBAR is a barotropic model. Of these four computer models, EPHC77 gave the best results, and these were subjectively improved by the EPI-IC forecasters.

5.4.2 Tropical Cyclones of the Central North Pacific

For forecast purposes, the central North Pacific is defined as the region between 140° W to the international dateline and from the equator to 35° N (see Fig. 5.57). The forecasts for this region are issued by the Central Pacific Hurricane Center in Honolulu. The 1978 season began on June 24 and ended on October 24; this was the season of greatest tropical cyclone activity since weather records were kept (SHAW, 1979). A total of 13 tropical cyclones either originated here or passed through this area during this season. Hurricane Fico of July 17 was an exceptional case in the sense that it maintained hurricane intensity for as long as 17 d and its track involved a total length of about 5000 mi (8000 km). Even on July 31, its effect was felt at Cold Bay in the Aleutians.

Another hurricane of this season, Susan, of October 18 was one of the two most intense hurricanes (in the central Pacific) on record with maximum sustained winds of 120 knots (222 km · h^{-1}). The other intense hurricane occurred on August 1972 and was referred to as Celeste. Hurricane Susan presented several interesting features. First of all, it began rather late in the season when the forecasters thought the hurricane season was over. After arriving 220 mi (354 km) southeast of the big island of Hawaii, it abruptly turned southwestward and dissipated rapidly. The central pressure rose more than 50 mb in 24 h.

Hurricane Gilma of July 22 was also somewhat unusual in the sense that it covered an area as large as 3×10^5 mi^2 (7.8×10^5 km^2). Hurricanes for the 1978 season in the central Pacific are summarized in Tab 5.29.

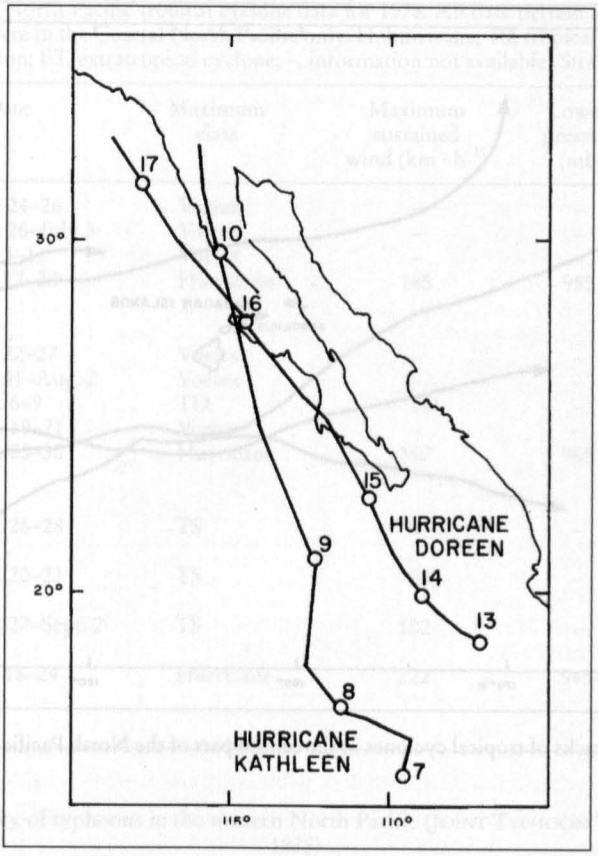

Fig. 5.56: Tracks of Hurricanes Kathleen of September 1976 and Doreen of August 1977 near Baja California (GUNTHER, 1978)

Table 5.28: Average forecast errors (km) in tropical cyclone movement using different models. Data in columns 2 to 6 show the average error (lun). Value in parentheses shows the number of cases. EPI4C, Eastern Pacific Hurricane Center; EPANALOG, Eastern Pacific analog model (For a description of these models, see the text.) (GUNTHER, 1978)

Forecast period (h)	EPHC forecasters	EPANALOG	EPHC-77	CLIPER	SANBAR
24	113 (126)	104 (141)	96 (129)	104 (129)	22 (137)
48	44 (239)	56 (265)	50 (255)	56 (255)	15 (271)
72	13 (284)	22 (365)	19 (292)	22 (378)	6 (508)

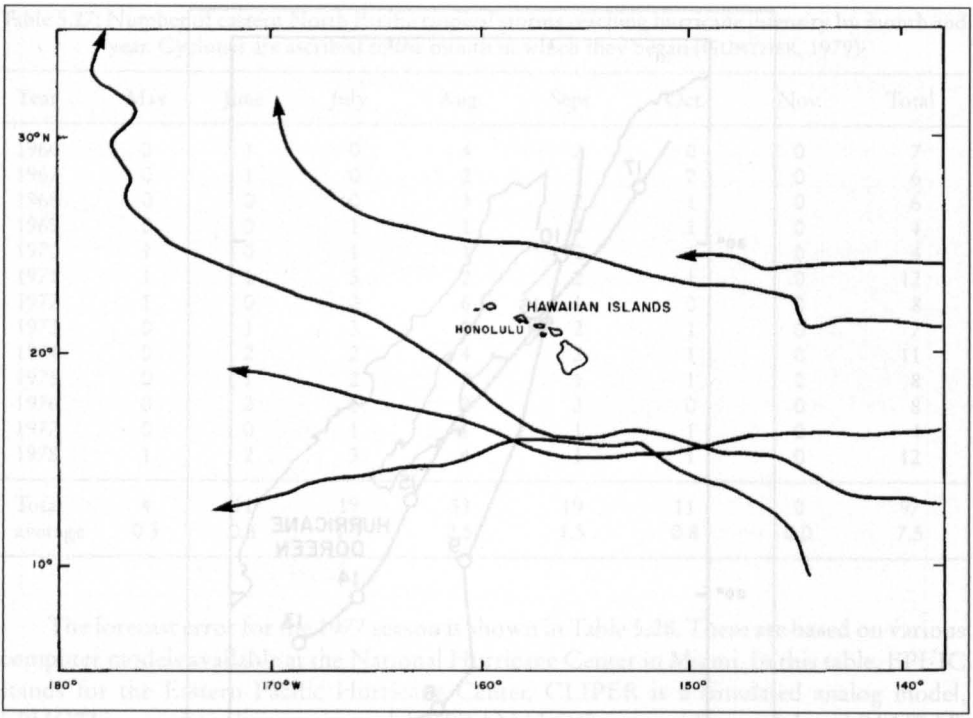

Fig. 5.57: Typical tracks of tropical cyclones in the central part of the North Pacific Ocean (SHAW, 1979)

5.4.3 Typhoons of the Western North Pacific

The Joint Typhoon Warning Center for the western North Pacific was set up at Guarn in 1959. The frequency of typhoons by month and year is listed in Table 5.30 and the western North Pacific tropical cyclones for the season of 1977 are listed in Table 5.31. The 1977 season began on March 13 and ended in January 1978. The 1978 season officially began on January 8 and ended on November 30. It can be seen that in the western North Pacific, typhoons can and do occur at any time of the year. In this respect this ocean basin is different from the central North Pacific, eastern North Pacific, and North Atlantic Ocean basins where the tropical cyclone season does not span the full year.

The seasons of 1977 and 1978 (JOINT TYPHOON WARNING CENTER, 1978, 1979) will be compared. The season of 1977 had the lowest number of tropical cyclones since 1959. Of a total of 21, 2 dissipated as depressions, 8 peaked out as tropical storms, and the remaining 11 matured into hurricanes. The monsoon systems of the Indian subcontinent and Southeast Asia appear to have some influence on tropical cyclones in the western North Pacific. During the 1977 season there were only 12 multiple storm days (a multiple storm day is one during which there is more than one tropical cyclone in the region). In 1970 and 1975, at certain times there were three or more tropical cyclones simultaneously. Storms with long durations could occur. Typhoon Kim of November 6, 1977, spanned 12 d. In this season, Typhoon Babe was classified as a super typhoon.

Table 5.29: Central North Pacific tropical cyclone data for 1978. All data pertain to the period during which the storms were in the Central North Pacific only. H, hurricane; TS, tropical storm; TD, tropical depression; ET, extratropical cyclone; –, information not available (SHAW, 1979)

Name of storm	Date	Maximum class	Maximum sustained wind (km · h^{-1})	Lowest pressure (mb)	Total hours observed
Bud	June 24–26	Vortex	–	–	48
Carlotta	June 26–July 3	Vortex	–	–	168
Daniel	July 3–11	Vortex	–	–	192
Fico	July 17–28	Hurricane	185	955	225 (H) 15 (TS) 36 (ET)
Gilma	July 22–27	Vortex	–	–	144
Hector	July 31–Aug. 2	Vortex	–	–	60
TD-10	Aug. 6–9	TD	56	–	84
Iva.	Aug. 19–21	Vortex	–	–	54
John	Aug. 23–30	Hurricane	167	965	48 (H) 72 (TS) 48 (TD)
Kristy	Aug. 26–28	TS	93	–	18 (TS) 45 (TD)
Lane	Aug. 20–23	TS	93	–	66 (TS) 27 (TD)
Miriam	Aug. 27–Sept. 2	TS	102	–	72 (TS) 6 (TD)
Susan	Oct. 18–24	Hurricane	222	945–954	81 (H) 30 (TS) 24 (TD)

Table 5.30: Frequency of typhoons in the western North Pacific (JOINT TYPHOON WARNING CENTER, 1978)

Year	Jan	Feb	Mar	Apr	May	Jun	Jul	Aug	Sep	Oct	Nov	Dec	Total
1954–58 (average)	0.4	0.1	0.3	0.4	0.7	1.1	2.0	2.9	3.2	2.4	2.0	0.9	16.3
1959	0	0	0	1	0	0	1	5	3	3	2	1	20
1960	0	0	0	1	0	2	2	8	0	4	1	1	19
1961	0	0	1	0	2	1	3	3	5	3	1	1	20
1962	0	0	0	1	2	0	5	7	2	4	3	0	24
1963	0	0	0	1	1	2	3	3	3	4	0	2	19
1964	0	0	0	0	2	2	6	3	5	3	4	1	26
1965	1	0	0	1	2	2	4	3	5	2	1	0	21
1966	0	0	0	1	2	1	3	6	4	2	0	1	20
1967	0	0	1	1	0	1	3	4	4	3	3	0	20
1968	0	0	0	1	1	1	1	4	3	5	4	0	20
1969	1	0	0	1	0	0	2	3	2	3	1	0	13
1970	0	1	0	0	0	1	0	4	2	3	1	0	12
1971	0	0	0	3	1	2	6	3	5	3	1	0	24
1972	1	0	0	0	1	1	4	4	3	4	2	2	22
1973	0	0	0	0	0	0	4	2	2	4	0	0	12
1974	0	0	0	0	1	2	1	2	3	4	2	0	15
1975	1	0	0	0	0	0	1	3	4	3	2	0	14
1976	1	0	0	1	2	2	3	0	4	1	0	0	14
1977	0	0	0	0	0	0	3	0	2	3	2	1	11
1959–77 (average)	0.3	0.1	0.1	0.7	0.9	1.1	2.8	3.6	3.2	3.2	1.6	0.5	18.3

Table 5.31: Tropical cyclones in the western North Pacific for the season of 1977. TV, typhoon; TS, tropical storm; STY, supertyphoon (JOINT TYPHOON WARMING CENTER, 1978)

Name of typhoon	Period of warning	Intensity	Maximum surface wind ($km \cdot h^{-1}$)	Minimum observed sea level pressure (mb)
Patsy	Mar. 23–31	TS	93	981
Ruth	June 14–17	TS	111	980
Sarah	July 16–21	TY	139	970
Thelma	July 21–26	TY	157	957
Vera	July 28–Aug. 1	TY	204	926
Wanda	July 31–Aug. 4	TS	83	986
Amy	Aug. 20–23	TS	74	990
Babe	Sept. 2–10	STY	241	906
Carla	Sept. 3–5	TS	65	994
Dinah	Sept. 14–23	TY	139	964
Emma	Sept. 15–20	TS	111	966
Freda	Sept. 23–25	TS	102	997
Gilda	Oct. 3–10	TY	130	968
Harriet	Oct. 16–20	TS	102	984
Ivy	Oct. 21–27	TY	167	945
Jean	Oct. 28–31, Nov. 2–3	TY	120	972
Kim	Nov. 6–17	TY	232	916
Lucy	Nov. 28–Dec. 7	TY	213	919
Maiy	Dec. 20–Jan. 3	TY	185	947

One important feature of the typhoons in the western North Pacific is that they could have rather erratic tracks and loops (usually the loops occur when the steering currents are weak). The 1978 season had about an average number of tropical cyclones. However, there were several surprises. Ten storms and typhoons had erratic tracks. Typhoon Carmen was almost stationary for 3 d. Typhoon Faye's track had a large anticyclonic loop and then it deepened explosively (surface central pressure decreased by 18 mb in just 6 h). Typhoon Trix was the most ill-behaved of all. Storms Hester and Phyllis attained speeds of movement of 40 and 50 knots (74 and 93 $km \cdot h^{-1}$), respectively, after recurvature in their extratropical transition. Typhoons Virginia and Mamie were so compact in size (but not in intensity) that they were called midget typhoons. Typhoon Virginia traveled farthest north (to 42° N) still behaving like a tropical cyclone. Super typhoon Rita covered an amazing distance of 4142 mi (6669 km) and is second only to Typhoon Sarah of 1976, which traveled 4499 mi (8000 km). Some typical tracks of typhoons in the western North Pacific are shown in Fig. 5.58.

Northwest Pacific Ocean

LAPPO and ROZHDESTVENSKIY (1977, 1979) studied the energy transferred to the ocean from a typhoon via the storm surge. They referred to the storm surge as meteorological ocean tides. In their calculations they ignored the influence of the wind but included the effect of the atmospheric pressure. When the cyclone is stationary, the energy transferred to the ocean is equal to the potential energy associated with the change in the sea level. For a moving cyclone, however, there is an additional transfer of kinetic energy.

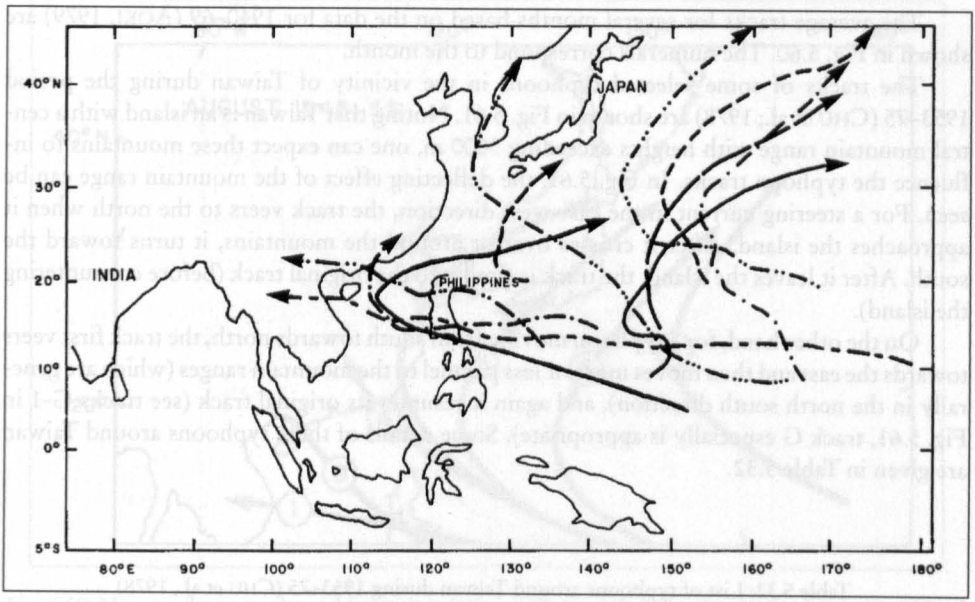

Fig. 5.58: Typical tracks of tropical cyclones in the western North Pacific (JOINT TYPHOON WARNING CENTER, 1977, 1978)

LAPPO and ROZHDESTVENSKIY (1977) formulated this problem along the lines of the classical quasi-stationary Proudman problem (PROUDMAN, 1929). For a plane pressure disturbance, with a pressure deficit of 40 mb, a cross-sectional diameter of the cyclone of 10^3 km, and the distance traveled as 5×10^3 km, these authors gave the following values for an average cyclone (Joules):

Total energy of cyclone $= E_1 = 5 \times 10^{17}$ to 8×10^{17}

Kinetic energy $= E_2 = 5 \times 10^{16}$ to 8×10^{16}

Mechanical energy imparted to the ocean (ignoring wind stress) $= E_l = 5 \times 10^{15}$

Potential energy of the storm surge created $= E_0 = 10^{15}$

Tropical Cyclone Tracks Near Japan, Taiwan And The Philippines

JAMISON (1956) described the average tracks of typhoons in this region for the month of August based on 11 yr of data (1945–55). These tracks are illustrated in Fig. 5.59.

During this period there was a total of 43 typhoons, of which 15 had rather erratic tracks (not known here). The number along each track is the number of typhoons that occurred during this 11-yr. period. Note that the lowest frequency is for the track that crosses Vietnam and the highest is for the Philippines area and continuing towards the Gulf of Tonkin. The number of tropical cyclones that traveled over Korea and Japan during this period was five.

The average tracks for several months based on the data for 1940–69 (AOKI, 1979) are shown in Fig. 5.60. The numerals correspond to the month.

The tracks of some selected typhoons in the vicinity of Taiwan during the period 1953–75 (CHU et al.; 1978) are shown in Fig. 5.61. Noting that Taiwan is an island with a central mountain range with heights exceeding 3000 m, one can expect these mountains to influence the typhoon tracks. In Fig. 5.61, the deflecting effect of the mountain range can be seen. For a steering current in the east-west direction, the track veers to the north when it approaches the island. After it crosses over or around the mountains, it turns toward the south. After it leaves the island, the track is similar to the original track (before encountering the island).

On the other hand, for a typhoon moving from south towards north, the track first veers towards the east and then moves more or less parallel to the mountain ranges (which are generally in the north south direction), and again it resumes its original track (see tracks G-1 in Fig. 5.61, track G especially is appropriate). Some details of these typhoons around Taiwan are given in Table 5.32.

Table 5.32: List of typhoons around Taiwan during 1953–75 (CHU et al., 1978)

Name of typhoon	Date	Maximum wind speed ($km \cdot h^{-1}$)	Name of typhoon	Date	Maximum wind speed ($km \cdot h^{-1}$)
Judy	June 1953	74–111	Gilda	Nov. 1967	148–185
Kit	July 1953	204	Elsie	Sept. 1969	194
Thelma	Apr. 1956	157	Betty	Aug. 1972	157–222
Trix	Aug. 1960	204–222	Joan	Aug. 1973	56–83
Agnes	Aug. 1960	74–102	Nora	Oct. 1973	111–176
Pamela	Sept. 1961	222–278	Jean	July 1974	93
Sally	Sept. 1961	130	Wendy	Sept. 1974	93
Wendy	July 1963	185–250	Nina	Aug. 1975	250
Dinah	June 1965	74–241	Betty	Sept. 1975	157–167
Nora	Aug. 1967	111–120	Elsie	Oct. 1975	222–259

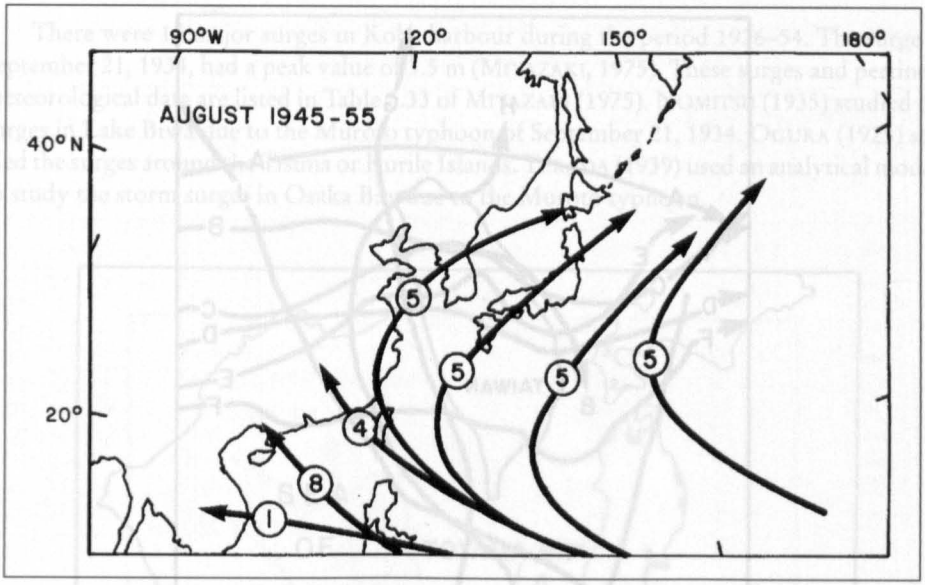

Fig. 5.59: Mean typhoon tracks and frequency (over an 11-yr period) for August in the western North Pacific (JAMISON, 1956)

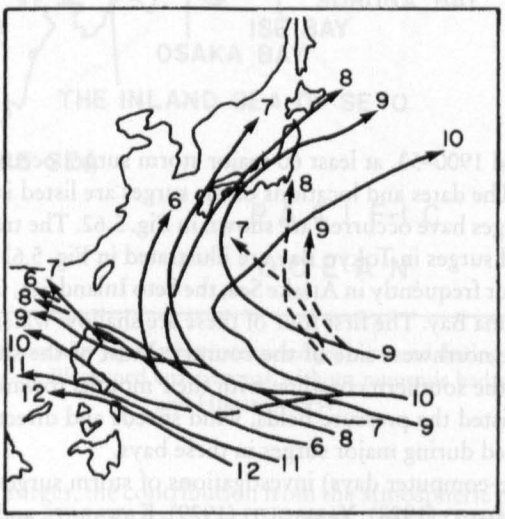

Fig. 5.60: Monthly mean tracks of tropical cyclones in the western North Pacific. Numbers refer to the months (AOKI, 1979)

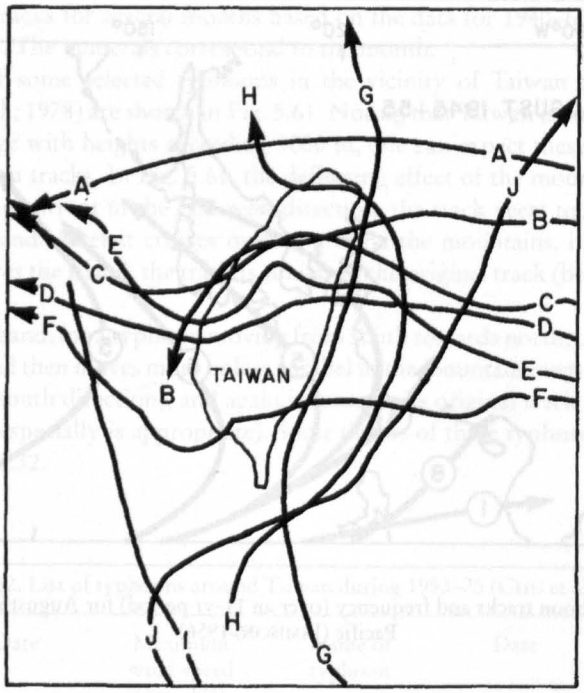

Fig. 5.61: Typical tracks of typhoons around Taiwan. A, Trix, 1960; B, Agnes, 1960; C, Pamela, 1961; D, Nora, 1967; E, Nina, 1975; F, Betty, 1975; G, Dinah, 1965; H, Wendy, 1974; I, Nora, 1973; J, Judy, 1953 (CHU et al., 1978)

Japan

During the period 1900–53, at least 60 major storm surges occurred in Japan (WADATI and HIRONO, 1954). The dates and locations of the surges are listed in Table 5.33. The locations where major surges have occurred are shown in Fig. 5.62. The tracks of some of the typhoons that generated surges in Tokyo Bay are illustrated in Fig. 5.63.

Storm surges occur frequently in Ariake Sea, the Seto Inland Sea, Osaka Bay, Tokyo Bay, Suruga Bay, and Toyama Bay. The first four of these are shallow water bodies; only Toyama Bay is situated on the northwest side of the country. Most of the shallow water bodies in Japan are situated on the southern coastline with their mouths towards southwest. WADATI and HIRONO (1954) listed the pressure fields, wind speeds and directions, damage, and the number of people killed during major surges in these bays.

For early (i.e. pre-computer days) investigations of storm surges in and around Japan, see TERADA and YAMAGUTI (1928), YAMAGUTI (1929), KAWABATA and FUJITO (1951), HONSYÛ (1932), and UNOKI (1959). TERADA (1912) and NAKANO (1949) investigated the secondary undulations associated with storm surges in Japan. RABE and BRAND (1980) studied the extreme sea states associated with typhoons.

MIYAZAKI (1975) studied the characteristics of storm surges along the coast of Japan. Some of the major surges (that exceeded 2 m) during the period 1900-73 are listed in Table 5.33. The damage associated with some selected surges is listed in Table 5.34.

There were 15 major surges in Kobe harbour during the period 1926–54. The surge of September 21, 1934, had a peak value of 3.5 m (MIYAZAKI, 1975). These surges and pertinent meteorological data are listed in Table 5.33 of MIYAZAKI (1975). NOMITSU (1935) studied the surges in Lake Biwa due to the Muroto typhoon of September 21, 1934. OGURA (1925) studied the surges around the Tisima or Kurile Islands. TERADA (1939) used an analytical model to study the storm surges in Osaka Bay due to the Muroto typhoon.

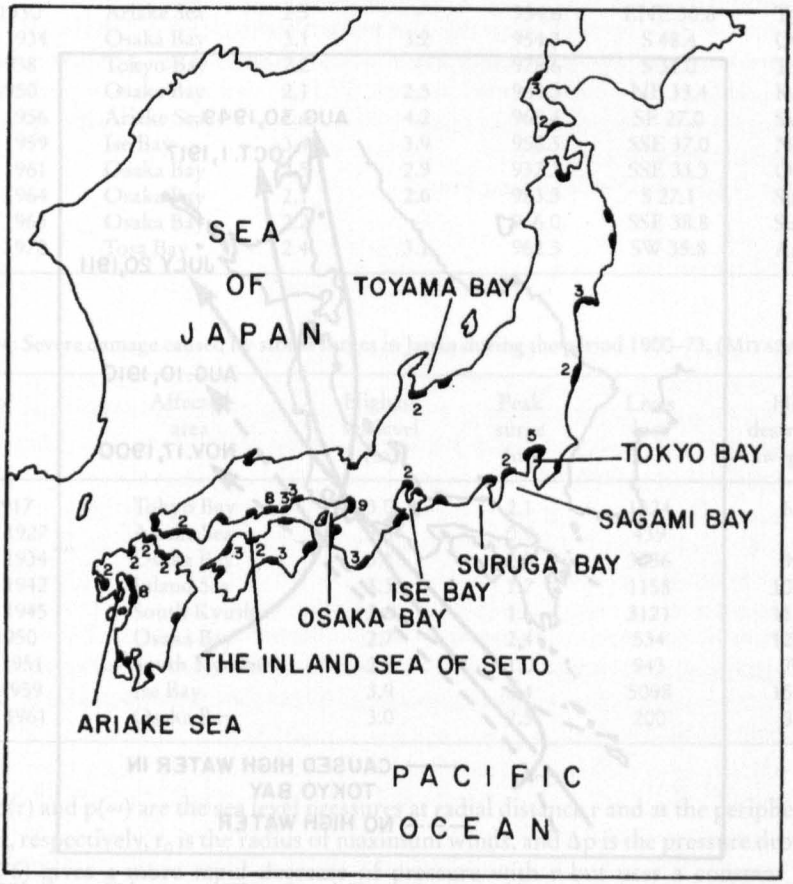

Fig. 5.62: Locations on the coast of Japan where storm surges occurred during 1900–53 (numerals indicate number of occurrences). Blackened coastal areas without numerals had one occurrence (WADATI and HIRONO, 1954)

In Japanese storm surges, the contribution from the atmospheric pressure gradients was at most 15 %. In the numerical model of ISOZAKI (1970a, 1970b, 1970c) the following pressure field distributions were specified:

$$p(r) = p(\infty) - \frac{\Delta p}{\left[1 + \left(\frac{r}{r0}\right)^2\right]^{1/2}} \qquad (5.75)$$

or

$$p(r) = 1010 - \frac{\Delta p}{\left(1 + \frac{r}{r_0}\right)^2} \qquad (5.76)$$

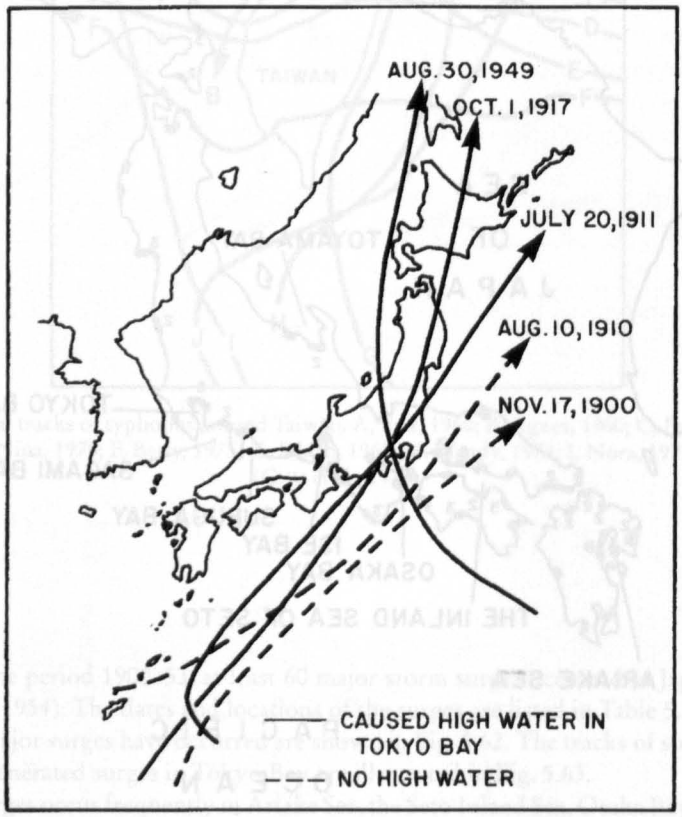

Fig. 5.63: Tracks of typhoons that passed near Tokyo Bay (WADATI and HIRONO, 1954)

Table 5.33: Storm surges in Japan during the period 1900–73 with maximum amplitudes ir, excess of 2 m; highest level includes surge and tide (MIYAZAKI, 1975)

Date	Affected area	Peak surge (m)	Highest level (m)	Meteorological extreme values: Central pressure (mb)	Wind ($m \cdot s^{-1}$)	Location
Oct. 1, 1917	Tokyo Bay	2.3	3.1	950.4	SSE 40.0	Tokyo
July 18, 1930	Ariake Sea	2.5	-	954.6	ENE 30.6	Tomie
Sept. 21, 1934	Osaka Bay	3.1	3.2	954.3	S 48.4	Osaka
Sept. 1, 1938	Tokyo Bay	2.2	-	978.6	S 31.0	Tokyo
Sept. 3, 1950	Osaka Bay	2.1	2.5	964.3	NE 33.4	Kobe
Aug. 17, 1956	Ariake Sea	2.4	4.2	968.4	SE 27.0	Saga
Sept. 26, 1959	Ise Bay	3.4	3.9	958.5	SSE 37.0	Nagoya
Sept. 16, 1961	Osaka Bay	2.5	2.9	937.3	SSE 33.3	Osaka
Sept. 25, 1964	Osaka Bay	2.1	2.6	983.5	S 27.1	Sumoto
Sept. 10, 1965	Osaka Bay	2.2	-	966.0	SSE 38.8	Sumoto
Aug. 21, 1970	Tosa Bay	2.4	3.1	962.3	SW 35.8	Ashizuri

Table 5.34: Severe damage caused by storm surges in Japan during the period 1900–73. (MIYAZAKI , 1975)

Date	Affected area	Highest sea level (m)	Peak surge (m)	Lives lost	Houses destroyed or swept away
Oct. 1, 1917	Tokyo Bay	3.0	2.1	1324	60 175
Sept. 13, 1927	Ariake Sea	3.8	0.9	439	2 211
Sept. 21, 1934	Osaka Bay	3.1	2.9	3036	92 323
Aug. 27, 1942	Inland Sea	3.3	1.7	1158	102 374
Sept. 17, 1945	South Kyushu	2.6	1.6	3121	115 984
Sept. 3, 1950	Osaka Bay	2.7	2.4	534	120 923
Oct. 14, 1951	South Kyushu	2.8	1.0	943	72 648
Sept. 27,1959	Ise Bay	3.9	3.4	5098	156 676
Sept. 16, 1961	Osaka Bay	3.0	2.5	200	54 782

where, p(r) and p(∞) are the sea level pressures at radial distance r and at the periphery of the typhoon, respectively, r_0 is the radius of maximum winds, and Δp is the pressure drop. Equation (5.76) gives a more rapid decrease of pressure with r but uses a constant value of 1010 mb at the typhoon periphery. The cyclostrophic wind corresponding to eq. (5.76) is

$$V^2 = 4V_m^2\left[\frac{\mu^2}{\left(1+\mu^2\right)^2}\right] \tag{5.77}$$

where, $\mu = r/r_0$ and V_m is the maximum wind at r_0. The maximum wind and the pressure drop are related through

$$V_m = C(V_v)^{1/2} \tag{5.78}$$

where, C is a constant.

In other studies, the JELESNIANSKI (1972) model is used:

$$v(r) = V(r_0)\frac{2r_0}{r_0^2 + r^2} \tag{5.79}$$

where, again, r_0 is the radius of maximum winds. MYERS and MALKIN (1961) determined the angle of inflow for a stationary storm using the equations of motion. The angle varies from 0 at the center of the storm to about 30° at a radial distance of about $3r_0$ (where r_0 is the radius of maximum winds) and is roughly constant after that. Usually, within the region up to r_0, the wind field computed from the pressure field (i.e. cyclostrophic or gradient winds) is reasonably correct. Outside r_0, the angle of inflow (i.e. the angle of the wind vector across circular isobars) must be considered.
TAKAHASHI (1939) used the following form:

$$p(r) = p(\infty) - \frac{\Delta p}{\left(1 + \frac{r}{r_0}\right)} \tag{5.80}$$

This formula underestimates the pressure field at the center. KAWAHARA et al. (1980) used a finite-element model for storm surge propagation in Suragawa Bay. They used eq. (5.75) to specify the pressure field.

China

In China, storm surges mainly occur on the southeastern coast. In the 1970s, the biggest storm surge in China occurred at Shantou on August 2, 1979. The peak surge was over 2 m. In the dynamic models for surge prediction used in China (JIN-CHUAN and GUANG, 1979), MYERS (1954) formula is used:

$$\Delta p = \Delta p_0 (1 - e^{-R/r}) \tag{5.81}$$

where,

$$\Delta p_0 = p_\infty - p_c \text{ and } \Delta p = p_\infty - p \tag{5.82}$$

where, p_c is the central pressure, p_∞ is the peripheral pressure, p is the pressure at any point at distance r from the centre, and R is the radius of maximum winds.

The tangential component of the wind field is expressed as

$$V_\theta = \begin{cases} V_{max}\,\frac{r}{R}\cos\alpha & \text{for} \quad r \le R \\ V_{max}\,\frac{R}{r}\cos\alpha & \text{for} \quad r > R \end{cases} \tag{5.83}$$

The radial component of the wind field is written as

$$V_r = \begin{cases} -V_{max}\dfrac{r}{R}\sin\alpha & \text{for} \quad r \le R \\ -V_{max}\dfrac{R}{r}\sin\alpha & \text{for} \quad r > R \end{cases} \tag{5.84}$$

where, α is the angle measured inward between the wind direction and the isobars. In the surge computations for the Chinese coast, α was taken as 30°.
The tangential and radial components of the wind stress are computed from:

$$\tau_\theta = K\rho_a \,|V|\, V_\theta$$
$$\tau_r = K\rho_a \,|V|\, V_r \tag{5.85}$$

where, $K = 2.5 \times 10^{-3}$ and $\rho_a = 1.2 \times 10^{-3}\ g \cdot cm^{-3}$.

Storm surges are quite frequent in Hong Kong. About three to four occur per year in Hong Kong Harbour (WORLD METEOROLOGICAL ORGANIZATION, 1978). A total of 35 surges with amplitudes varying from 0.2 to 1.8 m occurred in Hong Kong during 1954–64 (CHENG, 1967). Typhoon Wanda caused one of the important surges in September 1962. The surge was 1.8 m at Hong Kong and 3.2 m at Taipo (farther inland in a narrow channel).

CHAN and WALKER (1979) mentioned that two of the most disastrous surges in Hong Kong occurred on September 2, 1937, and September 1, 1962, in the Tolo Harbour region. WATTS (1959) concluded that pronounced surges occur in Hong Kong when the center of a westward moving storm passes over Hong Kong within several tens of kilometres to the south.

If the storm track lies to the west of Hong Kong, the wind field at Hong Kong will be strong (east-northeast to east-southeast) and a major surge could be generated. On the other hand, if the track is to the east of Hong Kong, the winds will be weak (west–northwest to west–southwest) and surges, if generated, will be small. Most of the storms that affect Hong Kong originate in the Philippine Sea. A few, however, develop in the South China Sea, and in this case, the above criterion (track to the east or west of Hong Kong) does not apply. Also, those storms that make a landfall at Hong Kong usually are associated with weak local winds and would not generate significant surges. The major surges at Hong Kong are associated with storms that make a landfall within 60 nautical miles (111 km) either to the north or south of Hong Kong.

Based on storm surge data at North Point, the storm surges are classified into three categories by CHAN and WALKER (1979): type 0 refers to storms whose centers lie within a 60 nautical mile radius of Hong Kong, type W for storms whose centers are outside the 60 nautical mile radius and which travel to the west of Hong Kong over the land, and type E for storms with centers outside the radius and traveling over the land to the east of Hong Kong. For these three categories, the average values of the peak surges are 2.49 ± 0.25, 1.71 ± 0.13, and 1.31 ± 0.18 ft (1 ft = 0.3048 m).

For type 0 storms, the following empirical relation was deduced:

$$s = 0.102\,(1009.1 - p) \tag{5.86}$$

where, s is the peak surge (feet) and p is the local minimum hourly sea level pressure (millibars). Note that in this relation, the local minimum hourly mean sea level pressure is used to represent the central pressure of the storm when it landfalls near Hong Kong. For type 0 storms, the coefficient of correlation between the central pressure and the peak surge was –0.89. For type W and E storms the correlation was poor.

Again, for type 0 storms, the correlation coefficient between the peak surge s and the maximum hourly mean wind speed W_{60} was 0.84 and the following regression equation was derived:

$$s = 0.088\ W_{60} - 0.75 \tag{5.87}$$

The local wind field appears to have more influence on the type W and E storm surges than type 0. For type W, maximum surges are associated with winds from east-northeast, east, or east-southeast. The following relation has been empirically deduced for type W storm surges:

$$s_w = 0.00217\ W^2_{60} + 0.43 \tag{5.88}$$

The correlation coefficient between s_w and W^2_{60} was 0.88. No correlation could be found for type E storm surges.

LAU (1980a, 1980b) adapted the SPLASH (JELESNIANSKI, 1972, 1974) model to predict storm surges in Hong Kong. Using 57 hypothetical storms, peak surge heights at various locations along the South China coast near Hong Kong were determined. In these calculations, a standard storm is chosen with the following six parameters: (a) a central pressure of 973 mb at nearest approach, (b) a movement on bearing 300° at nearest approach, (c) a speed of 10 knots at nearest approach, (d) a radius of maximum winds of 26 nautical miles at nearest approach, (e) a nearest approach of 26 nautical miles, and (f) landfalling to the west of Hong Kong. This standard storm will generate on an open coast a surge (using the SPLASH program) of 1.92 m at North Point.

5.4.4 Explosively developing tropical Cyclones and Superthypoons in the Pacific

CLARK (1978a, 1978b), using satellite imagery, studied rapidly developing tropical cyclones in the northeastern Pacific Ocean during the period 1973–76. In his analysis, he made use of the so-called T number (DVORAK 1975a, 1975b)[1]. During this 4-yr period, of a total of 62 cyclones, 12 underwent a rapid development. The tracks of these rapidly developing tropical cyclones fall within a small area near Mexico (Fig. 5.64). CLARK (1978a, 1978b) cited persistent atmospheric conditions as contributing to the existence of a relatively small area of rapid development.

HOLLIDAY and THOMPSON (1979) made a study of rapidly deepening typhoons in the western part of the North Pacific Ocean using data from the period 1956–76. Their defini-

[1] The T number is based on the maximum wind speed. For example, TI corresponds to 25 knots, T2 to 30 knots, T3 to 45 knots, T4 to 65 knots, etc., with T8 corresponding to 170 knots (1 knot = 1.852 km · h^{-1}).

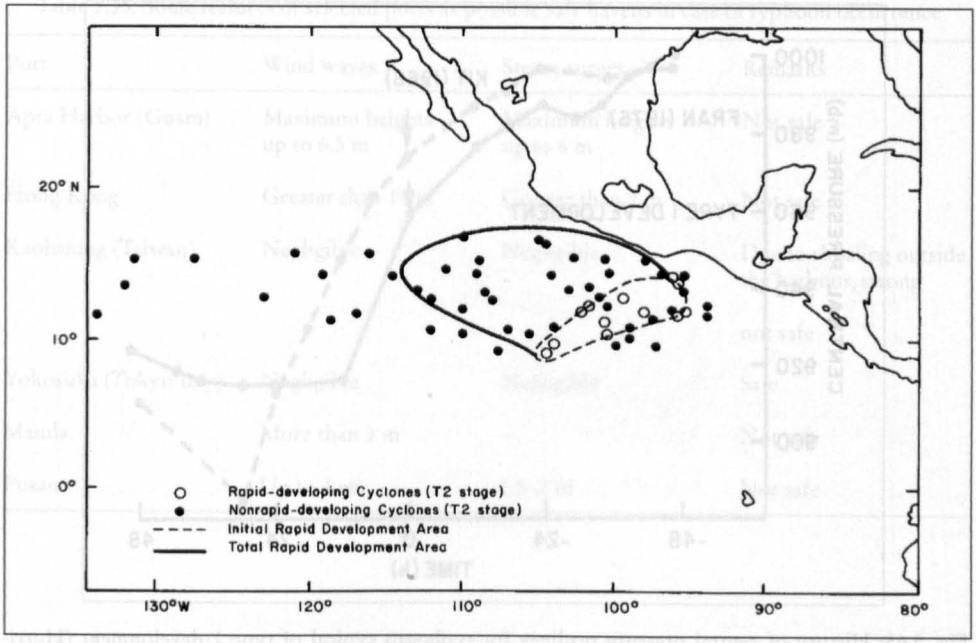

Fig. 5.64: Area of development of eastern North Pacific tropical cyclones, 1973–76 (CLARK, 1978b)

tion of rapid deepening is a fall in the central surface pressure by at least 42 mb in 24 h. In a total of 79 cases, rapid deepening (i.e. over an interval of 18 h with the steepest fall in the first 6 h) produced surface central pressures of 920 mb or less. For a tropical cyclone to mature into a typhoon, the underlying ocean temperature (up to a depth of 30 m) must be at least 28° C. This is a necessary condition for rapid deepening but not a sufficient condition.

Two basic types of deepening were noticed. In type 1 (Fig. 5.65) the central pressure falls at a moderate rate (≥ 0.8 mb $\cdot$ h^{-1}) at least over a period of 12–24 h. This is accompanied by accelerated development (≥ 1.75 mb h^{-1}). This behaviour for Typhoons Kit of 1966 and Fran of 1976 is shown in Fig. 5.65. In type 2 behaviour, initially there is slower development (< 0.8 mb $\cdot$ h^{-1}) suddenly followed by explosive (≥ 1.75 mb $\cdot$ h^{-1}). This is shown for Typhoons Virginia of 1957 and Anita of 1970 in Fig. 5.66. In the 79 case studies, 36 % exhibited type 1 behaviour and the remainder showed type 2 behaviour.

About 36 % of the rapid deepening occurred during daytime and 64 % occurred during nighttime. SHEETS (1969) suggested that this might be related to the differences in the atmospheric stability during day and night. However, SHEETS' (1969) study of hurricanes and FRANK's (1978) study of typhoons on diurnal variations showed little evidence for diurnal changes except in the temperature field and other Crameters in the upper troposphere and stratosphere.

The time interval between the weak circulation stages to the commencement of rapid deepening varied from 72 to 172 h. The time interval between the tropical storm stages to the onset of rapid deepening varied from 12 to 108 h. The interval between the time of reaching typhoon stage and initiation of rapid deepening varied from 0 to 72 h.

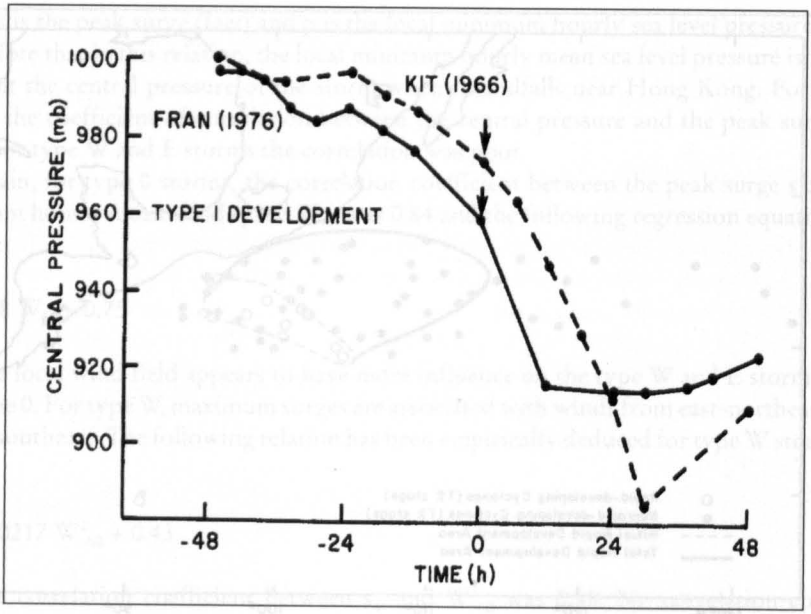

Fig. 5.65: History of central pressure readings for typhoons typical of type 1 development (Hurricanes Kit of June 1966 and Fran of September 1976). Arrow indicates onset of rapid deepening (≥ 1.75 mb $\cdot$ h^{-1}) (HOLLIDAY and THOMPSON, 1979)

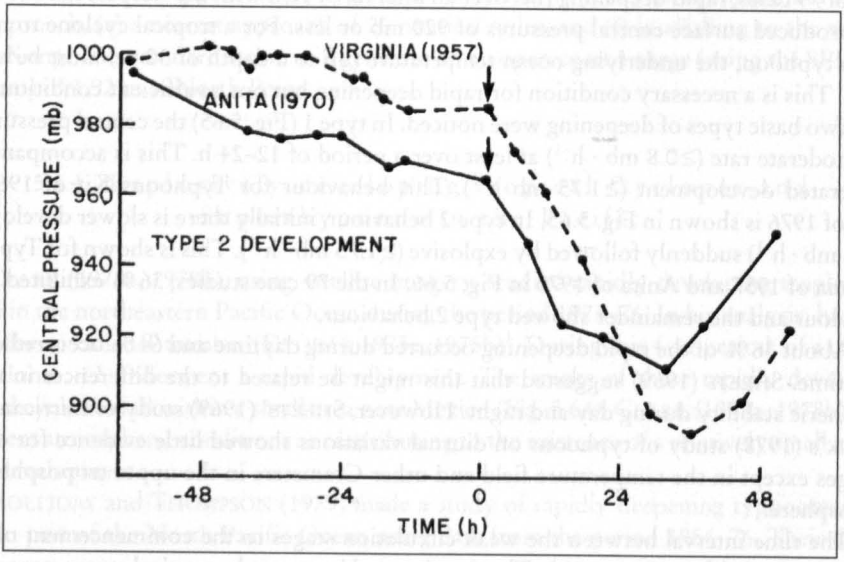

Fig. 5.66: History of central pressure readings for typhoons of type 2 development (Hurricanes Virginia of June 1957 and Anita of August 1970). Arrow indicates onset of rapid deepening (≥ 1.75 mb $\cdot$ h^{-1}) (HOLLIDAY and THOMPSON, 1979)

Table 5.35: Some features of selected ports as possible safe havens in case of typhoon occurrence

Port	Wind waves	Storm surges	Remarks
Apra Harbor (Guam)	Maximum heights up to 6.5 m	Maximum heights up to 6 m	Not safe
Hong Kong	Greater than 10 m	Greater than 2 m	Not safe
Kaohsiung (Taiwan)	Negligible	Negligible	Due to shoaling outside the harbour, strong not safe
Yokosuka (Tokyo Bay)	Negligible	Negligible	Safe
Manila	More than 3 m	–	Not safe
Pusan	Up to 4 m	1.5–2 m	Not safe

At the time of initiation of rapid deepening the eye diameters ranged from 29 to 37 km (average 33 km). Twelve hours after initiation of rapid deepening, the mean diameter of the eye decreased to 30 km, and 24 h after rapid deepening commencement, the average diameter was 26 km. Most of the rapid deepening occurred during the period July–November, with maximum activity in August and September. The area where rapid development began is shown in Fig. 5.67. The numerals show the number of cases during 1956–76.

Next, two interesting typhoons will be considered: Agnes of July 1978 and Tip of October 1979. The track of Typhoon Agnes is shown in Fig. 5.68. Because of the loop in the track, according to BELL (1979) it is the only tropical storm on record that caused gale signals to be hoisted twice at Hong Kong. Another unusual feature was that the so-called Fujiwara effect occurred between Typhoons Agnes and Wendy, although they were separated by 1000 mi (1600 km) apart. Another interesting feature from a public information point of view was that the American spacecraft *Apollo* ran into this with 60-knot (111 km · h^{-1}) winds and 25-ft (8 m) waves when it splashed down into the Pacific Ocean.

Super typhoon Tip developed in the western part of the North Pacific Ocean in early October 1979. This had at least two unique features: it holds the world record for the lowest minimum sea level pressure (870 mb) ever measured in a tropical cyclone (see Fig. 5.69) and it possessed the largest surface circulation pattern ever observed for a tropical cyclone (about 2200 km in diameter). Finally, this was transformed into an extratropical cyclone around October 18, 1979. Although it caused great destruction in Japan, the destruction was minimal for its size because the maximum intensity was reached while the system was still far away from inhabited areas.

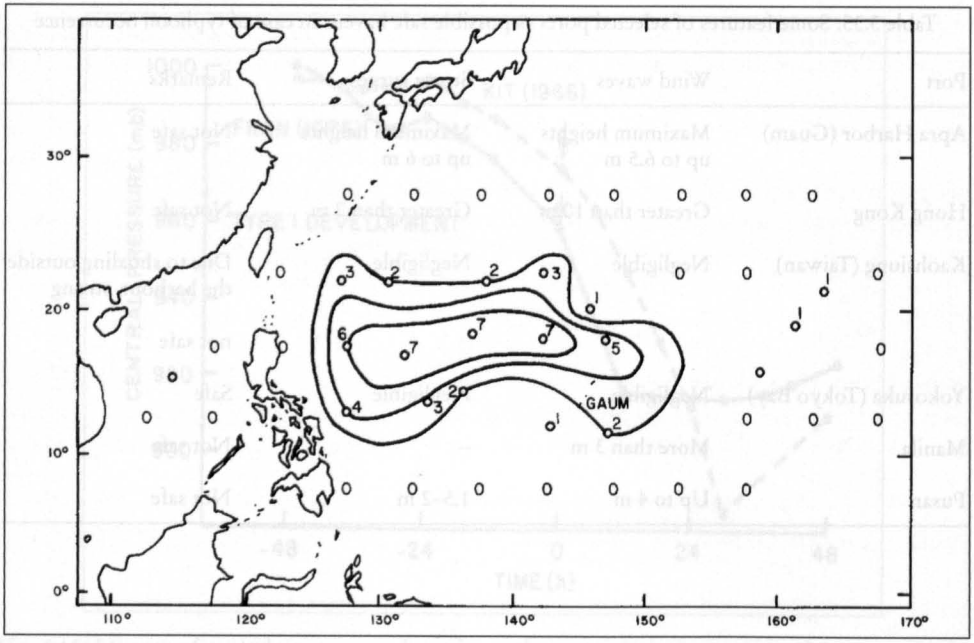

Fig. 5.67: Areas where typhoons intensified rapidly during summer and early fall (June 20–October 16). Numbers represent occurrences during 1956–76 (HOLLIDAY and THOMPSON, 1979)

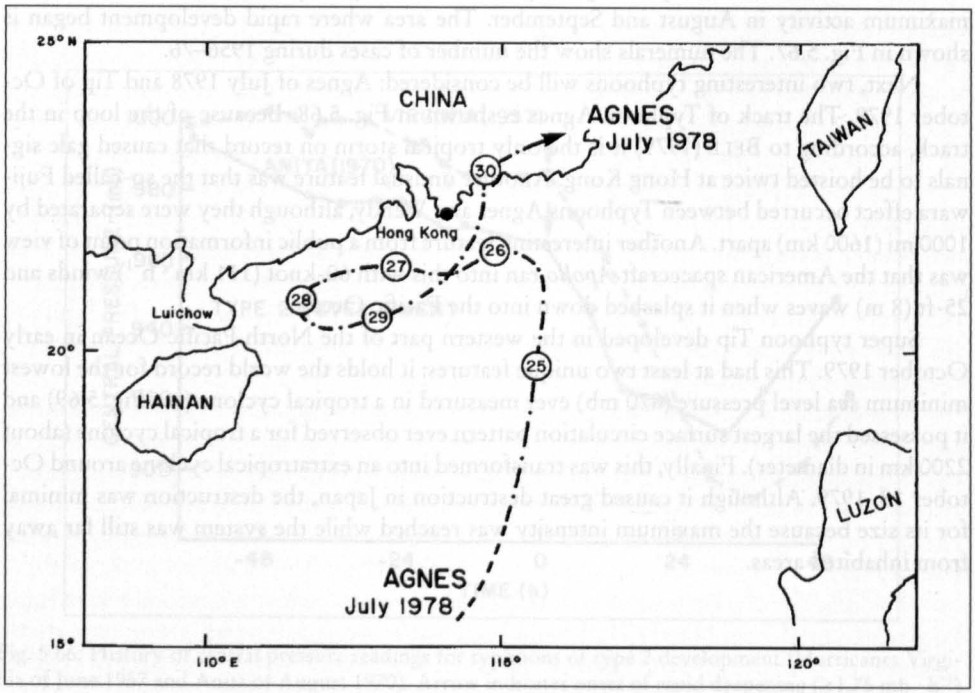

Fig. 5.68: Track of severe tropical storm Agnes from its formation on July 24, 1978, to its passage across the coast on July 30, 1978 (BELL, 1979)

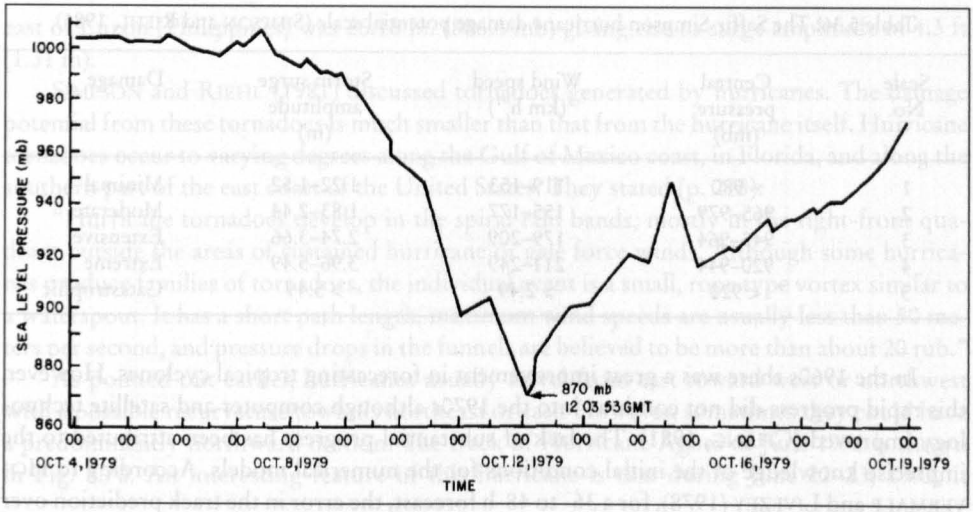

Fig. 5.69: Central pressure trace for Super typhoon Tip of October 1979 (DUNNAVAN and DIERCKS, 1980)

5.5 Tropical Cyclones of the Atlantic Ocean

Extratropical cyclones that affect North America are born in the western parts of the continent or in the Pacific Ocean and travel generally towards east (also east-northeast and north-east). Extratropical cyclones originating in the Atlantic generally do not affect North America but will travel towards Europe. Therefore this will be considered in chapter 5.1.3.

Here, basically, tropical cyclones originating in the Atlantic that affect mainly the North American continent will be considered.

5.5.1 Hurricanes Affecting the United States

The term "hurricane" comes from the Spanish word "huracon", which probably originated from Maya and Carib Indian usage meaning evil spirit, storm god, or devil. A hurricane is an intense tropical storm with wind speeds in excess of 74 mi · h^{-1} (64 knots or 33 m · s^{-1}). Hurricanes originating in the Atlantic Ocean, Caribbean Sea, and the Gulf of Mexico caused about thousands of deaths. About 90 % of the deaths were due to drowning in the storm surge. In the twentieth century, damage in the United States resulting from hurricanes exceeded more than $ 12 billion.

There appears to be no definite periodic cycle for hurricanes. For example during the 1940's Florida took the brunt, during the 1950s the east coast of the United States was mostly affected, and during the 1960s and 1970s most damage occurred along the coast of the Gulf of Mexico. There is some indication in the early 1980s that the same trend as in the 1940s and 1950s may occur (OWEN, 1980).

In the North Atlantic Ocean, from June through November, some 100 disturbances develop every year. Of these, about five to six intensify into hurricanes. About 70 % of these storms originate near the west coast of Africa and are referred to as Cape Verde storms. Locations were shown earlier (Fig. 1.19) at which Atlantic tropical storms reached hurricane intensity during the period 1901–63.

Table 5.36: The Saffir-Simpson hurricane damage potential scale (SIMPSON and RIEHL, 1981)

Scale No.	Central pressure (mb)	Wind speed (km h^{-1})	Storm surge amplitude (m)	Damage
1	~ 980	119–153	1.22–1.52	Minimal
2	965–979	155–177	1.83–2.44	Moderate
3	945–964	179–209	2.74–3.66	Extensive
4	920–944	211–249	3.96–5.49	Extreme
5	< 920	> 2.49	> 5.49	Catastrophic

In the 1960s there was a great improvement in forecasting tropical cyclones. However, this rapid progress did not continue into the 1970s although computer and satellite technology improved (CHANG, 1981). The lack of substantial progress has been attributed to the imprecise knowledge of the initial conditions for the numerical models. According to HOVERMALE and LIVEZEY (1978), for a 36- to 48-h forecast, the error in the track prediction over the oceans (where data is scarce) is three times the error at coastal stations. Not everybody agrees with this evaluation. The EOS Bulletin (Vol. 61, No. 28, July 15, 1980, p. 538) mentioned that a NOAA satellite that is 22 300 mi (35 680 km) out in space is locating Atlantic Ocean hurricanes with an average accuracy of about 17 nautical miles and is pinpointing their intensity within an average of 10 knots. For a recent summary of the status of operational prediction of tropical cyclone motion over the North Atlantic Ocean, see NEUMANN and PELISSIER (1981). These authors concluded that none of the seven models (five statistical and two dynamical) that are in use at the National Hurricane Center in Miami could be singled out as superior to the others in every respect. One disappointing aspect is that one cannot combine the good points from all these models into a single model.

Hurricanes are classified according to the Saffir-Simpson scale (named after Herbert Saffir, a consulting engineer, and Dr. R. H. Simpson, former director of the National Hurricane Center in Miami), which is an intensity scale based on the central pressure, wind speed, amplitude of the storm surge, and the resulting damage. This scale is illustrated in abbreviated form in Table 5.36. More details about this scale can be found in SIMPSON and RIEHL (1981). Note that in the twentieth century, only three storms affecting the United States are given the highest rank (5) on this scale. These are the Labour Day storm of 1935, Hurricane Camille of 1969, and Hurricane Allen of 1980.

Hurricane Statistics For The United States

Some of the most disastrous hurricanes of the twentieth century in the United States and the damage are listed in Table 1. 1. BRUUN et al. (1962) gave a list of major hurricanes affecting Florida during the period 1900–60. In this table there are 40 entries. The inverted barometer effect could be quite significant in the generation of storm surges here. For each inch (of mercury) of reduction of the central pressure of the hurricane (1 in. = 2.54 cm) the corresponding hydrostatic water head is 14 in. (BRETSCHNEIDER, 1967). For the storm of September 2, 1935, at Lower Matecumbe Key in Florida, the lowest central pressure was 26.35 in. Hg (892.3 mb). Taking the normal sea level pressure as 29.92 in. Hg (10 13.2 mb) gives a 4.1-ft (1.3 m) rise in water level. Similar inverted barometer effects could be noticed in typhoons, also. For the typhoon of August 18, 1927, the central pressure some 460 mi (740 km)

east of Luzon (Philippines) was 26.18 in. (886.6 mb) giving rise to surge amplitude of 4.3 ft (1.31 m).

SIMPSON and RIEHL (1981) discussed tornadoes generated by hurricanes. The damage potential from these tornadoes is much smaller than that from the hurricane itself. Hurricane tornadoes occur to varying degrees along the Gulf of Mexico coast, in Florida, and along the southern part of the east coast of the United States. They stated (p. 218):

"Hurricane tornadoes develop in the spiral rain bands, mostly in the right-front quadrant outside the areas of sustained hurricane or gale force winds. Although some hurricanes produce families of tornadoes, the individual event is a small, rope type vortex similar to a waterspout. It has a short path length, maximum wind speeds are usually less than 50 meters per second, and pressure drops in the funnels are believed to be more than about 20 rub."

As pointed out earlier, hurricanes usually travel from east toward west or northwest with a possible recurvature towards northeast or cast. However, sometimes they could have a predominantly northward motion. The track of Hurricane Agnes of June 1972 is shown in Fig. 5.70. An interesting feature of this hurricane is that during June 22–23, 1972, it

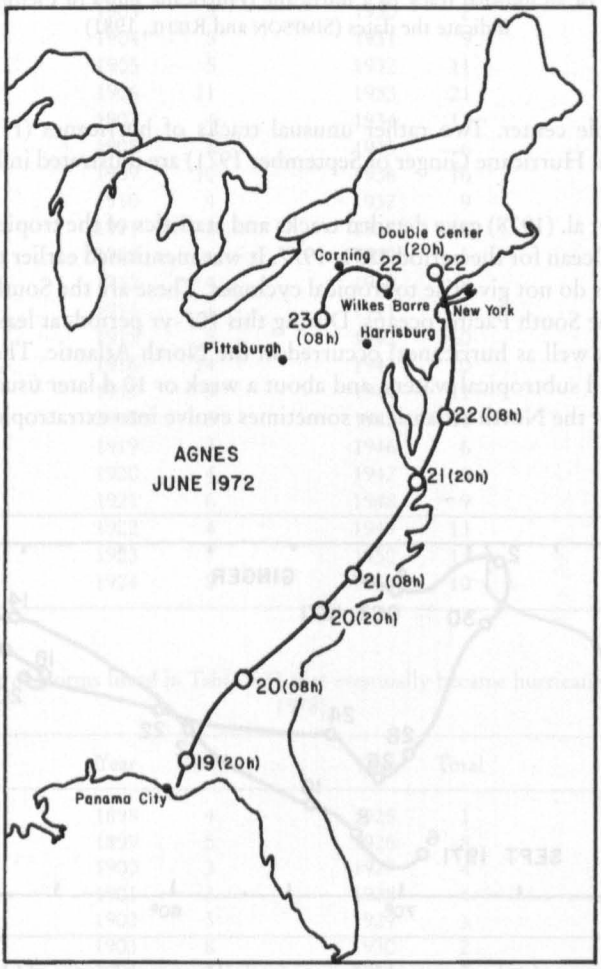

Fig. 5.70: Track of Hurricane Agnes of June 1972

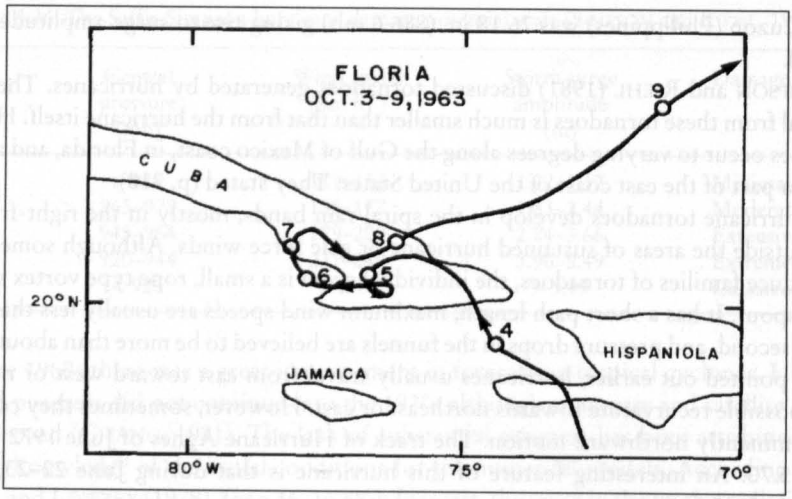

Fig. 5.71: Example of an unusual track of a hurricane (Hurricane Flora of October 1963). Numbers indicate the dates (SIMPSON and RIEHL, 1981)

exhibited a double center. Two rather unusual tracks of hurricanes (Hurricane Flora of October 1963 and Hurricane Ginger of September 1971) are illustrated in Fig. 5.71 and 5.72, respectively.

NEUMANN et al. (1978) gave detailed tracks and statistics of the tropical cyclones of the North Atlantic Ocean for the period 1871–1977. It was mentioned earlier that two large tropical ocean basins do not give rise to tropical cyclones. These are the South Atlantic and the eastern part of the South Pacific oceans. During this 107-yr period, at least 850 tropical cyclones (storms as well as hurricanes) occurred in the North Atlantic. These form over the warm tropical and subtropical waters, and about a week or 10 d later usually dissipate over the cold waters of the North Atlantic or sometimes evolve into extratropical cyclones.

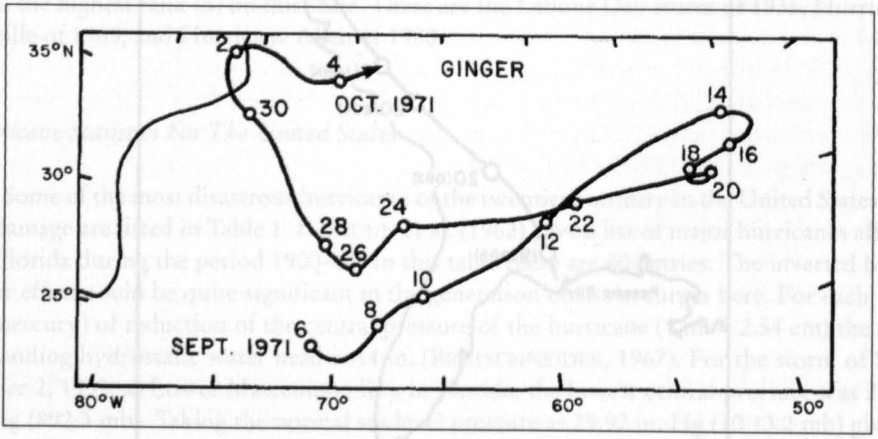

Fig. 5.72: Another example of an unusual hurricane track (Hurricane Ginger of October 1971). Numbers indicate the dates (SIMPSON and RIEHL, 1981)

These storms are listed in Table 5.37 for each of these years. Moreover the list of NEUMANN et al. (1978) encloses storms by month. It can be seen the dominance of storm events from August to October, which increase in number from May to August and decrease from October to December. Those that eventually became hurricanes are listed in Table 5.37. The distribution of the observed duration of hurricanes is given in Fig. 5.73.

Table 5.37: Number of recorded Atlantic tropical cyclones (excluding depressions and after 1967, including subtropical cyclones) that reached at least tropical storm intensity, 1871–1977 (NEUMANN et al., 1978)

Year	Total	Year	Total	Year	Total	Year	Total
1871	6	1898	9	1925	2	1952	7
1872	5	1899	6	1926	11	1953	14
1873	5	1900	7	1927	7	1954	11
1874	7	1901	10	1928	6	1955	12
1875	4	1902	5	1929	3	1956	8
1876	3	1903	9	1930	2	1957	8
1877	8	1904	5	1931	9	1958	10
1878	10	1905	5	1932	11	1959	11
1879	8	1906	11	1933	21	1960	7
1880	9	1907	4	1934	11	1961	11
1881	6	1908	8	1935	6	1962	5
1882	3	1909	10	1936	16	1963	9
1883	4	1910	4	1937	9	1964	12
1884	3	1911	4	1938	8	1965	6
1885	8	1912	6	1939	5	1966	11
1886	10	1913	4	1940	8	1967	8
1887	17	1914	1	1941	6	1968	8
1888	9	1915	5	1942	10	1969	18
1889	9	1916	14	1943	10	1970	10
1890	1	1917	3	1944	11	1971	13
1891	11	1918	5	1945	11	1972	7
1892	9	1919	3	1946	6	1973	8
1893	12	1920	4	1947	9	1974	11
1894	6	1921	6	1948	9	1975	9
1895	6	1922	4	1949	13	1976	10
1896	6	1923	7	1950	13	1977	6
1897	5	1924	8	1951	10		

Table 5.38: Number of storms listed in Table 5.37 that eventually became hurricanes (NEUMANN et al., 1978)

Year	Total	Year	Total	Year	Total	Year	Total
1871		1898	4	1925	1	1952	6
1872		1899	5	1926	8	1953	6
1873		1900	3	1927	4	1954	8
1874		1901	3	1928	4	1955	9
1875		1902	3	1929	3	1956	4
1876		1903	8	1930	2	1957	3
1877		1904	2	1931	2	1958	7
1878		1905	1	1932	6	1959	7

Table 5.38: (Continued)

Year	Total	Year	Total	Year	Total	Year	Total
1879		1906	6	1933	9	1960	4
1880		1907	0	1934	6	1961	8
1881		1908	5	1935	5	1962	3
1882		1909	4	1936	7	1963	7
1883		1910	3	1937	3	1964	6
1884		1911	3	1938	3	1965	4
1885		1912	4	1939	3	1966	7
1886	8	1913	3	1940	4	1967	6
1887	10	1914	0	1941	4	1968	5
1888	5	1915	4	1942	4	1969	12
1889	5	1916	11	1943	5	1970	5
1890	1	1917	2	1944	7	1971	6
1891	8	1918	3	1945	5	1972	3
1892	4	1919	1	1946	3	1973	4
1893	10	1920	4	1947	5	1974	4
1894	5	1921	4	1948	6	1975	6
1895	2	1922	2	1949	7	1976	6
1896	6	1923	3	1950	11	1977	5
1897	2	1924	5	1951	8		

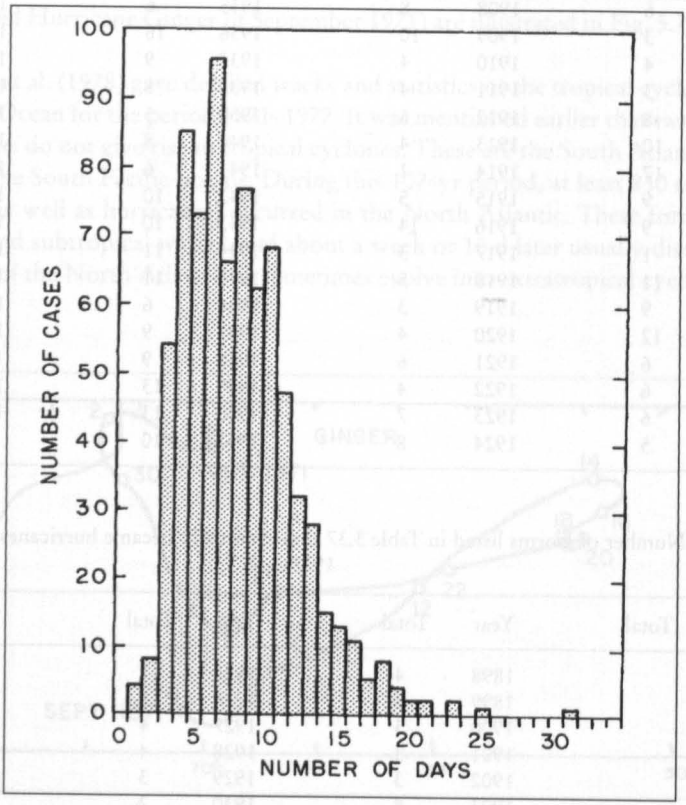

Fig. 5.73: Distribution of observed duration of Atlantic tropical cyclones, 1886–1977 (NEUMANN et al., 1979)

Die Küste, 63 Global Storm Surges (2001), 1-623

FRANK (1978) studied the geographical distribution of the generation areas and other characteristics of these Atlantic storms for the period 1968–77. During this 10-yr period, a total of 1044 systems appeared. Of these, 58 % originated near Dakar (Africa). Of the approximately 100 tropical weather systems developing in each hurricane season (June 1–November 30) about 25 % become depressions and about 10 % become storms.

NEUMANN and HILL (1976) described the computerized tropical cyclone climatological data at the National Hurricane Center in Miami. The tracks of the 680 recorded Atlantic tropical cyclones for the period 1886–1969 were plotted. Later, this number increased to 743 tracks up to the end of the 1975 hurricane season. Most of these data are based on ship reports, and in later years these data were supplemented by aircraft reconnaissance and satellite data. The storm track data are maintained at the National Climatic Center in Asheville, NC. Based on these computerized data. NEUMANN and CRY (1978) discussed the revised Atlantic tropical cyclone climatology.

Some Comparisons of the Tropical Cyclone Activity in the Atlantic and Pacific Oceans

NUNEZ and GRAY (1978) and GRAY (1978c) compared some meteorological parameters associated with Atlantic hurricanes and Pacific typhoons, and their findings are summarized in Table 5.39.

Table 5.39: Comparison of Atlantic hurricanes and Pacific typhoons

Parameter	Atlantic hurricanes (West Indies)	Pacific typhoons
Temperature anomaly. This is determined as follows. A mean temperature is calculated by averaging the temperature values at 9 and 15° to the east and west of the position of the cyclone. Deviation from this mean temperature is the anomaly	Warm core throughout most of the troposphere. Warmest temperature at about 300 mb. The anomaly is +4°C for the hurricane (at 300 mb) Cold core in the upper troposphere and lower stratosphere. This region occurs at a lower level than for typhoons and its radial extent is greater	Warm core throughout most of the troposphere. Warmest temperature at about 250 mb. The anomaly is +7° C for the typhoon (at 250 mb). Cold core in the upper troposphere and lower stratosphere
Relative humidity	About 10 % less than for typhoons at equivalent radii and heights Boundary layer relative humidity is about 15 % lower than for the West Pacific	Moister inner core with relative humidities greater than 90 % up to 400 mb whereas in the hurricane, such a high relative humidity cannot be found higher than at 575 mb
Radial winds	Maximum inflow at 950 mb with a wind of 8 ms-'. At 150 mb there are two outflow jets: northeast and southwest. The northeast jet is about four times stronger	Maximum inflow at 950 mb with a wind of 6 ms-'. At 150 mb there are two outflow jets: northeast and southwest. The southwest jet is somewhat greater

Table 5.39: (Continued)

Parameter	Atlantic hurricanes (West Indies)	Pacific typhoons
Tangential wind	Maximum cyclonic flow is at the top of the frictional boundary layer at 850 mb	Maximum cyclonic flow is at the top of the frictional boundary layer at 850 mb
	The tangential wind is smaller than in typhoons	
	The anticyclonic maximum occurs at 150 mb	The anticyclonic maximum occurs at 150 mb. The anticyclonic circulation is relevant also in determining the weather associated with the typhoon
	Generally the hurricane size is smaller than a typhoon's	
	Vertical shear between 950 and 150 mb is 10–15 ms-'	Vertical shear between 950 and 150 mb is 15–20 ms-'
Inflow angle	The boundary layer inflow angle decreases from quadrant to quadrant in the following order: right, front, back, left	The boundary layer inflow angle decreases in the following order: front, right, left, back
Steering current concept for predicting tracks	Applies	Applies
		West Pacific typhoons move more to the left of the mean current than do West Atlantic hurricanes

5.6 Tropical Cyclones of the Indian Ocean

There are no extratropical cyclones in the North Indian Ocean. The extratropical cyclones of the South Indian Ocean are not very relevant for storm surge studies and, in any case, these will be briefly considered. In this section will be considered mainly the tropical cyclones of the South and North Indian oceans with emphasis on the Bay of Bengal and to a lesser extent on the Arabian Sea. However, while discussing tropical cyclones, another type of cyclone (which is neither tropical nor extratropical) referred to as a subtropical cyclone will be considered.

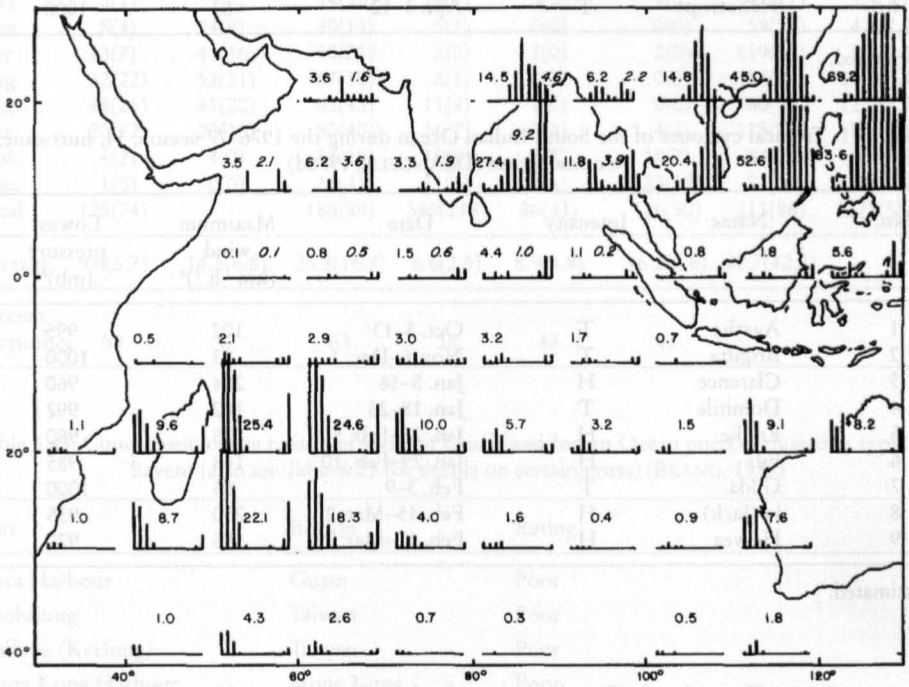

Fig. 5.74: Frequency of tropical cyclones in the Indian Ocean (average numbers of occurrences per 10 yr. for each 10° square by months). Roman-type numbers indicate average 10-yr totals over the northern Indian Ocean. The unblackened segments of the histograms and the italicized numbers given corresponding information for severe tropical storms (RAMAGE, 1971)

Tropical cyclones develop in all parts of the Indian Ocean. This is in contrast with the Atlantic and Pacific Oceans. There are no tropical cyclones in the South Atlantic and eastern part of the South Pacific. The average number of tropical cyclones during a 10-yr period for each 10° square by months is shown in Fig. 5.74. It can be seen that the highest frequencies occur north of Indonesia (not counting the Philippines area). In the Bay of Bengal and to the region east of the Malagasy Republic (Madagascar) high frequencies also occur. However, one difference is that whereas in the Bay of Bengal the highest frequencies are during September–December, in the region east of the Malagasy Republic (i.e. the western part of the South Indian Ocean) and in the region west of the west coast of Australia (i.e. the eastern part of the South Indian Ocean) the high frequencies occur during January–March.

Table 5.40: Tropical cyclones of the South Indian Ocean for the 1975–76 season. H, hurricane; T, tropical storm (DEANGELIS, 1977)

No.	Name	Intensity	Date	Maximum wind ($km \cdot h^{-1}$)[a]	Lowest pressure (mb)[a]
1	Audrey	T	Nov. 17–29	96	995
2	Barbara	H	Dec. 3–19	157	980
3	Clotilde	H	Jan. 7–20	250	980
4	Danae	H	Jan. 12–29	250	955
5	Gladys	T	Mar. 27–Apr. 10	111	998
6	Heliotrope	T	Apr. 3–12	83	1000

[a]Estimated.

Table 5.41: Tropical cyclones of the South Indian Ocean during the 1976–77 season; H, hurricane; T, tropical storm (DEANGELIS, 1978d)

No.	Name	Intensity	Date	Maximum wind ($km \cdot h^{-1}$)[a]	Lowest pressure (mb)[a]
1	Agathe	T	Oct. 3–13	102	995
2	Brigitta	T	Nov. 6–Dec. 1	83	1000
3	Clarence	H	Jan. 5–16	204	960
4	Domitile	T	Jan. 18–23	102	992
5	Emilie	H	Jan. 26–Feb. 5	176	980
6	Fifi	H	Jan. 29–Feb. 10	148	985
7	Gilda	T	Feb. 3–9	83	1000
8	Io (Jack)	H	Feb. 15–Mar. 2	250	935
9	Hervea	H	Feb. 17–Mar. 3	185	970

[a] Estimated.

5.6.1 Tropical Cyclones of the South Indian Ocean

Certain features of the tropical cyclones of the South Indian Ocean for the seasons 1975–76 and 1976–77 are summarised in Table 5.40 and 5.41, respectively. In the 1975–76 season there was a total of six tropical cyclones of which three reached hurricane strength. In the 1976–77 season, of a total of nine cyclones, five became hurricanes. The tropical cyclones for the period 1965–77 are summarised by month for various ocean basins in Table 5.42. Note that in terms of frequency, the North Indian Ocean has the lowest and the South Indian Ocean has the second lowest. However, this may be misleading when one considers the damage due to tropical cyclones (and storm surges generated by them). More than 60 % of the deaths and almost 40 % of the damage due to tropical cyclones occur on lands bordering the Bay of Bengal, which is only a small part of the North Indian Ocean.

Considered earlier were typhoon waves among harbours located around the Pacific Ocean. Some Indian Ocean harbours as well as some Pacific Ocean harbours (for comparison) are listed in Table 5.43. Among the Indian Ocean harbours, only Colombo is listed as "good" and Karachi as "marginal" (BRAND, 1978).

Table 5.42: Tropical cyclones in various ocean basins during the period 1965–77. Numbers in parentheses indicate tropical cyclones that reached hurricane intensity (i.e. winds ≥ 119 km · h^{-1}) (DE-ANGELIS, 1979a)

Month	North Atlantic	Eastern North Pacific	Western North Pacific	North Indian	South Indian	Australia-South Pacific	Total	Average
Jan.	0(0)	0(0)	9(5)	2(1)	29(17)	52(20)	92(43)	7.1(3.3)
Feb.	0(0)	0(0)	4(1)	0(0)	30(16)	41(16)	75(33)	5.8(2.5)
Mar.	0(0)	0(0)	6(1)	0(0)	15(5)	39(18)	60(24)	4.6(1.8)
Apr.	0(0)	0(0)	11(9)	4(2)	6(1)	18(6)	39(18)	3.0(1.4)
May	3(1)	5(3)	14(10)	14(5)	3(0)	4(3)	42(22)	3.3(1.7)
June	8(4)	24(9)	20(13)	5(1)	0(0)	0(0)	59(27)	4.4(2.1)
July	13(7)	41(16)	60(35)	2(0)	1(0)	2(0)	119(58)	9.2(4.5)
Aug.	32(22)	53(31)	67(38)	2(1)	0(0)	0(0)	154(92)	11.8(7.1)
Sept.	44(26)	41(20)	63(43)	11(4)	1(0)	0(0)	160(93)	12.3(7.2)
Oct.	20(12)	20(10)	50(40)	16(7)	5(3)	4(1)	115(73)	8.8(5.6)
Nov.	4(2)	4(0)	34(19)	19(8)	5(2)	18(7)	84(38)	6.5(2.9)
Dec.	1(0)	0(0)	11(4)	11(4)	21(6)	33(15)	77(29)	5.9(2.2)
Total	125(74)		188(89)	349(218)	86(33)	116(50)	211(86)	1075(550)
Average	9.6(5.7)	14.5(6.8)	26.8(16.8)	6.6(2.5)	8.9(3.8)	16.2(6.6)	82.7(42.3)	
Percent hurricanes	59	47	63	38	43	41		

Table 5.43: Comparison of the ratings of western Pacific and Indian Ocean ports evaluated as typhoon havens (also see Table 6.29 for details on certain ports) (BRAND, 1978)

Port	Region	Rating
Apra Harbour	Guam	Poor
Kaohsiung	Taiwan	Poor
Chilung (Keelung)	Taiwan	Poor
Hong Kong Harbour	Hong Kong	Poor
Yokosuka	Japan	Good
Nunazu operating area	Japan	Poor
Lwakuni	Japan	Marginal (but has easily accessible anchorages close by that are good)
Kure	Japan	Good
Saskebo	Japan	Good (except for carriers)
Kagoshima	Japan	Poor
Buckner Bay (Okinawa)	Japan	Poor
Naha (Okinawa)	Japan	Poor
Subic Bay	Philippines	Marginal to poor
Manila	Philippines	Poor
Cebu	Philippines	Poor
Inchon	Korea	Poor (unless shelter is available in the tidal basin, then it would be considered a good haven)

Table 5.43: (Continued)

Port	Region	Rating
Pusan	Korea	Poor
Chinhae	Korea	Marginal (but has easily accessible anchorage's nearby that are considered good)
Colombo	Sri Lanka	Good
Karachi	Pakistan	Marginal
Auckland	New Zealand	Good to marginal
Freemantle	Australia	Marginal (unless shelter is available in Cockburn Sound or the inner harbour, then it would he considered good)
Diego Garcia Harbour	Diego Garcia	Poor

Australia and New Zealand

Although storm surges are not a serious problem in Australia and New Zealand, they do occur and cause damage. In Australia, the areas particularly susceptible to storm surges are the central north coast of eastern Queensland and parts of the Gulf of Carpentaria. HOPLEY and HARVEY (1979) studied the storm surges all along the coast of Australia. The cyclones in this study are listed in Table 5.44. Cyclones affect the northern parts of the east and west coasts of Australia, as well as its north coast. The frequency of cyclones (capable of generating storm surges) varies from 0.4 to 2.8 per year. Lowest central pressures occur on the east and west coasts between 20 and 25° S. The central pressures on the west coast are usually 3–4 mb lower than those on the coast of Queensland. Central pressures drop gradually towards the north but more drastically towards the south.

Intense cyclones with central pressures less than 960 mb occur on the central part of the west coast (Northwest Cape to Port Hedland), the region between Princess Charlotte Bay and Mackay on the Queensland coast. However, in the Gulf of Carpentaria, central pressures less than 960 mb rarely occur.

Cyclones in the Australian region usually travel with speeds between 6 and 11 knots although sometimes with a speed as high as 35 knots (particularly on the Queensland coast between 25 and 30° S). They travel with low speeds over the Gulf of Carpentaria and off Arnhemland (COLEMAN, 1972). The variability in the meteorological parameters associated with cyclones in the Australian region, based on data for 1960–72, is shown in Table 5.44 of HOPLEY and HARVEY (1979). This variability was determined for the following three parameters: (a) variability in the direction of movement by measuring the difference between the point on the coast for which the cyclone was heading 24 h prior to landfall and the observed landfall location, (b) variability in pressure by comparing changes in the pressure field during the 24 h prior to landfall, and (c) variability in the speed of movement by comparing the average speed in the 24 h prior to landfall with the mean speed in the previous 24 h.

NELSON (1975) listed 30 severe tropical cyclones in the Australian region during the period 1880–1970 that generated storm surges with amplitudes of at least 0.5 m along the north coast of Australia. One of the lowest central pressures ever recorded, a storm on

March 5, 1899, that travelled over Bathurst Bay and struck Barrow Point on the Queensland coast, was 914 mb. The storm and the storm surge together killed 300 people and the surge penetrated 5 km inland (WHITTINGHAM, 1958).

Table 5.44: Cyclones in and around Australia (HOPLEY and HARVEY, 1979)

Name	Date of landfall or nearest point to coast	Tidal station closest to cyclone	Lowest central pressure (mb)	Highest record of surge at any station (m)	Remarks
Adeline	Jan. 28, 1973	Centre Island	990	0.52	
Agnes	Mar. 6, 1956	Townsville	961	1.4	
Althea	Dec. 24, 1971	Townsville	952	2.85	3.6 m at Toolakea
Bridget	Jan. 27, 1969	Lucinda	1002	0.34	
Emily	Apr. 2, 1972	Gladstone	920	1.78	Filled rapidly before crossing
Eva	Dec. 4, 1970	Broome	970	0.16	1.2- to 13-m surge reported at Broome (Met. Bur. 1973)
Gertie	Feb. 16, 1971	Lucinda	983	0.52	
Glynis	Feb. 6, 1970	Perth	970	1.01	Surge incorrectly reported as 4.1 m above normal at Carnarvon (Met. Bureau, 1973). Record tides elsewhere
Ida	Feb. 16, 1971	Mourilyan	980	0.37	
Ingrid	Feb. 16, 1970	Carnarvon	970	1.32	Surge incorrectly reported as 2.3 m above normal at Carnarvon (Met. Bur. 1973)
Joan	Dec. 7, 1975	Port Hedland	-992	1.52	Port Hedland recorder malfunction during rising surge
Leah	Feb. 28, 1973	Milner Bay	990	0.45	
Madge	Mar. 4, 1973	Milner Bay	990	0.42	Affected east coast and Gulf
Pam	Feb. 6, 1974	Kirra	930	0.4	Came within 450 km of Queensland but very large cyclone
Sheila-Sophie	Feb. 3, 1971	Port Hedland	970	1.8	
Tracy	Dec. 24, 1974	Darwin	940	1.6	2.0-m surge reported to north of city
Una	Dec. 19, 1973	Townsville	988	0.72	
Wanda	Jan. 25, 1974	Noosa	990	0.6	Associated with Brisbane floods
Zoe	Mar. 13, 1974	Broadwater	975	0.56	

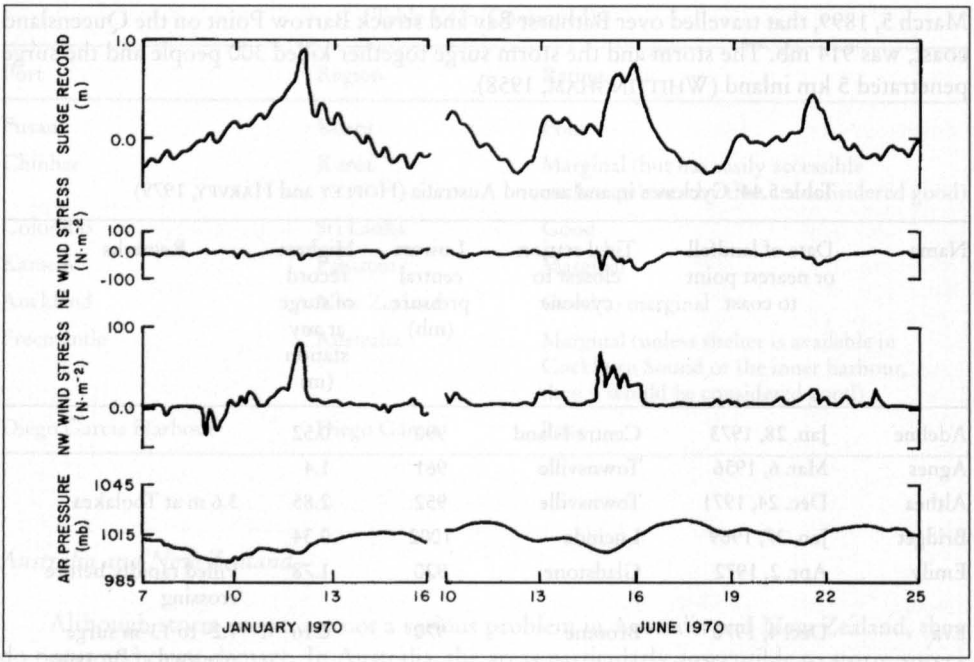

Fig. 5.75: Storm surges, atmospheric pressure, and wind stress at Adelaide, Australia (TRONSON and NOYE, 1973)

In the 1970s two storm surges did considerable damage in Australia. Cyclone Althea of December 24, 1971, made a landfall to the north of Townsville on the Queensland coast. Winds up to 196 km · h^{-1} and lowest central pressure of 971.5 mb generated a maximum surge of about 2.7 m at Townsville. Cyclone Tracy of December 25, 1974, hit Darwin; a central pressure of 955 mb and winds up to 200 km · h^{-1} generated a maximum surge of about 1.6 m.

TRONSON and NOYE (1973) developed statistical models to predict storm surges on the coast near Adelaide in South Australia. The storm surges in this region are particularly sensitive to the wind direction. On April 12, 1948, steady winds from the southwest with a speed of 90 km · h^{-1} caused a surge of about 1.2 m. On June 28, 1972, a surge with the same amplitude was generated by winds from the northwest, with a speed of about 45 km. h'. Surges with amplitudes of up to 4 m can occur at Adelaide, e.g. on May 12, 1960, and June 28, 1972. The atmospheric pressure field, the wind stress, and the surges at Adelaide for two cases (January 7–16 and June 10–25, 1970) are shown in Fig. 5.75.

HEATH (1979) discussed the storm surges on the coasts of New Zealand. Storm surge amplitudes on the coasts of New Zealand are rather small and are usually less than 1 m (AGNEW, 1966; GILMOUR, 1963; PICKRILL, 1972). Even though the amplitudes may be small, they could cause severe erosion, especially on the west coast of the North Island, in the Bay of Plenty, and on the east coast of the North Island, north of Auckland.

HEATH (1979) studied the following three surges: April 9–11, 1968, on the east coast of the North Island, July 30–August 1, 1975, on the east coast of the South Island, and September 11–14, 1976, on the west coast of the North Island. The surface weather chart for the third case is given in Fig. 5.76.

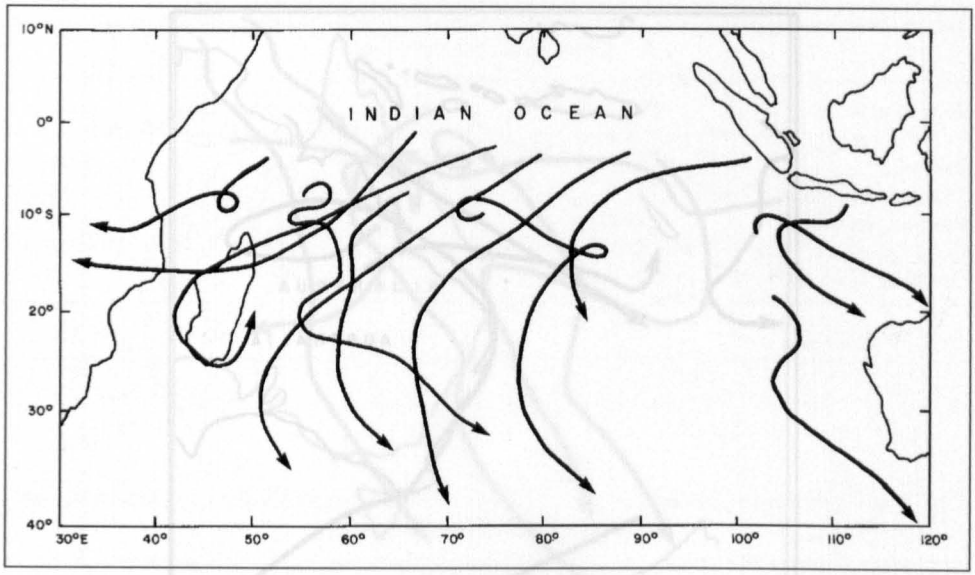

Fig. 5.76: Typical tropical cyclone tracks in the South Indian Ocean between the Malagasy Republic and the west coast of Australia

Australia is the only continent that is affected by tropical cyclones on both the east and west coasts. Certain features of the tropical cyclones of Australia are described in Tables 5.45–5.47. The average tropical cyclone frequencies for the west and east coasts of Australia for the months of December and January are given in Fig. 5.81 and 5.82, respectively. The frequency of cyclone days in Australia is given in Fig. 5.83 and the cyclone frequency change (i.e. trend) during the period 1905–55 is shown in Fig. 5.84.

Some typical tropical cyclone tracks in the region between the Malagasy Republic and the west coast of Australia are illustrated in Fig. 5.77 and typical tracks near the west coast of Australia in Fig. 5.78. For comparison, tropical cyclone tracks near the east coast of Australia and those affecting New Zealand are shown in Fig. 5.79 and 5.80, respectively.

Australia is the only continent that is affected by tropical cyclones on both the east and west coasts. Certain features of the tropical cyclones of Australia are described in Tables 5.45–5.47 The average tropical cyclone frequencies for the west and east coasts of Australia for the months of December and January are given in Fig. 5.77 and Fig. 5.78, respectively. The frequency of cyclone days in Australia is given in Fig. 5.79 and the cyclone frequency change (i.e. trend) during the period 1905–55 is shown in Fig. 5.80.

Fig. 5.77: Typical tropical cyclone tracks near the west coast of Australia

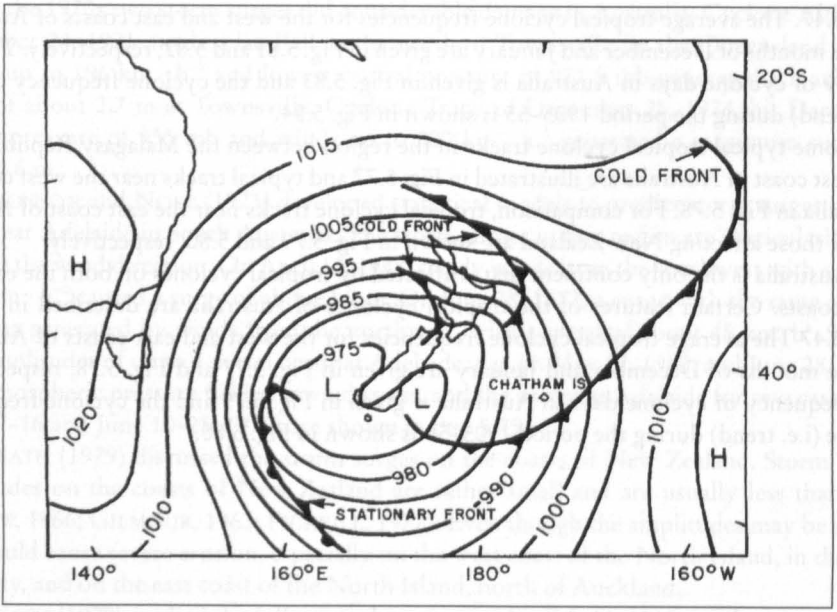

Fig. 5.78. Simplified surface weather chart at 0 h (New Zealand Standard Time) on September 13, 1976 (HEATH, 1979)

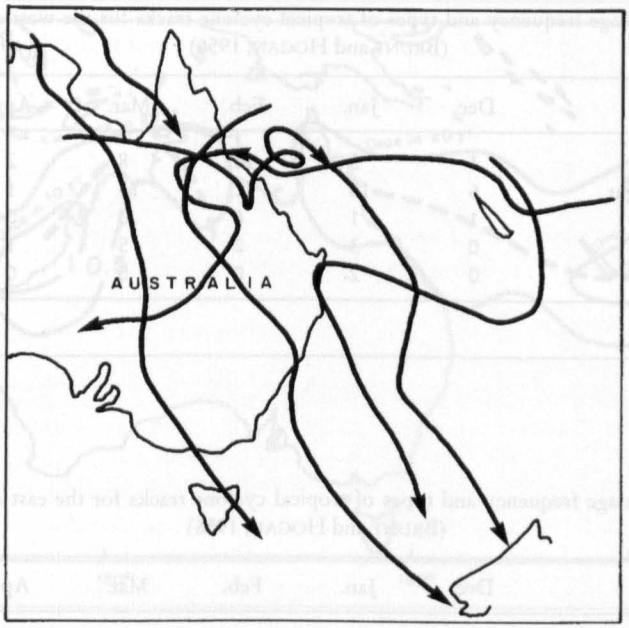

Fig. 5.79: Typical tropical cyclone tracks near the east coast of Australia

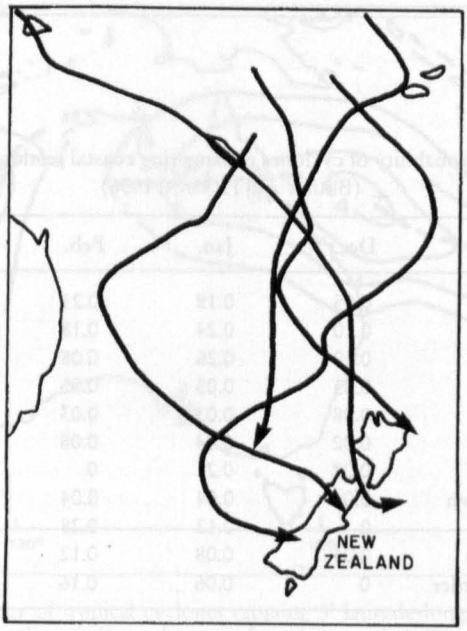

Fig. 5.80: Typical tropical cyclone tracks near New Zealand

Table 5.45: Percentage frequency and types of tropical cyclone tracks for the west coast of Australia (BRUNT and HOGAN, 1956)

Type of path	Dec.	Jan.	Feb.	Mar.	Apr.	Season
Parabolic	4	5	12	8	2	31
More or less straight	6	16	12	13	1	48
Reverse curvature	1	1	6	0	0	8
Cusp	0	3	2	5	1	11
Doubling of track	0	2	0	0	0	2
Total						100

Table 5.46: Percentage frequency and types of tropical cyclone tracks for the east coast of Australia (BRUNT and HOGAN, 1956)

Type of path	Dec.	Jan.	Feb.	Mar.	Apr.	Season
Parabolic	2	6	14	15	2	39
More or less straight	2	11	8	11	5	37
Reverse curvature	1	8	0	1	2	12
Cusp	0	2	7	1	0	10
Doubling of track	1	0	0	0	1	2
Total						100

Table 5.47: Probability of cyclones endangering coastal sections in Australia (BRUNT and HOGAN, 1956)

Section of coast	Dec.	Jan.	Feb.	Mar.	Apr.
Hamlin Pool-Roebourne	0.05	0.18	0.21	0.18	0
Roebourne-Broome	0.10	0.24	0.18	0.13	0.03
Broome-Wyndham	0.10	0.26	0.08	0.13	0.03
Wyndham-Darwin	0.03	0.03	0.05	0.03	0
Darwin-Melville Bay	0.08	0.03	0.03	0.03	0.03
N.T. Gulf coast	0.02	0.14	0.08	0.08	0
Queensland Gulf coast	0.02	0.21	0	0	0
Thursday Island-Cooktown	0.04	0.04	0.04	0.08	0.04
Cooktown-Townsville	0	0.12	0.28	0.12	0.04
Townsville-Rockhampton	0.04	0.08	0.12	0.16	0.06
Rockhampton-N.S.W. border	0	0.06	0.16	0.16	0.06

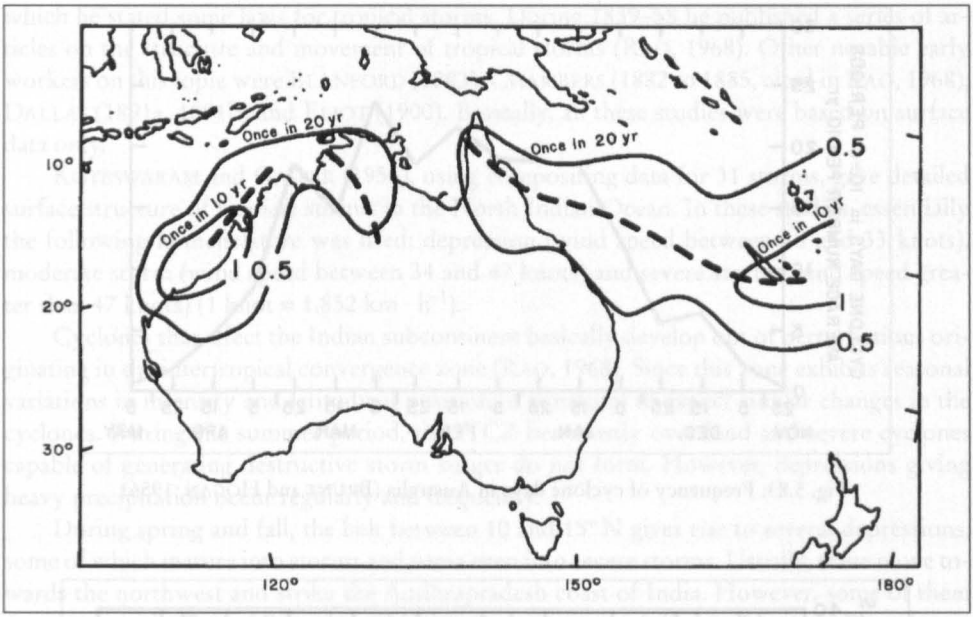

Fig. 5.81: Average frequency of tropical cyclones crossing 5' latitude-longitude squares per 10 yr. in December; heavier broken lines indicate the axes of maximum values (BRUNT and HOGAN, 1956)

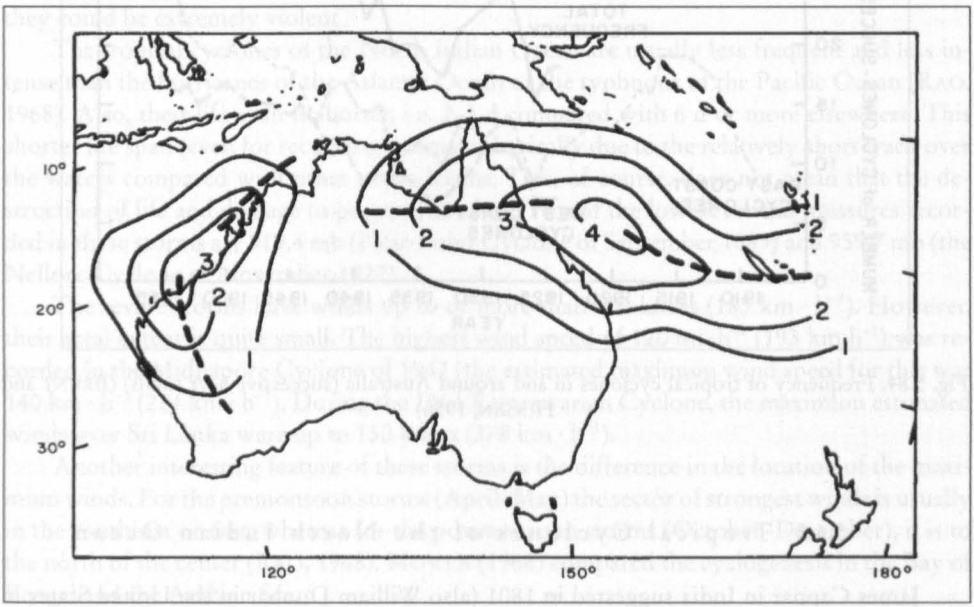

Fig. 5.82: Average frequency of tropical cyclones crossing 5' latitude-longitude squares per 10 yr. in January. Heavier broken lines indicate the axes of maximum values (BRUNT and HOGAN, 1956)

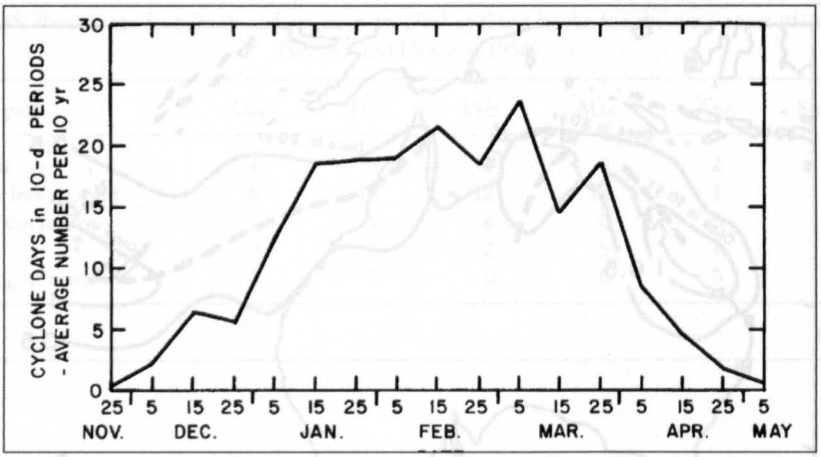

Fig. 5.83: Frequency of cyclone days in Australia (BRUNT and HOGAN, 1956)

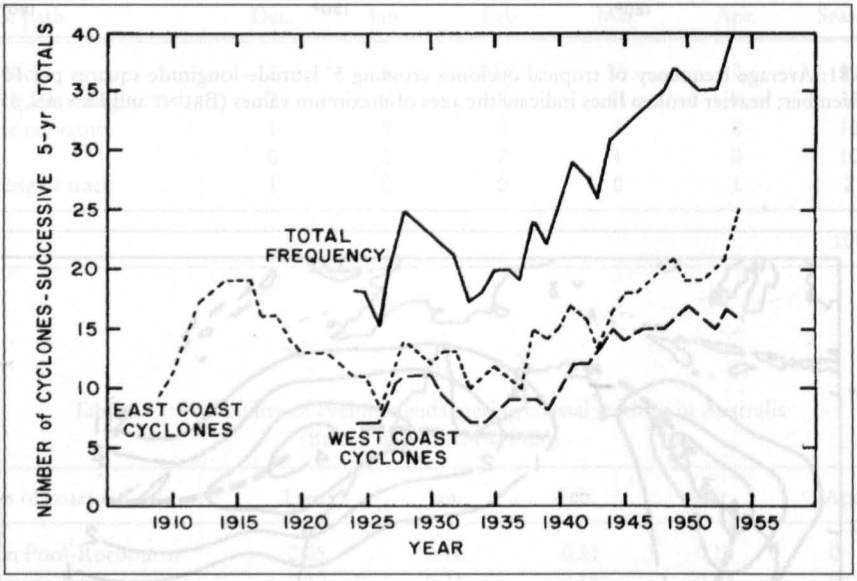

Fig. 5.84: Frequency of tropical cyclones in and around Australia (successive 5-yr totals) (BRUNT and HOGAN, 1956)

5.6.2 Tropical Cyclones of the North Indian Ocean

James Cappar in India suggested in 1801 (also William Dunbar in the United States in the same year) that there is a vortex in the center of a tropical cyclone (LUDLAM, 1963). However, it was Henry Piddington who, in 1851, coined the word "cyclone" from the Greek word „kyklon" meaning coil of snake to describe the rotary motion. Piddington was the president of the Marine Courts at Calcutta, India, and in 1851 he published a sailor's handbook in

which he stated some laws for tropical storms. During 1839–58 he published a series of articles on the structure and movement of tropical storms (RAO, 1968). Other notable early workers on this topic were BLANFORD (1883), CHAMBERS (1882 to 1885, cited in RAO, 1968), DALLAS (1891a, 1891b) and ELIOT (1900). Basically, all these studies were based on surface data only.

KOTESWARAM and GASPER (1956), using compositing data for 31 storms, gave detailed surface structure of tropical storms in the North Indian Ocean. In these studies, essentially the following nomenclature was used: depression (wind speed between 18 and 33 knots), moderate storm (wind speed between 34 and 47 knots) and severe storm (wind speed greater than 47 knots) (1 knot = 1.852 km · h^{-1}).

Cyclones that affect the Indian subcontinent basically develop out of perturbations originating in the intertropical convergence zone (RAO, 1968). Since this zone exhibits seasonal variations in intensity and latitudinal position, it is natural to expect similar changes in the cyclones. During the summer period, the ITCZ lies mostly over land and severe cyclones capable of generating destructive storm surges do not form. However, depressions giving heavy precipitation occur regularly and frequently.

During spring and fall, the belt between 10 and 15° N gives rise to several depressions, some of which mature into storms and some even into severe storms. Usually, these move towards the northwest and strike the Andhrapradesh coast of India. However, some of them recurve over the Bay of Bengal and hit the northern coast of the bay (the west Bengal state of India and the coast of Bangladesh). During autumn, the storms take a more southerly course and strike the peninsular part of India. Some of these storms recurve and strike the north coast of the bay (the Sunderban coast). Some cross the peninsula and redevelop over the Arabian Sea and travel west-north-west and strike the Arabian Sea coast of the subcontinent. Usually, there are no storms during winter. On the rare occasion when they occur, they could be extremely violent.

The tropical cyclones of the North Indian Ocean are usually less frequent and less intense than the hurricanes of the Atlantic Ocean or the typhoons of the Pacific Ocean (RAO, 1968). Also, their life span is shorter, i.e. 2–3 d compared with 6 d or more elsewhere. This shorter life span (even for recurving storms) is basically due to the relatively short track over the waters compared with other ocean basins. This, of course, does not mean that the destruction of life and damage to property are less. Two of the lowest central pressures recorded in these storms are 919.4 mb (False Point Cyclone of September 1885) and 959.7 mb (the Nellore Cyclone of November 1927).

The severe storms have winds up to or more than 100 knots (185 km · h^{-1}). However, their areal extent is quite small. The highest wind speed of 120 mi · h^{-1} (193 km h^{-1}) was recorded in the Midnapore Cyclone of 1942 (the estimated maximum wind speed for this was 140 km · h^{-1} (224 km · h^{-1}). During the 1964 Rameswaram Cyclone, the maximum estimated winds over Sri Lanka were up to 150 knots (278 km · h^{-1}).

Another interesting feature of these storms is the difference in the location of the maximum winds. For the premonsoon storms (April–May) the sector of strongest winds is usually in the southeast or east, whereas for the postmonsoon storms (October–December), it is to the north of the center (RAO, 1968). MOWLA (1968) compared the cyclogenesis in the Bay of Bengal and the Arabian Sea.

Table. 5.48: Number of cyclonic disturbances that originated over the Bay of Bengal and the Arabian Sea in different months for the period 1891–1960. Note that "storms" includes "severe storms" also, whereas „cyclonic disturbances" include storms and severe storms in addition to cyclonic disturbances (RAO, 1968)

	Cyclonic disturbances	Storms	Severe storms
Jan.	13	4	1
Feb.	3	1	1
Mar.	5	4	2
Apr.	26	18	7
May	56	28	18
June	93	34	4
July	132	38	7
Aug.	145	25	1
Sept.	151	27	8
Oct.	132	53	19
Nov.	102	56	23
Dec.	52	26	9
Year	910	314	100

After the Second World War, using radiosonde data, the upper structure of these storms was studied, and several articles appeared in the *Indian Journal of Meteorology and Geophysics* (now called *Mausam),* especially on the tracks of cyclonic disturbances in various months with emphasis on the recurvature. These studies revealed that the areas of generation and the tracks in every month are closely related to the anticyclonic cell in the upper troposphere at a 10- to 12-km height. However, variations in the tracks could occur due to changes in the general circulation produced by troughs in the midlatitude westerlies.

Frequencies of Cyclonic Storms in the Bay of Bengal

The number of cyclonic disturbances over the Bay of Bengal for each month during the period 1891–1960 is given in Table 5.48. RAGHAVENDRA (1973) performed a statistical analysis of the number of tropical storms and depressions in the Bay of Bengal for the period 1890–1969. The average annual number of storms and depressions is 13. The monsoon season accounts for 56 % of these and the postmonsoon season accounts for 31 %. The highest number (20 storms) occurred in 1927. The frequency distribution of storms and depressions of monsoon and postmonsoon seasons is normal and that of the annual season is almost normal with slight kurtosis. The decade of 1920–29 had the highest mean and the decade of 1950–59 the lowest mean for the annual and monsoon seasons, thus indicating a cycle of 60 yr.

SADLER and GIDLEY (1973) gave tracks of the storms in the North Indian Ocean. CHAKRAVORTHY (1956) discussed the dimensions of the eye of the Bay of Bengal storms. He found that the eye diameter varied from 7 to 20 mi (11.5–32 km).

MOOLEY (1980a, 1980b) studied the severe cyclonic storms of the Bay of Bengal for the period 1877–1977. He found that during the period 1965–77, a higher percentage (than the average) of storms intensified into severe storms and a higher percentage of storms made landfall. Generally, the formation and landfall of these severe storms are random events and are consistent with the Poisson stochastic process.

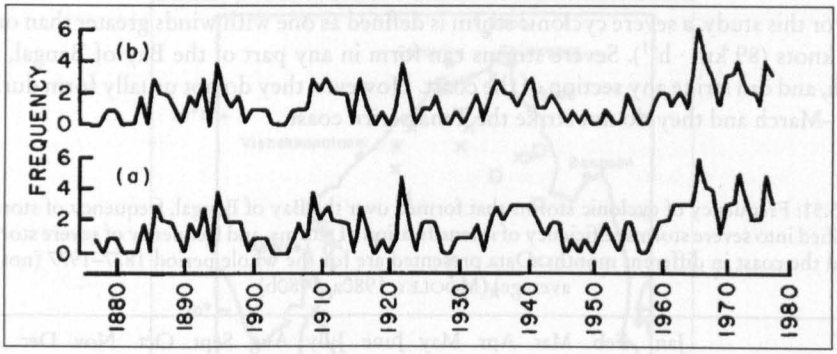

Fig. 5.85: Annual frequency of severe cyclonic storms that over the period 1877–1977 (a) formed over the Bay of Bengal and (b) struck the coast (MOOLEY, 1980a, 1980b)

Table 5.49: Mean and variance of the number of severe storms forming over the Bay of Bengal, and the number of severe storms striking the coast in a year (MOOLEY, 1980)

	Severe storms forming over the Bay of Bengal		Severe storms striking the coast	
Period	Mean	Variance	Mean	Variance
1891–1964	1.50	1.420	1.22	1.087
1877–1964	1.42	1.374	1.16	1.091
1877–1977	1.67	1.910	1.40	1.530
1965–1977	3.38	1.923	3.00	1.833

Table 5.50: Number of cyclonic storms that formed over the Bay of Bengal, number that intensified into severe storms over the bay, and number that struck the coast as severe storms in different 13-yr periods (MOOLEY, 1980a, 1980b)

Period	Number of storms that formed	Number of storms that intensified into severe storms	Number of severe storms that struck the coast	Intensification of storms into severe storms over the bay	Efficiency of Ratio of severe storms that struck the coast to storms that struck the coast
1877–99	49	13	12	0.26	0.31
1890–1902	56	19	18	0.34	0.36
1903–15	64	19	17	0.30	0.30
1916–28	61	19	16	0.31	0.36
1929–41	70	24	19	0.34	0.39
1942–54	46	13	8	0.28	0.28
1952–64	45	21	13	0.47	0.43
1965–77	70	44	39	0.63	0.66
1886–98	74	24	23	0.32	0.35
1924–36	74	16	13	0.22	0.25
1932–44	71	27	22	0.38	0.47

For this study, a severe cyclonic storm is defined as one with winds greater than or equal to 48 knots (89 km · h^{-1}). Severe storms can form in any part of the Bay of Bengal, in any month, and can strike any section of the coast. However, they do not usually form during January–March and they do not strike the Tenasserirn coast.

Table 5.51: Frequency of cyclonic storms that formed over the Bay of Bengal, frequency of storms that intensified into severe storms, efficiency of intensification of storms, and frequency of severe storms that crossed the coast in different months. Data presented are for the whole period 1877–1977 (not annual average) (MOOLEY, 1980a, 1980b)

	Jan.	Feb.	Mar.	Apr.	May	June	July	Aug.	Sept.	Oct.	Nov.	Dec.	Annual
Frequency of storms	5	0	5	21	48	43	48	30	42	77	91	43	453
Frequency of storms that intensified into severe storms	2	0	3	9	32	6	8	3	14	30	44	18	169
Efficiency of intensification				0.43	0.67	0.14	0.17	0.10	0.33	0.39	0.49	0.42	0.37
Frequency of severe storms that crossed the coast	1	0	2	6	29	6	8	3	12	28	35	11	141

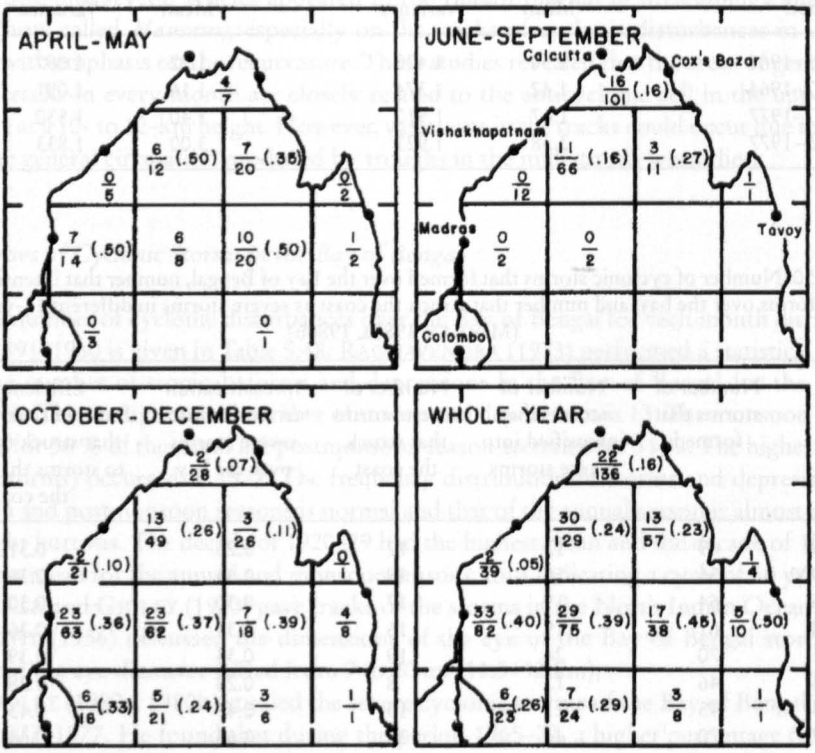

Fig. 5.86: Number of storms located (denominator), number of storms intensified into severe storms (numerator), and the efficiency of intensification (in parentheses) in the different sectors of the Bay of Bengal for the period 1877–1977 (MOOLEY, 1980a, 1980b)

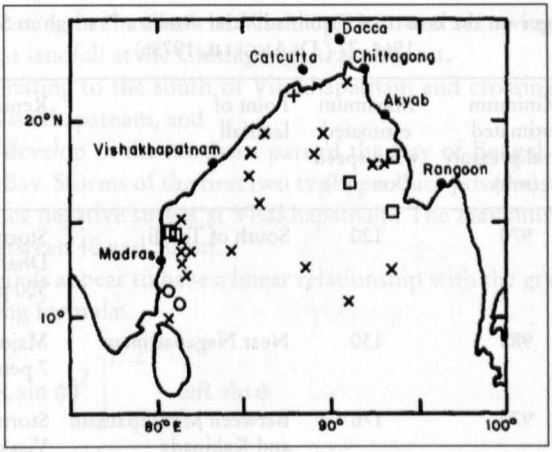

Fig. 5.87: Locations of severe storms just prior to their weakening into storms and depressions over the Bay of Bengal during the period 1877–1977. ○, January–March; □, April and May; June–September; ×, October–December (MOOLEY, 1980a, 1980b)

The annual frequency of severe cyclones that formed over the Bay of Bengal and those that struck the coast is shown in Fig. 5.85. The mean and variance of the number of severe storms forming over the Bay and those striking the coast are listed in Table 5.49. Further details are provided in Table 5.50 and 5.51. The efficiency of intensification (i.e. a cyclonic storm maturing into a severe storm) for different areas in the Bay of Bengal, for the periods April–May, June–September, October–December, and the whole year, is shown in Fig. 5.86. The locations of severe storms just prior to their weakening into storms or depressions are illustrated in Fig. 5.87.

In principle, the entire coast of the Bay of Bengal from Sri Lanka to Thailand is vulnerable to storm surges, although in practice, storm surges occur only on certain stretches. Storm surges are not frequent in Sri Lanka; however, in 1978 a major surge occurred that caused great devastation. Most of the storms developing in the Andaman Sea travel towards northwest and strike the coast of Tamilnadu or Andhrapradesh (south-east part of India), rather than travel towards the west and strike the coast of Sri Lanka. Certain storms have a more northerly component in their motion and these can landfall on the coast of Orissa. Those that recurve can hit the coasts of West Bengal, Bangladesh, and Burma.

On the coasts of Tamilnadu and Andhrapradesh, at least six storm surges occurred during the period 1964–77. These are listed in Table 5.52 along with the minimum central pressure and maximum wind speed. There appears to be some controversy regarding the intensity of the November 1977 cyclone (last entry in Table 5.52). PANT et al. (1980) suggested that the minimum central pressure was 943 mb and the maximum wind speed was 125 knots (231 km · h^{-1}). This cyclone intensified from T6 to T7 between November 17 and 19 (see Table 5.53 for the classification of T numbers in terms of pressure drop and wind speed). GHOSH (1980) suggested that the lowest pressure was 919 mb and not 943 mb. In intensity, this cyclone was comparable with that of the 1927 cyclone. However, the 1927 cyclone generated a surge smaller than the 1977 cyclone (in the storm surge of 1927, 300 people died compared with at least 10 000 in the 1977 surge). The 1927 cyclone made a landfall near Nellore where the topography was much steeper and hence the surge was smaller. Another cyclone that had a pressure drop in excess of 90 mb occurred in 1885 (ELIOT, 1890).

Table 5.52: Storm surges on the coasts of Tamilnadu and Andhra Pradesh in Southeast India during 1964–77 (DEANGELIS, 1978a)

Date	Minimum estimated central pressure (mb)	Maximum estimated wind speed ($km \cdot h^{-1}$)	Point of landfall	Remarks
Dec. 17–24, 1964	970	120	South of Tondi	Storm surge amplitude at Dhanushkodi about 5 m, 500 people died
Dec. 4–8, 1967	988	130	Near Nagapattinam	Major storm surge, 7 people died
Nov. 4–9, 1969	970	176	Between Masulipatnam and Kakinada	Storm surges at Visakhapatnam, 200 people died
Sept. 7–14, 1972	957	204	Near Baruva	Storm surges of 1–3 m between Baruva and Chandbali
Nov. 15–23, 1972	983	148	South of Nellore	Minor storm surge
Nov. 14–20, 1977	919	250	Chirala	Surges up to 6 m near Divi. At least 10 000 people died. Surges occurred on a coastal stretch 80 km long and penetrated 8–15 km inland

Table 5.53: Relationship between T number, maximum wind speed, and pressure drop in a cyclone (DVORAK, 1975a; MISHRA and GUPTA, 1976)

T	Maximum wind speed ($km \cdot h^{-1}$)	Pressure drop (mb)	T	Maximum wind speed ($km \cdot h^{-1}$)	Pressure drop (mb)
1	46	-	5	167	40
1.5	46	-	5.5	189	52
2	56	-	6	213	66
2.5	65	6	6.5	235	80
3	83	10	7	259	97
3.5	102	15	7.5	287	119
4	120	21	8	315	143
4.5	143	29			

At Visakhapatnam, on the east coast of India, the maximum (positive or negative) surge appears to occur usually about a day after the winds attain their maximum intensity. The amplitude of the surge depends more on the wind direction than on the wind speed (RAMANADHAM and VARADARAJULU, 1965). The storm surges at Visakhapatnam are usually associated with three types of storm tracks:

(a) storms originating to the south of Visakhapatnam and recurving near the east coast of India and making a landfall at the Chittagong-Arakan coast,

(b) storms originating to the south of Visakhapatnam and crossing the coast between Masulipatnam and Visakhapatnam, and

(c) storms that develop in the northern part of the Bay of Bengal and cross the coast near the head of the Bay. Storms of the first two types produce positive surges and storms of the third type produce negative surges at Visakhapatnam. The maximum amplitudes of the surges are usually between 40 and 50 cm.

The observed winds appear to have a linear relationship with the gradient wind calculated from the following formula:

$$V_g = \left[\frac{R}{\rho} \frac{\partial p}{\partial r} + (\omega R \sin \phi)^2 \right]^{1/2} - \omega R \sin \phi \qquad (5.89)$$

where, V_g is the gradient wind, ω is the angular velocity of the earth's rotation, ϕ is the latitude, R is the radius of curvature of the isobars, and p is the density of air. It was found that

$$\frac{V}{V_g} = 0.6$$

where, V is the wind as measured from ships offshore.

Although storm surges may be of small amplitude at Visakhapatnam, south of it, storm surges could have very large amplitudes. The cyclone of October 28, 1949, made a landfall north of Masulipatnam (Fig. 5.88). Winds up to 90 knots (167 km · h^{-1}) produced storm surges with amplitudes of 3–4 m along a stretch of the coast shown in Fig. 5.88. The storm crossed the coast at the time of high tide (RAO, 1968).

Another severe storm struck the Coromandel Coast on November 30, 1952 (RAO, 1968). Again, winds up to 90 knots produced surges with amplitudes up to 2.5 m along a stretch of the coast shown in Fig. 5.89. Another severe cyclonic storm travelled towards the west over the northern boundary of the Palk Strait (between India and Sri Lanka) on November 30–December 1, 1955. Two different storm surges occurred (RAO, 1968). The first one was along the coast between Point Calimere and Vettaikaran lruppu and had amplitudes up to 2 m. The second surge occurred between Thambkottai and Kattumavedi with amplitudes over 1 m.

One of the most destructive storm surges in southern India occurred on December 23, 1964 (Fig. 5.92). Winds up to 120 knots (322 km · h^{-1}) created storm surges over the islands of Mannar (Sir Lanka) and Rameswaram (India) and the maximum amplitudes of the surges were 5–6 m. This storm exhibited some interesting features: (a) the major surges occurred to the left of the storm track (at Pamban-Dhanushkodi Islands), (h) the surges preceded the arrival of the storm by approximately 3–4 h, (c) although winds up to 80 knots (148 km · h^{-1}) were recorded to the west of the Pamban Bridge, no surges occurred along this part of the coastline

It was mentioned that the amplitude of storm surges at Visakhapatnam, is not significant. Generally, north of Visakhapatnam, the storm surge activity is not severe, except on some stretches of the Orissa coast, until one arrives at the coast of Bangladesh. Saugor Island (India) is situated near the head of the Bay of Bengal where the Hoogly Estuary empties into the Bay. On this island, the surge heights usually range from 1/3 to 1 m (JANARDHAN, 1967).

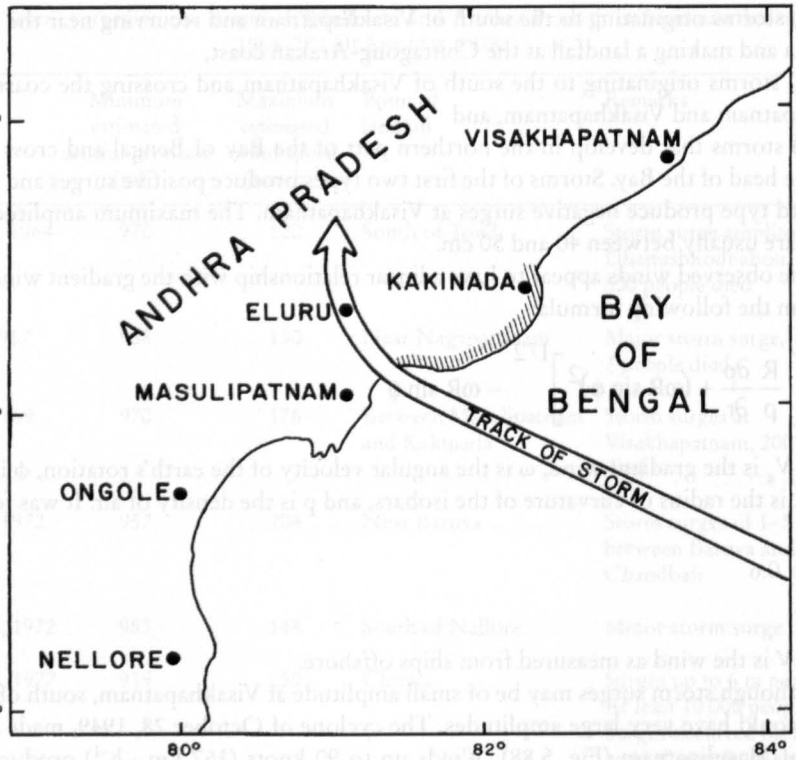

Fig. 5.88: Track of the storm of October 1949 on the southeast coast of India. Hatched area shows the coastline affected by the storm surge (RAO, 1968)

JOHNS and ALI (1980) used the following pressure distribution in their simulation of the November 1970 storm surge that caused great devastation in Bangladesh.

$$p = p_a - \Delta p \exp\left(-\frac{r}{R}\right) \tag{5.90}$$

where, p is the pressure field at radius r, p_a is the ambient pressure, Δp is the difference between the ambient and central pressures, and R is the e-folding radius of the pressure distribution.

A value of 350 km was given to HOLLAND (1980) pointed out that R should be the radius of maximum winds and that a typical value of R should be about 35 km.

The argument that R should be the radius of maximum winds was developed by HOLLAND (1981) as follows. For tropical cyclones, a typical Rossby number will be about 100, in the strongest wind region. One may assume a cyclostrophic balance and write

$$V_c = \left(\frac{r}{\rho}\frac{\partial p}{\partial r}\right)^{1/2} \tag{5.91}$$

where, V_c is the cyclostrophic tangential wind and p is the air density. Substituting eq. (5.90) into (5.91)

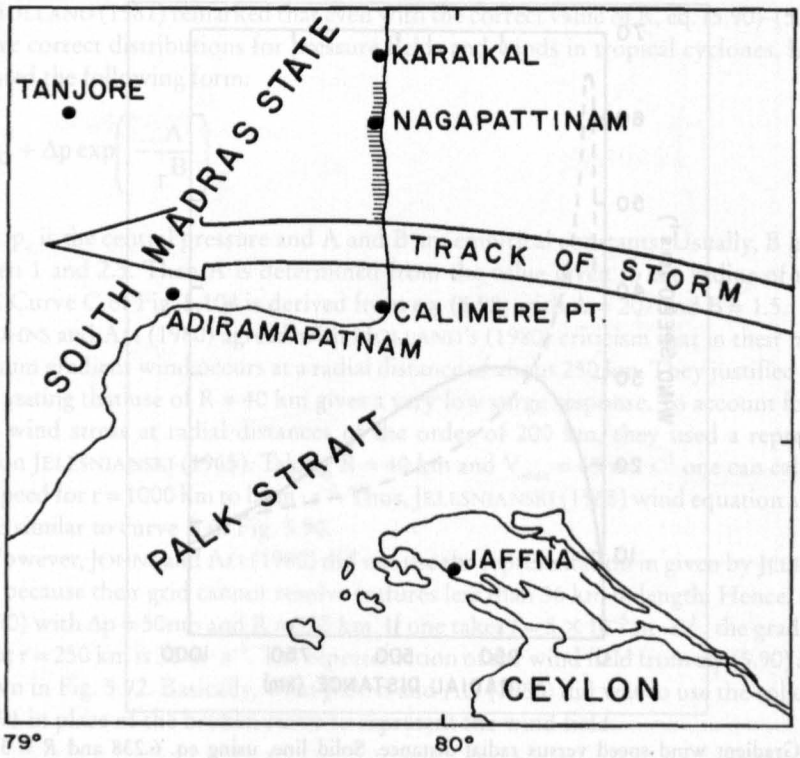

Fig. 5.89: Track of the storm of November 1952 on the southeast coast of India. Hatched area shows the coastline affected by the storm surge (RAO, 1968)

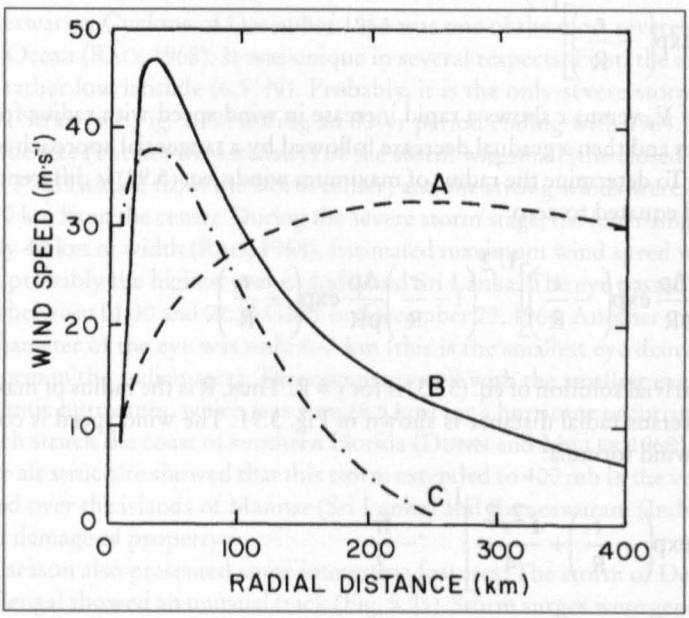

Fig. 5.90: Gradient wind speed versus radial distance. Curve A, R = 350 km; curve B, R 35 km; curve C, from eq. 6.243 (HOLLAND, 1981)

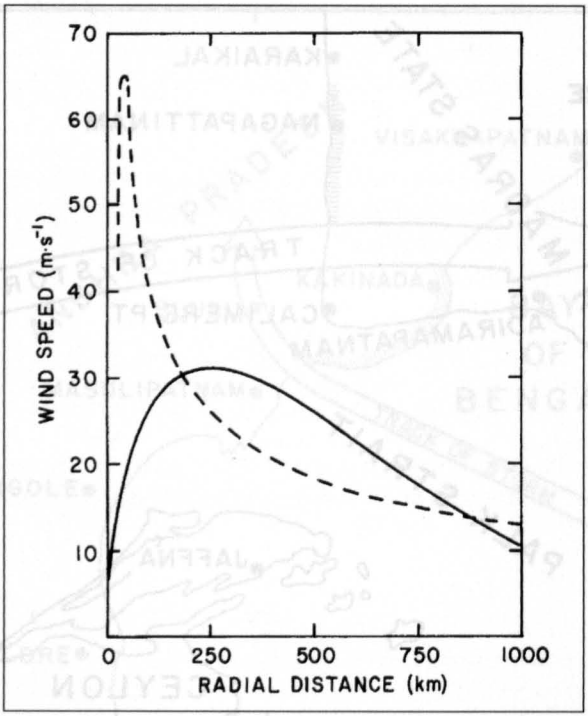

Fig. 5.91: Gradient wind speed versus radial distance. Solid line, using eq. 6.238 and R = 350 km; broken line, using eq. 6.143, R = *40* km, and V, = 65 m. s-' (JOHNS and ALI, 1981)

$$V_c = \left[\frac{r\Delta p}{\rho R}\exp\left(-\frac{r}{R}\right)\right]^{1/2} \tag{5.92}$$

A plot of V_c versus r shows a rapid increase in wind speed with radius from the center to a maximum and then a gradual decrease followed by a tangential approach to zero at infinite distance. To determine the radius of maximum winds, eq. (5.92) is differentiated with respect to r and equated to zero:

$$\frac{\partial V_C}{\partial r} = \frac{1}{2}\left[\frac{r\Delta p}{\rho R}\exp\left(-\frac{r}{R}\right)\right]^{1/2}\left(1-\frac{r}{R}\right)\frac{\Delta p}{\rho R}\exp\left(-\frac{r}{R}\right) \tag{5.93}$$

The nontrivial solution of eq. (5.93) is for r = R. Thus, R is the radius of maximum winds. Wind speed versus radial distance is shown in Fig. 5.91. The wind speed is computed from the gradient wind formula:

$$V_g = \left[\frac{r\Delta p}{\rho R}\exp\left(-\frac{r}{R}\right)+\frac{f^2r^2}{4}\right]^{1/2} - \frac{fr}{2} \tag{5.94}$$

where, V_g is the gradient wind and f is the Coriolis parameter. The following values were used: Δp = 50 mb, p = 1.2 km · m^{-3}, $f = 5 \times 10^{-5} \cdot s^{-1}$.

HOLLAND (1981) remarked that even with the correct value of R, eq. (5.90)–(5.94) might not give correct distributions for pressure fields and winds in tropical cyclones. Instead, he suggested the following form:

$$p = p_c + \Delta p \exp\left(-\frac{A}{r^B}\right) \tag{5.95}$$

where, p_c is the central pressure and A and B are empirical constants. Usually, B has a value between 1 and 2.5. Then A is determined from the value given to the radius of maximum winds. Curve C of Fig. 5.104 is derived from eq. (5.95) with A = 207 and B = 1.5.

JOHNS and ALI (1980) agreed with HOLLAND'S (1980) criticism that in their model, the maximum gradient wind occurs at a radial distance of about 250 km. They justified their model by stating that use of R = 40 km gives a very low surge response. To account for the role of the wind stress at radial distances of the order of 200 km, they used a representation based on JELESNIANSKI (1965). Taking R = 40 km and $V_{max} = 65\ m \cdot s^{-1}$ one can calculate the wind speed for r = 1000 km to be $m \cdot s^{-1}$. Thus, JELESNIANSKI (1965) wind equation also shows a curve similar to curve B of Fig. 5.90.

However, JOHNS and ALI (1980) did not use the representation in given by JELESNIANSKI (1965) because their grid cannot resolve features less than 36 km in length. Hence, they used eq. (5.90) with Δp = 50mb and R = 350 km. If one takes $f = 5 \times 10^{-5}\ m \cdot s^{-1}$, the gradient wind speed at r = 250 km is $30\ m \cdot s^{-1}$. The representation of the wind field from eq. (5.90) and (5.95) is shown in Fig. 5.92. Basically, what JOHNS and ALI (1980) did was to use the solid curve of Fig. 5.91 in place of the broken curve to represent the wind field.

Case Studies of Cyclonic Storms in the Bay of Bengal During the Period 1964–99

The Rameswaram Cyclone of December 1964 was one of the most severe storms of the North Indian Ocean (RAO, 1968). It was unique in several respects. First, the intensification occurred at a rather low latitude (6.5° N). Probably, it is the only severe storm that moved across the Palk Strait (see Fig. 5.92) during an 80-yr period ending with 1964. Another feature was that the size (but not the intensity) of the storm was small (the closed isobaric field extended only 3° in latitude from the storm center) and the strong winds were confined to a region 100–150 km from the center. During the severe storm stage, the inner ring of hurricane winds was only 40 km in width (RAO, 1968). Estimated maximum wind speed was 175 knots ($324\ km \cdot h^{-1}$), probably the highest ever in India and Sri Lanka. The eye passed over Rameswaram (India) between 01:30 and 02:30 GMT on December 23, 1964. Another unusual feature was that the diameter of the eye was only 6–7 km (this is the smallest eye diameter reported for a severe storm in the Indian area). This compares well with the smallest eye diameter reported for Atlantic hurricanes, which was 4 mi (6.5 km) for a hurricane occurring on July 27, 1936, and which struck the coast of southern Florida (DUNN and MILLER 1960).

The upper air structure showed that this storm extended to 400 mb in the vertical. Storm surges occurred over the islands of Mannar (Sri Lanka) and Rameswaram (India) with great loss of life and damage of property.

The 1965 season also presented some interesting features. The storm of December 1965 in the Bay of Bengal showed an unusual track (Fig. 5.93). Storm surges were generated on the coast of Bangladesh and heavy casualties followed. Not only was the track unusual, but also the duration of the storm was 9 d compared with the usual 1–3 d. During a 70-yr period,

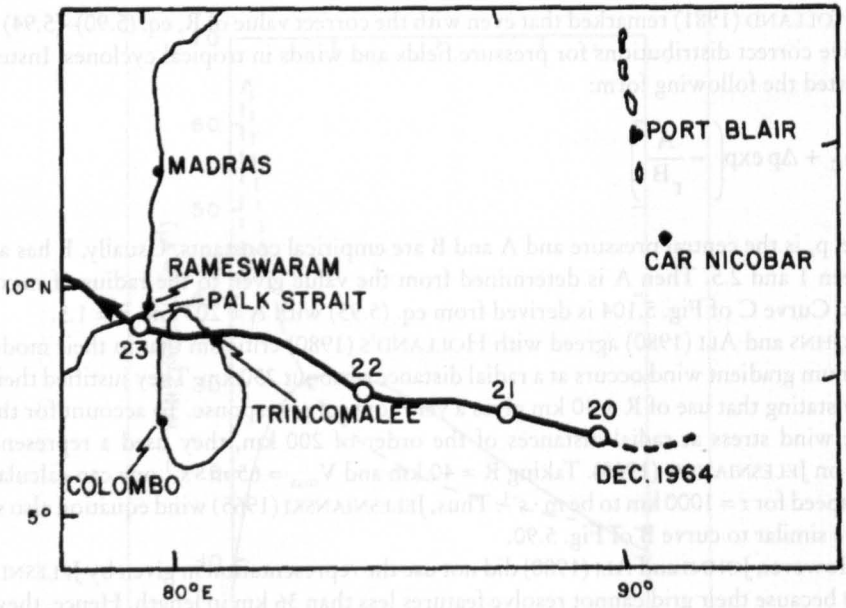

Fig. 5.92: Track of the severe storm of December 1964 over Sri Lanka (RAO, 1968)

about 77 % of the storms in the Bay of Bengal lasted only 1–4 d, 17 % lasted for 5–6 d, and only 7 % (i.e. three storms) lasted for 7 d. The average duration for the Bay of Bengal storms is 3.5 d (compared with the average life span of global tropical cyclones, which is 6.5 d according to RIEHL, 1954). Another unusual feature was that this storm hit Bangladesh and Burma in December. Note that in the 70-yr period only 13 storms did this. A final unusual feature was the simultaneous presence of another storm in the Arabian Sea (see Fig. 5.93). Only five times before has a similar situation existed (i.e. storms in the Bay of Bengal and the Arabian Sea at the same time). These cases are listed in Table 5.54 and their tracks are illustrated in Fig. 5.93.

The 1966 season produced a maximum number of storms in the postmonsoon season (RAMAN et al., 1967). The following deductions were made by RAMAN et al. (1967).

The thermodynamical conditions necessary for the development of cyclone storms, as discussed by PALMÉN (1955), are found in all the postmonsoon months. However, additional conditions must be satisfied. One of the reasons for the high cyclone activity in the 1966 season was the continued northward position of the equatorial trough. Even though the low latitude wind fields in 1959 and 1966 were similar, the absence of northward horizontal shear in the wind field of 1959 inhibited the development.

The required minimum energy for development is available at the air-sea interface during all postmonsoon months. However, for maturity into severe storms, the zones of maximum evaporation should also take place in preferred areas. During the 1966 season, the atmosphere gained the maximum heat over the southwest and west central parts of the Bay of Bengal. Generally, only in this region do all disturbances mature into cyclonic storms. On the other hand, in November 1954, maximum evaporation took place over the southwest part of the bay, south of 10° N. Finally, the origin, intensification and movement of cyclonic storms coincide with the zones of convergence of the total energy that is available in the atmosphere.

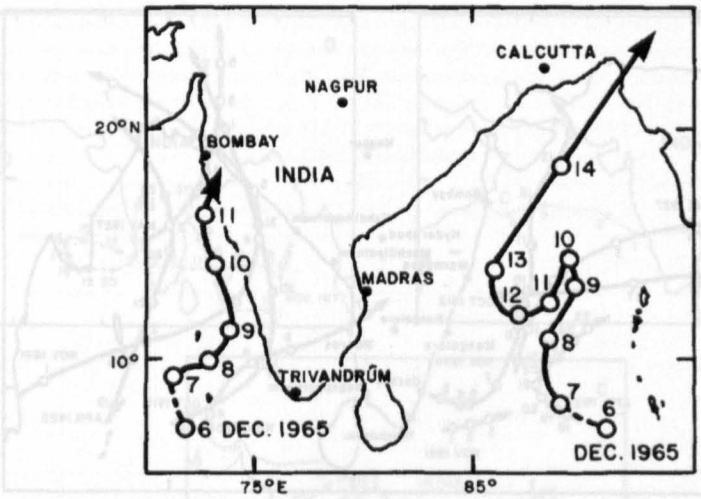

Fig. 5.93: Tracks of a storm pair in the Bay of Bengal (December 7–15, 1965) and Arabian Sea (December 7–12, 1965) (SWAMINATHAN, 1966)

Table 5.54: Details of storm pairs in the Bay of Bengal and the Arabian Sea during the period 1891–1960. Date indicated refers to the original date of the storm. In each pair, the top row is for the Bay of Bengal and the bottom row for the Arabian Sea (SWAMINATHAN, 1966)

	Origin	
Date	Latitude (°N)	Longitude (°E)
Nov. 1, 1981	8.0	74.5
Nov. 1, 1891	9.5	98.5
Oct. 25, 1912	15.0	72.5
Oct. 28, 1912	8.5	89.0
Apr. 18, 1922	9.0	68.5
Apr. 19, 1922	9.5	93.0
May 31, 1927	11.5	71.0
May 31, 1927	17.5	91.5
Nov. 3, 1936	9.5	75.0
Nov. 4, 1936	9.0	88.0

However, the 1977 season was an especially bad one. On November 19, a cyclone hit the coast of Andhra Pradesh (India) and produced storm surges greater than 5 m in amplitude. The path of this storm is shown in Fig. 5.95 a (track A). Between November 21 and 22, another Bay of Bengal originated storm struck the west coast of India (Fig. 5.95 a, track B). This storm also caused great damage. On October 28, a storm originating in the Bay of Bengal struck the coast of Arabia between November 4 and 5 (Fig. 5.95 b, track C).

WINCHESTER (1979) provided the following details about the Andhra coast storm of November 19. The storm made a landfall near the mouth of the Krishna River with a speed of 12 mi · h^{-1} (19.5 km · h^{-1}) with wind speeds of 75 mi · h^{-1} (121 km · h^{-1}) and gusting to 120 mi · h^{-1} (193 km · h^{-1}). The storm surge was 5 m in amplitude and penetrated at least 10 mi

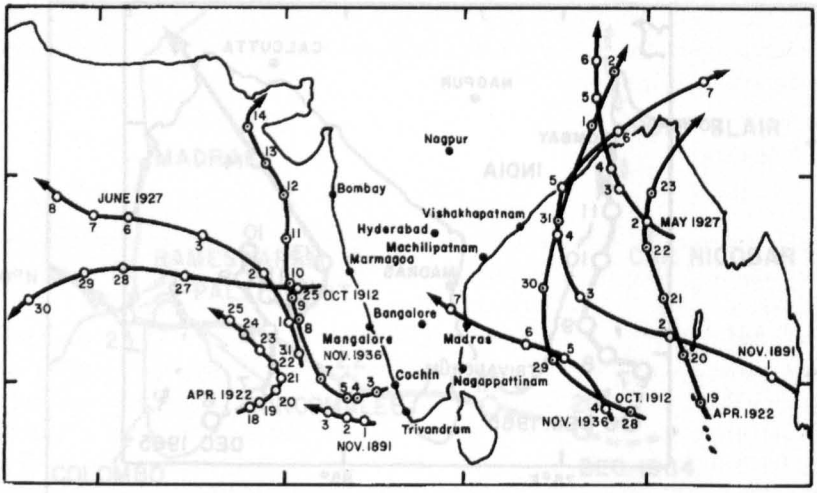

Fig. 5.94: Tracks of storm pairs in the Bay of Bengal and the Arabian Sea during 1891–1960 (SWAMINATHAN, 1966)

(16 km) inland with a speed of about 10 mi · h^{-1} (16 km · h^{-1}) over a coastal stretch of 35 mi (56 km). The high water due to the surge remained for about 10 h. The cyclone and the storm surge together totally damaged an area of about 7500 mi^2 (195 000 km^2). At least 20 000 people died and 2 million people were left homeless (DEANGELIS, 1978a, 1978b, 1978c, 1978d).

There was no significant storm surge activity in India during 1978. However, Sri Lanka experienced a very devastating storm surge during this year (damage of $ 50 million). On November 21, 1978, a tropical storm generated near the Nicobar Islands matured to hurricane strength and on November 23 it struck the east coast of Sri Lanka (Fig. 5.95 c, track D). The resulting storm surge together with the cyclone and the resulting landslides that occurred killed 373 people and destroyed 80 000 houses. Wind gusts up to 204 km · h^{-1} occurred. The storm surge inundated rice fields up to 8 km inland. The storm then moved to India over the Gulf of Mannar where it killed 10 people (DEANGELIS, 1979a, 1979b, 1979c).

One humorous sidelight of this cyclone was that 160 convicts escaped when the roof blew off the jail in Batticaba (Sri Lanka). The fact that not everybody is inconvenienced by a natural disaster such as a storm surge can be seen from the fact that, invariably, after the disaster looters descend upon the scene and helped themselves. These are also good times for black marketeers and food hoarders, especially in the developing countries.

When one of the author of this book (T. S. Murty) visited his native village in Andhrapradesh, India, in 1978 (1 yr after the disastrous storm surge of November 1977), tales of how village officers confiscated the emergency relief funds (provided by the federal government of India as well as by several international agencies) for their own use were mentioned to him. Although this author is not an expert on sociological aspects, his early background in developing countries convinced him that there is much truth to these tales. He was given to understand by the villagers that corruption is minimal to nonexistent with federal (central) government officers (due to the higher calibre of the federal civil service and also due to various built-in checks against corruption), and that corruption increases by an order of magnitude with the provincial (state) government officers, then by another order of magnitude with the district (county) level of government, and to absolute and total corruption at the municipal

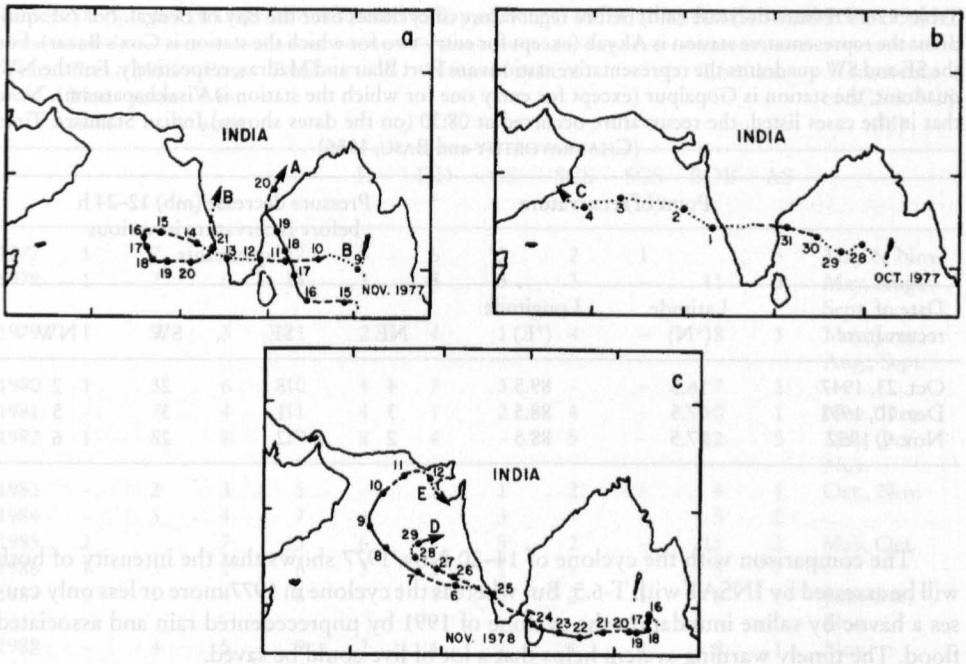

Fig. 5.95: (a) Track A: storm of November 1977 that caused great damage to the Andhra Pradesh Coast of India; track B: storm of November 1977 that did moderate damage to the west coast of India. (b) Track C: storm originating in the Bay of Bengal on October 28, 1977, that struck the coast of Arabia. (c) Track D: storm of November 1978 that did great damage on the cast coast of Srilankas; track E: storm of November 1978 originating in the Arabian Sea and striking the Gujarat coast of India (DE ANGELIS, 1978a,1978b, 1978c, 1978d)

(city, town, village) level. We would like to recommend to the international agencies that provide emergency relief funds to any developing country that only the federal government officials be involved in the handling of the relief operations.

SOM and SOM (1995) describe the Machilipatnam cyclone on 9th May 1990, which hit the Andrha coast (eastern coast of India) with an estimated force reaching 200 to 250 kph. Over the coastal area heavy rainfall has been happened. 967 people died and 650,000 people were evacuated from 546 coastal villages. They pointed out that the storm affected a population of about 7.78 million in 5160 villages in Andhra Pradesh. It was one of the severest cyclones in the Bay of Bengal whereas in Andhra coast another earlier cyclone struck the coast with an equal intense.

Table 5.55: Storms and depressions in the Bay of Bengal, 1945–54. A, total number; B, number that recurved. Storms and depressions that recurved on land or while in the Arabian Sea have been excluded (CHAKRAVORTHY and BASU, 1956)

Type	Jan.	Feb.	Mar.	Apr.	May	June	July	Aug.	Sept.	Oct.	Nov.	Dec.
A	5	1	1	5	6	11	18	19	19	18	12	11
B	2	0	0	1	1	0	0	0	0	5	1	4

Table 5.56: Pressure decrease (mb) before recurvature of cyclones over the Bay of Bengal. For NE quadrant the representative station is Akyab (except for entry two for which the station is Cox's Bazar). For the SE and SW quadrants the representative stations are Port Blair and Madras, respectively. For the NW quadrant, the station is Gopalpur (except for entry one for which the station is Visakhapatnam). Note that in the cases listed, the recurvature occurred at 08:30 (on the dates shown) Indian Standard Time (CHAKRAVORTHY and BASU, 1956)

	Point of recurvature		Pressure decrease (mb) 12–24 h before recurvature in various quadrants			
Date of recurvature	Latitude (°N)	Longitude (°E)	NE	SE	SW	NW
Oct. 23, 1947	16.5	89.5	4	8	2	2
Dec. 10, 1951	17.5	88.5	3	1	3	5
Nov. 9, 1952	17.5	88.5	2	2	2	6

The comparison with the cyclone of 14–20 Nov. 1977 shows that the intensity of both will be assessed by INSAT with T-6.5. But whereas the cyclone in 1977 more or less only causes a havoc by saline inundation the cyclone of 1991 by unprecedented rain and associated flood. The timely warning system helps that a lot of live could be saved.

SOM and SOM (1995) although describe the cyclone on 29 April, 1991 which has been happened about 12 hours long and occurred a 5 meter high storm surge. 10 Million people were affected and the country had suffered incalculable economic damage. SOM and SOM (1995) described the situation as follows:

"Whether it was an island (like Sandwip or Kutubdia) or a place on the main land, one moment there were communities of ten thousands or more, three hours later there was absolutely nothing. Just enormous street of salt water dwarfing everything save the tall palm trees. It swept heavily populated areas several kilometres inland along a 240 km coastal stretch of Bangladesh and all the offshore islands. The seawater took merely 10 minutes to reach neck deep water levels at highest points of Sandwip islands. The official tally of the casualties was approximately 132,000. But exact number of deaths would never be known as no one knew how many people had been washed away in the Bay of Bengal. However, unofficial estimate of casualties was half a million."

Arabian Sea

Compared with the Bay of Bengal, the storms of the Arabian Sea are less frequent, generally less intense, and the accompanying storm surges are usually less destructive (Table 5.57). The statistics by month for the period 1891–1960 are given in Table 5.58.

PEDGLEY (1969) mentioned that cyclones develop preferentially over the southeastern quadrant of the Arabian Sea and move in a west to northwest direction towards Arabia. However, sometimes they recurve to the north or northeast towards northwestern India and Pakistan (Fig. 5.96). About one storm in three passes over the western part of the Arabian Sea and strikes the coast of the Arabian peninsula.

Table 5.57: Number of Depressions formed in Bay of Bengal and Arabian Sea (SOM and SOM, 1995)

Year	Pre-Monsoon	Monsoon	Post Monsoon	Total	Name of system					Location		Occurence of SCS & SCS (H)
					D	DD	CS	SCS	SCS (H)	BOB	AS	
1977	1	7	9	17	5	6	3	2	1		5	May & Nov.
1978	1	7	6	14	3	5	3	3	-	11	3	May, Aug., Sept.
1979	1	7	3	11	2	4	1	4	-	8	3	May, June, Aug., Sept.
1980	1	3	6	10	4	3	3	-	-	7	3	-
1981	-	7	4	11	4	1	2	4	-	10	1	Nov., Dec.
1982	1	8	8	17	8	4	-	5	-	12	5	May, Oct. Nov.
1983	-	2	3	5	-	2	1	2	-	4	1	Oct., Nov.
1984	-	3	4	7	4	-	3	-	-	5	2	-
1985	2		7	13	6	-	5	2	-	11	2	May, Oct.
1986	1	3	2	6	3	2	1	-	-	5	1	-
1987	1	1	4	6	-	1	2	2	1	6	-	Jan., Oct, Nov.
1988	-	4	5	9	2	4	1	1	1	8	1	Nov.
1989	1	5	4	10	3	4	1	-	2	9	1	May & Nov.
1990	1	3	5	9	4	3	-	1	1	8	1	May & Dec.
1991	2	3	3	8	4	1	2	-	1	8	-	April
1992	1	3	8	12	1	4	5	1	1	8	4	Nov.

D – Depression, DD – Deep Depression, CS – Cyclonic Storms, SCS – Severe Cyclonic Storms, SCS (II) – Severe Cyclonic Storms with Hurricane Wind, BOB – Bay of Bengal, AS – Arabian Sea.

Table 5.58: Data on the cyclonic storms of the Arabian Sea during the period 1891–1960 (RAO, 1968)

Type of storm	Jan.	Feb.	Mar.	Apr.	May	June	July	Aug.	Sept.	Oct.	Nov.	Dec.	Year
Total number of cyclonic disturbances	6	0	1	7	20	30	11	21	0	36	36	8	165
Total number that intensified into storms	2	0	0	5	13	13	3	1	4	17	21	3	82
Total number that intensified into severe storms	0	-	-	4	11	8	0	0	1	7	16	1	48

The frequency of cyclonic storms for the period 1891–1967 is given in Table 5.59. About one cyclonic storm in 3 yr strikes the coast and about half of these that strike have cyclone strength. Usually the cyclones make landfall near Salalah and they show a tendency to turn to the left at a distance of a few hundred kilometres from the coast. The 10 cyclones that hit the Arabian coast during 1943–67 are listed in Table 5.60.

Table 5.59: Number of occurrences of cyclones (Beaufort ≥ 12) and cyclonic storms (BF ≥ 8) over the whole Arabian Sea during the period 1890–1950 and number of occurrences along the Arabian coast during the period 1891–1967. For the Beaufort wind scale, see Tables 5-6-18 (PEDGLEY, 1969)

Type of storm	Jan.	Feb.	Mar.	Apr.	May	June	July	Aug.	Sept.	Oct.	Nov.	Dec.	Year
Cyclones and Cyclonic storms over the whole Arabian Sea	1	0	0	4	10	11	2	1	4	15	12	3	63
Cyclones and Cyclonic storms along the coast of Arabia	0	0	0	0	8	5	1	0	0	7	6	1	28
Cyclones along the coast of Arabia	0	0	0	0	6	2	0	0	0	2	2	1	13

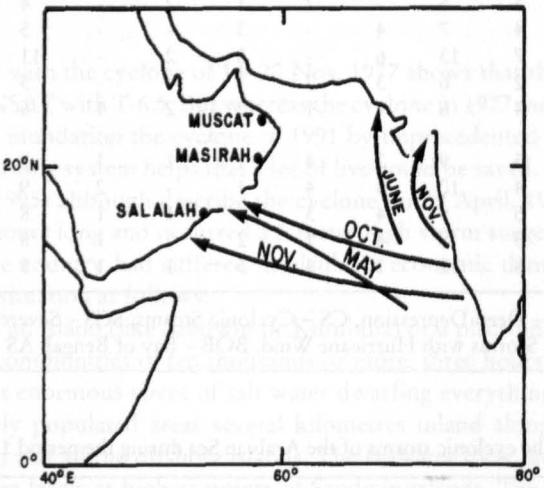

Fig. 5.96: Common tracks of Arabian Sea cyclones (PEDGLEY, 1969)

Table 5.60: Cyclones near the coast of the Arabian peninsula during 1943–1967 (PEDGLEY, 1969)

Date of approach or crossing the coast	Nature of the cyclone
June 6, 1946	Decaying before approaching Masirah from east-southeast
October 1, 1948	Decaying before approaching coast between Masirah and Ra's al Hadd from east
October 25, 1948	Cyclonic storm crossed Salalah, approaching from southeast
May 24, 1959	Severe cyclone crossed Salalah, approaching from east-southeast
October 18, 1959	Severe cyclone crossed near Ras Madraka, approaching from east
May 18, 1960	Severe cyclone crossed coast at Ras Fartak
November 23, 1960	Cyclonic storm approached entrance to Gulf of Aden from east
May 30, 1962	Decaying before crossing coast at Ras Madraka
May 26, 1963	Severe cyclone, passed just south of Salalah, approaching from east-southeast and then turning towards west-southwest
November 13, 1966	Severe cyclone with a track similar to that of May 1963

The following pressure distribution

$$p = 1008 - 1.64(v_r r) \tag{5.96}$$

appears to fit the central pressure of the Arabian Sea cyclones. Here, p is the central pressure (millibars) and v_r is the radial wind speed in knots at a distance from the center of r degrees latitude (KRUEGER, 1959). The maximum wind speed v_m can be estimated from MYERS (1957):

$$v_m = K\sqrt{p' - p} \tag{5.97}$$

where p' is the surrounding pressure and K is a constant (equal to 11). For example, taking p = 960 mb and p' = 1010 mb gives v_m = 80 knots (148 km · h^{-1}).

Although most of the Arabian Sea cyclones originate locally, some (6 of the 28 mentioned in Table 5.59) originated in the Bay of Bengal. Usually, cyclones with this distant origin occur towards the end of the cyclone season (i.e. towards November). Occasionally, the Arabian Sea cyclones cross the Gulf of Aden and even rarely the Gulf of Oman.

One difference between the cyclones of the Arabian Sea and the Bay of Bengal is that, whereas in the Bay of Bengal more cyclones occur in the postmonsoon season (September to December) than in the premonsoon season (April to May), in the Arabian Sea they are about equally distributed between the two cyclone seasons (i.e. May to June and October to November). Most of these originate over the southeastern Arabian Sea and move towards west-northwest. However, a few originate in the Bay of Bengal and cross southern Indian peninsula before emerging over the Arabian Sea.

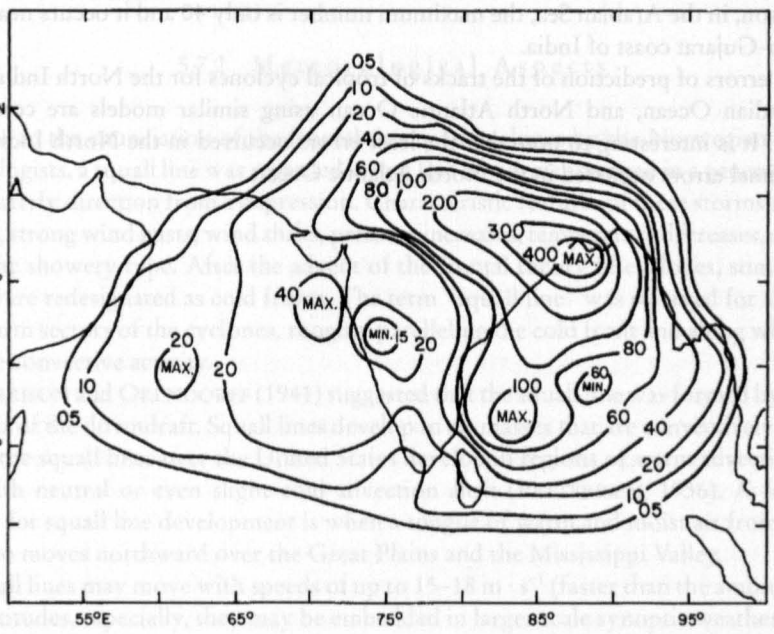

Fig. 5.97: Contours of a number of tropical cyclones (including depressions) passing through 2.5° latitude-longitude squares for the period 1877–1974 (NEUMANN and MANDAL, 1978)

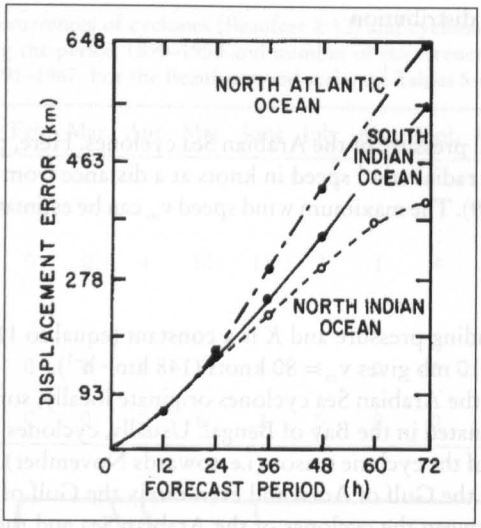

Fig. 5.98: Forecast errors in the tracks of tropical cyclones for three different ocean basins (NEUMANN and MANDAL, 1978)

NEUMANN and MANDAL (1978) used statistical techniques to predict the storm movement over the Arabian Sea and the Bay of Bengal. The number of tropical cyclones (including depressions) passing through 2.5° latitude-longitude squares for the period 1877–1974 is given in Fig. 5.97. It can be seen that maximum values of up to 400 cyclones and depressions occurred near the coasts of West Bengal (India) and Bangladesh in the Bay of Bengal. By comparison, in the Arabian Sea, the maximum number is only 40 and it occurs near the Maharashtra-Gujarat coast of India.

The errors of prediction of the tracks of tropical cyclones for the North Indian Ocean, South Indian Ocean, and North Atlantic Ocean using similar models are compared in Fig. 5.98. It is interesting to note that the least errors occurred in the North Indian Ocean and maximal errors occurred in the North Atlantic Ocean.

5.7 Mesoscale Weather Systems

HOBBS (1981) defined a mesoscale weather system as one with horizontal scales in the range of a few to 1000 km and time scales ranging from several hours to 1 d. Squall lines, thunderstorms, and tornadoes fall into the classification of mesoscale weather systems. Here, squall lines are specifically examined, since, as will be seen later, they can give rise to storm surges.

Squall lines are nonfrontal lines of active thunderstorms, several to some tens of kilometers wide and hundreds of kilometers long, which exist for a considerably longer period than the lifetime of the component cumulonimbus clouds (RAMAGE, 1971).

Stationary as well as traveling mesoscale weather systems such as those that occur over the Great Plains of the United States are classified further into the following: regional scale (200–2000 km), or meso-alpha; squall line scale (20–200 km), or meso-beta; cloud scale (2–20 km), or meso-gamma (ANONYMOUS, 1978).

5.7.1 Regions Where Squall Lines Occur

Squall lines occur in midlatitudes as well in the tropics. They occur mainly over the United States, Central, West, and South Africa, Venezuela, northern India, and northern Australia. In the United States they occur predominantly during spring and summer.

According to HAMILTON and ARCHBOLD (1945) and TSCHIRHART (1958), sub-Saharan Africa is a fertile ground for squall lines and, in fact, these account for most of the rainfall. Another area where squall lines occur is the Caribbean Sea. On rare occasions, squall lines can also be observed over the southern part of the North Sea.

5.7.2 Meteorological Aspects

Prior to the enunciation of the frontal theory of cyclones by the Norwegian School of Meteorologists, a squall line was regarded as any line of storms arranged in a general southerly and easterly direction from a depression. Characteristic features of these storms are strong intensity, strong wind gusts, wind shifts, pressure increases, temperature decreases, and heavy rain of the showery type. After the advent of the frontal theory of cyclones, some of these storms were redesignated as cold fronts. The term "squall line" was reserved for the storms in the warm sectors of the cyclones, roughly paralleling the cold front and along which there is intense convective activity.

HARRISON and ORENDORFF (1941) suggested that the squall line was formed by the rain-cooled air of the downdraft. Squall lines develop in air masses that are convectively unstable. Most of the squall lines over the United States develop in regions of warm advection at low levels with neutral or even slight cold advection aloft (PETTERSSEN, 1956). A favourable situation for squall line development is when a tongue of warm and moist air from the Gulf of Mexico moves northward over the Great Plains and the Mississippi Valley.

Squall lines may move with speeds of up to 15–18 $m \cdot s^{-1}$ (faster than the ambient wind). In midlatitudes, especially, they may be embedded in larger scale synoptic weather systems. In such situations, the intense part of the weather might be concentrated only in about 10 % of the area of the synoptic system. The life span of a squall line is much shorter

than that of the synoptic scale system in which it is embedded (e.g. a few hours versus a few days).

Squall lines have low-level indraft along their forward edge due to rapid motion (RIEHL, 1979). Individual cumulonimbus clouds in a squall line have life times of at most a few hours. Hence, for a squall line to survive, new convective elements continually replace dissipating elements (RAMAGE, 1971). Squall lines usually become most intense during late afternoons when the convective activity is the highest.

NEWTON and NEWTON (1959) and NEWTON (1967) showed that the continuous exchange of mass between the storm and the surroundings leads to a nonhydrostatic pressure that aids the convection process. On the downshear side the convective elements continually develop whereas on the upshear side they dissipate. Hence, the storm moves in the direction of developing elements and away from dissipating elements.

Over the Central United States the squall lines move 25° to the right of and about 4 $m \cdot s^{-1}$ slower than the mean wind at the 700-mb level. Squall lines over the midwestern and northeastern parts of the United States deviate 50 and 70°, respectively, to the right of the wind direction at the 700-mb level.

Squall lines usually develop near topographic discontinuities (mountains and valleys). Generally, squall lines tend to dissipate when they cross a coast because cool and relatively stable surface air suppresses ascent due to buoyancy (RAMAGE, 1971).

In northern India, squall lines occur in spring and fall (DE, 1963). In northern Australia, squall lines occur mainly in spring. The West African squall lines resemble those over the United States in the following respects: they tend to develop and are most intense in the afternoon and are most frequent in spring. However, there are certain differences also. The West African squall lines are usually embedded in an environment possessing easterly vertical shear and they travel westward with velocities of up to 10 $m \cdot s^{-1}$. Although the life span of most squall lines is less than 24 h, some persist for several days and travel more than 3000 km. Although most squall lines weaken after crossing a coastline, some do not (e.g. over the warm Guinea current).

Probably the first systematic study of squall lines emerged from the U.S. thunderstorm project during 1946–48. WILLIAMS (1948) used the data from the automatic recording stations in Ohio operated by the U.S. Weather Service's cloud physics project to deduce the microstructure of squall lines.

TEPPER (1950a, 1950b) described the meteorological features associated with the arrival of an intense squall line at the ground. Initially there is an abrupt rise in the surface pressure, which he referred to as a "pressure jump". FUJITA (1955) called it the "pressure surge". Within 1 min after the pressure jump there is a sudden change in the wind direction, which was referred to as „wind shift." Then, the temperature begins to drop rapidly within 2 min after the wind shift. This drop of temperature was referred to as the „temperature break. The peak wind gust, the onset of rain, and the pressure maximum follow the temperature break.

On the other hand, FUJITA (1955) described the situation somewhat differently. Following the pressure surge, the thunderstorm high occurs and then the pressure decreases. The low pressure areas following the wake drop in pressure are called wake depressions.

BEDARD et al. (1977) and BEDARD and MEADE (1977) described an inexpensive instrument system that was deployed at the Dulles Airport in Washington, DC, to measure the gust fronts associated with squall lines. NOAA (ANONYMOUS, 1978) described the various modeling activities on squall lines that are being done at the National Severe Storms Laboratory (United States). A model being developed by Fritsch (ANONYMOUS, 1978) incorporates the effects of deep convection and shows how a series of thunderstorms can become organized

into groups and how they can influence the winds and pressures in the surroundings. Warm moist air accumulates in front of the squall line, and this leads to a low pressure system at the surface; colder air from the thunderstorm downdraft forms a high pressure area behind the squall line. Presently used weather forecast models cannot resolve the squall lines adequately because the grids used are of the order of 200 km in size.

The official U.S. Weather Service definition of pressure jump (associated with a squall line) is an increase of pressure of more than 0.17 mb min^{-1} with at least a total increase of 0.7 mb. TEPPER (1950) suggested that the detection of the pressure jump could be used as an indication of the movement of the squall line.

Time series data on pressure jumps were published by TEPPER (1950b), FUJITA (1959), and CHARBA (1974). These data show increases of several millibars in surface pressure during a period of a few minutes. TEPPER's (1950a,b) data showed pressure increases of 2.3 mb in 5 min. WILLIAMS' (1948) data showed a 2- to 5-mb rise in 5 min. GOFF (1975) found an average increase of 2.5 mb in 100 s. BLECKER and ANDRE (1950) found significant pressure increases in 10 min.

As for the speed of travel, WILLIAMS (1948) gave a value of 13.4 m s^{-1}, TEPPER (1950) found 20.4 m s^{-1}, and GOFF (1975) found 10 m s^{-1}. On the other hand, DE (1963), based on a study of 44 squall lines in northern India, found a value of 33 km · h^{-1}. He quoted values from other authors ranging from 35 to 40 km · h^{-1}. DE (1963) also found that the direction of movement of the squall lines is generally within 90° to the right (looking downwind) of the 700-mb wind. They occurred mainly during March–May and their life span varied from 3 to 10 h. Their lengths varied from 40 to 400 km and their speed of travel varied from 20 to 50 km · h^{-1}. For comparison, some data on squall lines in Venezuela are listed in Table 5.61.

Table. 5.61: Squall lines over Venezuela (BETTS et al., 1976)

Major axis of squall line (km)	Minor axis of squall line (km)	Life span (min)	Observed track length (km)	Speed of travel (km · h^{-1})
96	32	200	136	51.1
90	46	240	131	38.5
120	27	211	170	55.0
95	20	215	161	59.4
100	30	140	154	52.4
100	31	195	150	52.0

The cross-section through a squall line system is shown schematically in Fig. 5.100. Important results on squall lines may be found in LILLY (1979), OGURA and LIOU (1980), BETTS et al. (1976), ZIPSER (1969, 1977), HOUZE (1977), MITCHELL and HOVERMALE (1977), CHARBA (1974), MONCRIEFF and MILLER (1976) and MILLER and BETTS (1977).

5.7.3 Squall Line Forcing Terms for Storm Surge Calculation

WILSON (1978) developed simplified pressure and wind profiles for a "historical maximum squall line" for use in estimating water levels near United States nuclear power plants. One very important point to be made is that, whereas with synoptic scale weather systems

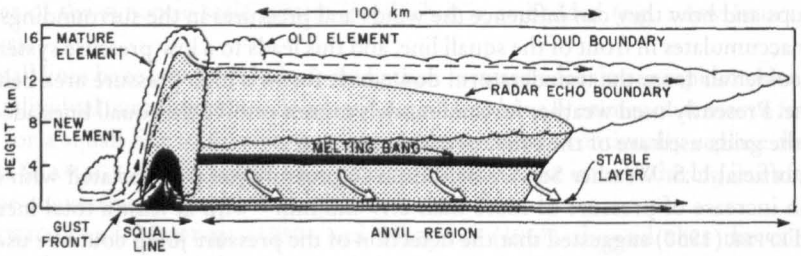

Fig. 5.99: Schematic cross-section through a squall line system. Streamlines show flow relative to the squall line. Broken lines show updraft circulation. Thin solid streamlines show mesoscale downdraft below the base of the anvil cloud. Dark shading shows strong radar echo in the melting band and in the heavy precipitation zone of the mature squall line element. Light shading shows weaker radar echoes. Scalloped line shows visible cloud boundaries (Houze, 1977)

(e.g. tropical and extratropical cyclones) usually the wind stress is much more important than the atmospheric pressure gradients, for squall lines, the pressure gradient terms are at least of equal importance and sometimes much bigger than the wind stress terms.

Following FUJITA (1955), WILSON (1978) developed a simple model for a squall line system, as shown in Fig. 5.100. He also made the following assumptions: (a) the squall line is in a steady state and is in the mature stage, (b) the leading edge of the pressure surge and the gust front move with the same speed (this is in contrast with FUJITA's [1955]) result that the pressure surge moves with a speed some 40 % greater than that of the gust front), and (c) the squall line moves perpendicular to the shoreline.

Making use of these assumptions and the model shown in Fig. 5.100, WILSON (1978) developed the pressure and wind profiles (Fig. 5.101) for a historical maximum squall line. For example, FUJITA et al. (1956) gave a value for the pressure gradient of 9 mb in 50 mi (80 km)

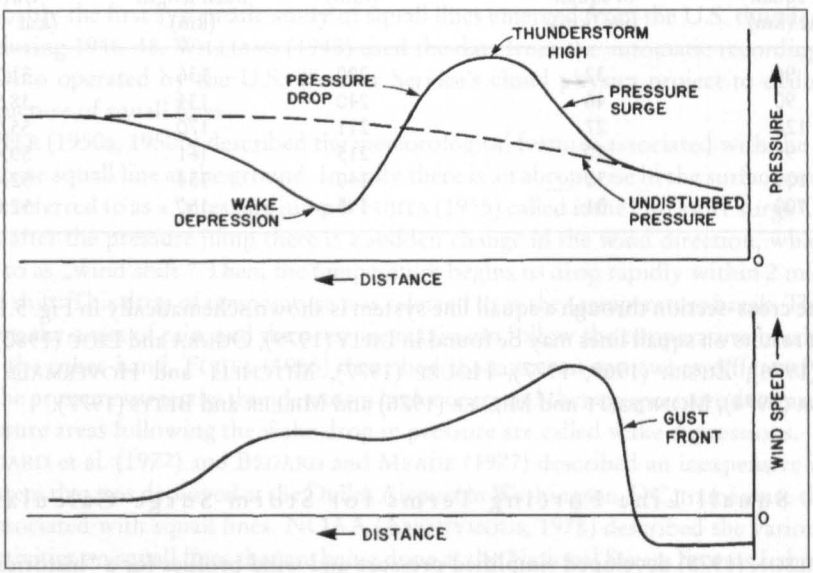

Fig. 5.100: Idealized pressure (top) and wind speed (bottom) field profiles for a squall line system. Negative wind speed denotes inflow into storm system (WILSON, 1978)

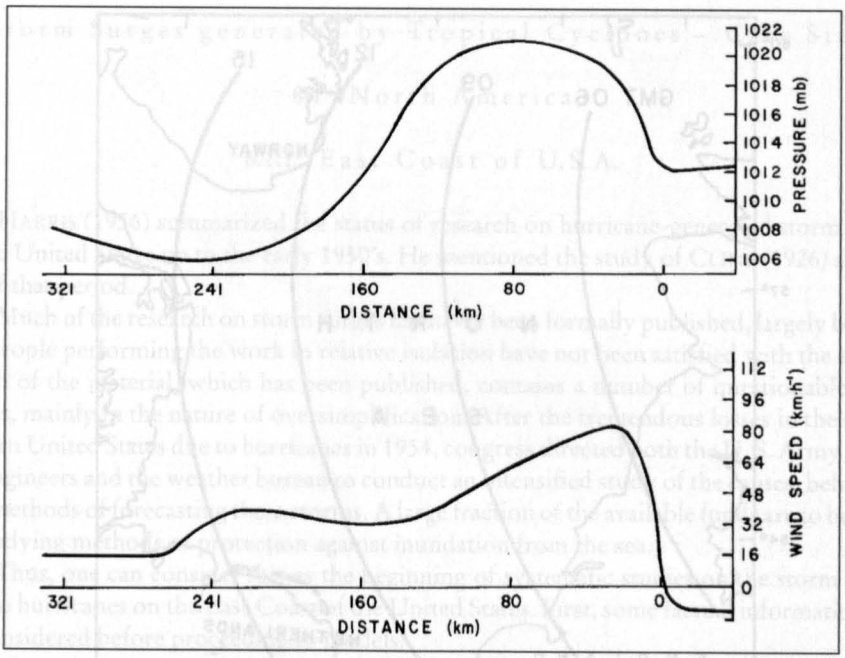

Fig. 5.101: Simplified pressure (top) and wind speed (bottom) profiles for historical maximum squall line system (WILSON, 1978)

for a squall line over Nebraska on June 25, 1953, with a sustained post-gust front wind speed of 45 mi · h^{-1} (73 km · h^{-1}). In this model Wilson used a value of 50 mi · h^{-1}.

It was mentioned that for squall lines the pressure gradient terms are comparable in magnitude with wind stress terms. This is also borne out by the studies of FREEMAN and MURTY (1972) and MURTY and FREEMAN (1973) for the squall line of August 22, 1971, over Lake Huron. For the squall line, a sharp rise of pressure (δp_a) of 4.5 mb and wind (W) of 112.6 km · h^{-1} were deduced from the observations. Taking the average depth (D) of the southern part of Lake Huron as 54.7 m, a horizontal scale (δx) of 8 km, a time interval during which the pressure increased as 5 min, and the speed of travel of the squall line as 96.5 km · h^{-1}, the pressure gradient term becomes

$$\frac{1}{\rho} D \frac{\delta p_a}{\delta x} = 34 \text{ cm}^2 \cdot \text{s}^{-2}$$

The wind stress term gives

$$\tau_S = 3 \times 10^{-6} W^2 = 30 \text{ cm}^2 \cdot \text{s}^{-2}$$

For the synoptic scale, the atmosheric pressure gradient as taken from the isobaric plot is a 4-mb change (δpa) in a 161-km distance (δx). A wind speed (W) of 32 km · h^{-1} is used as a typical value. The preessure gradient term and the wind stress term become 1.5 and 2.4 cm · s^{-2}, respectively.

Earlier, the storm surge calculations in idealized situations using the method of characteristics (e.g. RAO, 1967, 1969; MURTY, 1971) were discussed. The calculations of the storm

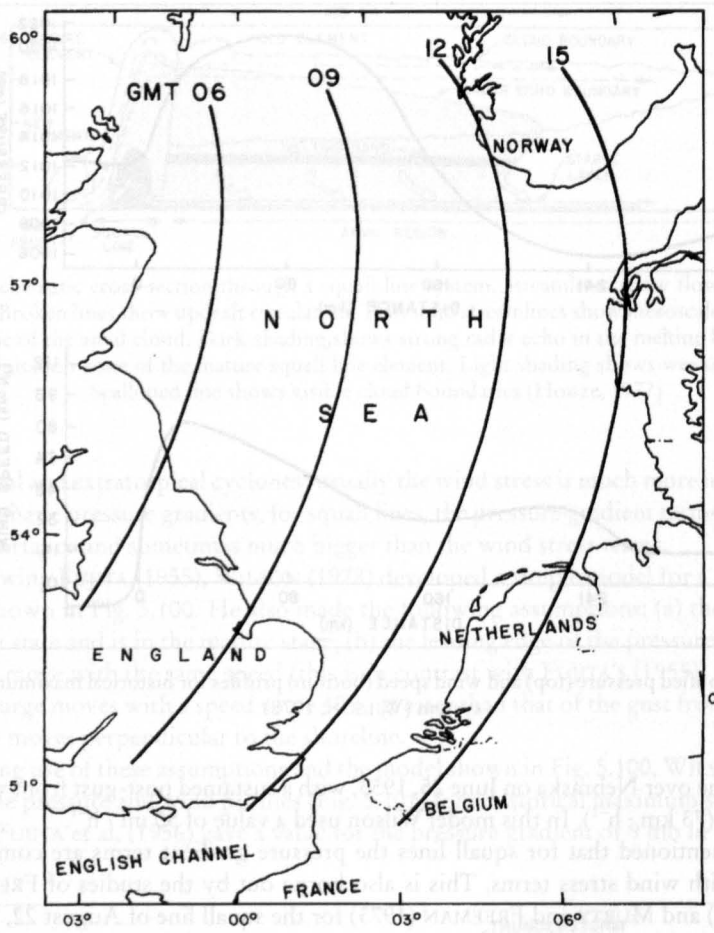

Fig. 5.102: Position of the leading edge of the squall line at four different times (GMT) on December 13, 1956 (TIMMERMANN, 1971)

surge in Lake Michigan due to a squall line on June 26, 1954 (PLATZMAN, 1958a, 1965; IRISH, 1965; HUGHES, 1965) are included elsewhere in the book. DONN and BALACHANDRIAN (1969) discussed the water level oscillations in Long Island Sound (east of New York City) due to a squall line on November 23, 1953. DONN (1959) studied the storm surges in Lake Huron and Erie due to a squall line on May 5, 1952. KRAUSS (1978) studied the response of a stratified sea to a moving squall line.

DOUGLAS (1929) made a simple calculation of the water level oscillations in the English Channel due to a squall line on July 20, 1929. TIMMERMANN (1971) studied the water level oscillations (he referred to therm as "cold fronts") on the Dutch coast of the North Sea. When the speed of the squall line is between 29 and 36 knots, resonance occurs between the squall line and the long gravity waves in the North Sea, and this leads to water level oscillations. During the period December 13, 1956, to January 4, 1968, 20 squall lines with speeds ranging from 25 to 36 knots travelled over the southern part of the North Sea. The positions of tile leading edge of the squall line at four different times on December 13, 1956, are shown in Fig. 5.102.